Title
ELECTRONIC DENSITIES OF STATES OF SOLIDS FROM X-RAY PHOTOEMISSION SPECTROSCOPY

Author
Pollak, Roger Alan.

Publication Date
1972-12-01

LBL-1299

ELECTRONIC DENSITIES OF STATES OF SOLIDS FROM X-RAY PHOTOEMISSION SPECTROSCOPY

Roger Alan Pollak
(Ph. D. thesis)

December 1972

Prepared for the U. S. Atomic Energy Commission
under Contract W-7405-ENG-48

LBL-1299

DISCLAIMER

ELECTRONIC DENSITIES OF STATES OF SOLIDS FROM
X-RAY PHOTOEMISSION SPECTROSCOPY

Contents

INDEX OF SPECTRA

ELECTRONIC DENSITIES OF STATES OF SOLIDS FROM X-RAY PHOTOEMISSION SPECTROSCOPY

Roger Alan Pollak

Lawrence Berkeley Laboratory
University of California
Berkeley, California 94720

December 1972

ABSTRACT

High-resolution, monochromatic x-ray photoemission valence-band spectra for a variety of solids are presented, related to ground state eigenvalue spectra, and compared with existing theory. Valence-band spectra of C (diamond), Al, Si, Ga, Ge, As, Pd, Ag, Cd, In, Sn, Sb, Te, Ir, Pt, Au, Tl, Pb, Bi, GaAs, ZnSe, PbS, PbSe, PbTe, NiO, CoO, Tl_2O, GaP, GaSb, ZnO, ZnS, ZnTe, CdS, CdSe, CdTe, InSb, HgTe, NaI, NaBr, NaCl, NaF, KI, KBr, KCl, and KF are reported.

With increasing atomic number in the 4d5s5p elements Pd through Te the 4d structure evolves from d bands to spin-orbit split atomic-like core levels. Band-structure broadening was detectable in Cd, for which the 4d doublet is 11 eV below the Fermi energy. Structure was observed in the 5s5p bands for the first time by this method.

Structural features in the valence-band XPS spectra vary from Ir to Au as expected on the basis of 5d6s band filling. Spin-orbit splitting of the 6p band is manifest in the XPS spectra of Pb and Bi. Lowered energies of the 6s band indicate the presence of the mass-velocity and Darwin terms.

The total valence bands of crystalline and amorphous silicon and germanium are reported. For the crystals, the XPS spectra yield results

that are strikingly similar to current theoretical calculations of the electron density of states, $\rho(E)$. Amorphous Si and Ge exhibit definite band structures that are similar to one another but markedly different from the crystalline results.

The XPS valence-band spectra for the isoelectronic series Ge, GaAs, and ZnSe are compared with theoretical valence-band density-of-states calculations using the empirical pseudopotential method. The agreement between the experimental and theoretical results is quite good, particularly for Ge and GaAs. For ZnSe the x-ray photoemission spectrum shows the Zn 3d-states to be higher in energy than the lowest valence-band s-states. In order to obtain this ordering of states in the theoretical calculation, a pseudopotential with an explicit energy dependence is required.

The high-resolution XPS valence-band spectrum from a cleaved natural diamond single crystal is reported. The absence of extrinsic structure allows a reliable comparison with band theory. The XPS molecular-orbital spectra of methane, silane, and germane are also given. The modulation of photoelectric cross section in the valence bands of diamond, Si, and Ge are discussed and compared with atomic XPS cross sections derived from the spectra of CH_4, SiH_4, and GeH_4.

XPS spectra of the valence bands of As, Sb, and Bi show a splitting, ΔE, of the "s-like" peak for the crystalline phase that disappears in the amorphous phase. This similarity to tetrahedrally coordinated semiconductors is explained by describing the semimetals as layers of distorted covalently bonded hexagonal rings. This generalizes the "even-odd" ring effect to the A7 lattice. The relation of ΔE to interatomic distance is described by a universal curve.

XPS valence-band spectra of PbS, PbSe, and PbTe are compared with available band theory results. Relativistic OPW results exhibit the best overall agreement with experiment. EPM results show similar agreement for all but the most tightly bound valence bands.

The charging behavior of 26 semiconductors and insulators is reported and discussed. Charging is found to be correlated with the energy band gap between the valence and conduction bands.

The XPS characteristic energy loss structure of Ag through Te is reported. It can be almost entirely accounted for by excitations similar to those observed in electron reflection experiments. Most of the structure can be assigned to bulk and surface plasmon excitations.

The XPS valence-band spectra of CoO and NiO are presented and discussed in terms of our current understanding of their electronic structure. A 3.5 eV wide structure with two components whose separation appears related to the exchange splitting Δex is assigned to the 3d electrons.

Preliminary results from studies of the oxidation of Tl and Ni demonstrate the ability of XPS to monitor the chemistry of surfaces. Preliminary ultrahigh vacuum XPS spectra of the valence-band and 2s level of aluminum are reported. The valence band exhibits the expected free electron structure.

SECTION I. INTRODUCTION

The language of solid state chemistry and physics is quantum theory. Theoretically one attempts to describe a solid by specifying its Hamiltonian and determining its complete set of eigenfunctions and eigenvalues. This is a many-body problem with $\sim 10^{23}$ atoms/cc and thus its solution can only be approached by using many simplifying and often sizable approximations. This inability to calculate exact solutions leads to a multitude of theories each attempting to treat part of the problem and many taking different approaches to describe the same phenomenon. The employment of the experimental sciences for verification of existing theories and for insight during development of new theories is essential in guiding us in our attempt to understand the solid state.

This thesis presents the experimental valence-band x-ray photoemission spectra for a wide variety of solids, relates these spectra to their ground state eigenvalue spectra, and compares these results with existing theory. Experimentally several techniques are presently used to investigate the electronic density of states $\rho(E)$:

I. Photoemission spectroscopy
   - A. Ultraviolet photoemission spectroscopy[1,2,3]
   - B. X-ray photoemission spectroscopy[4,5,6,7]
   - C. Synchrotron radiation photoemission spectroscopy[8]

II. Soft x-ray spectroscopy[9,10]

III. Ion-neutralization spectroscopy[11]

None of these spectroscopies directly yields the density of states in the one-electron approximation,

$$\rho(E) = \sum_i \delta(E - \varepsilon_i)$$

where the ε_i are the single-particle energies, however each spectroscopy has methods for relating its own measured response function to $\rho(E)$.

The uncorrected response function $I(E)$ measured in x-ray photoemission spectroscopy for several systems with well understood band structures quite closely resembles the calculated densities of states and thus suggests that even uncorrected XPS spectra will yield many of the features of less well understood materials. This is proving to be the case.

REFERENCES

1. W. E. Spicer, in Proc. 3rd Int. Mat. Res. Symp., Electronic Density of States, Nat. Bur. Stand. (U.S.), Spec. Pub. 323 (1971), p. 139.

2. D. E. Eastman, in Electron Spectroscopy, ed. by D. A. Shirley (North-Holland Publishing Co., Amsterdam and London, 1972) p. 487.

3. N. Smith, CRC Critical Reviews in Solid State Sciences 2, 45 (1971).

4. K. Siegbahn, C. Nordling, A. Fahlman, R. Nordberg, K. Hamrin, H. Hedman, G. Johansson, T. Bergmark, S.-E. Karlsson, I. Lindgren, and B. Lindberg, Electron Spectroscopy for Chemical Analysis (Almqvist and Wiksells AB, Stockholm, Sweden, 1967).

5. C. S. Fadley, Ph.D. dissertation, University of California, Berkeley, 1970 (Lawrence Berkeley Laboratory Report UCRL-19535 (1970)).

6. C. S. Fadley and D. A. Shirley, J. Nat. Bur. Stand. 74A, 543 (1970).

7. S. B. Hagström, in Electron Spectroscopy, ed. by D. A. Shirley (North-Holland Publishing Co., Amsterdam and London, 1972) p. 515.

8. D. E. Eastman and W. D. Grobman, Phys. Rev. Letters 28, 1327 (1972).

9. D. W. Fischer, J. Appl. Phys. 41, 3561 (1970).

10. D. J. Nagel, Advan. X-Ray Anal. 13, 182 (1970).

11. H. D. Hagstrum, Phys. Rev. B4, 4187 (1971).

SECTION II. THE ELECTRONIC DENSITY OF STATES AND X-RAY PHOTOEMISSION SPECTROSCOPY--THE ONE ELECTRON TRANSITION MODEL

The use of x-ray photoemission spectroscopy (XPS) to determine the electronic density of states of filled valence and conduction bands in solids is still in its infancy and only several dozen spectra have been reported in the literature. No quantitative theoretical description of the XPS of solids exists at this time. The experimental state of the art is presently advancing quite rapidly, however XPS of valence bands* has not yet become a routine technique.

In solid state XPS a beam of x-ray photons of known energy is directed at a solid surface and the kinetic energy spectrum of the emitted photoelectrons is measured and then related to the eigenvalue spectrum of the solid.[1] This relationship is not yet theoretically or empirically well defined. Presently the very close similarity of the uncorrected XPS spectrum to calculated densities of states in some well understood cases leads us to a series of assumptions and approximations which permit us to compare XPS results with band theory results even though at this stage of development many of these assumptions and approximations must yet be tested and refined.

Photoemission from solids can conceptually be decomposed into a three step process: I. excitation of an electron from a level of the ground state to a free-electron like state of high kinetic energy within the solid, II. passage of the photoelectron to the surface of the solid, and III. escape of the electron from the solid. Conservation of energy requires that the measured kinetic energy of the photoelectron equal the

*All bands formed from the atomic valence electrons will be termed valence bands.

x-ray photon energy minus the energy expended in steps I, II, and III above. A corrected XPS spectrum I'(E) can be obtained from step I after correcting for contributions from steps II and III. It is I'(E) that is compared with the calculated one-electron density of states $\rho(E)$.

The energy required by an electron to escape from a solid (Step III) is the electrochemical potential $\bar{\mu}$. The zero of energy of $\bar{\mu}$ is conventionally the potential energy at infinity. The Fermi level E_F of a metal at 0° K is the uppermost filled electron energy level. In general E_F is defined by the Fermi distribution function and the density of electronic states of the system. The Fermi level is equal to the electrochemical potential $\bar{\mu}$ at 0°K. Conventionally XPS spectra of solids are reported relative to the Fermi level. The relationship among some commonly encountered potentials is illustrated in Fig. 1. The electrochemical potential is the sum of the Volta potential, surface potential jump, and chemical potential. The Volta potential is the electrostatic potential just outside the solid surface ($\sim 10^{-3}$ cm away). Charging of the solid or external fields produce the Volta potential. The surface potential jump is the electrostatic potential difference between a point just outside the surface and a point inside the solid. The chemical potential accounts for the interaction of the measuring probe, the electron, with the system. The inner potential is defined as the sum of the Volta potential and surface potential jump. The work function is defined as the sum of the surface potential jump and the chemical potential. When the Volta potential is zero the work function equals the electrochemical potential.

Photoelectrons excited within a solid must pass through the solid to the surface (Step II). Many suffer inelastic energy losses. The

secondary electron energy spectrum of monoenergetic electrons reflected from a solid surface contains inelastic loss structure similar to that observed in XPS spectra. Figure 2 after Seah[2] is the secondary electron energy spectrum of silver bombarded with 100 eV electrons incident at 70° from the normal. For convenience this spectrum is divided into three regions. Region III contains the elastically scattered electrons and those which have lost a few hundredths of an electron volt to phonons. Region II is composed of those electrons which have suffered characteristic energy losses by producing, for example, collective excitations or interband transitions of the lattice electrons. Characteristic energy loss peaks usually occur between 2 eV and 50 eV below the elastically scattered peak. The electrons of region I are called the true secondary electrons. They are of low energy and it is believed they are produced by a cascade background. Thus we see that the initially monoenergetic beam of electrons after passing through the solid has a very broad energy distribution with much structure. As the kinetic energy of the incident electron beam increases the ratio R of elastically scattered to inelastically scattered electrons decreases.[2] R for XPS valence band spectra is usually much smaller than unity. XPS results are more complex than those from electron reflection measurements since there are as many primary electron energies in XPS as there are orbitals of different energy. The spectral distributions from all orbitals are superimposed in the XPS spectrum.

At present XPS kinetic energy spectra I(E) are corrected for inelastic scattering (step II) and the electrochemical potential (step III) and then compared directly with one-electron densities of states

calculated within the self-consistent field approximation. The theoretical densities of states are usually broadened to be consistent with experimental resolution. By making this comparison one assumes the validity of the one-electron transition model. The applicability and limitations of the one-electron transition model to XPS have been discussed by Fadley and Shirley;[1] Hedin, B. I. Lundqvist, and S. Lundqvist;[3] and Hagström.[4] They have pointed out the experimental contributions to lineshape and cases where the one-electron transition model is inadequate.

The one-electron density of states is given by:

$$\rho(E) = \sum_i \delta(E - \varepsilon_i) \tag{1}$$

where ε_i is the single particle energy which is equated with the electron binding energy in the one-electron transition model. The binding energy E_B relative to the Fermi level of the solid is given by the energy conservation equation for photoemission:

$$E_B = h\nu - E_{kin} - \bar{\mu} \tag{2}$$

where $h\nu$ is the photon energy, E_{kin} is the photoelectron's kinetic energy, and $\bar{\mu}$ is the electrochemical potential. In practice the contact potential between the spectrometer and sample must be subtracted from this equation. This yields the familiar equation:

$$E_B = h\nu - E_{kin} - q\phi_{sp} - q\psi_{sa} \tag{3}$$

where ϕ_{sp} is the spectrometer work function, ψ_{sa} is the Volta potential of the sample and q is the electronic charge (-e). (See Fig. 1.)

Within this model we can directly compare the XPS kinetic energy spectrum with the one-electron density of states modulated by the appropriate transition probabilities.[1]

REFERENCES

1. C. S. Fadley and D. A. Shirley, in Proc. 3rd Int. Mat. Res. Symp., Electronic Density of States, Nat. Bur. Stand. (U.S.), Spec. Pub. 323 (1971), p. 163.

2. M. P. Seah, Surface Science 17, 132 (1969).

3. L. Hedin, B. I. Lundqvist, and S. Lundqvist, in Proc. 3rd Int. Mat. Res. Symp., Electronic Density of States, Nat. Bur. Stand. (U.S.), Spec. Pub. 323 (1971), p. 233.

4. S. B. Hagström, in Electron Spectroscopy, ed. by D. A. Shirley (North-Holland Publishing Co., Amsterdam and London, 1972) p. 515.

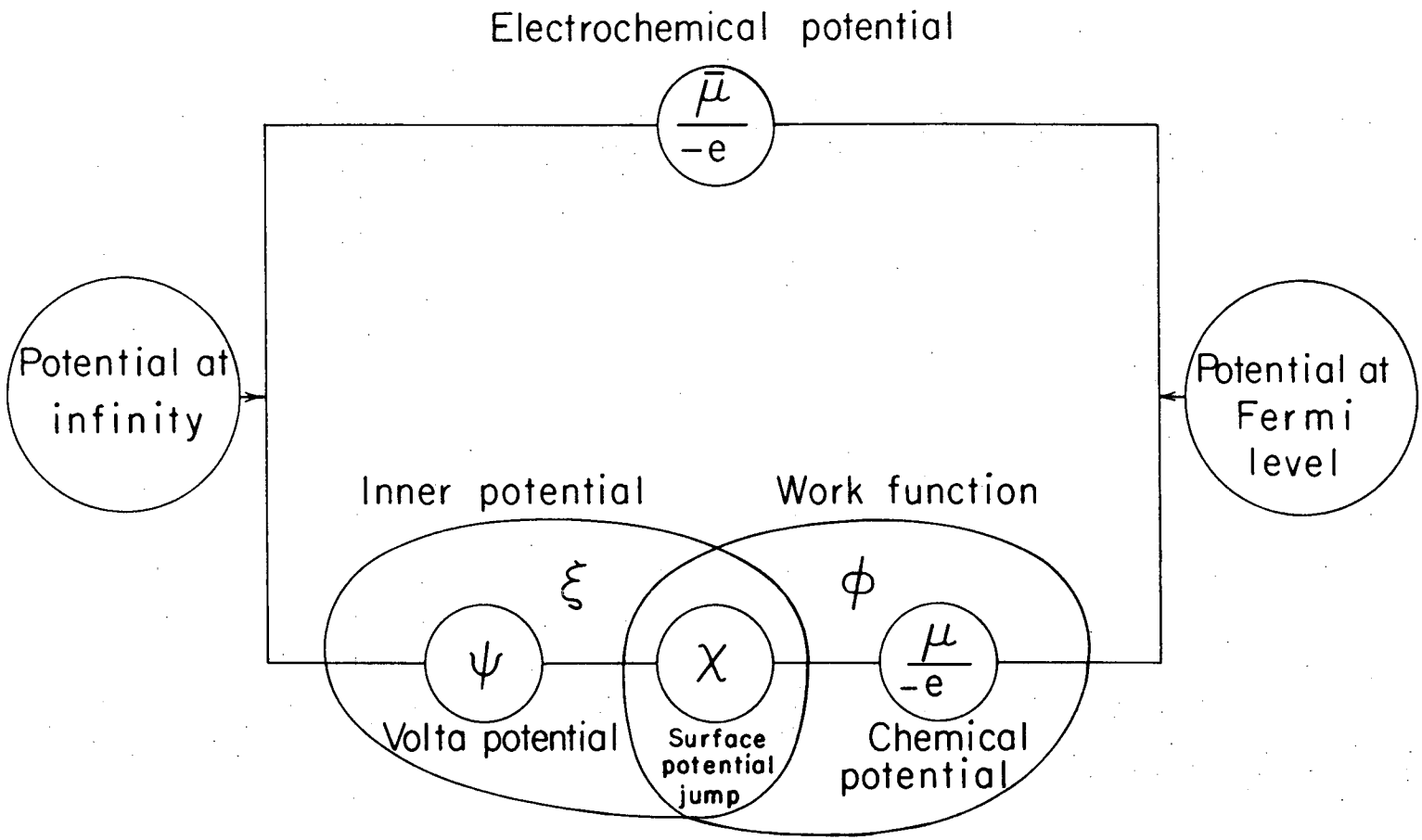

XBL7210-4232

Fig. 1. Electrochemical Potential.

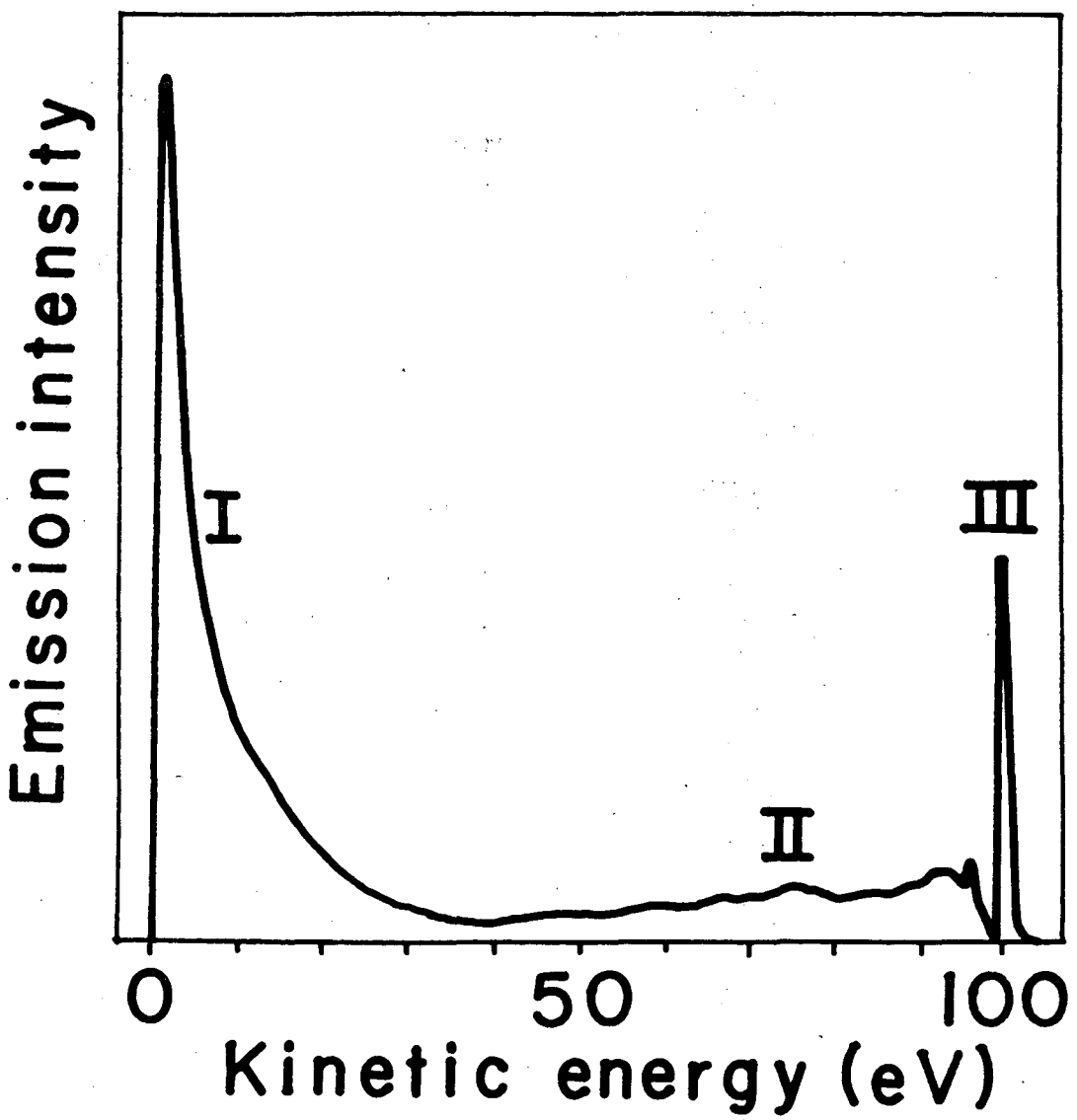

XBL 7211-7435

Fig. 2. Secondary electron energy spectrum of silver bombarded with 100 eV electrons (after Seah[2]).

SECTION III. EXPERIMENTAL METHOD

Siegbahn *et al.*[1] in 1967 proposed a design for an x-ray photoemission spectrometer that would allow one to improve resolution beyond the limit set by the natural linewidth of the exciting x-radiation and also eliminate the photoelectron background excited by satellite x-rays and bremsstrahlung radiation produced at the x-ray anode. This is accomplished by Bragg reflecting from a quartz single crystal only the Al $K\alpha_{1,2}$ region of radiation produced in the x-ray tube. On reflection from the crystal the Al $K\alpha_{1,2}$ doublet is dispersed in wavenumber across the sample being studied. Dispersion-compensated electron optics are then used to energy analyze the photoelectron spectrum. The Scientific Instruments Division of the Hewlett-Packard Company manufacture a spectrometer based on this design. This spectrometer, the HP 5950A ESCA photoelectron spectrometer[2] has been used for the majority of the work reported here. A measure of the instrumental resolution has been extracted from the slope of the Fermi edges in the spectra of Pd, Ag, Cd, In, and Sn. For each of these cases the observed slope can be obtained by folding a Fermi distribution function with a Gaussian instrumental response function of 0.55 ± 0.02 eV FWHM (see Sec. IV). The error only applies to the precision of the measurement. It is believed that with the elimination of some systematic contributions to linewidth this resolution can yet be improved. This problem is now under study.

Figure 1 is a photograph of the HP 5950A. The major components are the monochromator, the electron optics, the electron detection system, the data system, the sample inlet system, and the vacuum system. A schematic of the monochromator, the electron optics, and data system is

given in Fig. 2, a schematic of the sample inlet system in Fig. 3, and a schematic of the vacuum system in Fig. 4. The x-rays strike the sample 20° from the surface normal and photoelectrons emitted 51.5° from the normal enter the energy analyzer. The analyzer consists of an electron lens system which retards and focusses the photoelectrons at the entrance of a constant energy 15.5 cm radius electrostatic hemispherical analyzer. A glass multi-channel electron multiplier projects the electron distribution at the exit focal plane of the analyzer onto a phosphor which coats the inside of a vacuum port window. A vidicon system transfers the information from the phosphor to the data system. A multichannel analyzer is used to store the data. The MCA is presently addressed by an analogue signal generated by the vidicon system. The number of horizontal vidicon lines does not equal the number of MCA channels used. We believe that there is a systematic contribution to both linewidth and noise associated with the present addressing system and are in the process of building a system which will digitally address the MCA and digitally step the retarding voltage of the energy analyzer. Presently the retarding voltage is swept continuously. In the new system the information from each vidicon line will be stored in a different MCA channel. We believe this will eliminate the systematic noise which now dominates random statistical noise and thereby requires counting times several times longer than statistics alone would require.

The need for ultrahigh vacuum photoelectron spectrometers has been recognized for some time. The sensitivity of XPS to only the first few surface layers[3] requires the production and maintenance of clean

surfaces to insure no contribution to spectra from contaminants. During normal operation the residual gas pressure in the unbaked, unmodified HP 5950A analyzer chamber ranges from 5×10^{-9} Torr to 3×10^{-8} Torr. The pressure was measured with a nude Bayard-Alpert gauge in the analyzer chamber. The residual gas consists mainly of water, CO, and H_2 with small quantities of hydrocarbons and rare gases. A typical residual gas spectrum obtained with an EAI QUAD 250 quadrupole residual gas analyzer attached to the electron energy analyzer chamber is shown in Fig. 5. The residual gas pressure in the sample preparation chamber ranged from 2×10^{-7} Torr to 8×10^{-7} Torr. This pressure was measured with a nude Bayard-Alpert gauge attached to the sample preparation chamber. The x-ray monochromator chamber is vacuum isolated from the analyzer chamber by a 0.25 mil aluminum window. The whole system is pumped with Varian Noble Vac-Ion pumps (Fig. 4). The above vacuum conditions have been adequate for studying elemental semiconductors, binary tetrahedrally coordinated semiconductors, the alkali halides, some other binary semiconductors, and the less electropositive metals on the right side of the periodic table. The conditions were inadequate for materials with reactive surfaces. The majority of the work reported here was performed in the unmodified, unbaked HP 5950A which will be termed the high vacuum (HV) mode.

The HP 5950A is bakeable and constructed of materials compatible with ultrahigh vacuum. All seals are metal except for one sliding C-ring seal through which the samples are introduced into the system on a long rod. This sliding seal system appears to be incompatible with ultrahigh vacuum. The conductance of air through the seal system limits

in the energy analyzer does not have to be regenerated unless the system has been contaminated. These modifications necessary for UHV operation have just been completed. Preliminary results are discussed in Sec. XVI.

REFERENCES

1. K. Siegbahn, C. Nordling, A. Fahlman, R. Nordberg, K. Hamrin, J. Hedman, G. Johansson, T. Bergmark, S.-E. Karlsson, I. Lindgren, and B. Lindberg, Electron Spectroscopy for Chemical Analysis (Almqvist and Wiksells AB, Stockholm, Sweden, 1967).

2. K. Siegbahn, D. Hammond, H. Fellner-Feldegg, and E. F. Barnett, Science 176, 245 (1972).

3. M. Klasson, J. Hedman, A. Berndtsson, R. Nilsson, and C. Nordling, Physica Scripta 5, 93 (1972).

4. Figure from HP 5950A manual.

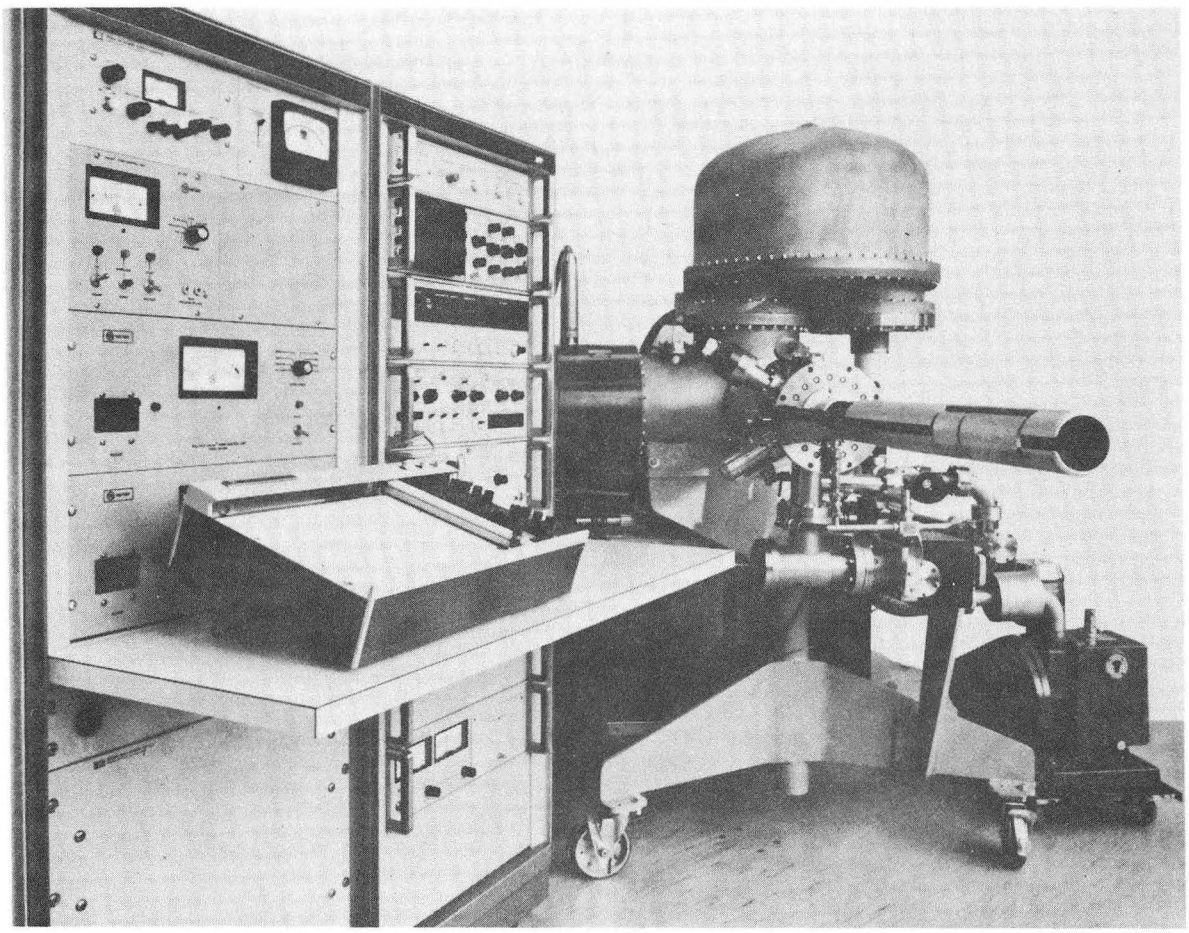

XBB 7211-5762

Fig. 1. HP 5950A ESCA photoelectron spectrometer.[4]

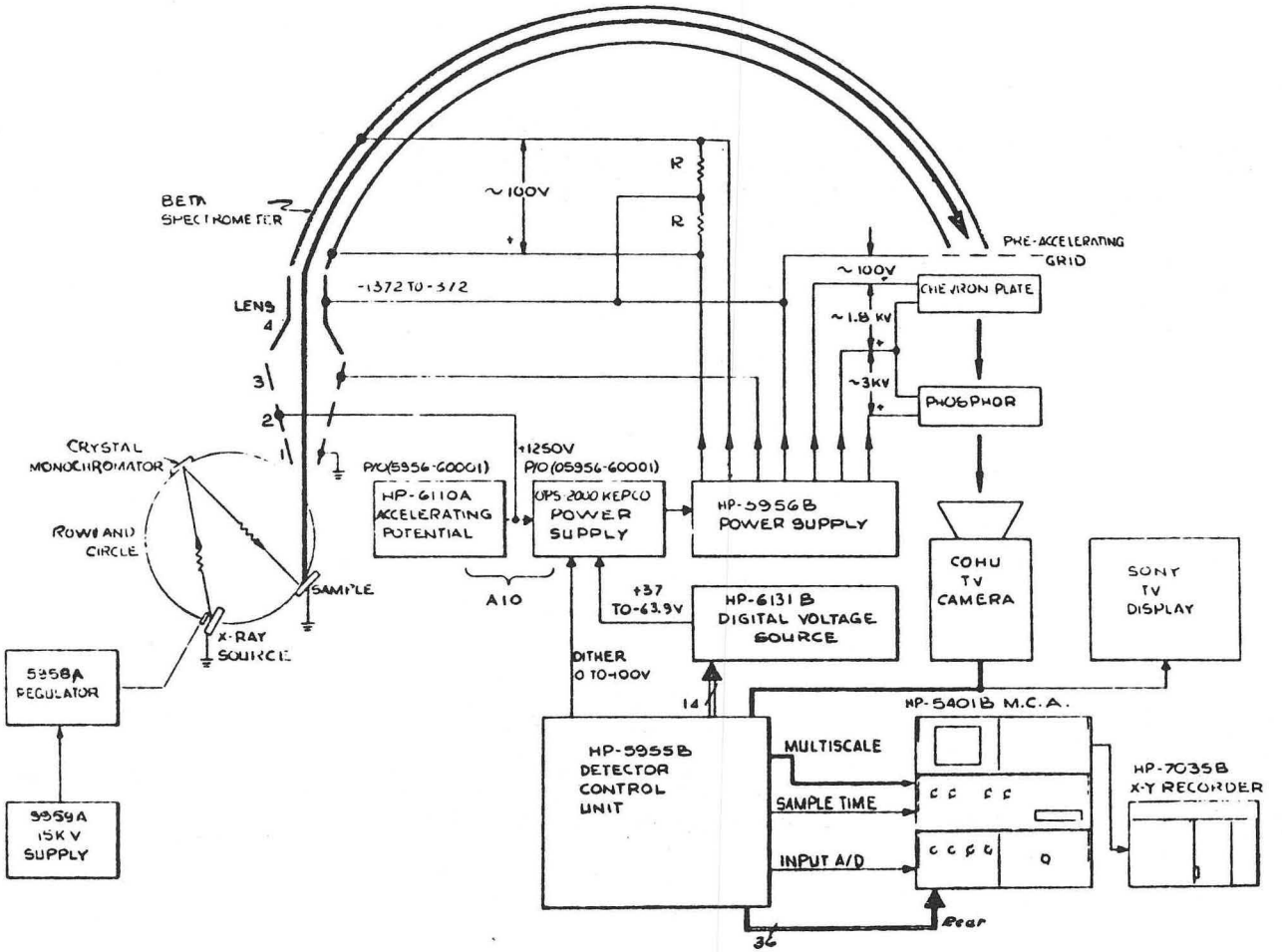

XBL 7211-7401

Fig. 2. Schematic of HP 5950A monochromator, electron optics, and data system.[4]

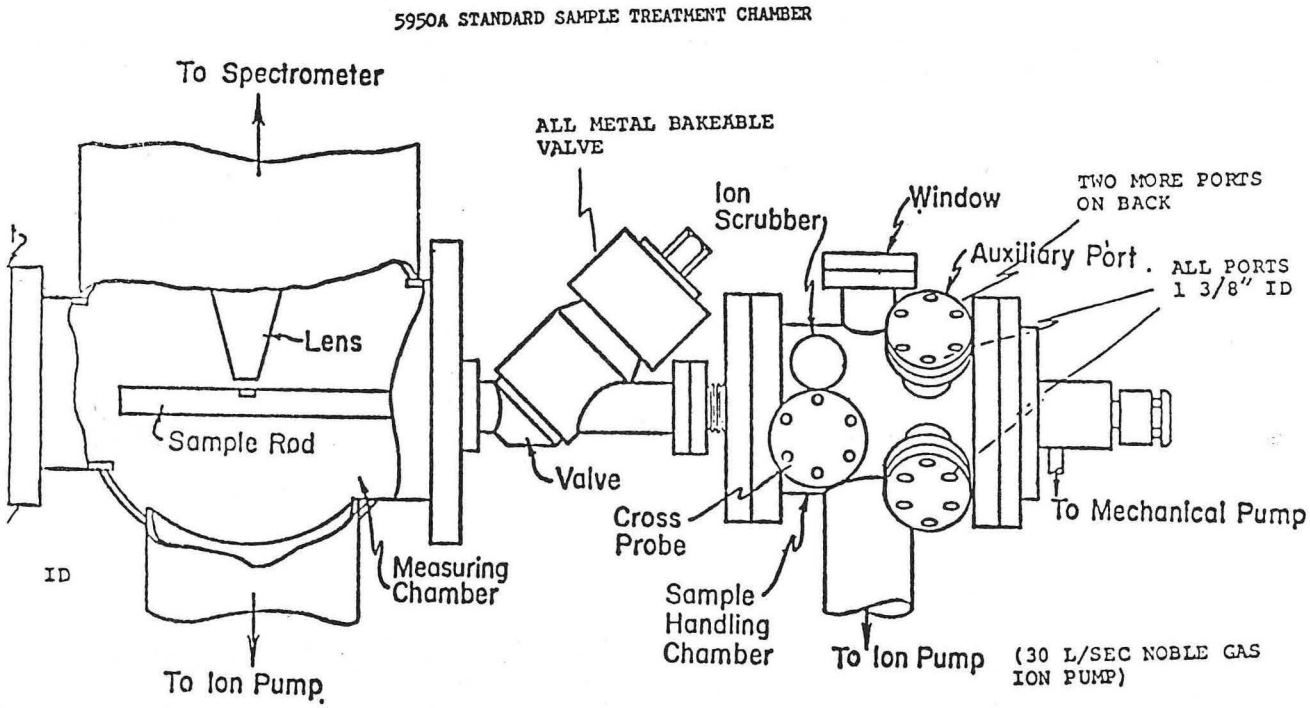

XBL 7211-7402

Fig. 3. HP 5950A sample inlet system.[4]

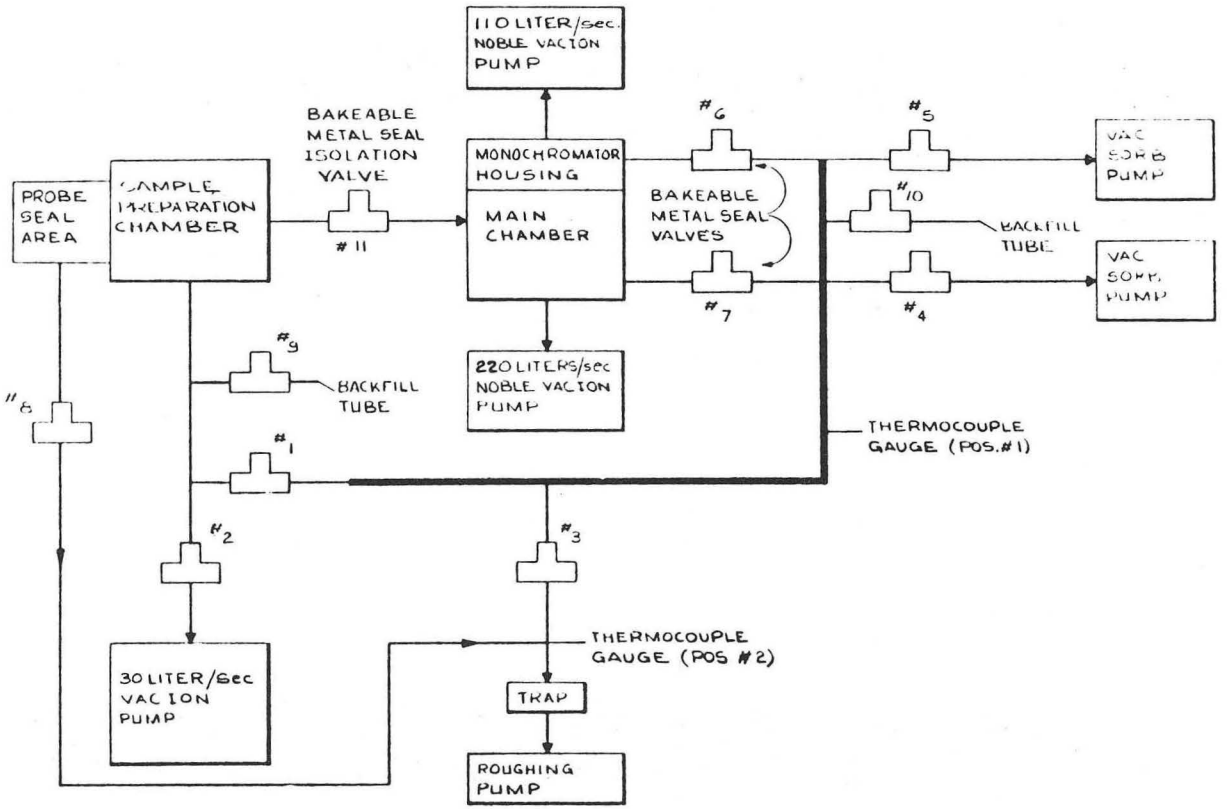

XBL 7211-7400

Fig. 4. HP 5950A vacuum system block diagram.[4]

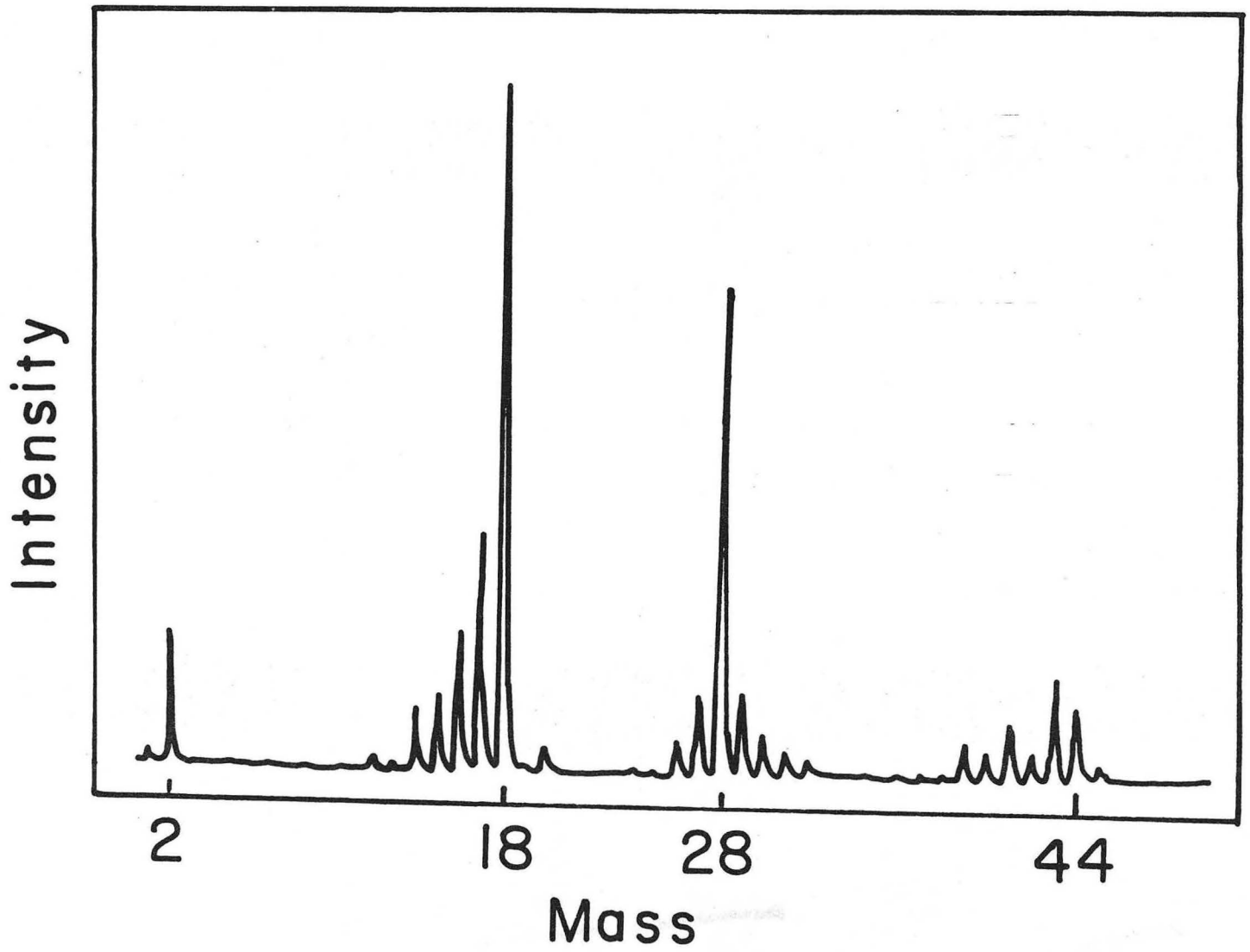

XBL 7211-7434

Fig. 5. Typical residual gas spectrum in the HP 5950A analyzer chamber. (Obtained with an EAI Quad 250 quadrupole residual gas analyzer.)

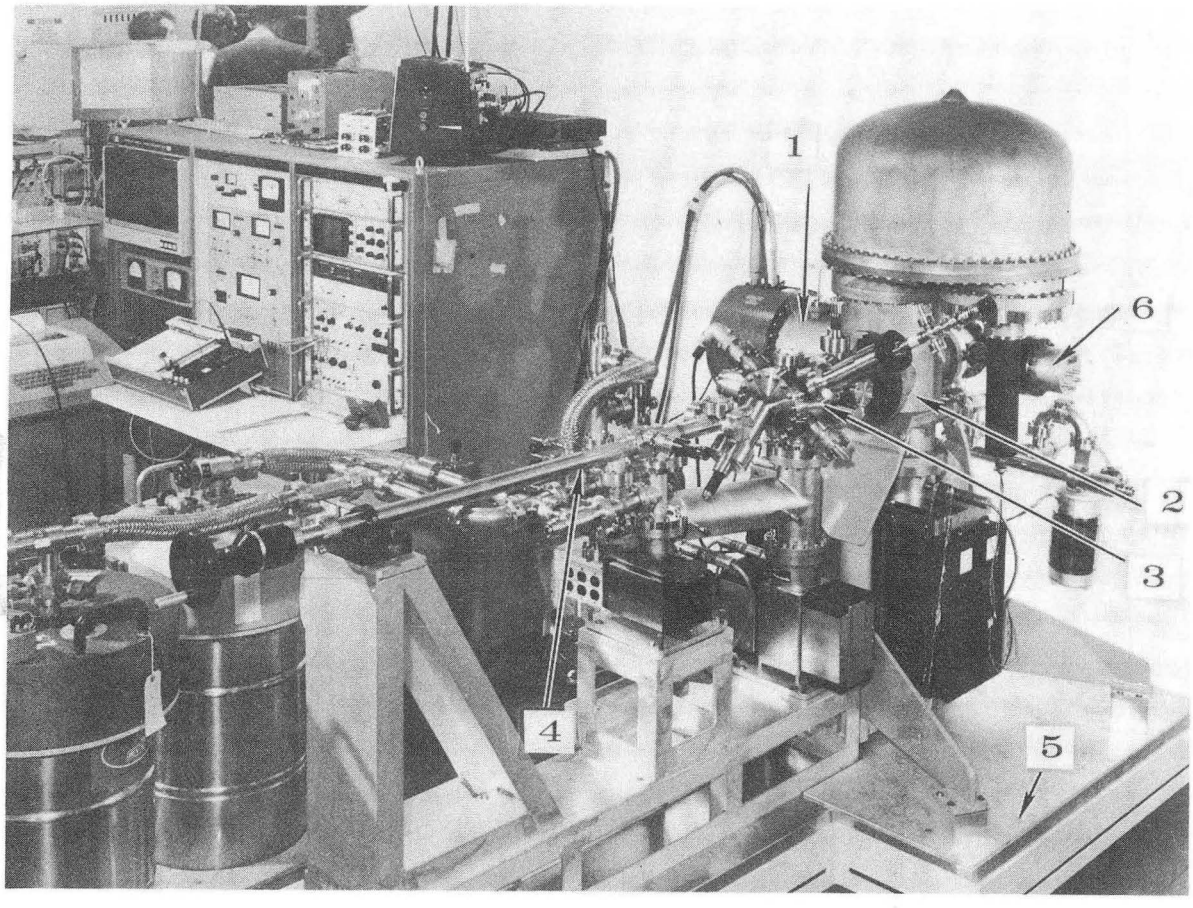

XBB 7210-5115A

Fig. 6. Modified HP 5950A ESCA photoelectron spectrometer. 1) Monochromator vacuum chamber; 2) Analyzer vacuum chamber; 3) Sample preparation chamber; 4) Sample introduction chamber; 5) Bakeout oven base; 6) Quad 250 residual gas analyzer.

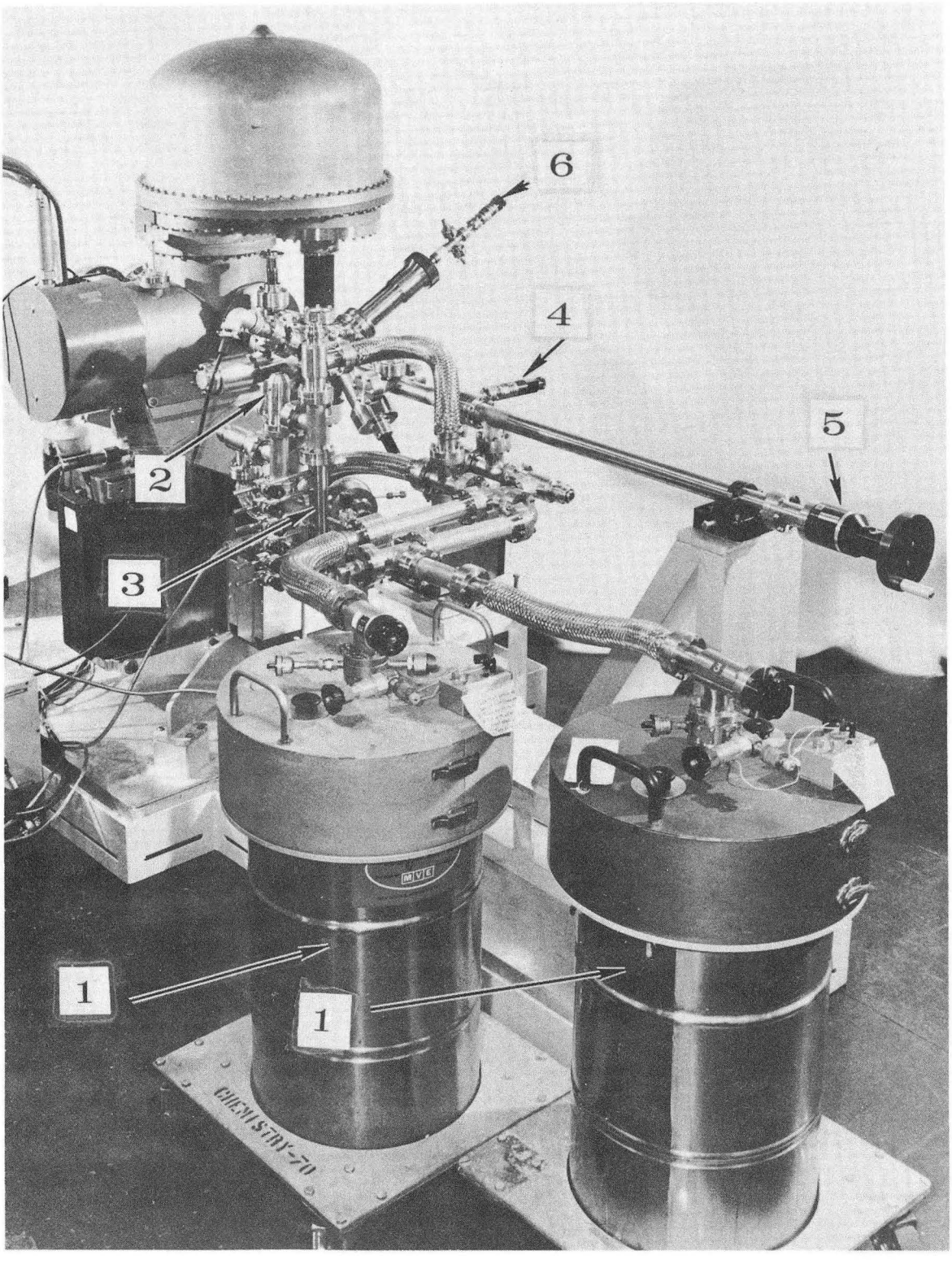

XBB 7210-5119A

Fig. 7. Modified HP 5950A ESCA photoelectron spectrometer. 1) roughing cryosorption pumps; 2) leak valve between gas manifold and TSP; 3) gas manifold; 4) sample-rod rotary drive mechanism; 5) sample-rod linear drive mechanism; 6) sample preparation manipulator.

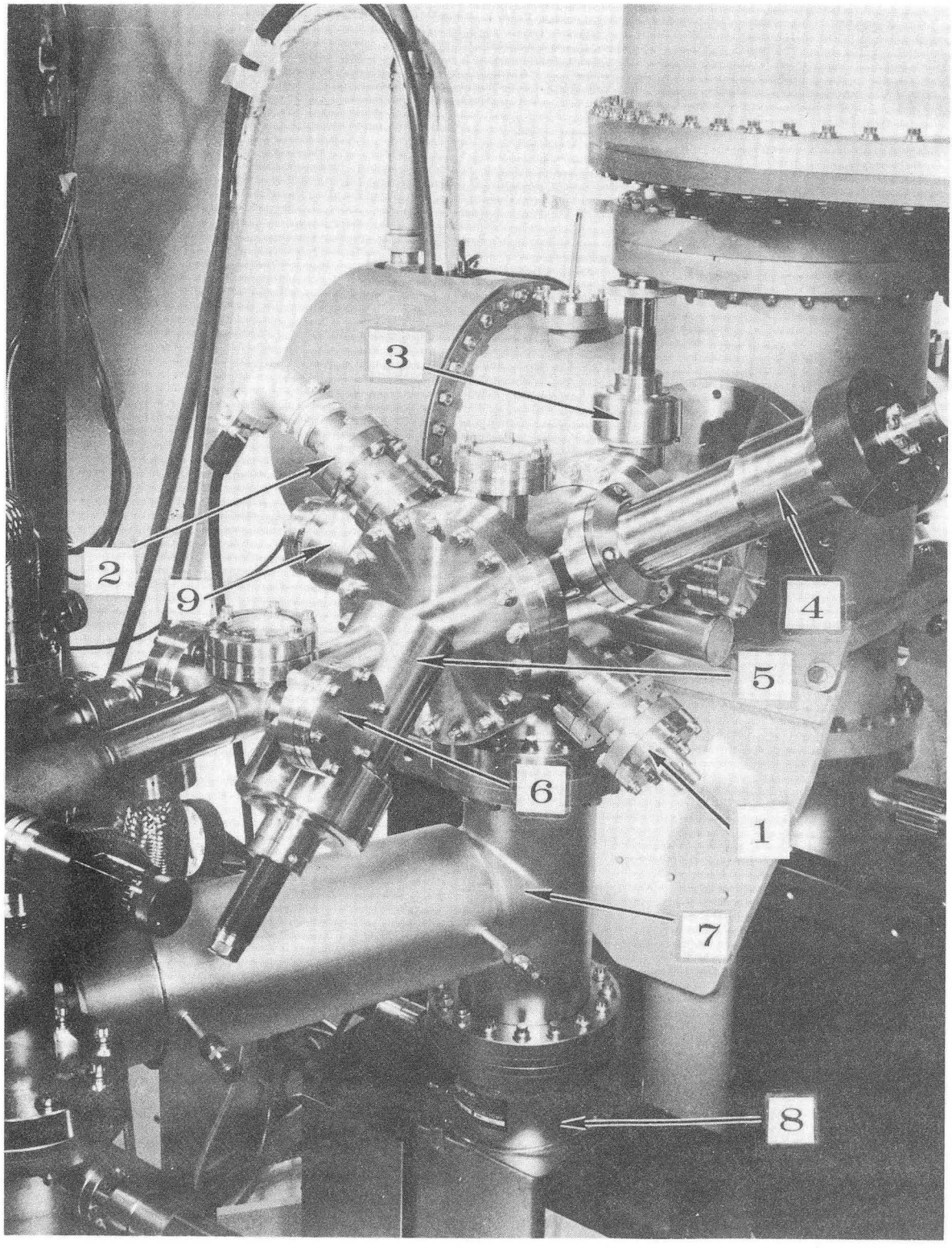

XBB 7210-5120A

Fig. 8. Modified HP 5950A sample preparation and introduction chambers. 1) electron bombardment heater (Physical Electronics); 2) argon ion gun (Physical Electronics); 3) conductance barrier; 4) sample preparation manipulator; 5) straight-through valve (Cal Physics); 6) sample introduction port; 7) 350 l/s titanium sublimation pump (Varian); 8) 60 l/s triode ion pump; (Varian); 9) Bayard-Alpert ion gauge.

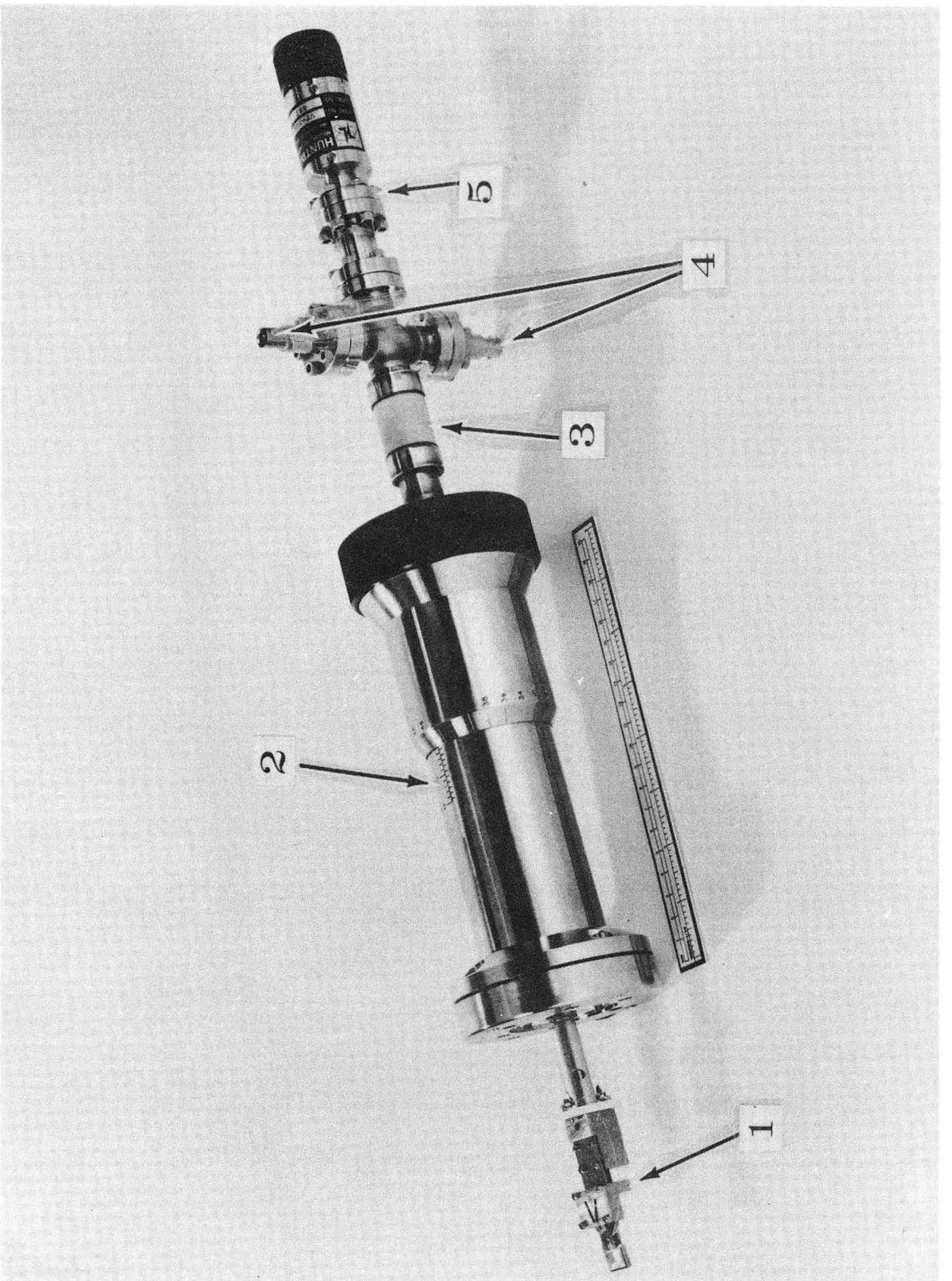

Fig. 9. Sample preparation manipulator. 1) scissor device for grabbing sample platens; 2) linear drive mechanism; 3) 10 KV insulator; 4) connectors to Pt-Pt (10% Rh) thermocouple; 5) rotary feedthrough that drives scissor device which spreads or closes pins that grab sample platen.

(XBB 7210-5318A)

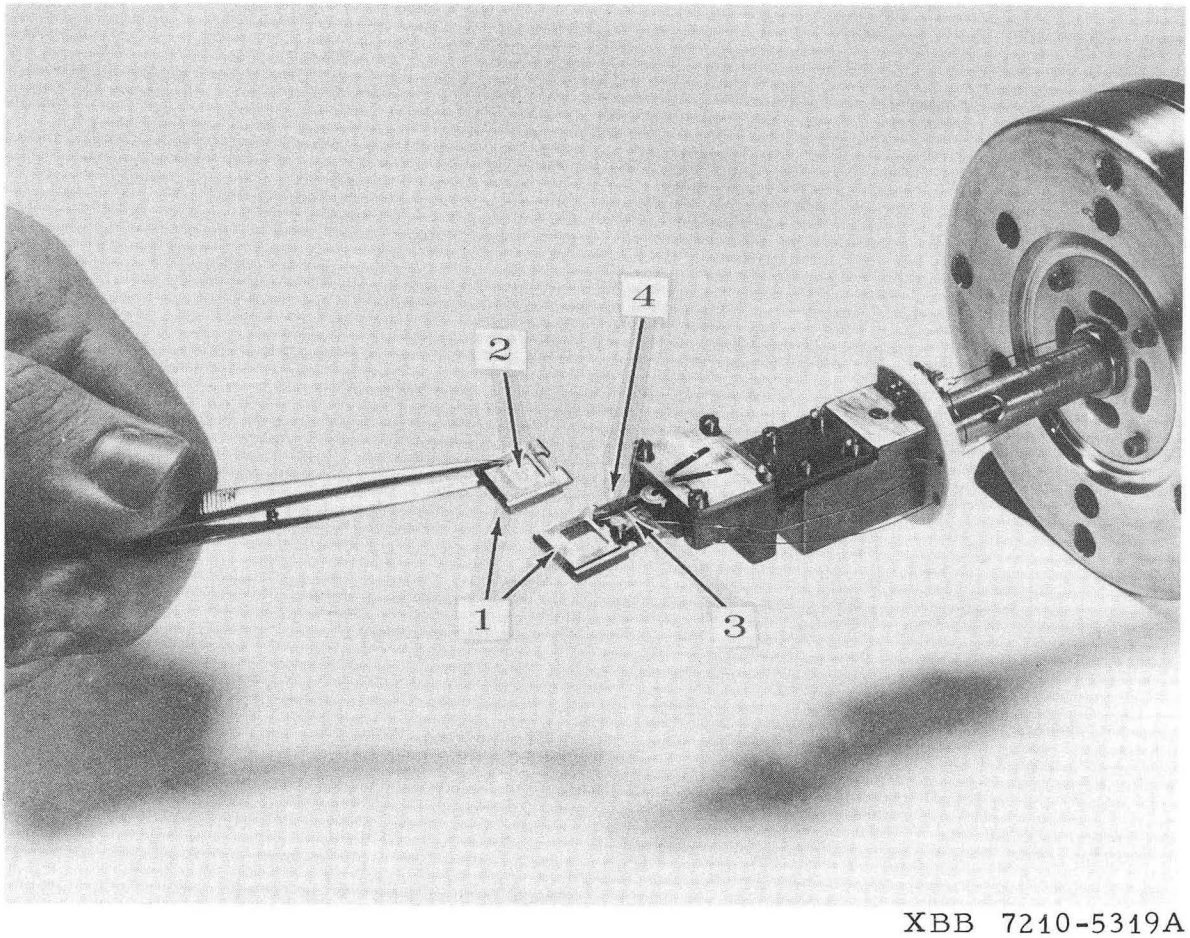

XBB 7210-5319A

Fig. 10. Sample preparation manipulator. 1) sample platens; 2) mounted sample; 3) Pt-Pt (10% Rh) thermocouple; 4) scissor arms with pins engaged in slot of platen.

SECTION IV. THE EVOLUTION OF CORE STATES FROM ENERGY BANDS IN THE $4d5s5p$ REGION FROM Pd TO Xe*

Abstract

X-ray photoemission studies were carried out on high-purity specimens of the $4d5s5p$ elements Pd through Te using monochromatized Al ($K\alpha$) radiation. With increasing atomic number the $4d$ structure evolves from d bands to spin-orbit split atomic-like core levels. Band-structure broadening was detectable in Cd, for which the $4d$ doublet is 11 eV below the Fermi energy. Structure was observed in the $5s5p$ bands for the first time by this method. The cohesive energy was attributed to the $5p$ bands in In through Sb. The two-component $5p$ peak in Te is interpreted as a bonding valence band at 4.0 eV and a non-bonding band at 1.2 eV.

— — —

Most discussions of band structure in metals are predicated on the assumption that the tightly-bound electrons can be regarded as belonging to separate ion cores, while those that are more loosely bound occupy valence bands. In passing beyond the end of a transition series one would expect the d bands to become narrower, fall below the Fermi energy E_F, and evolve into core levels. It is not always clear, however, just which atomic levels can be safely treated as core states and which ones must be explicitly included as part of the band structure. In this paper we report x-ray photoelectron spectroscopy (XPS)[1] experiments addressed to this question for the $4d5s5p$ elements Pd ($Z=46$) through I ($Z=53$). By following the $4d_{3/2} - 4d_{5/2}$ spin-orbit splitting from I down through Cd to Ag one can unambiguously trace the onset of band-structure broadening.

---

*Section IV was published in Phys. Rev. Letters 29, 274 (1972) in co-authorship with S. Kowalczyk, L. Ley, and D. A. Shirley.

We also report the first observation by XPS of structure in the sp bands. This structure exhibits systematic changes between Cd and Te.

The specimens studied were high-purity single crystals in each case except Sb and I, for which polycrystalline samples were used. All the specimens except I were studied in a Hewlett Packard 5950A spectrometer with a monochromatic Al(Kα) x-ray source. The working pressure was always less than 5×10^{-9} Torr. Iodine was examined in the Berkeley iron-free spectrometer. Standard metallographic methods were used to produce clean surfaces. The typical procedure consisted of spark-cutting discs from single crystal rods, mechanically polishing, and finally electropolishing just prior to insertion into the vacuum chamber. Surface purity was monitored in situ and the sample was repeatedly argon etched until all impurity XPS lines were eliminated. This typically required 15 minutes of bombardment with a 10 μA beam of 900 V Ar^+ ions. Oxygen 1s and carbon 1s spectra taken after each valence-band measurement indicate that there was no oxygen build-up. A carbon layer corresponding to 1/10 the intensity of the carbon 1s line of graphite accumulated on the surface after 10 hrs.

Valence-band spectra are displayed in Fig. 1 and derived parameters are set out in Table 1. The position of the Fermi energy E_F in these spectra is known to ± 0.09 eV relative to the Fermi edge of Au, which was measured together with each sample.

In the spectra of Pd, Ag, Cd, In, and Sn, E_F appears to fall at an energy where the density of states is rather large, and the maximum slope of the leading edge is consistent with the resolution of the instrument. For each of these cases the observed slope can be obtained by folding a Fermi distribution function with a Gaussian instrumental response function

of 0.55 ± 0.02 eV FWHM. For Sb and Te there is no visible leading edge at E_F.

Doublet structure in the 4d shell is evident from Ag through I. The energy splitting ΔE between the two components of the doublet is plotted in Fig. 2a. Also plotted is a theoretical splitting which was estimated by normalizing orbital energy differences taken from free-atom relativistic Hartree-Fock-Slater calculations[2] to ΔE(Sb). That the free-atom values of spin-orbit splitting are appropriate in metals is confirmed by the good agreement of this normalized curve with the experimental splitting in gaseous xenon,[3] also shown in Fig. 2a. The free-atom values are lowered 0.1 eV by this normalization. The trend from Sn to I is in excellent agreement with the theoretical curve. The intensity ratio of the two components is in each case close to 1.3, in only fair agreement with the value 1.5 expected for a $d_{3/2}$, $d_{5/2}$ doublet on the basis of multiplicity alone. For the heavier elements Sn to I the 4d electrons can be assigned to the ion cores with confidence. The splitting in indium may be just slightly larger than the free-atom spin-orbit splitting. For Cd the experimental splitting ΔE = 0.99 eV greatly exceeds the predicted spin-orbit splitting of 0.73 eV, and is in fact even larger than the observed splitting in indium. We conclude that band structure affects the 4d shell in Cd, at 11 eV below E_F, and is perhaps perceptible even for the 4d shell of In at E_F - 17 eV.

The spin-orbit splitting energy ΔE is a uniquely reliable parameter for detecting the onset of lattice effects because it is independent of component linewidth, which can be affected by lifetime broadening. Nevertheless, the total "4d bandwidth" can also be used to study broadening by

the lattice. In Fig. 2b the 4d bandwidth (FWHM) is plotted against Z. The bandwidth drops monotonically with increasing Z across the 4d transition series from 6 eV in Mo (not shown) to 3.4 eV in Ag, going through a minimum in In and increasing thereafter because of spin-orbit splitting. The width in Cd is greater than in In, showing again that band structure effects are present in Cd metal.

In the past, XPS studies of valence bands in transition-series metals have yielded little information about s and p bands.[1,4,5,6] This was a consequence of their small cross section for photoemission, the presence of $K\alpha_{1,2}$ lines, and bremsstrahlung in the exciting radiation. With these unwanted components removed by monochromatization it was possible to observe for the first time a considerable amount of structure in the 5s5p bands of Cd, In, Sn, Sb, and Te. A detailed analysis of the spectra must await more intensive measurements and further density of states calculations, but the systematic variation of the 5s5p spectra from Cd to Te (Fig. 1) suggests a preliminary interpretation in terms of a transition from band structure to atomic core-level character for the 5s band with a simultaneous filling of the 5p band. Three systematic effects occur between Cd and Te. First, the s-p valence band which shows structure even in Cd resolves into two peaks in Sn and Sb and three in Te. Second, the higher binding-energy peak which we designate as 5s, falls monotonically below E_F as Z increases. We designate the lower binding-energy bands in In, Sn, Sb, and Te as 5p. Finally, the experimental area ratio (5s/5p) in In to Te agrees well with the occupation number ratio (n/m) for the respective free-atom ground state configurations $5s^n5p^m$ (Table 1).

We interpret this behavior in terms of the evolution of core-like 5s and 5p shells. Figure 2c illustrates the approach of the 5s and 5p bands toward the core s and p levels of Xe. The bars in Fig. 2c represent the widths (FWHM) of the 5s and 5p bands. In Cd through Te all bands are considerably broader than the corresponding levels in Xe. It should also be noted that the 5p splitting in Te is dominated by band structure effects, yielding a splitting much larger (2.9 eV) than the spin-orbit splitting in Xe (1.3 eV). Thus the systematic trend toward core-like levels aids assignment of the peaks, although solid-state interactions are clearly present in Cd to Te.

Further analysis of the 4d, 5s, and 5p peak positions permits us to attribute the cohesive energy to the 5p orbitals. Examination of the peak positions in Cd through Te shows that the 5s and 5p binding energies are nearer the 4d binding energies than are the corresponding free-atom orbital energies from Hartree-Fock-Slater estimates. We ascribe this discrepancy in part to the cohesive energy of the solid and in part to relaxation of the passive orbitals during photoemission. Valence-shell relaxation energies are usually much smaller than those of more tightly-bound levels.[7] Assuming this to be true for these elements, we may calculate the d-shell relaxation shift Δ according to

$$\Delta = [E_c + n(E_{5s} - \eta_{5s}) + m(E_{5p} - \eta_{5p})]/(n + m) \quad .$$

Here E_c is the cohesive energy as taken from Refs. 8 and 9, $\eta_{5s,5p} = \varepsilon(5s, 5p) - \varepsilon(4d)$ is the difference between the s or p orbital energy and the

4d orbital energy in the free atom, $E_{5s,5p} = E_B(4d) - E_B(5s,5p)$ is the corresponding measured binding-energy difference in the solid, and n and m are the numbers of 5s and 5p electrons. Figure 3 shows the results of these simple calculations. The relaxation energies range from 1.1 eV to 2.0 eV for the elements In to Te. The values of Δ show very good agreement with expectations. A theoretical estimate of the magnitude of Δ for iodine may be obtained by comparing the orbital- and binding-energy estimates for the 4d, 5s, and 5p levels as given by Rosen and Lindgren[10] (their Methods "A" and "B"). The result, $\Delta(I) = 2.4$ eV, agrees quite well with our values.

An important result of this analysis is that the cohesive energy is almost entirely accounted for by the 5p electrons. In Te there are two 5p peaks of equal area at binding energies of 1.1 eV and 4.0 eV relative to E_F. The higher binding energy band alone accounts for most of the cohesive energy, and it is also wider than the 1.1 eV band. These observations strongly support the model for group-VI elements in two-fold coordination as discussed by Kastner.[11] In the chalcogens the valence band is formed by unshared-electron states in contrast to the tetrahedral semiconductors in which the bonding band forms the valence band and the antibonding band forms the conduction band. We assign the 4.0 eV peak in tellurium as the bonding band and the 1.1 eV peak as the unshared or lone-pair band.

We thank Professor G. Somorjai for giving us single crystal Ag, In, and Sn.

REFERENCES

1. C. S. Fadley and D. A. Shirley, Phys. Rev. Letters 21, 980 (1968).

2. T. A. Carlson, C. C. Lu, T. C. Tucker, C. W. Nestor, and F. B. Malik, Oak Ridge National Laboratory Report ORNL-4614 (1970).

3. K. Siegbahn, C. Nordling, G. Johansson, J. Hedman, P. F. Hedén, K. Hamrin, U. Gelius, T. Bergmark, L. O. Werme, R. Manne, and Y. Baer, ESCA-Applied to Free Molecules (North-Holland Publishing Co., Amsterdam, 1969).

4. G. Broden, S. B. M. Hagström, and C. Norris, Phys. Rev. Letters 24, 1173 (1971).

5. C. S. Fadley and D. A. Shirley, J. Res. Nat. Bur. Stand. 74A, 543 (1970).

6. Y. Baer, P. F. Hedén, J. Hedman, M. Klasson, C. Nordling, and K. Siegbahn, Physica Scripta 1, 55 (1970).

7. L. Hedin and A. Johansson, J. Phys. B 2, 1336 (1969).

8. K. S. Pitzer and L. Brewer, Thermodynamics (New York, 1961) p. 669 ff.

9. C. A. Wert and R. M. Thompson, Physics of Solids (New York, 1964) p. 184.

10. A. Rosen and I. Lindgren, Phys. Rev. 176, 114 (1968).

11. M. Kastner, Phys. Rev. Letters 28, 355 (1972).

Table 1. Summary of experimental data.

	Ag	Cd	In	Sn	Sb	Te	I	Xe
Binding energy $4d_{3/2}$ (eV)	--	11.46(9)[a]	17.64(9)	24.76(9)	33.44(9)	41.80(9)	--	--
Binding energy $4d_{5/2}$ (eV)	--	10.47(9)	16.74(9)	23.68(9)	32.14(9)	40.31(9)	--	--
FWHM $4d_{3/2}$ = FWHM $4d_{5/2}$	--	0.81(18)	0.78(15)	0.83(8)	0.76(18)	0.94(2)	--	--
4d Splitting (eV)	1.6(1)	0.990(46)	0.899(10)	1.075(34)	1.254(42)	1.51(1)	1.76(16)	1.97[b]
HFS free atom 4d splittings normalized to Sb	0.59	0.73	0.88	1.06	1.25	1.48	1.72	1.98
Binding energy 5s (eV)	--	2.2(5)	4.1(4)	7.0(5)	9.1(2)	11.5(2)	--	--
FWHM 5s (eV)	--	5.0(7)	4.0(5)	5.8(5)	4.0(5)	5.3(5)	--	--
Binding energy 5p (eV)	--	--	0.75(13)	1.25(27)	2.35(25)	4.0(2) 1.13(5)	--	--
FWHM 5p (eV)	--	--	2.0(2)	3.5(5)	3.9(2)	2.3(2) 2.1(2)	--	--
4s/4p rel. areas	--	--	1.85	0.7	0.63	0.5	--	--
n/m	--	--	2.00	1	0.66	0.5	--	--

[a]Errors in last place given in parenthesis.

[b]Ref. 3.

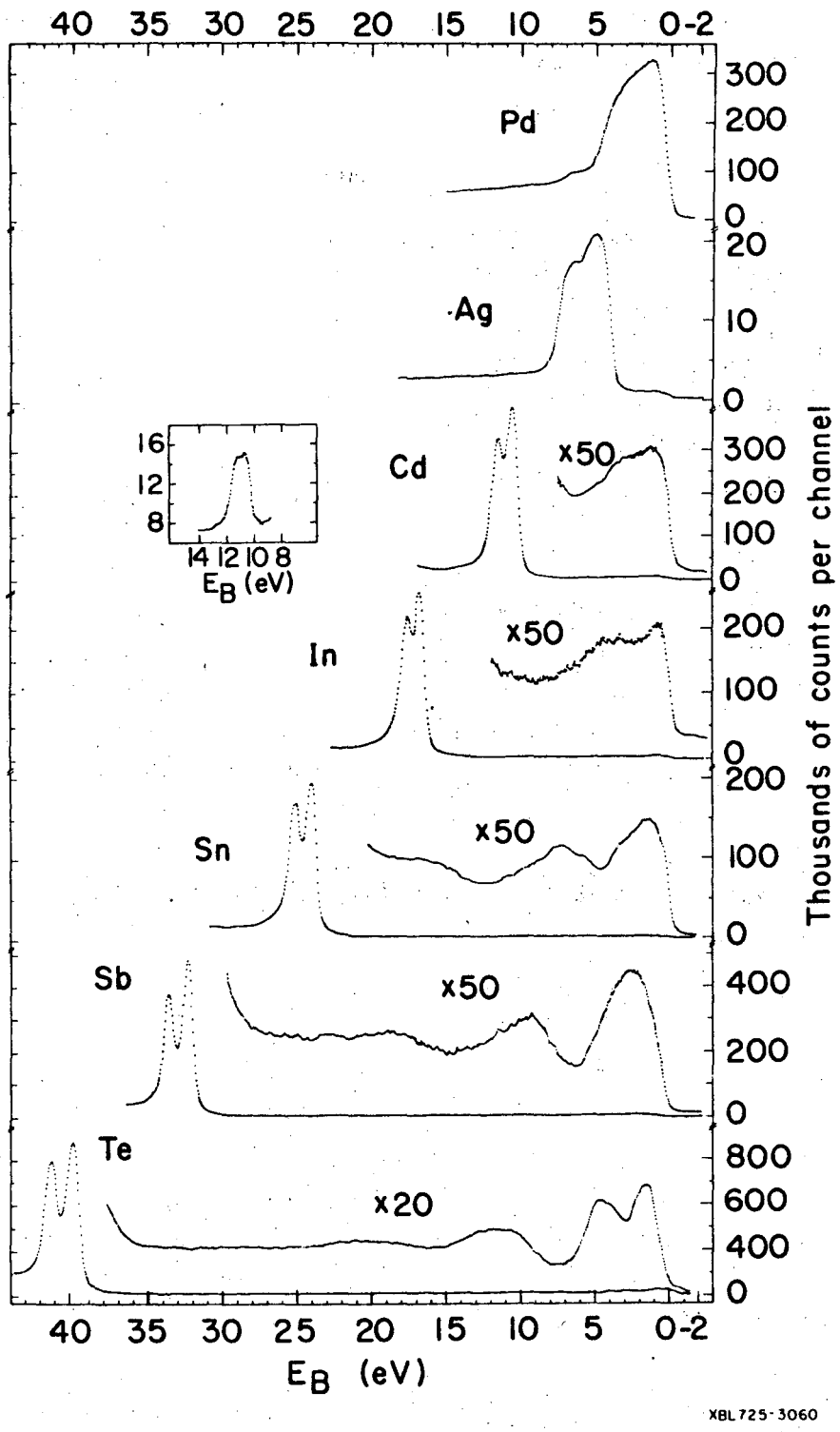

Fig. 1. X-ray photoelectron spectra of the valence-band region for Pd through Te.

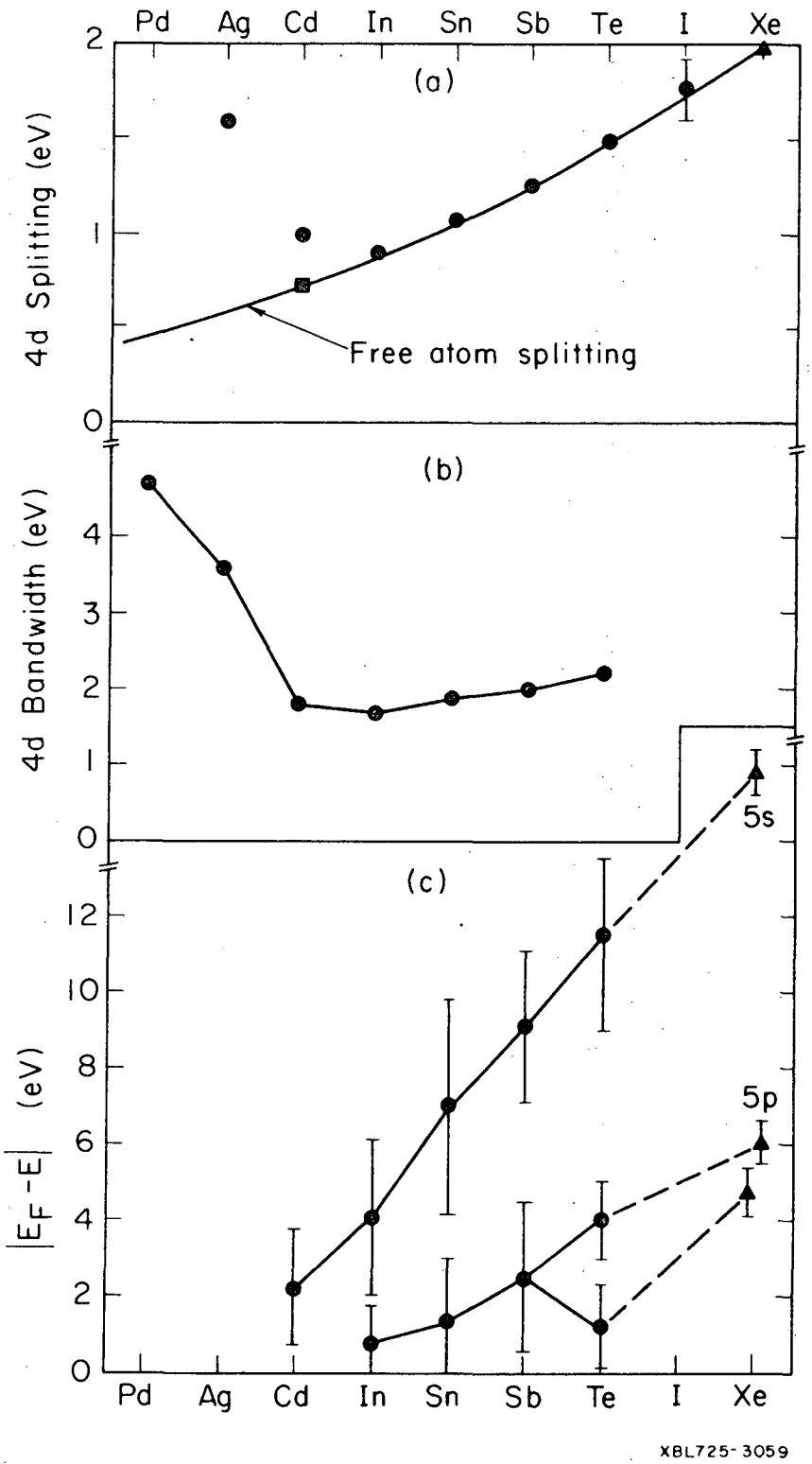

Fig. 2. a) Comparison of the experimental 4d level splitting with free atom HFS calculations[2] ; the Cd-point ■ refers to the experimental value for Cd atoms sputtered onto a Au (111) surface. b) The experimental 4d-bandwidths. c) Positions of the 5s- and 5p-bands relative to the Fermi level; the vertical bars represent the bandwidths at half maximum. The Xe-values in a) and c) are taken from Ref. 3.

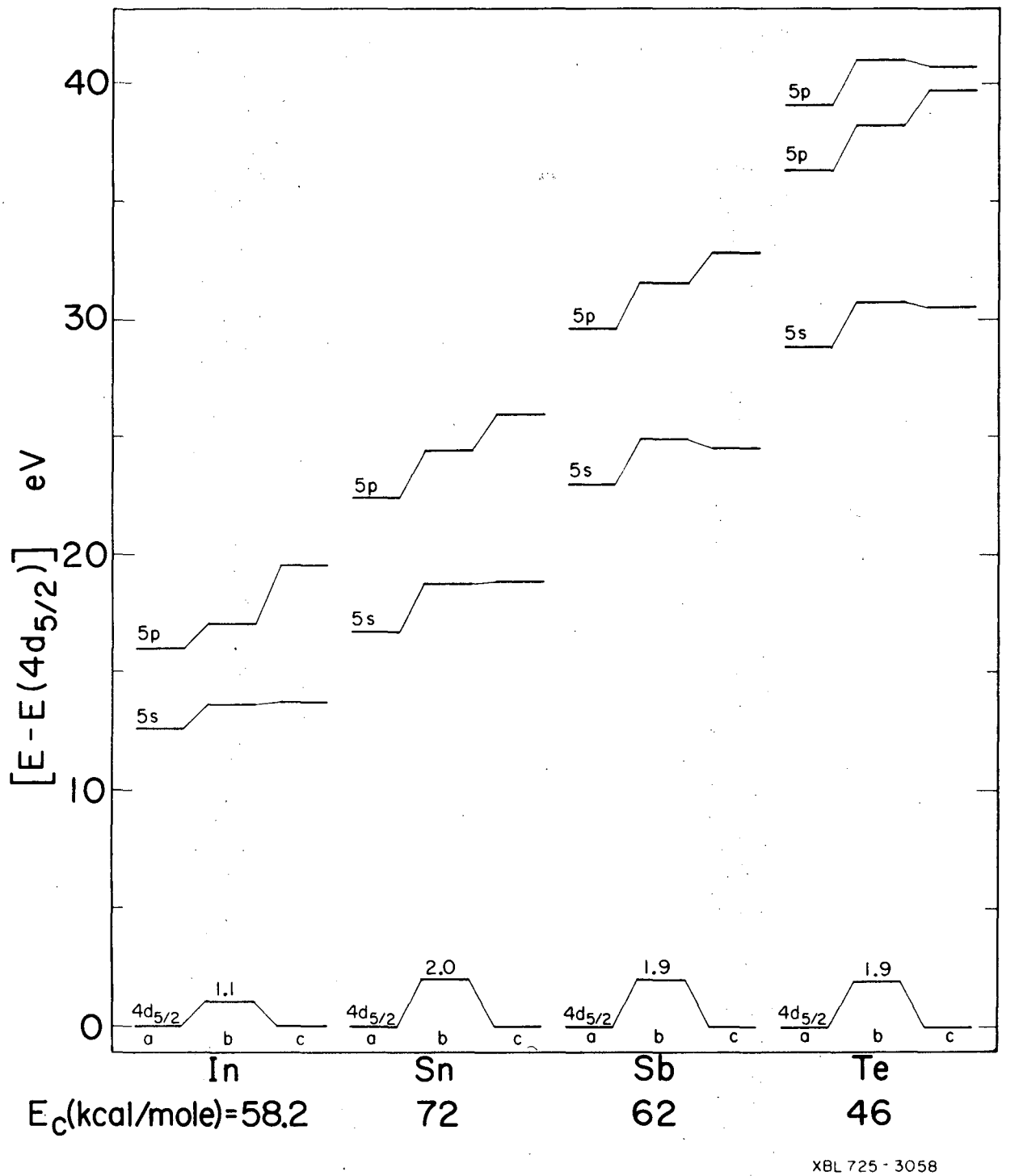

Fig. 3. The 5s- and 5p-band contributions to the cohesive energy E_c of the metals In through Te. a) Experimental values. b) Experimental values shifted by the 4d relaxation energy Δ given by equation (1). c) Free atom HFS values (Ref. 2).

SECTION V. HIGH-RESOLUTION XPS SPECTRA OF Ir, Pt, AND Au VALENCE BANDS*

Abstract

Structural features in the valence-band XPS spectra vary from Ir (Z = 77) to Au (Z = 79) as expected on the basis of 5d6s band filling.

— — —

X-ray photoelectron spectroscopy (XPS) spectra (hereafter denoted by I(E)) of the valence bands of several sixth-row elements have been reported earlier.[1,2] Those spectra were obtained from heated metal foils at resolutions of $\sim$ 1 eV, in the presence of hydrogen gas. Although trends in I(E) for the fcc-metals Ir, Pt, and Au were suggestive of band filling, detailed interpretation was precluded both by experimental limitations and by a lack of appropriate theoretical densities of states, $\rho(E)$, with which to compare I(E). Several relativistic $\rho(E)$ calculations on Au have recently become available. Two of them[3,4] compare very well with the high-resolution ($\sim$ 0.6 eV) XPS spectrum of Au.[5] In this paper we report the results of a high-resolution study of I(E) for Ir, Pt, and Au that confirms the band-filling model for these elements.

The experimental procedures have been described in Sec. IV. Briefly, high-purity single crystals were spark-cut, mechanically polished, electropolished, and introduced into a sample-preparation chamber at 2×10^{-7} Torr. They were then argon-ion bombarded (10 μA, 1000 eV) at 8×10^{-5} Torr of argon and introduced into a Hewlett-Packard HP 5950A ESCA spectrometer at 8×10^{-9} Torr. In-situ monitoring of the carbon 1s and oxygen 1s lines showed these elements to be present in negligible amounts.

*Section V was published in Phys. Letters 41A, 455 (1972) in co-authorship with S. Kowalczyk, L. Ley, and D. A. Shirley.

The raw spectra I(E) are shown in Fig. 1, together with I'(E), the spectra after correction for inelastic scattering. The similarity of I'(E) for these three elements is striking and its variation from Ir to Pt to Au confirms band-structure expectations. To permit discussion of these I'(E) within the framework of theoretical $\rho(E)$ predictions, we have truncated the $\rho(E)$ for Au, as calculated by Connolly and Johnson,[2] to correspond to occupancies of 9 and 10 electrons in the 5d6s bands, thus simulating Ir and Pt, respectively. The results were broadened to simulate the experimental resolution,[1,5] and the energy scales were expanded by 1.35 for Ir and 1.20 for Pt, to roughly match the experimental bandwidths. The resulting very approximate $\rho(E)$'s are also shown in Fig. 1.

Proceeding from Ir to Pt to Au, the band-filling phenomenon is quite evident. Four features, numbered in Fig. 1, are present in all three cases. These are: (1) A shoulder at 6.8 eV in Ir, 6.1 eV in Pt, and 7.0 eV in Au. (2) A peak at 3.8_5 eV in Ir, 4.3_5 eV in Pt, and 6.1 eV in Au. (3) A minimum at 3.0 eV in Ir, 3.3 eV in Pt, and 5.0 eV in Au. This feature is present in the calculated $\rho(E)$ for Au only if spin-orbit interaction is included. It may be less pronounced in Ir and Pt because for these lighter elements the ratio of lattice interactions to spin-orbit interactions is larger. (4) Another peak component at 1.4_5 eV in Ir, 1.7_5 eV in Pt, and 3.5_5 eV in Au. The quoted energies are known to $\pm$ 0.1 eV.

A fifth feature--a second component of the second peak--appears at 0.8 eV in Pt and at 2.65 eV in Au. This part of $\rho(E)$ is at least partially unoccupied in Ir. The dip between features 4 and 5 is very

shallow, especially in Au. In Au the 5d bands have become filled and dropped below E_F, as expected. The width of the occupied 5d bands as measured between the outermost inflection points of I'(E) decreases systematically from 7.4 eV (Ir) to 7.1 eV (Pt) to 5.4 eV (Au). This is also expected. In auxiliary studies on liquid Hg (Z = 80) we found that the 5d states have assumed the character of a spin-orbit split core doublet, at 7.7 eV and 9.5 eV.

In summary, these high-resolution XPS spectra support the band-filling concept in considerable detail. It would be of interest to compare these I'(E) spectra with $\rho(E)$ results from a systematic theoretical study of these three adjacent isostructural elements.

We thank Professor G. A. Somorjai for providing us with single crystals of Ir, Pt, and Au.

the base pressure (especially in the sample preparation chamber) and each time the sample rod is introduced from atmosphere into the vacuum chamber it carries adsorbed gases with it. We have modified the sample introduction mechanism in order to overcome these limitations.

The modified HP 5950A is shown in Figs. 6 to 10. The new system consists of a sample introduction chamber (4 in Fig. 6), sample preparation chamber (3 in Fig. 6), and sample transport system. The sample preparation chamber is pumped with a 60 l/s Varian Noble Vac-Ion pump (8 in Fig. 8) and Varian 350 l/s Tee type titanium sublimation pump (7 in Fig. 8) and the sample introduction chamber is pumped with a 30 l/s Varian Noble Vac-Ion pump. The sample preparation chamber can be vacuum isolated from the analyzer chamber by a wedge shaped conductance barrier which is operated by a metal bellowed valve actuator (3 in Fig. 8). The sample introduction chamber can be isolated from the sample preparation chamber by a straight-through bakeable valve with copper knife-edge seat (5 in Fig. 8). The sample transport system is totally enclosed in vacuum. A long drive screw is attached to a rotary motion feed through (5 in Fig. 7) and a nut rides along the screw as it is turned. A tube is welded to the nut and a solid rod into which 12 sample positions are milled is welded to the other end of the tube. The center of a gear is drilled out such that the tube slides through the center of the gear. A groove is milled along the length of the tube's outer wall and the gear is keyed to this groove. A worm gear attached to a small rotary motion feedthrough (4 in Fig. 7) turns the gear and thus rotates the rod. The screw drive gives linear motion and the worm drive gives rotation. All seals are metal. The system is a closed system.

This system is designed to allow the study of up to 12 samples each minor bake cycle and several sets of 12 between each major bake cycle. The samples are each placed in a platen mount (1 in Fig. 10), inserted through a 2-3/4" sample introduction chamber port, and placed into one of the 12 sample rod slots. During this operation the sample rod is in its fully retracted position; it is totally enclosed by the sample introduction chamber. The straight-through bakeable valve isolates the rest of the system while the samples are being loaded. The sample introduction chamber is then sealed with a 2-3/4" blank flange and pumped down. The whole spectrometer is then baked at 150° C for 48 hours. The bakeout oven encloses the whole spectrometer. After the base operating pressure is attained the bakeable valve is opened and the sample rod is cranked into the sample preparation chamber where there are facilities for preparing a clean surface. A manipulator (Figs. 9 and 10) removes one sample platen from the sample rod. The sample rod is retracted into the sample introduction chamber and the bakeable valve closed. The sample is then alternately heated with an electron gun from the back and argon bombarded from the front. When the surface is clean and annealed the sample rod is returned to pick up the sample platen from the manipulator. The conductance barrier is opened and the sample is transported into the electron spectrometer analyzer chamber and the XPS spectrum taken. The other samples are processed similarly. The sample rod is then retracted into the sample introduction chamber and the bakeable valve closed. The sample introduction chamber is back-filled with dry N_2 and a new set of samples introduced. Then the chamber is sealed and pumped down. During this cycle only the sample introduction chamber is baked. The vacuum

REFERENCES

1. C. S. Fadley and D. A. Shirley, J. Res. Nat. Bur. Stand. 74A, 543 (1970).

2. Y. Baer, P. F. Hedén, J. Hedman, M. Klasson, C. Nordling, and K. Siegbahn, Physica Scripta 1, 55 (1970).

3. J. W. D. Connolly and K. H. Johnson, MIT Solid State and Molecular Theory Group Report No. 72, p. 19, 1970 (unpublished); and private communication.

4. N. E. Christensen and B. O. Seraphin, Phys. Rev. B4, 3321 (1972).

5. D. A. Shirley, Phys. Rev. B5, 4709 (1972).

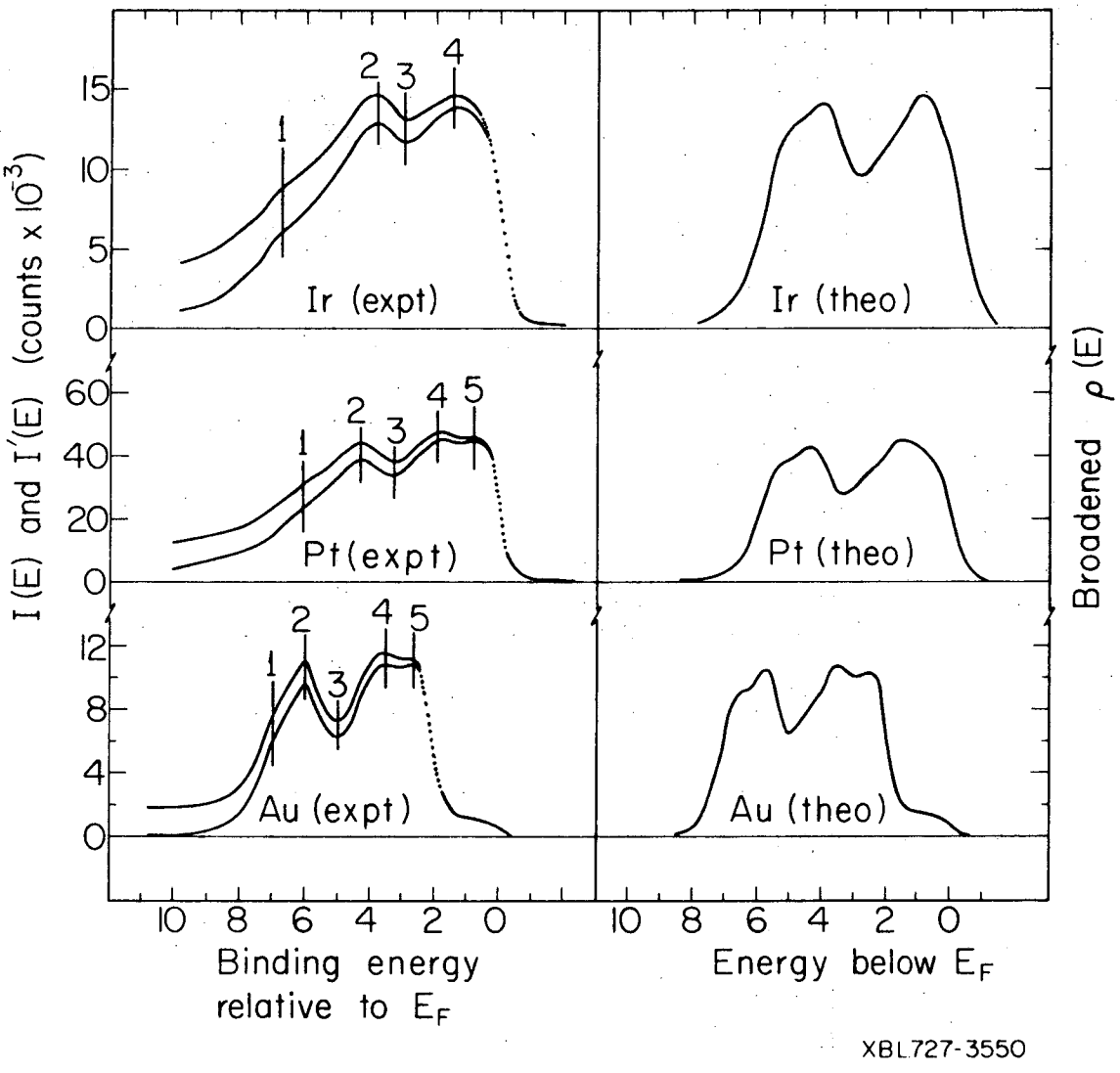

Fig. 1. Left panels and left ordinate: experimental XPS spectra of 5d6s bands of Ir, Pt, and Au. Upper curve in each case shows raw spectrum I(E); lower curve is the corrected spectrum I'(E). Data were all taken digitally. They are shown as points only for the leading edges of the 5d bands, where data density permits. Right panels and right ordinate: Theoretical densities of states obtained by broadening Connolly and Johnson's ρ(E) results. For Ir and Pt this ρ(E) was truncated and the energy scale expanded.

SECTION VI. THE ONSET OF RELATIVISTIC EFFECTS IN THE DENSITY OF STATES OF THE 6s6p ELEMENTS Tl, Pb, AND Bi*

Abstract

Spin-orbit splitting of the 6p band is manifest in the XPS spectra of Pb and Bi. Lowered energies of the 6s band indicate the presence of the mass-velocity and Darwin terms.

— — —

Relativistic effects, e.g. spin-orbit splitting, have to be taken into account in electronic level calculations for even the lightest atoms. For the valence and conduction electrons, however, crystal-field interactions are usually stronger by several orders of magnitude. Therefore spin-orbit splitting may well be treated as a small perturbation in band structure calculations.

This is certainly not the case for the elements Tl, Pb, and Bi, with atomic numbers 81, 82, and 83. Relativistic band structure calculations[1,2,3] show that spin orbit interactions result in band splittings that are comparable to crystal-field splittings. We report in this paper experimental evidence that spin-orbit splitting in the valence p-electrons of Pb and Bi prevails in the presence of crystal-field splitting.

Figure 1a shows the XPS-spectra of the valence region of Tl, Pb, and Bi obtained with monochromatic Al K_α x-rays in a Hewlett-Packard HP 5950A spectrometer. The samples were cleaned by argon-ion bombardment (1000 eV, 10 μA) and were studied at 6×10^{-9} Torr. Other experimental details are described in Sec. III. The valence bands extend to 7 eV

*This section was published in Phys. Letters 41A, 429 (1972) in co-authorship with L. Ley, S. Kowalczyk, and D. A. Shirley.

below E_F in Tl, to about 12 eV in Pb, and to 13.5 eV in Bi. Included in these spectra are the high intensity 5d peaks at energies which are listed in Table 1.

The single broad peak at the bottom of the valence band represents electrons with mainly 6s-like character. The shift of this peak to higher binding energy as one goes from Tl to Bi can be explained by the increasing depth of the atomic potential with increasing atomic number. In Bi the 6s state is already very nearly a core level.

In Tl the p-like electrons are concentrated in one narrow peak near E_F. By contrast, Pb and Bi show two peaks at the top of the valence band which are split apart by 1.8 eV in Pb and 2.2 eV in Bi. The calculated spin-orbit splittings obtained at certain symmetry points in the Brillouin Zone are[4] 0.3 eV for Tl,[1] 1.4 eV for Pb,[2] and 2 eV for Bi.[3] The excellent agreement between these figures and the experimental values strongly supports our interpretation of these bands as being split by spin-orbit interactions rather than by the crystal field. In this connection it is of interest to note (Table 1) that even free-atom HFS-calculations[5] reproduce the 6p-band splitting quite well.

In this discussion we have neglected the differences in crystal structure among these three elements. This is somewhat justified by the fact that the rhombohedral Bi lattice can be regarded as a slightly distorted cubic lattice, as compared with the cubic lattice of Pb. Of course the lattice symmetries were taken into account in the band-structure calculations.[1-3]

Two other relativistic effects--the Darwin and mass-velocity terms--should also be considered. These terms should have the effect of lowering

the energies of the s bands. Comparison of the positions of the s-bands in Tl, Pb, and Bi with those of In, Sn, and Sb[6] shows a relative depression of the s-band energies in the heavier elements. We interpret this as a probable indication of these other relativistic effects. Loucks' relativistic APW calculation on Pb[2] located the 6s band lower relative to the 6p band than did an interpolated OPW calculation of Anderson and Gold.[7] Since the former used a relativistic Hamiltonian, it is probable that part of the difference is a consequence of the 6s bands being lowered somewhat by the Darwin and mass-velocity terms.

A more detailed interpretation awaits density-of-states calculations for these elements.

REFERENCES

1. P. Soven, Phys. Rev. 6A, 1706 (1972).

2. T. L. Loucks, Phys. Rev. Letters 14, 1072 (1965).

3. L. G. Ferriera, J. Phys. Chem. Sol. 28, 1891 (1967).

4. We deduced these splittings from published band-structure work. Theoretical densities of states are not yet available.

5. C. C. Lu, T. A. Carlson, F. B. Malik, T. C. Tucker, and C. W. Nestor, Jr., Atomic Data 3, 1 (1971).

6. R. A. Pollak, S. Kowalczyk, L. Ley, and D. A. Shirley, Phys. Rev. Letters 29, 274 (1972) (and Sec. IV).

7. J. R. Anderson and A. V. Gold, Phys. Rev. 139, A1459 (1965).

Table 1. Valence-band binding energies

	Tl	Pb	Bi
Bind. Energ. $5d_{3/2}$	14.53(5) eV	20.32(5) eV	26.94(7) eV
Bind. Energ. $5d_{5/2}$	12.30(5)	17.70(5)	23.90(7)
d-splitting	2.23(2)	2.62(2)	3.04(2)
Free atom d-splitting (HFS theory, Ref. 5)	2.44	2.83	3.26
6s-band	4.90(25)	7.68(20)	9.95(18)
6p-band	0.80(12)	{2.33(8) 0.53(5)	{3.34(12) 1.18(12)
6p-splitting	--	1.80(5)	2.16(8)
Free atom 6p splitting (HFS theory) Ref. (5)	--	--	2.16

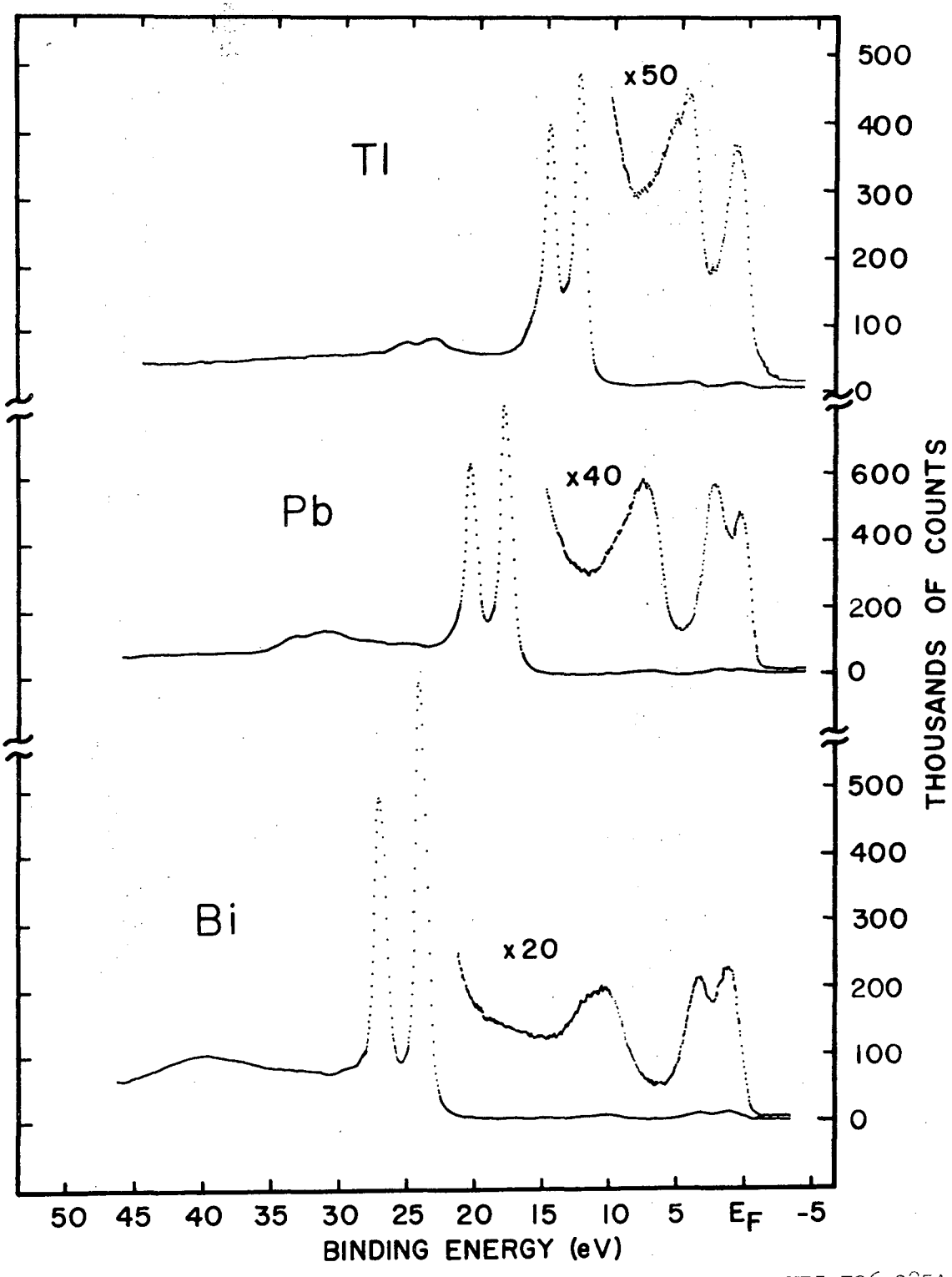

Fig. 1. High-resolution XPS spectra of thallium, lead, and bismuth. The $5d_{3/2}$ - $5d_{5/2}$ doublet is the strongest feature in each spectrum. Characteristic energy-loss maxima appear to the left in each case, with the losses in thallium showing up as two well-resolved peaks. The broad peak to the right of the 5d doublet is the 6s band, and the narrower, spin-orbit split 6p bands fall near the Fermi energy.

SECTION VII. X-RAY PHOTOEMISSION SPECTRA OF CRYSTALLINE AND AMORPHOUS Si AND Ge VALENCE BANDS*

Abstract

The high resolution x-ray photoemission spectra of the total valence bands of crystalline and amorphous silicon and germanium are reported. For the crystals, the XPS spectra yield results that are strikingly similar to current theoretical calculations of the electron density of states, $\rho(E)$. Amorphous Si and Ge exhibit definite band structures that are similar to one another but markedly different from the crystalline results. They agree very well with the theoretical model of Joannopoulos and Cohen.

— — —

Although several density of states calculations have been carried out on silicon[1] and germanium,[2] relatively little experimental information is as yet available concerning the densities of states, $\rho(E)$, of the more tightly-bound valence electrons of these semiconductors. The valence-band densities of states of the crystalline modifications of Si and Ge are of current and continuing interest. In addition, a considerable amount of recent activity has been directed toward elucidating the electronic structure in the amorphous forms. For example, Thorpe and Weaire[3] have discussed three alternative models for the densities of states of amorphous Si and Ge, and Joannopoulos and Cohen[4] have recently given quantitative predictions for $\rho(E)$. In this paper we present the first high-resolution XPS spectra for the densities of states of crystalline and amorphous Si and Ge and compare these spectra with theory.

*This section was published in Phys. Rev. Letters 29, 1088 (1972) in co-authorship with L. Ley, S. Kowalczyk, and D. A. Shirley.

The crystalline samples were cleaved in a dry inert atmosphere from 20 Ω-cm n-type silicon and intrinsic germanium single crystals. The spectra were taken with a Hewlett Packard HP5950A photoelectron spectrometer with monochromatic AlKα x-rays. After cleaving, the samples were introduced into the analyzer vacuum of 8×10^{-9} Torr within 30 seconds. The intensity ratios of the Si(2p) to the contaminant O(1s) and C(1s) lines were 5:1 and 12:1, respectively. No oxygen contamination was detected on the Ge sample, whereas the intensity ratio of Ge(3p) to C(1s) was 10:1. To prepare amorphous specimens, Si and Ge films were evaporated onto clean gold surfaces at room temperature in the spectrometer sample preparation chamber. The background pressure was initially 4×10^{-7} Torr; it rose to 3×10^{-6} Torr for 4 minutes during the evaporations. The films were then directly transferred to the analyzer vacuum of 8×10^{-9} Torr. The only contaminant detected was oxygen on the Si film (Si(2p):O(1s) = 7:1). The raw data for the valence band regions of all four specimens are shown in Fig. 1. The spectra are referenced to the Fermi level E_F of a thin layer of Au evaporated after the valence band measurement onto the semiconductor surfaces. The Au 4f lines are used as a secondary standard, by assuming that their binding energies are the same relative to E_F in the evaporated film and in bulk gold. The densities of states of the semiconductors extend $\sim$ 15 eV below E_F in both Si and Ge. The structure at the foot of the unresolved Ge 3d doublet can be entirely assigned to the first characteristic energy loss structure of the valence-band photoelectrons, as can most of the satellite structure that is found at 17 eV below the valence band peaks in Si. The energy-loss spectra from typical core levels are shown in Fig. 2. To

correct for energy losses, the inelastic loss spectrum was approximated by the sum of a continuous tail with magnitude at each point proportional to the spectrum area at lower binding plus a discrete loss structure constructed by folding a response function determined from the discrete inelastic structure of a sharp core peak and the valence band structure. This correction accounted for the structure at 19 eV in Ge and for 95% of the structure at 23 eV in Si. The remaining 5% is accounted for by the contaminant oxygen 2s peak. A correspondingly small portion of the peak at 6.6 eV can be attributed to the O(2p) line. The corrected valence-band spectra are shown in Fig. 3.

Several band structure calculations have predicted $\rho(E)$ for crystalline Si and Ge. These calculations show very good agreement among themselves. They yield three characteristic peaks in $\rho(E)$. We shall label these peaks according to the symmetry points X_4, L_1, and L_2', in order of increasing binding energy. Of course the peaks do not arise entirely from bands at these symmetry points. This notation is used only for identification. To facilitate comparison with experiment we have plotted for Si and Ge in Fig. 3 both $\rho(E)$ as calculated[1c,2b] and a broadened version that is consistent with the experimental resolution.

The agreement between theoretical and experimental peak positions and shapes is striking for crystalline Si and Ge. Table 1 lists the energies of the characteristic features, the theoretical densities of states $\rho(E)$, and the corrected XPS spectra, which we denote as $I'(E)$. The marginal ability to locate the feature W_2 gives an indication of the resolving power of our spectrometer.

As Table 1 shows, I'(E) provides very strong confirmation of all three theoretical methods for calculating $\rho(E)$. The relative intensities of the p-like X_4 and the s-like $L_1 + L_2'$ peaks in I'(E) vary markedly between Si and Ge and in neither case agree with $\rho(E)$. This is not unexpected, since I'(E) resembles $\rho(E)$ weighted with the photoemission cross section σ. Extrapolating measured 3s/3p and 4s/4p core-level intensity-ratios[8] to the valence electrons of Si and Ge yields

$$[\sigma(3s)/\sigma(3p)]_{Si} : [\sigma(4s)/\sigma(4p)]_{Ge} = 2.3:1 \quad .$$

The observed change in the intensity ratio of the corresponding valence band structures is 2.2:1. Our Si intensities agree well with earlier XPS[5] and Si $L_{2,3}$ (SXS) results.[6]

The excellent agreement observed for crystalline Si and Ge provides a firm basis for further XPS and theoretical band-structure work on semiconductors. It also suggests that these two approaches may profitably be used together.

The results for amorphous Si and Ge are significantly different from the respective crystalline modifications. From the I'(E) spectra (Fig. 3) we note the following observations:

1. The gross variation of intensity with respect to energy is similar for the amorphous and crystalline materials in both elements.

2. The "X_4" peak remains essentially intact from crystalline to amorphous material.

3. The L_1 and L_2' peaks merge into a single broad peak of intermediate energy.

4. I'(E) shows a distinct minimum between the "X_4" peak and the broader peak in the amorphous materials.

5. The centroid of the "X_4" peak shifts toward E_F in each case, by 0.4 eV in Si and 0.5 eV in Ge.

6. The amorphous Ge spectra were in good agreement for samples prepared by evaporation and by Ar^+ ion bombardment (1000 eV, 10 μA for 1 hour).

Observations 1-3 are in agreement with the Si $L_{2,3}$ (SXS) results of Wiech and Zöpf.[6] Observation 2 is expected because X_4 arises from localized p-like bonding orbitals,[7] which are relatively insensitive to long-range order. Observation 6 indicates that I'(E) for amorphous Ge was reproducible even though the method of sample preparation was varied.

Observations 3-5 are the ones that allow a distinction to be made among different theoretical models for amorphous semiconductors.

Thorpe and Weaire[3] have recently discussed three theoretical models for amorphous Si and Ge. The Brust model[9] yields a $\rho(E)$ that resembles a somewhat broadened version of the crystalline $\rho(E)$. Thorpe and Weaire indicated that the Penn model[10] might apply to amorphous semiconductors. The $\rho(E)$ curve for the Penn model shows no minimum, but rather a (broadened) logarithmic divergence near E_F and a free-electron $\rho(E)$ below. Our data exclude both of these shapes for $\rho(E)$, thereby ruling out these two models as being applicable to amorphous Si and Ge. Our spectra definitely require a model that predicts large changes in the s-like L_1 and L_2' peaks but not in the p-like X_4 peak on going from the crystalline to the amorphous state. Thorpe and Weaire described a model that distinguished between the effects of local and long-range interactions. They sketched a curve for $\rho(E)$ that is in good agreement with our amorphous Si and Ge spectra, especially Observations 2-4.

A more quantitative comparison with theory is provided by the recent EPM calculations of Joannopoulos and Cohen[4] on several forms of Ge. Their $\rho(E)$ results for Ge (ST-12), after smoothing to eliminate sharp features associated with long-range order, show very good agreement with our $I'(E)$ curve. They have also calculated Si (ST-12) with similar results. Their $\rho(E)$ curves are shown in Fig. 3. As they pointed out, Ge (ST-12) shows short-range disorder, but the peak near E_F still arises from p-like bonding orbitals. Their model predicts the shift of this peak toward E_F (Observation 5). The crucial feature of the ST-12 structure, according to Joannopoulos and Cohen, is the presence of five- and seven-membered rings. This feature causes the two lower-energy peaks in $I'(E)$ to merge.

In summary, our $I'(E)$ results strongly support the Joannopoulos-Cohen model for amorphous Si and Ge. It appears that future theoretical developments on the band structure of amorphous Si and Ge should be constrained to reproduce the first five observations listed above.

It is a pleasure to acknowledge the generous contributions of Professor Marvin Cohen and Mr. John Joannopoulos to this research.

REFERENCES

1. See for example: (a) E. O. Kane, Phys. Rev. 146, 558 (1966); (b) D. J. Stuckel, T. C. Collins, and R. N. Euwema, Proc. 3rd Int. Mat. Res. Symp., Electronic Density of States, Nat. Bur. Stand. (U.S.), Spec. Pub. 323 (1971); (c) M. L. Cohen, and J. D. Joannopoulos (private communication).
2. See for example: (a) F. Herman, R. L. Kortum, C. D. Kuglin, and J. L. Shay, in Proc. Int. Conf. on II-VI Semiconducting Compounds, Providence, 1967 (W. A. Benjamin, Inc., New York, 1967); (b) M. L. Cohen and J. D. Joannopoulos (private communication); (c) M. Cardona and F. H. Pollak, Phys. Rev. 142, 530 (1966).
3. M. F. Thorpe and D. Weaire, Phys. Rev. Letters 27, 1581 (1971).
4. J. D. Joannopoulos and M. L. Cohen, to be published.
5. D. W. Langer, Z. Naturforschung. 24a, 1555 (1969).
6. G. Wiech and E. Zopf, Proc. Int. Conf. on Band Structure Spectroscopy of Metals and Alloys, Univ. of Strathclyde, Glasgow, Scotland, September, 1971.
7. J. P. Walter and M. L. Cohen, Phys. Rev. B 4, 1877 (1971).
8. K. Siegbahn, C. Nordling, G. Johansson, J. Hedman, P. F. Hedén, K. Hamrin, U. Gelius, T. Bergmark, L. O. Werme, R. Manne, and Y. Baer, ESCA Applied to Free Molecules (North-Holland Publishing Co., Amsterdam, 1969).
9. D. Brust, Phys. Rev. Letters 23, 1232 (1969).
10. D. Penn, Phys. Rev. 128, 2093 (1962).

Table 1. Energies of characteristic features in the valence band spectra of Si and Ge. The theoretical entries are taken from density of states calculations after appropriate broadening.

Crystalline Silicon

	Experiment[a]	Theory[b]	
	I'(E)	EPM M. L. Cohen et al.[1c]	SCOPW Stukel et al.[1a]
X_4	2.2 eV	2.6 eV	2.5
W_2	3.6	4.0	3.1
V[c]	4.4	5.1	4.5
L_1	6.6	7.1	6.9
W_1	7.8	8.2	8.2
L_2'	9.2	10.0	9.6
Γ_1	14.7	13.0	11.8

Crystalline Germanium

	Experiment[a]	Theory[b]		
	I'(E)	EPM M. L. Cohen et al.[2b]	OPW Herman et al.[2a]	SCOPW Stukel et al.[1a]
X_4	2.4 eV	2.3 eV	2.7 eV	2.6
W_2	3.6	3.4	3.8	3.6
V[c]	4.9	4.4	4.9	4.9
L_1	7.2	6.9	7.3	6.8
W_1	8.6	8.5	8.6	7.8
L_2'	10.3	9.7	10.2	9.4
Γ_1	13.0	12.4	12.7	11.7

[a] Positions relative to gold Fermi level.

[b] Positions relative to the top of the valence bands.

[c] The valley between W_2 and L_1 is arbitrarily called V.

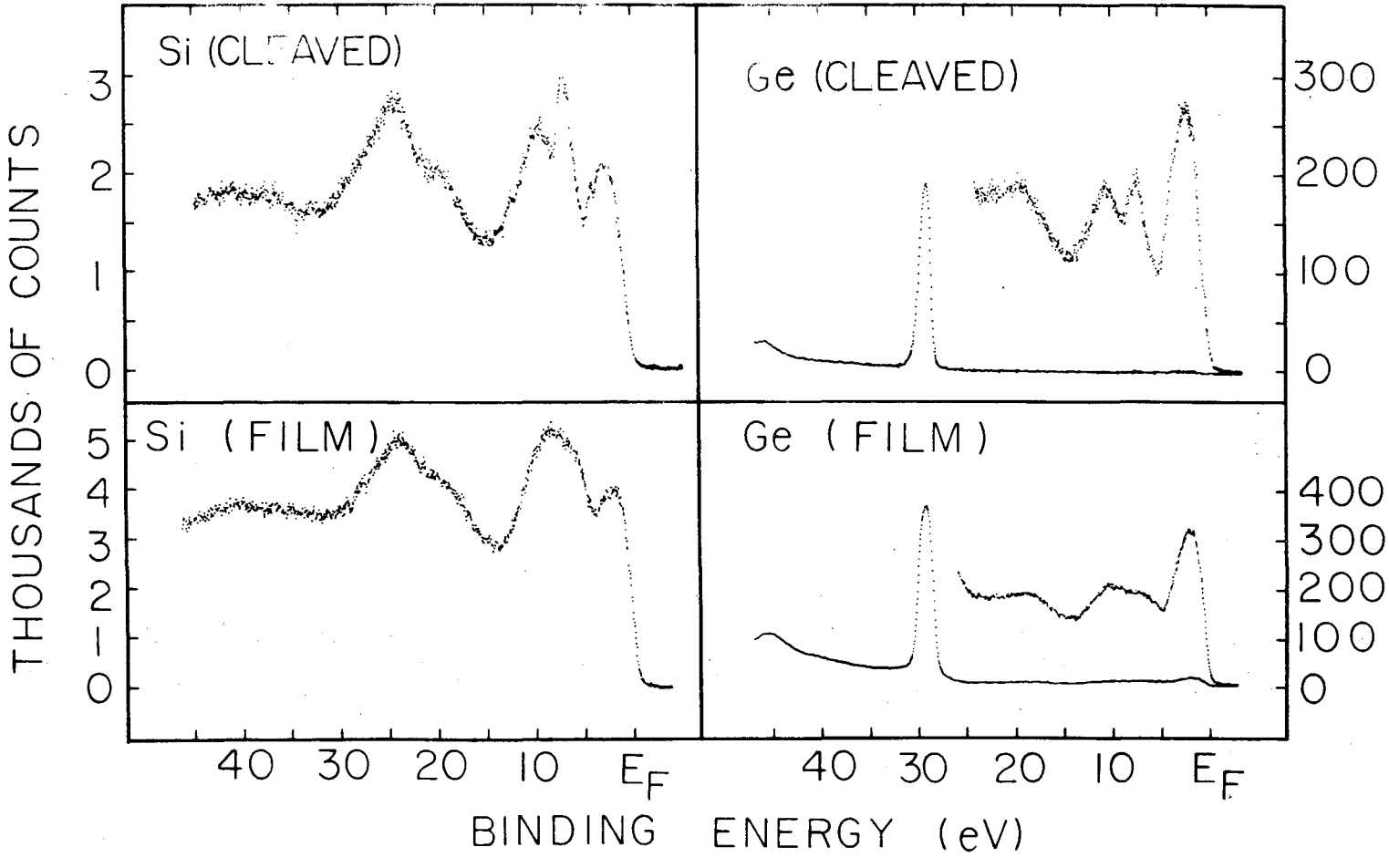

XBL 726-1232

Fig. 1. XPS valence-band spectra of crystalline and amorphous Si and Ge.

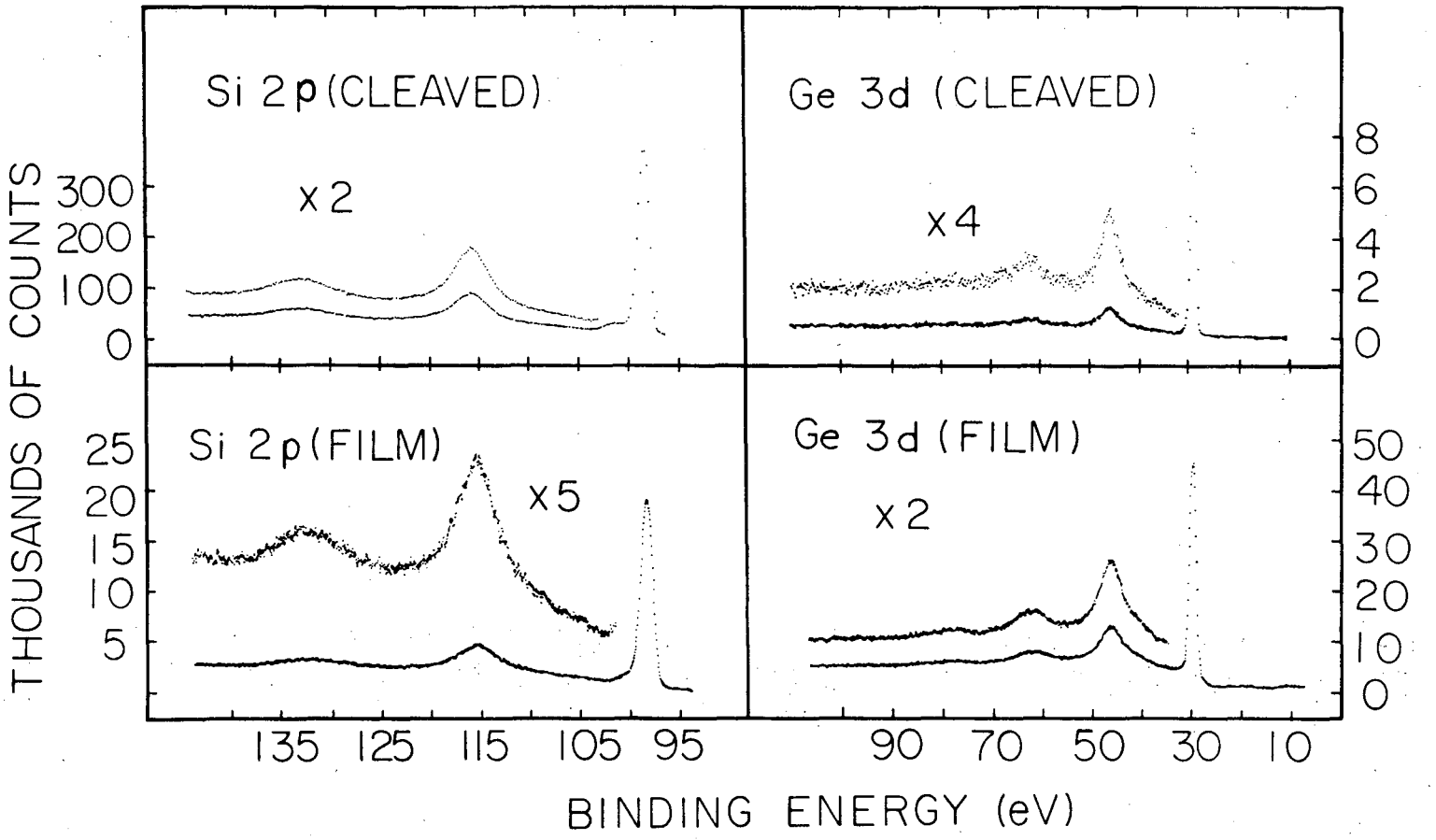

XBL 726-1231

Fig. 2. Si 2p and Ge 3d core levels exhibiting the characteristic energy loss structure (plasmons) used in the valence-band correction procedure.

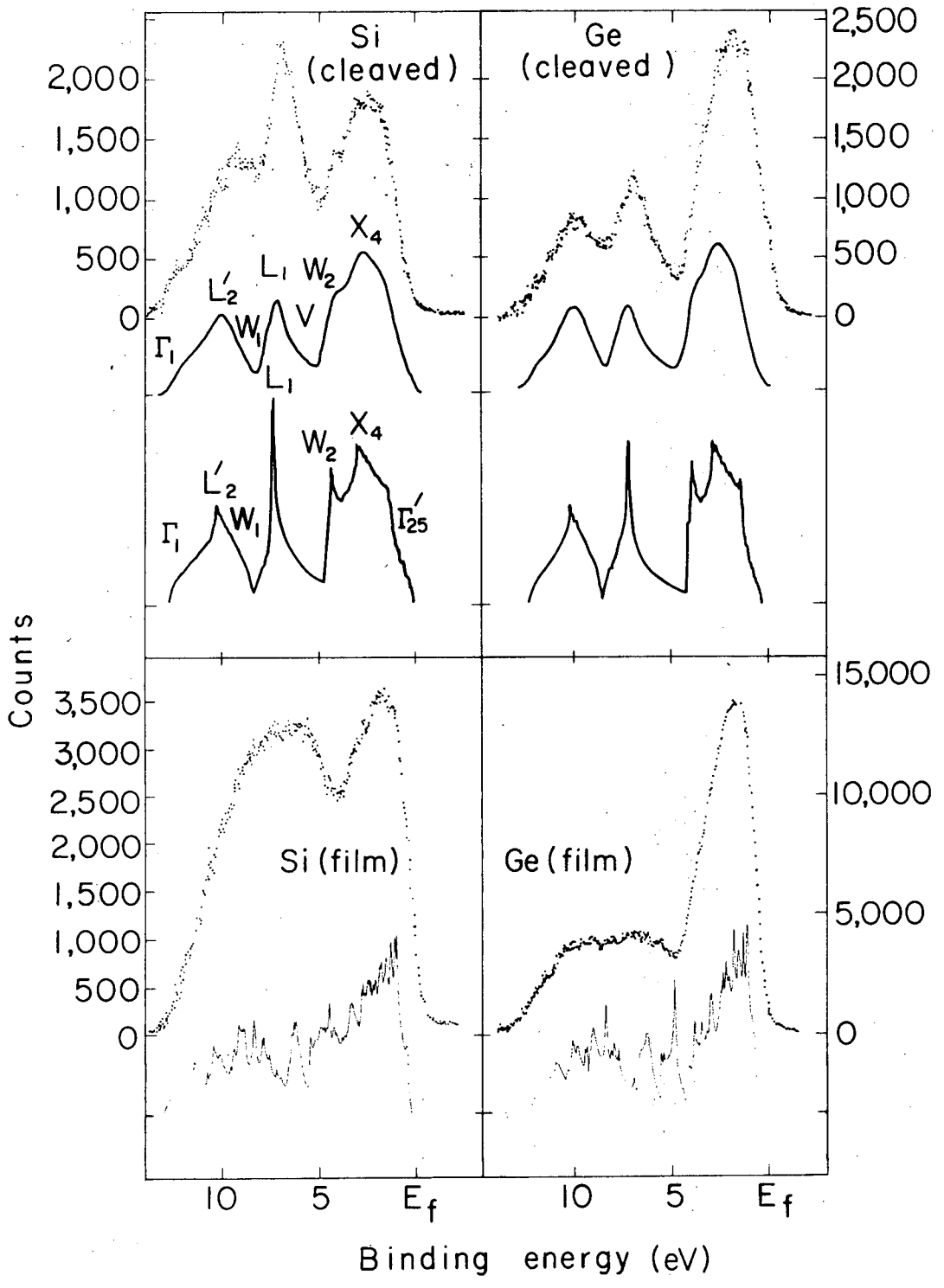

XBL727-3392A

Fig. 3. Corrected spectra I'(E) (point plots) and calculated densities of states ρ(E) (lower curves)[1c,2b,4] for the valence bands of crystalline and amorphous (ST-12) Si and Ge. A broadened ρ(E) is also shown for crystalline Si and Ge (middle curves).

SECTION VIII. X-RAY PHOTOEMISSION VALENCE BAND SPECTRA AND THEORETICAL VALENCE BAND DENSITIES OF STATES FOR Ge, GaAs, AND ZnSe*

Abstract

We report the first high resolution valence-band x-ray photoemission spectra for the isoelectronic series Ge, GaAs, and ZnSe. The results are compared with a theoretical valence-band density-of-states calculation using the empirical pseudopotential method. The agreement between the experimental and theoretical results is quite good, particularly for Ge and GaAs. For ZnSe the x-ray photoemission spectrum shows the Zn 3d-states to be higher in energy than the lowest valence-band s-state. In order to obtain this ordering of states in the theoretical calculation, a pseudopotential with an explicit energy dependence is required.

— — —

Much theoretical and experimental effort has been devoted to the study of the band structures of tetrahedrally coordinated semiconductors because of their numerous applications. Most earlier measurements (optical spectroscopy, transport properties, etc.) have been useful in yielding information concerning electronic properties near the Fermi energy. Only recently have there been any experimental data (e.g. soft x-ray spectroscopy) which yield information about the density of states in regions near the bottom of the valence band.

---

*Section VIII was published in Phys. Rev. Letters 29, 1103 (1972) in co-authorship with L. Ley, S. Kowalczyk, D. A. Shirley, J. D. Joannopoulos, D. J. Chadi, and Marvin L. Cohen.

We report here the first high resolution XPS (X-ray Photoemission Spectroscopy) spectra for all valence bands in the isoelectronic series Ge, GaAs, and ZnSe. These experimental results are compared with theoretical valence band density-of-states calculations using the EPM[1] (Empirical Pseudopotential Method). Since the lattice constants and ion cores are essentially constant for the series, the band spacings are used to obtain information about the increasing ionicity from purely covalent Ge to the more ionic ZnSe. The experimental results also yield information about the asymmetric part of the pseudopotential.

High-purity single crystals were cleaved in a dry nitrogen atmosphere immediately before insertion into the spectrometer vacuum ($\sim 8 \times 10^{-9}$ Torr). The spectra were obtained on an HP 5950A electron spectrometer using monochromatized Al K_α x-rays (1486.6 eV). The possibility of using this method to study the valence band density of states in semiconductors has recently been demonstrated by L. Ley et al.[2] (see Sec. VII) and the experimental resolution of the HP 5950A has been discussed by R. Pollak et al.[3] (see Sec. IV). The spectra were referenced to the Fermi level E_F of a thin layer of Au evaporated onto the semiconductor surfaces after the valence band measurement. The Au 4f lines were used as a secondary standard by assuming that their binding energies are the same relative to E_F in the evaporated film and in bulk gold.

In Fig. 1 are shown the experimental and theoretical densities of states for Ge, GaAs, and ZnSe, and the corresponding theoretical band structures. The theoretical valence-band densities of states were obtained from band-structure calculations for Ge,[4] GaAs,[5] and ZnSe[6] using the EPM. A broadened theoretical density of states is also provided to

facilitate comparison with experiment. The experimental curves have not been corrected for energy losses. This tends to exaggerate the intensities of the peaks at the bottom of the valence-band. In Table 1 we list the energies of the various peaks from the theoretical density of states and from the XPS spectra.

For Ge there is good agreement between theory and experiment in regard to the energy positioning and the widths of the peaks, as was reported earlier.[2] In the XPS spectrum the 3d states of Ge fall at 29.0 eV, 18.7 eV lower than the first peak shown in Fig. 1. In GaAs we again find good agreement between theory and experiment. The first peak on the left in the XPS spectrum (Fig. 1) comes from the 3d states of Ga. The lowest s-like valence band has shifted to a lower energy and has become dissociated from the next peak. This shift to a lower energy occurs because of the localization of electrons in the first band around the strong As potential, and can be related to the antisymmetric form factors. The "antisymmetric gap" (between the lowest s-like valence band and the second valence band) may provide some measure of the ionicities of these compounds. It is surprising that the EPM agrees so well with experiment for this lowest valence band. This does not make any contribution to optical transitions in the 2.8 to 6 eV range, which were used to determine[5] the pseudopotential form factors. Furthermore these states are far from E_F and the energy dependence of the pseudopotential has not been taken explicitly into account.

The largest differences between the experimental and theoretical spectra are found in ZnSe. Here the XPS spectrum shows that the Zn 3d-states lie higher in energy than the s-like states at the bottom of

the valence band, and the "antisymmetric gap" has become larger. The agreement between theory and experiment is less satisfying than for Ge and GaAs. The widths of the theoretical peaks are smaller than the corresponding experimental widths and the theoretical energy gap between the first two valence bands is larger than the experimental energy gap. It appears that the explicit energy dependence of the pseudopotential form factors cannot be neglected for ZnSe. It is interesting to note that the introduction of an explicit energy dependence[7] to lowest order, by using an effective mass, gives better agreement with experiment for the two peaks at the top of the valence band but leaves the antisymmetric gap almost unchanged. OPW calculations[8] for several II-VI compounds give band structures and density of states curves very similar to EPM results.

The 3d-states can be included in the EPM by using a non-local d-potential in addition to the usual pseudopotential form factors in the EPM calculation. Band structure calculations using the KKR method for hexagonal II-VI compounds have been carried out by Rössler,[9] who found d-states close in energy to valence bands for some of these compounds. We expect the KKR to give similar results for the II-VI zincblende structure.

This research illustrates the way in which XPS and band-structure calculations can be used together. The EPM calculations provided a framework within which to interpret the XPS spectra. The spectra in turn gave empirical valence-band energies with which to calibrate the EPM results. We are confident that further research combining the two methods will continue to provide valuable information about the electronic structure of crystalline and amorphous semiconductors.

We thank Prof. G. Somorjai for a single crystal of GaAs and Prof. Y. Petroff for a single crystal of ZnSe.

REFERENCES

1. M. L. Cohen and V. Heine, Solid State Physics 24, 37 (1970).

2. L. Ley, S. Kowalczyk, R. Pollak, and D. A. Shirley, Phys. Rev. Letters 29, 1088 (1972).

3. R. Pollak, S. Kowalczyk, L. Ley, and D. A. Shirley, Phys. Rev. Letters 29, 274 (1972).

4. M. L. Cohen and T. K. Bergstresser, Phys. Rev. 141, 789 (1966).

5. R. L. Zucca, J. P. Walter, Y. R. Shen, and M. L. Cohen, Solid State Comm. 8, 627 (1970).

6. J. P. Walter and M. L. Cohen, Phys. Rev. B1, 2661 (1970).

7. J. Chelikowsky, private communication.

8. F. Herman et al., Proceedings of the 1967 Int. Conf. on II-VI Semiconducting Compounds, D. G. Thomas, ed. (Benjamin, New York, 1967), p. 503. F. Herman et al., Aerospace Research Laboratories Report ARL69-0080, May 1969. D. J. Stuckel, T. C. Collins, and R. N. Euwema, Proc. 3rd Int. Mat. Res. Symp., Electronic Density of States, Nat. Bur. Stand. (U.S.), Spec. Publ. 323 (1971). The OPW results for the lowest ZnSe valence band agree better with experiment than the EPM results.

9. U. Rössler, Phys. Rev. 184, 733 (1969).

Table 1. Energies of characteristic features in the valence band spectra of Ge, GaAs, and ZnSe. The theoretical entries are taken from the density of states calculations after appropriate broadening

	Ge		GaAs		ZnSe	
	Expt.†	Theory††	Expt.†	Theory††	Expt.†	Theory††
X_4	2.4 eV	2.4 eV	2.4 eV	2.4 eV	3.0 eV	3.0 eV
W_2	3.6	3.5	3.9	3.4	--	--
V*	4.9	4.5	5.1	4.6	5.2	4.6
L_1	7.2	7.0	6.8	6.5	6.3	5.3
W_1	8.6	8.6	8.9	--	--	--
L_2'	10.3	9.8	11.5	11.2	13.8	15.6
Γ_1	13.0	12.5	13.8	12.9	14.5	16.4

†Positions relative to gold Fermi level.

††The positions are normalized to the experimental values of X_4.

*The valley between W_2 and L_1 is arbitrarily called V.

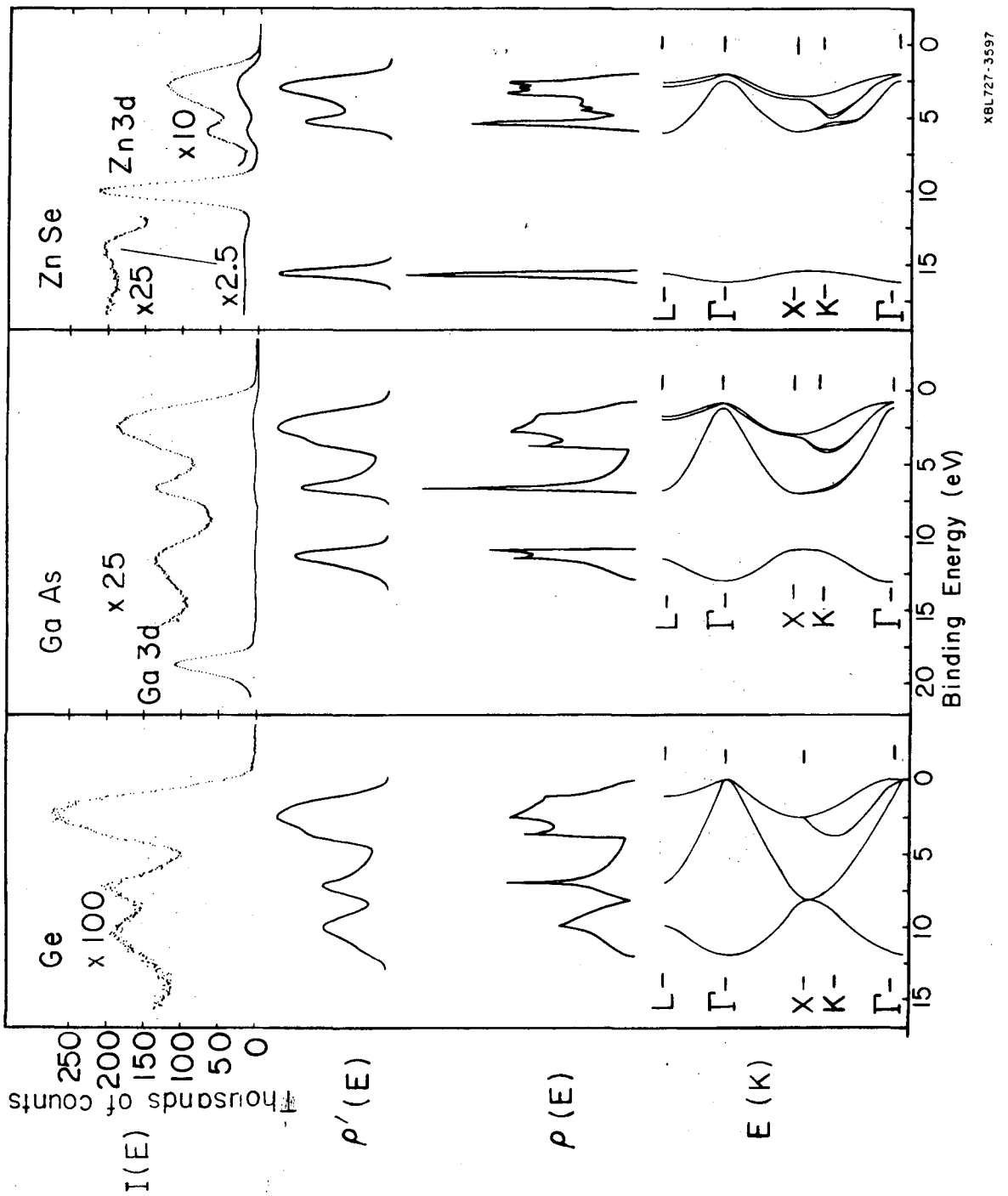

Fig. 1. XPS-spectra, band structures and densities of states for Ge, GaAs, and ZnSe. The top row I(E) shows the uncorrected experimental spectra. At the bottom the corresponding band structures E(k) and densities of states ρ(E) as derived from EPM calculations are shown. The broadened theoretical densities of states ρ'(E) in the second row facilitate comparison with experiment.

SECTION IX. X-RAY PHOTOEMISSION CROSS-SECTION MODULATION IN DIAMOND, SILICON, GERMANIUM, METHANE, SILANE, AND GERMANE*

Abstract

The high-resolution XPS valence-band spectrum from a cleaved natural diamond single crystal is reported. The absence of extrinsic structure allows a reliable comparison with band theory. The XPS molecular-orbital spectra of methane, silane, and germane are also given. The modulation of photoelectric cross sections in the valence bands of diamond, Si, and Ge are discussed and compared with atomic XPS cross sections derived from the spectra of CH_4, SiH_4, and GeH_4.

— — —

The allotropic form of carbon, diamond, is the prototype for Group IV crystals of the diamond structure. Many calculations of the energy-band structure have been carried out,[1] yielding results that vary more widely than is the case for its congeners, silicon, and germanium. Thus, it is especially desirable to determine the positions of the diamond energy bands experimentally. We report the total valence-band density-of-states spectrum of a cleaved single crystal of diamond. The spectrum was obtained using x-ray photoemission spectroscopy (XPS) which has recently been employed to yield total valence-band spectra for silicon and germanium.[2] The diamond spectrum is compared with theory after discussing the relationship between the XPS spectrum $I'(E)$ and the calculated density of states $\rho(E)$. The XPS molecular orbital spectra of CH_4, SiH_4, and GeH_4 are presented and used to derive relative atomic photoelectric cross sections which are compared with peak intensities in the XPS valence spectra of

*Section IX is to be published in co-authorship with R. G. Cavell, S. P. Kowalczyk, L. Ley, B. Mills, D. A. Shirley, and W. Perry.

diamond, Si, and Ge. These intensities are consistent with predictions based on the theoretical orbital symmetries of the valence bands.

A diamond single crystal was cleaved in a dry N_2 atmosphere and introduced directly through a vacuum interlock into the analyzer chamber of an HP 5950A electron spectrometer in which a pressure of 8×10^{-9} Torr was maintained. The crystal was irradiated with monochromatized Al $K\alpha_{1,2}$ radiation. Monochromatization has the effect of improving the resolution in XPS somewhat (the resolution of our instrument is 0.55 eV[3]): a more important advantage is the elimination of unwanted $K\alpha_{3,4}$ and bremmstrahlung radiation.

Since the effective XPS sample depth is only a few atomic layers, the production of a clean surface is essential. Previous XPS studies of diamond[4,5] were done on powdered samples which yielded valence band spectra that were seriously modified by surface contamination (apparently oxygen). The resultant structures were clearly not intrinsic, and no detailed comparisons with band structure theory were possible. In a preliminary experiment on an untreated diamond single crystal, we observed a valence-band spectrum that was similar to the previously reported spectra.[4,5] An indication of the extent of oxygen contamination is given by the intensity ratio for the 1s core peaks, C(1s)/O(1s) = 4. After cleaving the diamond this ratio rose to C(1s)/O(1s) = 13, and the valence-band spectrum showed no evidence of oxygen contamination.

The uncorrected spectra I(E) of the diamond valence band and the diamond C 1s core region are shown in Fig. 1. The satellite structure on the high binding energy side of the C 1s line is assumed to be "extrinsic"; i.e., to be characteristic of the energy losses suffered by an electron

traveling through a diamond lattice, rather than characteristic of the C 1s level itself. Using this assumption we are able to correct the valence-band spectrum quantitatively for inelastic losses. This yields the corrected spectrum I'(E) shown in Fig. 2. As can be seen by comparing Figs. 1 and 2, this correction does not appreciably affect the valence-band structure below 25 eV binding energy and thus any inadequacy of the above assumption will have only minor influence on I'(E).

Direct measurement of binding energy in insulators and semiconductors is not possible because of space-charge effects. A thin layer of gold was evaporated onto the diamond crystal after the valence-band measurements were completed, and the separation of the Au $4f_{7/2}$ and the underlying diamond C 1s line was measured. The binding energy of the Au $4f_{7/2}$ relative to the Fermi edge in gold metal was measured to be 84.00 ± 0.01 eV, which when added to the above separation yields for the diamond C 1s binding energy relative to the Fermi level of a thin surface film of gold, E_B = 284.44 ± 0.07 eV. This agrees fairly well with the value 284.0 ± 0.3 reported by Thomas et al.[4] which was obtained by a similar referencing procedure using platinum.

To a certain point the valence-band spectrum is extremely straightforward. There are three peaks in I'(E) as was the case for Si and Ge,[2] which are also shown in Fig. 2 for comparison. The wider spacing of I'(E) for diamond is consistent with theoretical expectations[1] and is due to the smaller lattice constant in diamond. With two atoms per unit cell and four electrons per atom, diamond has four doubly-occupied valence bands as indicated in Fig. 3. These bands produce three peaks in the density

of states, $\rho(E)$, with the top two bands forming a single peak. Labeling the $I'(E)$ peaks as I, II, and III (Fig. 3), we identify the majority of peak I with band 1, peak II with band 2, and peak three with bands 3 and 4.

The photoemission spectrum $I'(E)$ is essentially a joint density of states. In a one-electron picture we have

$$I'(E) \propto \rho(E)\, \sigma(E,h\nu)\, \rho_e(h\nu - E) \quad .$$

Here $\rho(E)$ is the density of states of the valence bands, $\sigma(E,h\nu)$ the cross-section for photoemission, and $\rho_e(h\nu - E)$ the continuum final state of the photoelectron. This last term can be regarded as constant over the valence-band width ΔE, provided that[6] $h\nu \gg \Delta E$. Thus

$$I'(E) \propto \rho(E)\, \sigma(h\nu,E) \quad ,$$

and a detailed comparison of $I'(E)$ with $\rho(E)$ would require an understanding of the cross-section modulation.

For molecules cross-section modulation is readily understood, and Gelius has given a good discussion.[7] The cross section is proportional to the square of the overlap between the initial one-electron state and the continuum final state of the electron

$$\sigma(h\nu,E) \propto |\langle \psi_i(E) | \chi_f(h\nu - E) \rangle|^2 \quad .$$

Taking $\chi_f(h\nu - E)$ as a plane wave, the de Broglie wavelength of an electron ejected from the valence bands by AlKα radiation is 0.32Å. Thus, the major contributions to $\sigma(h\nu,E)$ must come from those regions in which $\psi_i(E)$ has a curvature corresponding to this wavelength; i.e., the atomic-like regions

near the nucleus. The carbon 2s orbital has a larger cross section for photoemission at this energy than the carbon 2p orbital, because its radial node makes the 2s wavefunctions curvature similar to that of the photoelectron.

Inspection of Fig. 2 and Fig. 3 reveals that cross section modulation is very important in diamond, Si, and Ge. The wavefunctions of the valence electrons are of course eigenfunctions of the linear momentum rather than the angular momentum operator because of the periodicity of the crystal lattice. An expansion into atomic angular momentum eigenfunctions extends therefore in principle over the whole Hilbert space which is orthogonal to the core wavefunctions. It is however true that--especially near the nucleus--the prevailing contributions to this expansion came from the ns and np orbitals, where n is the principal quantum number of the valence electrons in C, Si, and Ge respectively. In this sense band 1 is mostly s-like and bands 3 and 4 are mostly p-like.[8] Band 2 is a mixture of s- and p-like functions. The variation in the peak area ratio (I + II)/III should therefore correspond to a similar variation in the cross-section ratio $\sigma(s)/\sigma(p)$ for the atomic orbitals. This has been noted earlier for Si and Ge (see Sec. VII).[2]

In order to investigate this point more quantitatively we deduced atomic cross section ratios from x-ray photoemission spectra of methane (CH_4), silane (SiH_4), and germane (GeH_4). The latter two were prepared applying the techniques of Refs. 9 and 10. Electron spectra of the valence regions of these simple gaseous compounds were measured in the Berkeley iron-free spectrometer using a $MgK\alpha_{1,2}$ x-ray source. The resulting spectra (see right side of Fig. 3 and Table 1) exhibit in all three cases two peaks

which correspond to the singly degenerate level A_1 (s-like) and the triply degenerate level T_2 (p-like).

An LCAO calculation for the three molecules yields the parentages of the two levels in terms of the atomic s and p orbitals. From these parentages and from the measured line intensities we deduce the ratios of the s and p cross sections for the atomic orbitals as listed in Table 2. These numbers demonstrate the dramatic change in the cross section ratios as one proceeds from C to Ge, thus supporting our arguments on the intensity variation of peaks I, II, and III in the valence-band spectra of the elements. These variations (Table 2) are however much smaller than those of the atomic cross sections. This discrepancy cannot arise from the different energies of the exciting x-rays for the crystals and the molecules. (See Ref. 11.) This still leaves a valid objection against an atomistic LCAO interpretation of the intensity ratios: the electronic wavefunctions of the valence bands of a crystalline solid such as diamond are not well described by LCAO basis functions. Even in the tight binding approach, which means restriction to the atomic valence orbitals in constructing the valence bands, the states which make up $\rho(E)$ are mixtures of the s and p basis functions for every value of E. This mixture alone tends to equalize the cross-section over the valence region. A more realistic approach however would require a rigorous calculation of the valence-band wave-functions and the cross section for photoemission at each energy. It is thus clear that cross-section modulation can shift slightly the apparent positions of characteristic features from $\rho(E)$ to $I'(E)$.

The point Γ marks the center of the Brillouin zone, and bands 2-4 all have p character at this point. Since they all approach Γ'_{25} with

zero slope the density-of-states falls rather sharply at this energy--the top of the valence bands. Thus, in principle, $E(\Gamma'_{25})$ could be determined rather accurately, without ambiguity due to s,p mixing or unfavorable structure in $\rho(E)$. In fact, the right side of Peak III shows some tailing which tends to worsen the accuracy with which $E(\Gamma'_{25})$ can be determined. This small amount of tailing could arise from surface states or instrumental resolution. By extrapolating down from the steepest part of the Peak III, we obtained $E(\Gamma'_{25}) = 1.8 \pm 0.3$ eV relative to $E_F(Au)$ (the Fermi energy provides a convenient reference point, but we shall not discuss it further because its meaning under the experimental conditions of a high x-ray flux is not clear).

The peaks in $I'(E)$ should fall at maxima in $\rho(E)$ with small shifts between the two sets of maxima arising from instrumental broadening of unsymmetrical peaks and from s/p mixing. The former effect is easily corrected for. The latter effect should be small because both Bands 1 and 2 have high s symmetries at the peaks in $I'(E)$. The overall increase of s character with energy below E_F tends to bias $I'(E)$ downward in energy relative to $\rho(E)$. With all these factors considered, we assign the positions of peak I and II as 17.9 ± 0.2 eV and 13.2 ± 0.1 eV below $E_F(Au)$ respectively.

Detailed comparison of XPS valence bands with theory requires theoretical densities of states modulated by XPS cross sections. The upper portion of Fig. 3 compares the calculated density of states for diamond of Painter, Ellis, and Lubinsky[12] (solid line) with our experimental results. They used a discrete variational method in an ab initio approach with an LCAO Bloch basis set which allows inclusion of nonspherical terms

in the potential. The band structure from which $\rho(E)$ was calculated is shown in the lower portion of Fig. 3. The calculated density of states and our experiment show excellent agreement in the positions of all characteristic features. It is therefore possible to deduce the variation of the photoelectric cross section over the valence region, as indicated by the broken line in Fig. 3. This line exhibits the smooth decrease from the bottom of the valence band to its top, as expected from the discussion given above. Thus the relative intensities in photoelectron spectra can provide a valuable tool in exploring the atomic origin of different regions in the valence bands of solids.

REFERENCES

1. Detailed references to the early literature appear in Refs. 4 and 5 below.

2. L. Ley, S. Kowalczyk, R. A. Pollak, and D. A. Shirley, Phys. Rev. Letters 29, 1088 (1972), and Sec. VII.

3. R. A. Pollak, S. Kowalczyk, L. Ley, and D. A. Shirley, Phys. Rev. Letters 29, 274 (1972), and Sec. IV.

4. J. M. Thomas, E. L. Evans, M. Barber, and P. Swift, Trans. Faraday Soc. 67, 1875 (1972).

5. T. Gora, R. Stanley, J. D. Rimstidt, and J. Sharma, Phys. Rev. B 5, 2309 (1972).

6. C. S. Fadley and D. A. Shirley, J. Res. Nat. Bur. Stand. 74A, 543 (1970).

7. U. Gelius, Electron Spectroscopy, ed. by D. A. Shirley (North-Holland Publishing Co., Amsterdam and London, 1972), p. 311

8. J. P. Walter and Marvin L. Cohen, Phys. Rev. B4, 1877 (1971).

9. A. D. Norman, J. R. Webster, and W. L. Jolly, Inorganic Syntheses, ed. by W. L. Jolly, XI, 170 (1968).

10. W. L. Jolly, The Synthesis and Characterization of Inorganic Compounds (Prentice-Hall, Inc., Englewood Cliffs, New Jersey, 1970), p. 496.

11. K. Siegbahn, C. Nordling, G. Johansson, J. Hedman, P. F. Hedén, K. Hamrin, U. Gelius, T. Bergmark, L. O. Werme, R. Manne, and F. Baer, ESCA Applied to Free Molecules (North-Holland Publishing Co., 1969), p. 40.

12. G. S. Painter, D. E. Ellis, and A. R. Lubinsky, Phys. Rev. B4, 3610 (1971).

Table 1. Binding energies E_B and widths (FWHM) of molecular orbitals of methane, silane, and germane. Energies in eV.

Orbital	CH_4	SiH_4	GeH_4
$\underline{A_1}$			
E_B	23.08(4)	18.01(4)	18.46(4)
FWHM	1.71(3)	1.16(6)	1.17(6)
$\underline{T_2}$			
E_B	14.5(2)	12.67(4)	12.28(4)
FWHM	2.8(5)	1.69(6)	1.75(6)

*Binding energies were measured using neon as a standard. The Ne 2s peak was assigned a value of 48.72 eV.

Table 2. Comparison of the atomic cross section ratio for photoemission $\sigma(s)/\sigma(p)$ with the intensity ratio of peaks I + II to peak III in the valence band spectra of diamond, Si, and Ge.

	$\frac{I + II}{III}$	$\frac{\sigma(s)}{\sigma(p)}$
C	2.9 ± 0.3	12
Si	1.6 ± 0.2	3.4
Ge	0.7 ± 0.1	1.0

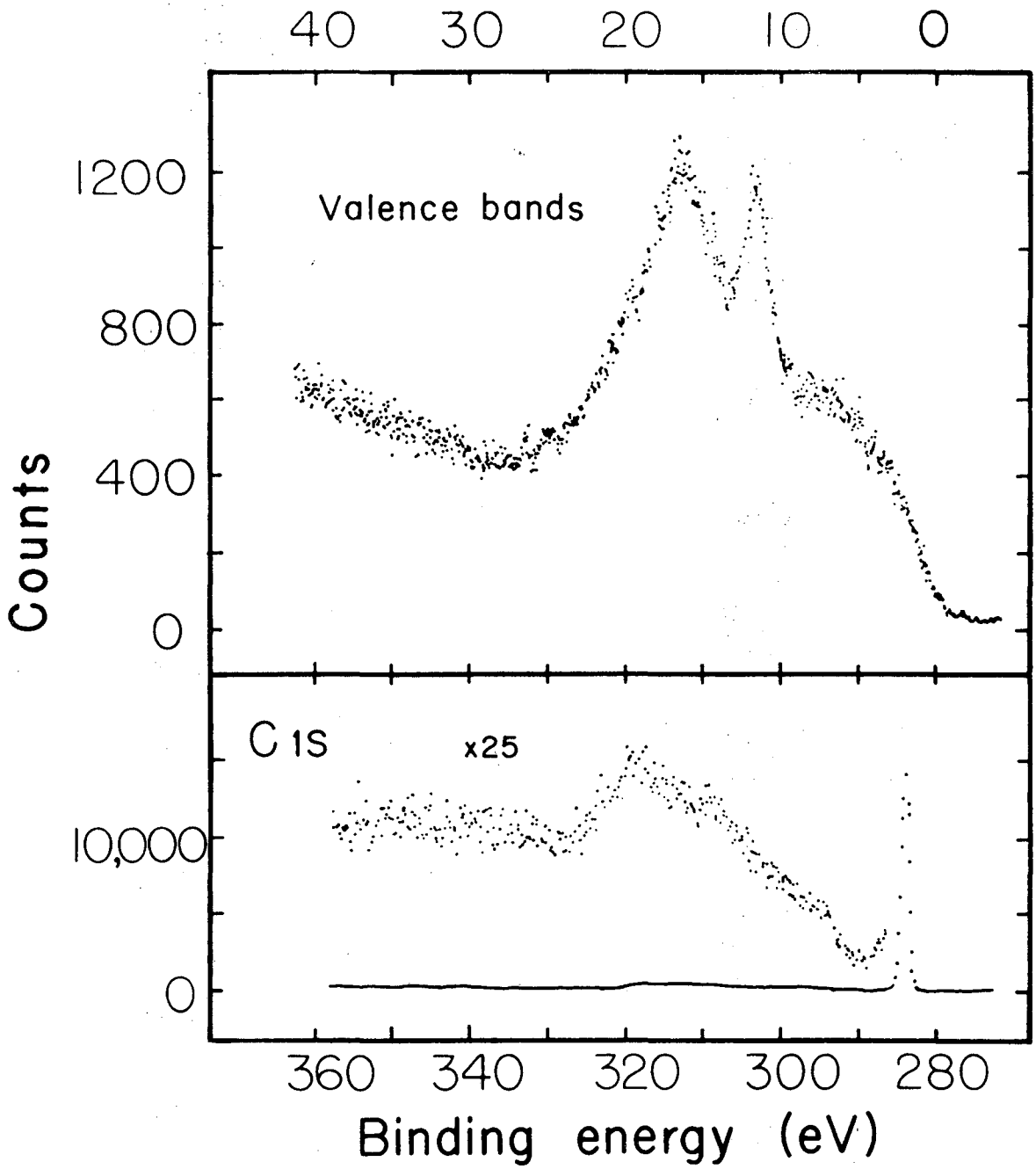

XBL 728-1458

Fig. 1. XPS valence band (upper curve) and C 1s core region (lower curve) of diamond.

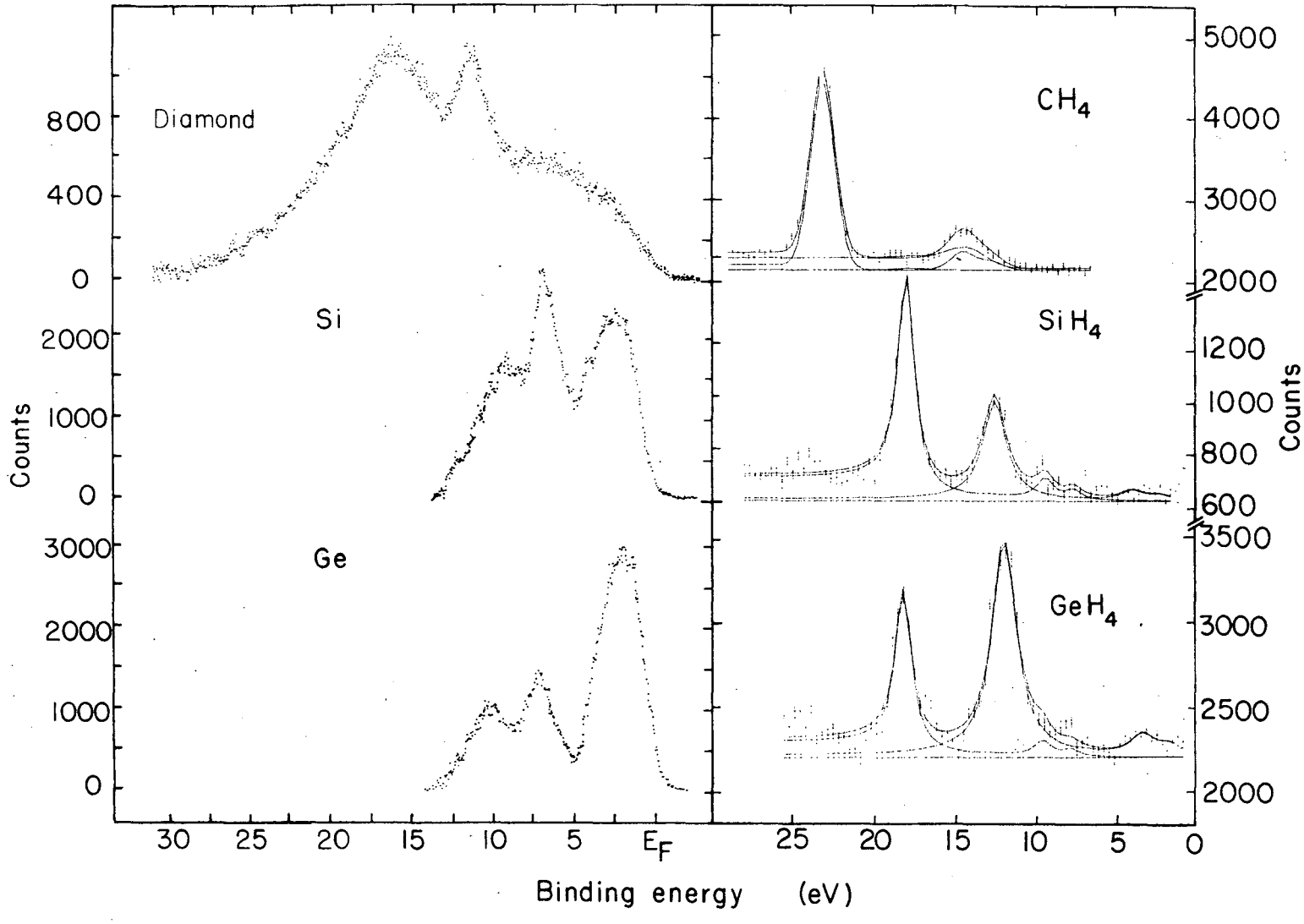

XBL721-4391

Fig. 2. a) Corrected valence-band spectra I'(E) for diamond, Si and Ge.
b) Molecular orbitals for CH_4, SiH_4, and GeH_4. The $K_{\alpha_{3,4}}$ satellites are accounted for in the least-squares computer fit.

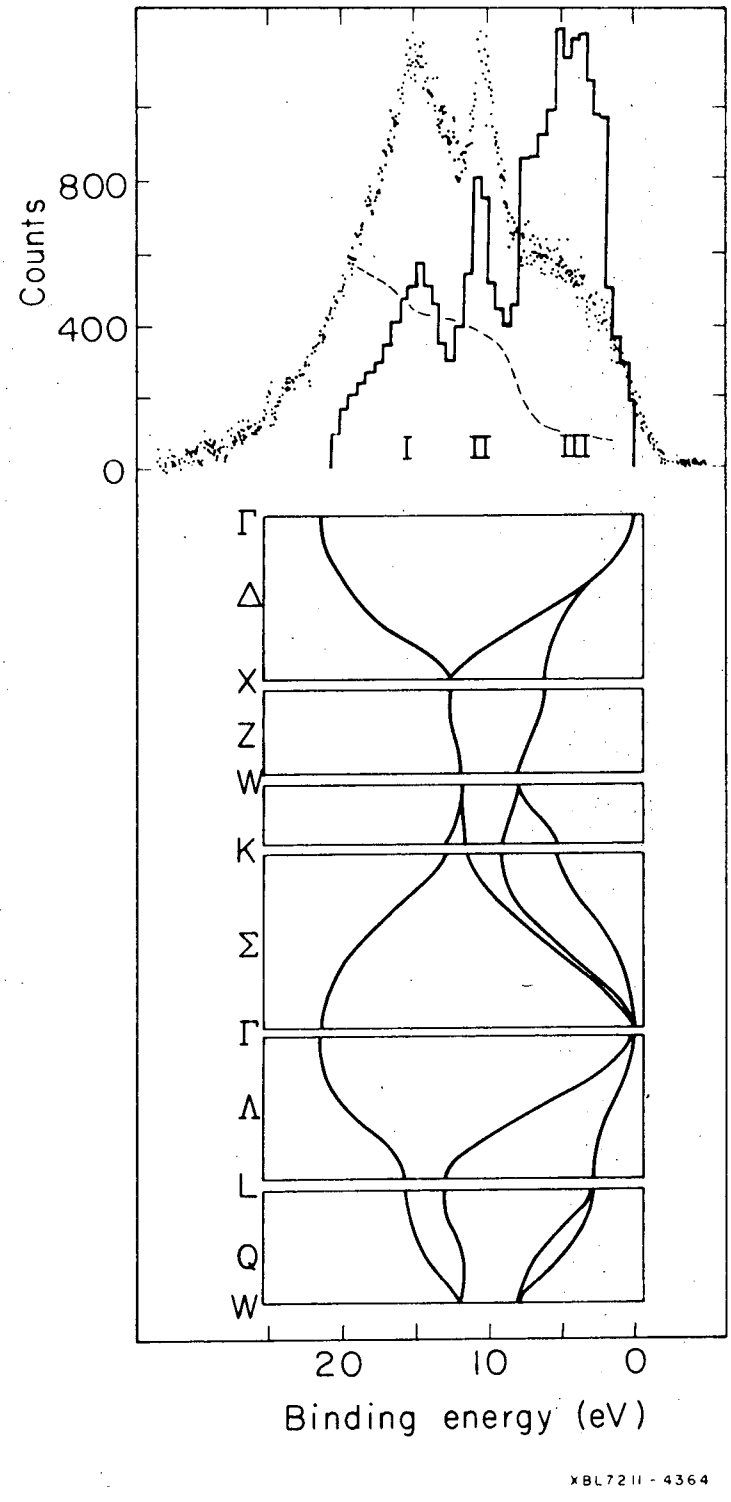

Fig. 3. Comparison of the calculated density of states (Ref. 12) with I'(E) for diamond. The broken line gives the cross section modulation as obtained by dividing I'(E) into $\rho(E)$.

SECTION X. EVIDENCE FOR COVALENT BONDING IN CRYSTALLINE AND AMORPHOUS As, Sb, AND Bi FROM VALENCE BAND PHOTOEMISSION SPECTRA*

Abstract

X-ray photoemission spectra of the valence bands of As, Sb, and Bi show a splitting, ΔE, of the "s-like" peak for the crystalline phase that disappears in the amorphous phase. This similarity to tetrahedrally coordinated covalent semiconductors is explained by describing the semimetals as layers of distorted covalently bonded hexagonal rings. This generalizes the "even-odd" ring effect to the A7 lattice. The relation of ΔE to interatomic distance is described by a universal curve.

— — —

Weaire and Thorpe have used the concept of topological disorder in attempting to understand the properties of amorphous semiconductors.[1-3] They used model Hamiltonians of the tight binding type to calculate the density of states in crystals of the diamond structure, and obtained the characteristic splitting in the lowest "s-like" peaks in the valence bands using these Hamiltonians. They emphasized the importance of six-membered rings in the diamond structure, and suggested that a random-network amorphous structure, with both five-fold and six-fold rings, would not exhibit well-resolved splitting in the s-like peak. Joannopoulos and Cohen carried out EPM band-structure calculations on several forms of silicon and germanium.[4] They found a single broad s-like peak in $\rho(E)$ for the ST-12 structure, which has five- and seven-membered rings. Single s-like peaks were indeed observed in the XPS spectra of amorphous silicon

*Section X is to be published in co-authorship with L. Ley, S. P. Kowalczyk, F. R. McFeely, and D. A. Shirley.

and germanium.[5] Both the form of Weaire and Thorpe's one-band Hamiltonian and the discussion by Joannopoulos and Cohen may be interpreted as implying splitting in the s-like peak in a broader context than the diamond lattice, and loss of this splitting in the amorphous state. In this paper we report XPS spectra on crystalline and amorphous As, Sb, and Bi which show exactly this behavior. Furthermore, for the six elements studied to date, the s-peak splitting falls on a universal curve when plotted against nearest-neighbor distance. Thus both s-peak splitting in the crystalline state and its disappearance in the amorphous state appear to be general phenomena for simple covalent solids. In addition to its intrinsic theoretical importance, this result should prove valuable both as a diagnostic device for identifying amorphous phases and as a covalent reference point for establishing an ionicity scale.

Monocrystalline samples of As, Sb, and Bi were cleaved in a dry N_2 atmosphere immediately prior to insertion into the Hewlett-Packard 5950A ESCA spectrometer. No oxygen contamination was detected by in situ monitoring of the O 1s line on the As sample. Small amounts of oxygen on the Sb and Bi samples were easily removed by gentle (200 eV, 10 μamp) argon-ion bombardment for 45 seconds and 2 minutes, respectively. During the measurement a pressure of $\sim 5 \times 10^{-8}$ Torr was maintained, and no oxygen or carbon buildup was observed.

The uncorrected photoelectron spectra I(E) of the valence-band regions of crystalline As, Sb, and Bi are shown on the left side of Fig. 1 together with corrected spectra I'(E). To generate I'(E) from I(E), a response function was constructed from the low-energy tails of

the nearby d levels (not shown) in each case. These response functions were then used to correct the valence-band spectra for inelastic secondary processes. Also shown in Fig. 1 are the measured I(E) and I'(E) for amorphous samples of As, Sb, and Bi. Amorphous As was prepared in the spectrometer by flash evaporation of a thin film onto a gold substrate at room temperature. The amorphous Sb and Bi samples were prepared by argon-bombarding single crystal surfaces for about 30 minutes with 10 μamp of 900 eV Ar^+ ions. Earlier experience[5] with Si and Ge yielded essentially identical "amorphous" spectra for evaporated films and argon-bombarded crystals.

The overall similarity of the XPS spectra in Fig. 1 reflects the similarities of electronic configuration (s^2p^3) and, for the crystalline samples, of crystal structure (A7 in each case) in these Group V elements. There are two atoms per unit cell in the A7 structure, with ten electrons filling five valence bands. In free atoms of these elements, the valence s electrons are bound 8-10 eV more tightly than the valence p electrons. The mean splittings between peaks 1-2 (Fig. 1) and peaks 3-4 (Fig. 1) are approximately 8.4 eV (As), 7.2 eV (Sb), and 8.6 eV (Bi). Using the free-atom configuration $s^2p_{1/2}^2p_{3/2}$, the mean s-p splittings in free atoms[9] can be estimated as 9.8 eV (As), 8.4 eV (Sb), and 9.7 eV (Bi). Since the cohesive energies of these elements[10] are only 2-4 eV per atom, one would expect <u>a priori</u> to find separate peaks corresponding to s and p electrons, in the absence of unusual s-p mixing, with the s peak(s) lying lower. Theoretical band-structure calculations do indeed show two reasonably well-separated s-like bands several eV below the Fermi level E_F, and three p-like bands near E_F.[6-8] We assign the lower peak (labeled 1-2 in Fig. 1)

to the former and the upper peak (3-4 in Fig. 1) to the latter. Derived energies of characteristic features in I'(E) for the crystalline samples are set out in Table 1. Although the same two general features were observed in the spectra of the amorphous materials, most of the finer structure was completely lost.

Moving down from As to Bi, changes in the structure of the p-like peak arise dominantly from relativistic effects rather than from crystal-field effects. The single asymmetric peak 3 in As splits into two peaks (3 and 4) in Sb. The splitting increases to 2.2 eV in Bi. It has been shown for Bi[11] that this splitting can be identified with the effect of spin-orbit interaction on the p-like bands near the center of the Brillouin zone (Γ). The relativistic Hartree-Fock-Slater free-atom value[9] of 2.16 eV for the 6p spin-orbit splitting in Bi corresponds closely to the observed splitting in the p-like band. The measured value for Sb of 0.76(8) eV compares equally well with the calculated 5p free-atom value of 0.71 eV. It is unusual for the spin-orbit splitting to come through so cleanly as a splitting in the valence-band density of states, because the Hamiltonians for the spin-orbit and crystal-field interactions do not commute and the corresponding energies are not additive. The d-bands of silver[12] and gold[13] provide counter-examples in which the splitting, far exceeds the free-atom spin-orbit splitting in magnitude. Shoulders 3' and 4' in the I'(E) curve for Sb most likely arise from bands near the symmetry points L_4 and T_1 and X_3, X_4 in the Brillouin zone.

Turning now to the s-like bands, we observe for the first time a pronounced splitting of the s-peak (1-2 in Fig. 1) in the densities of

states of all three Group V semimetals As, Sb, and Bi. This splitting decreases from 2.62(8) eV in As to 1.67(6) eV in Sb to 1.18(8) eV in Bi (see Table 2). A parallel decrease in width (FWHM) of this peak from 5.2(2) to 4.6(2) to 4.0(1) eV is also evident. The two components of the s-peak differ in intensity in each case. After decomposition into two peaks, we obtain an intensity ratio of 1.3 for As, 1.3 for Sb, and 1.2 for Bi. Since only two nondegenerate bands are responsible for the doublet structure, this intensity difference is most likely due to cross-section modulation of the photoelectric effect. An admixture of p-like character into band 2 would increase its photoelectron cross section relative to that of band 1 as was earlier observed for Ge.[5] In Bi the drop in the intensity ratio coincides with a marked increase in the mean s-p band separation because of the relativistic lowering of the s-electron energy. This provides direct experimental evidence for the dehybridizing effect of relativistic corrections in solids.

The density-of-states results for amorphous As, Sb, and Bi are significantly different from those of the respective crystalline modifications. The s-bands do not exhibit double-peaked structure and there is much less structure in the p-like bands in As and Sb, while the spin-orbit splitting in Bi is essentially the same. In all three cases the maximum in the density of states is shifted toward the Fermi energy by a few tenths of an electron volt. This shift gives for the amorphous state under study a direct measure of the deviation of the sample from its ground equilibrium state. The replacement of peaks 1 and 2 in the crystalline samples by a single peak in the amorphous spectra is caused by a redistribution in the density of states rather than simply by broadening of the two

peaks. This is especially true in Sb and Bi. As evidence for this we note that the total widths of the s-band peaks as well as the valley between the s- and p-bands remain essentially the same in going from the crystalline to the amorphous material.

The startling agreement between these observations and those made earlier[5] for the prototypical covalent crystals Si and Ge suggests an interpretation of the semimetal spectra along similar lines. The distortions which lead from the diamond fcc lattice to the A7 lattice of As, Sb, and Bi obviously do not destroy the main features in the density of states. The experimental s-band splitting in the semimetals is rather well reproduced by the separation of these bands at points T_1 and T_2' in the Brillouin zone, as shown by a comparison with available theoretical data in Table 2. Points T_1 and T_2' correspond to points L_1 and L_2' in the diamond lattice. It has been pointed out that the existence of sixfold rings in the diamond structure is crucial for the preservation of well-separated s-bands (peaks 1 and 2) in the density of valence band states which correspond to the bonding and antibonding s-levels of covalently bonded atoms.[3,4] In As, Sb, and Bi the lattice is composed of layers normal to the trigonal axis. There are three weak bonds per atom between layers, and within a layer there are three stronger bonds which produce a two dimensional array of distorted hexagonal rings.[14] We therefore interpret the XPS spectra of As, Sb, and Bi as extending the generality of the "odd-even" ring effect on the valence bands. Apparently s-peak splitting is present in these covalently-bonded A7-lattice crystals because of the even-numbered rings, while the odd-numbered rings that presumably are

present in the amorphous materials preclude resolution of these peaks into two simple components.

Finally, the observed splitting in the valence-band s peaks of the covalent Groups IV and V elements C(diamond), Si, Ge, As, Sb, and Bi are related in a very simple way. When plotted against nearest-neighbor distance d, these splittings follow a universal curve given by

$$\Delta E(\text{eV}) = 8.0 - 2.2 \times d\ (\text{Å}) \quad ,$$

as shown in Fig. 2. That ΔE should follow such a simple equation is somewhat surprising, because differences in coordination and hybridization might be expected to play a larger role. Apparently the effect of overlap, which of course decreases strongly with distance, is dominant. With further study it may be feasible to give a detailed explanation for the variation of ΔE. Meanwhile the observed ΔE vs d relation can serve as a covalent reference point in establishing an experimental ionicity scale based on valence-band spectra.

We thank Dr. W. Ellis for a single crystal of As. We greatly appreciate helpful discussions with J. Joannopoulos.

REFERENCES

1. D. Weaire and M. F. Thorpe, Phys. Rev. 4B, 2508 (1971).
2. M. F. Thorpe and D. Weaire, to be published.
3. D. Weaire and M. F. Thorpe, in Computational Methods for Large Molecules and Localized States in Solids, ed. by F. Hermann, A. D. McLean, and R. K. Nesbet, Plenum Press, New York (1972).
4. J. D. Joannopoulos and M. L. Cohen, to be published in Phys. Rev.
5. L. Ley, S. Kowalczyk, R. A. Pollak, and D. A. Shirley, Phys. Rev. Letters 29, 1088 (1972), and Sec. VII.
6. a) L. M. Falicov and S. Golin, Phys. Rev. 137A, 871 (1965);
   b) S. Golin, Phys. Rev. 140A, 993 (1965).
7. L. M. Falicov and P. J. Lin, Phys. Rev. 141, 562 (1965).
8. a) L. G. Ferreira, J. Chem. Phys. Solids 28, 1891 (1967);
   b) S. Golin, Phys. Rev. 166, 643 (1968).
9. C. C. Lu, T. A. Carlson, F. B. Malik, T. C. Tucker, and C. W. Nestor, Jr., Atomic Data 3, 1 (1971).
10. In C. Kittel, Introduction to Solid State Physics, J. Wiley and Sons, Inc., New York (1956), p. 78.
11. L. Ley, R. A. Pollak, S. Kowalczyk, and D. A. Shirley, Phys. Letters 41A, 429 (1972), and Sec. VI.
12. R. A. Pollak, S. Kowalczyk, L. Ley, and D. A. Shirley, Phys. Rev. Letters 29, 274 (1972), and Sec. IV.
13. D. A. Shirley, Phys. Rev. 5B, 4709 (1972).
14. J. L. Yarnell, J. L. Warren, R. G. Wenzel, and S. H. Koenig, IBM J. Res. Develop. 8, 234 (1964).

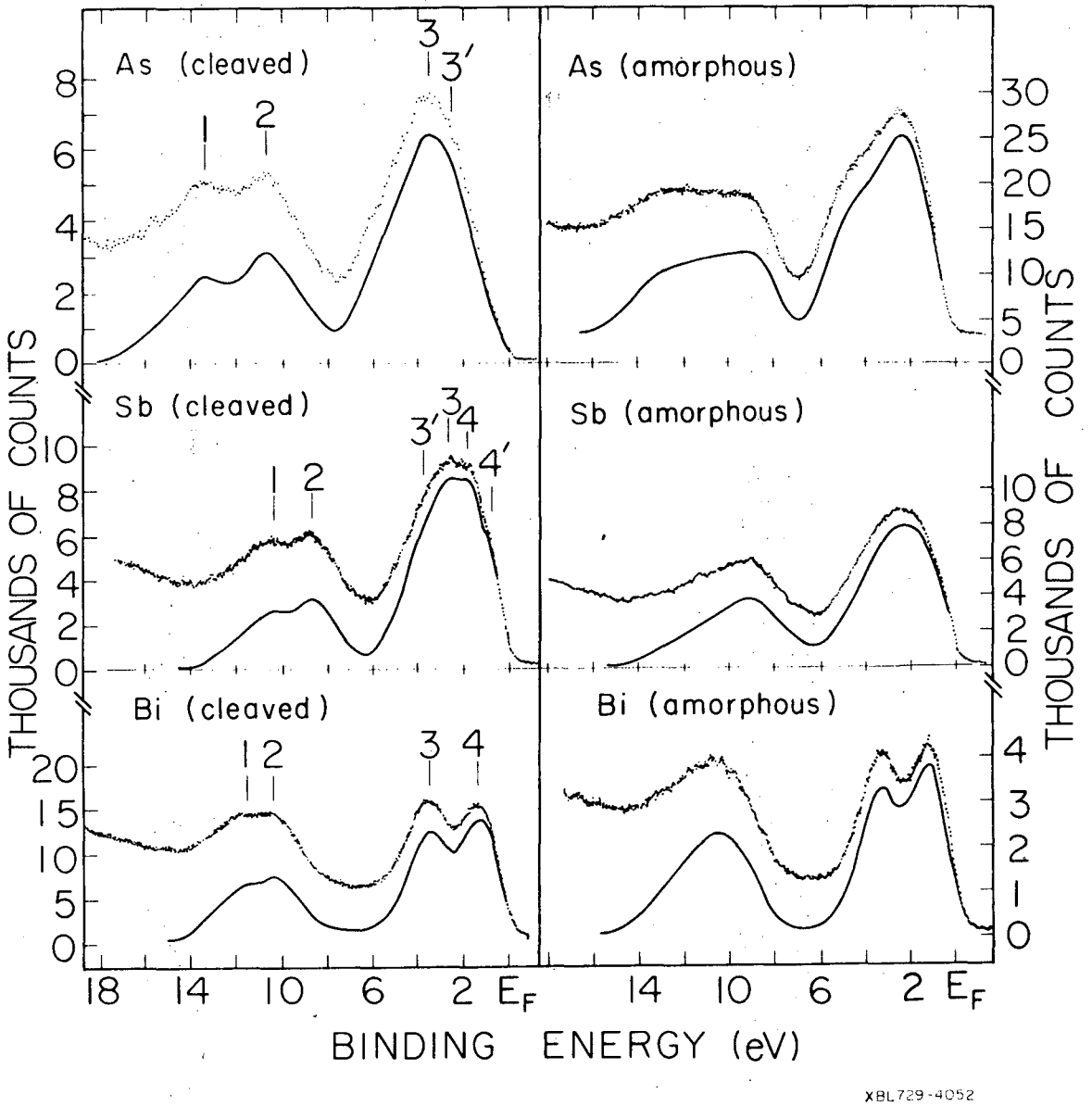

Fig. 1. Uncorrected (dots) and corrected (line) photoelectron spectra of the crystalline and amorphous semimetals.

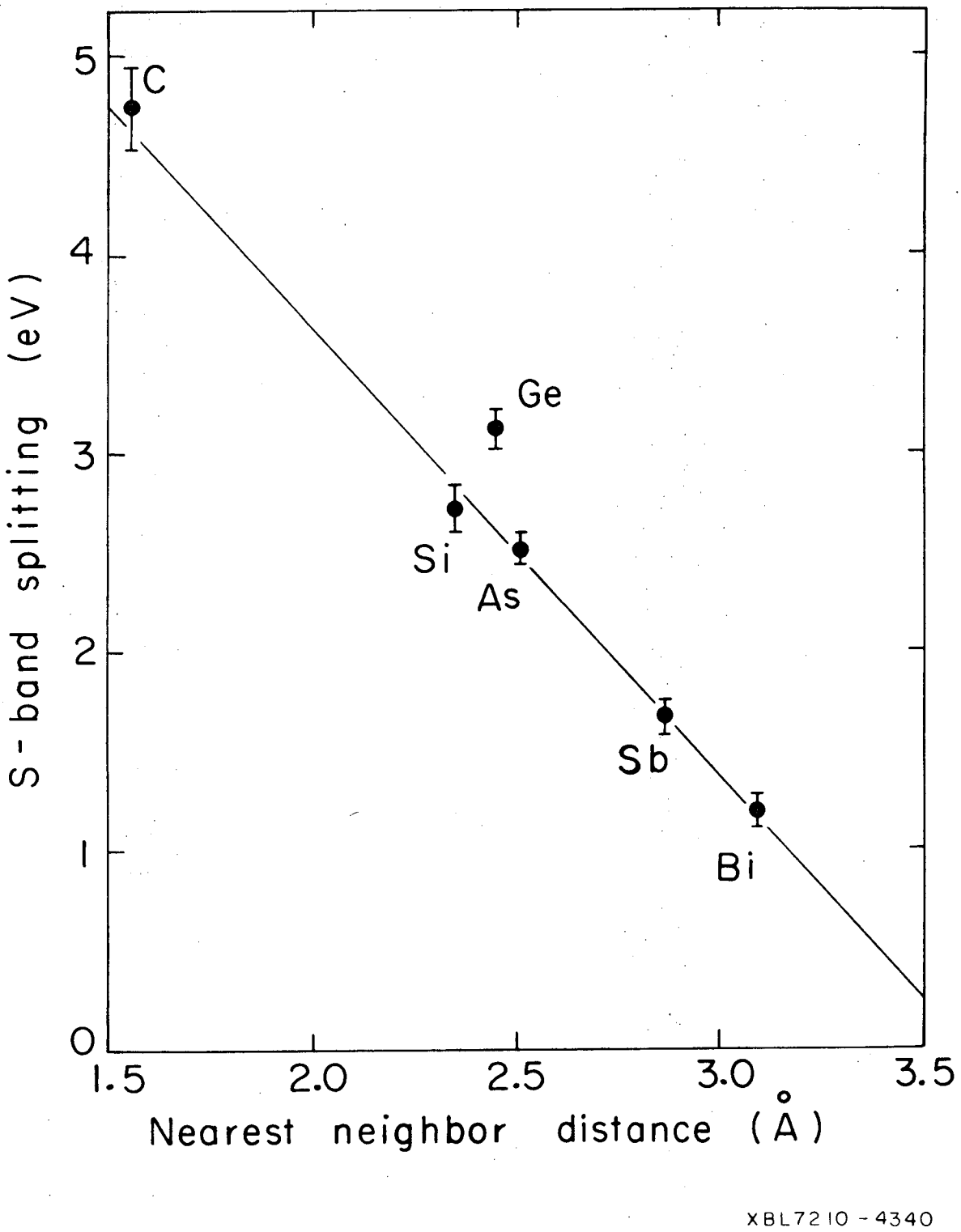

Fig. 2. Plot of the s-band splitting versus the nearest-neighbor distance for covalently bonded elements; the carbon point (diamond) is taken from Sec. IX.

SECTION XI. HIGH-RESOLUTION X-RAY PHOTOEMISSION SPECTRA OF PbS, PbSe, AND PbTe VALENCE BANDS*

Abstract

High-resolution x-ray photoelectron valence-band spectra (0 to 45 eV binding energy) of cleaved single crystal PbS, PbSe, and PbTe are reported. The spectra are compared with available band theory results. Relativistic OPW results exhibit the best overall agreement with experiment. EPM results show similar agreement for all but the most tightly bound valence band. The uppermost peak, corresponding to the three least tightly-bound bands, shows detailed structure in good agreement with the EPM predictions. The PbTe valence-band spectrum can be synthesized from the XPS valence-band spectra of Pb and Te.

A. Introduction

The "lead salts", PbS, PbSe, and PbTe, have in recent years been the object of considerable experimental and theoretical study, due in part to the technological importance of these materials as infrared and visible radiation detectors and in part to interest in their fundamental properties. All three salts crystallize in the rock-salt structure which consists of two interlocking fcc lattices separated by a translation of (a/2, a/2, a/2) where the lattice constant, a, at 300°K is 5.9362 Å for PbS,[1] 6.1243 Å for PbSe,[2] and 6.4603 Å for PbTe.[3] In this work, x-ray photoemission spectroscopy (XPS) has been used to determine the valence band density of states for each of the lead salts. Derived quantities are compared with several theoretical band structure calculations, which are critically examined in light of these results.

*Section XI has been submitted to Phys. Rev. B in co-authorship with F. R. McFeely, S. Kowalczyk, L. Ley, and D. A. Shirley.

Experimental procedures are described in Sec. B. Results are given in Sec. C and compared with theory in Sec. D.

B. Experimental

The samples used for these experiments were high-purity single crystals. In order to minimize contamination of the samples by adsorption of hydrocarbons and/or oxygen, the crystals were cleaved under dry nitrogen in a glove bag and placed in a Hewlett-Packard 5950A electron spectrometer at 5×10^{-9} Torr without exposure to the atmosphere. They were then irradiated with monochromatized $AlK\alpha_{1,2}$ radiation (1486.6 eV), and the ejected photoelectrons were energy-analyzed.

In addition to the valence band region, spectra were taken over a binding energy range of 0 - 1000 eV in order to detect core level peaks from any impurities which might be present. Experience has shown that even small amounts of impurities can give rise to extraneous peaks in the valence-band region. The only impurities present in detectable quantities were carbon and oxygen, and they were present in sufficiently small amounts so as to preclude any serious effects on the valence-band spectra. The area ratios of the Pb $4f_{7/2}$ line to the oxygen 1s line before and after the scan of each Pb salt valence band are given in Table 1. Furthermore, the symmetric shape of the Pb core levels indicate that the oxygen present was in adsorbed molecules on the surface of the sample rather than as oxide. This is further verified by the fact that the intensity of the O 1s line decreased when the crystal was left in vacuum overnight.

Energy conservation gives the photoemission equation

$$h\nu = E_B + E_{kin} + q\,\phi_{sp}$$

where E_{kin} is the kinetic energy of the photoelectron, ϕ_{sp} is the work function of the spectrometer, and E_B is the binding energy with respect to the Fermi energy. This equation presumes that the emitting region of the crystal is electrically grounded to the spectrometer. If this were not the case it would be necessary to include an extra additive term to account for charging. Our experience has shown that small band-gap semiconductors, such as the lead salts, show little or no charging.

The Fermi level of the Pb salts with respect to that of the spectrometer was determined with a Au reference as follows. A small quantity of Au was evaporated onto the surface of each Pb salt after the valence-band measurement, and the Au $4f_{7/2}$ line position was determined with respect to a core level in each case. The measured binding energy for gold metal of the Au $4f_{7/2}$ level with respect to the Au Fermi energy is 84.00 ± 0.01. Thus the binding energy of the Pb salt core level with respect to the Au Fermi level is 84.00 ± 0.01 eV minus its separation from the Au $4f_{7/2}$ peak. This binding energy then defines the Fermi level for the Pb salt valence band spectrum which includes the Pb salt core level. All binding energies quoted in this paper are given with respect to this reference energy. It is assumed that the Fermi level of the deposited Au is equal to the Fermi level of the emitting portion of the sample.

C. Results

The spectra I(E) for each of the three lead salts are shown in Fig. 1. There is striking similarity in the valence-band spectra of the three salts. The positions of the core-like Pb $5d_{5/2}$ peaks for these

salts vary within a range of 0.2 eV and the values of the spin-orbit splitting in the Pb 5d peaks are identical to within experimental error (0.02 eV). The spectra show in each case a strong broad peak, which we call peak 1, centered at about 2 - 2.5 eV below E_F, and exhibiting quite prominent structure on the low binding-energy side. This structure is evident only as a shoulder in PbTe, but in progressing through PbSe to PbS it becomes a well-defined extra peak which we label 1'. Between the (1-1') peak and the Pb 5d lines there are two less intense peaks labeled 2 and 3 in Fig. 1. The absolute binding energies of these peaks show no monotonic trend with the atomic number of the group VI element. Peaks 2 and 3 have the highest binding energies in PbSe. However, the energy difference between peaks 2 and 3 increases monotonically in going from the telluride to the sulfide. The 3-2 splitting is 3.5 eV in the telluride, 4.3 eV in the selenide and 4.4 eV in the sulfide.

We have deconvoluted and subtracted from the valence band spectra I(E) contributions from inelastically scattered electrons and contributions from the low binding energy tail of the Pb 5d peaks. The shape of the inelastic tail was obtained from a near-lying core level and the 5d-tail was approximated by smoothly extending the low binding energy edge of the Pb $5d_{5/2}$ peak. We label the corrected spectra I'(E). The uncertainty of these corrections are included in the quoted errors. The corrected experimental binding energies are summarized in Table 2.

D. Discussion

These IV-VI compounds have a total of ten valence electrons per Pb atom, which must occupy five valence bands. In light of many recent

band structure calculations, the (1-1') peak structure of the photoelectron spectra in all three lead salts may be unequivocally identified with three p-like bands. At the Γ point, two of these bands are degenerate and have Γ_8^- symmetry while the third band has Γ_6^- symmetry. Calculations of the band structure by the EPM,[4,5,6] OPW[7] and relativistic APW[8,9] methods give qualitative agreement on this point.

While there is reasonable agreement on the positions of the three p-like bands and the corresponding maxima in the densities of states, agreement among theoretical predictions of the two lower-lying peaks (2 and 3) is much poorer. Clearly these peaks can only represent the two s-like (Γ_6^+) bands arising from the 6s level of Pb and the highest s-level of the group VI atom. Neither peak can be due to impurities since, as stated previously, no core level peaks were observed for any element which would contribute significant intensity to the valence-band region. Nor can peak 3 be an energy loss peak arising from the 1-1' peak, first because the energy difference of $\sim$ 10 eV is too small compared to the $\sim$ 16 eV loss structure observed for the Pb 5d electrons in these salts and secondly because the intensity of peak 1-1' relative to peak 3 is far lower than the corresponding ratio of Pb 5d peak to its energy loss structure. The assignment of the spectra therefore appears to be completely straightforward. The 1-1' complex arises from the top three "p-like" bands and peaks 2 and 3 each arise from an "s-like" band.

Band-structure experiments and theory enjoy a symbiotic relationship. This relation is valuable because neither would be very effective alone. However, the closeness of the two requires that in the interpretation of spectra one should clearly differentiate between results that are

derived directly from the spectra and results that are inferred by comparing the spectra with calculated band structures. We have already identified the peaks in the lead salts spectra with energy bands, so some interplay of theory and experiment has already taken place. In fact these peaks are sufficiently well-resolved that they could have been assigned to the energy levels of the pure elements without reference to band structure, as we shall show below. We assume throughout this discussion that the one-electron transition model described by Fadley and Shirley[10] can be used for the Pb-salts. We also assume that calculated eigenvalue spectra of band theory represent experimental one-electron binding energy spectra (Koopmans' Theorem).[11] It should be emphasized at this point that disagreement between theory and experiment may result from the inapplicability of either of these assumptions.[10,11] Turning now to a more detailed interpretation of the spectra within this model, we can proceed at two distinct levels of sophistication:

Level 1. The mean peak positions and widths can be extracted directly from the spectra and used to assess the relative accuracies of the band-structure calculations. This is an empirical approach, and therefore less subject to error, but it yields information only about the gross features of the bands.

Level 2. After one or more band structure calculations have been judged to be in good agreement with experiment, these energy bands can be compared in more detail with the shape or at least the width of the peaks to estimate the energies of the bands at symmetry points in the Brillouin zone. This procedure is somewhat speculative, but it yields information of reasonable reliability about the really interesting features of the band structure.

In the discussion below we shall first discuss each of the available band-structure calculations at Level 1, then go on to Level 2.

Overhof and Rössler[12] calculated the band structures of all three Pb salts using a relativistic Green's function technique. Their calculation is unique among those considered here in that the d electrons are included. Unfortunately their band structures must be viewed in light of our results as being qualitatively wrong. The highest s level is predicted in all three cases to lie so close to the p-like bands so as to give rise to only one broad peak in the density of states rather than one p-peak and a smaller s-peak $\sim$ 6 eV away. Furthermore the lower lying s peak would in all three cases be buried under the core-like Pb 5d peaks. The Pb $5d_{3/2}$ and $5d_{5/2}$ are predicted to lie at $\sim$ 13.5 and 15.5 eV for PbS, $\sim$ 13.3 and 15.4 for PbSe, and $\sim$ 13.6 and 15.5 for PbTe instead of the ($\sim$ 18.5 - 21) given for the three salts by our spectra. We have not corrected our XPS spectra for polarization or relaxation about the final state hole and thus the reported binding energies for the Pb 5d electron--and to a lesser extent peaks 2 and 3--may be smaller than the Koopmans' theorem value of theory. This correction may consist of adding approximately 1 eV to the Pb 5d binding energies.

The Augmented Plane Wave (APW) method was used by Conklin, Johnson, and Pratt[8] to calculate the band structure of PbTe. The Hamiltonian used for this calculation included a spin-orbit term and Darwin and mass-velocity corrections. The results obtained agree reasonably well with our spectra. The calculation indicates that the highest s-peak should occur near 6 eV while the other s peak should be at 11 eV, compared with the experimental values 8.2 eV and 11.7 eV obtained here.

Augmented plane wave calculations very similar to those above were undertaken by Rabii[9] on PbS and PbSe. The upper Γ_6^+ levels were calculated and it appears that they would lead to maxima in the density of states around 7 eV in both PbSe and PbS, with the peak probably lying slightly lower in energy for PbSe. This compares with experimental values for this peak of 8.6 and 8.4 eV respectively. Thus the discrepancy is similar to that in the PbTe case.

A different approach to the problem was taken by Lin and Kleinman[4] in a pseudopotential calculation of the lead salt band structures. In this calculation there were 5 variable parameters which were adjusted to give the best agreement with reflectivity data.[13] The charge of Pb and the VI atom are allowed to vary and there was also a spin-orbit parameter. The remaining two parameters were used to adjust an extra repulsive potential term which applies only to s-like levels. The variation of these parameters ultimately produced shifts of up to 17.7 eV in PbS and 7.6 eV in PbTe. A comparison of the predictions of their band structures and experiment is given in Table 3. As can be seen the overall agreement is quite good in PbS and PbSe, except that, as with the APW calculations, the predicted binding energy of Peak 2 is too low. In the PbTe calculation, however, the agreement is poor for Peak 3 as well.

Tung and Cohen[5] and Tsang and Cohen[6] have calculated the band structures for PbTe and for PbSe and PbS respectively using the Empirical Pseudopotential Method (EPM). In these calculations spin-orbit interaction was included but other relativistic effects were not. In addition to band structures, the resulting densities of states curves were calculated.

The results of these calculations, shown in Fig. 2 match the experimental results for the p-like peak(s). Particularly striking is the way in which the calculation shows the origin of the 1' peak out of the 1 peak in progressing from PbTe to PbS. The position indicated for the highest s-band (not shown) is also reasonable though not exactly correct.

The major disagreement of this calculation with experiment lies in the predicted energy of the lowest s-peak (not shown in the density of states curve). This level is predicted to lie at 17 eV in PbTe, 24.5 in PbSe, and 27.5 in PbS. This discrepancy is not unexpected, because a local pseudopotential was used. In the case of ZnSe[14] a local pseudopotential was shown to be inadequate for the lowest bands. Thus the nonlocal nature of the pseudopotential should be considered when calculating these bands.

The most successful band structure calculation was undertaken by Herman et al.[7] In this calculation the OPW method, with relativistic effects included directly in the Hamiltonian, was used to calculate the energy levels at certain symmetry points in the Brillouin zone. A pseudopotential technique was then used to connect the regions between the summetry points. The resulting band structures were not fitted to any experimental data. The results for PbTe, PbSe, and PbS are shown in Table 4. While the predicted binding energy for Peak 2 in PbS and PbSe is lower than observed (as is the case in all the band structures), the results for PbTe agrees very well with experiment.

Proceeding now to the more sophisticated--and less certain--Level 2 of interpretation, we shall try to derive information about the positions

of bands at symmetry points in the Brillouin zone, we treat one salt at a time.

In PbS the 1-1' peak shows well-developed structure that can be identified with the structure of $\rho(E)$ in this region as given by the EPM results. The well-resolved peak in $\rho(E)$ at 1.5 eV below the top of the valence band (which falls at L_6^+) is presumably shoulder 1' in I'(E). We shall use this as a fiducial point. The EPM $\rho(E)$ and the experimental I'(E) are superimposed in Fig. 2 using this fiducial. Thus peak 1' appears, from the EPM results, to arise largely from maxima in the top valence band near symmetry points Δ (1.6 eV below L_6^+) and Σ (0.9 eV below L_6^+). The OPW calculation gives these last two energies as 1.8 and 0.9 eV, respectively. Since the 1' maximum in I'(E) falls 1.25 eV below our measured E_F, it follows that the top of the valence band must lie within 1.25 eV of the 1' energy, if this E_F can be regarded as being intrinsic to PbS. We regard the agreement of this figure 1.25 eV with the EPM result of 1.5 eV to the top of the valence bands as satisfactory.

Proceeding to Peak 1 in PbS, the characteristic shape of this peak in $\rho(E)$ is apparent in I'(E). The peak is rounded on the left side, and steep on the right side, with a well-defined breaking point at the top. This point, which we shall call 1", falls at E_F - 2.38 eV, or 1.13 eV below 1'. The highest intensity point in the EPM $\rho(E)$ for this band falls 3.0 eV below the top of the valence band, or 1.5 eV below the maximum corresponding to 1'. While this value exceeds the experimental result somewhat, we note that in the OPW calculations the relevant bands tend to lie higher. We may roughly relate the 1' - 1" energy difference to the difference in energy between the maximum in the top band near Δ and

the flat regions of the second (and third) bands from the top, along L - Γ - K. These energy differences are approximately 1.3 (EPM) and 0.7 eV (OPW). This 0.6 eV difference provides room for the 0.4 eV discrepancy between our data and the EPM results. Further strong evidence that the two maxima in question are too widely separated in the EPM bands is provided by the qualitative appearance of the 1-1' peak. If the two points 1' and 1" were really 1.5 eV apart, there would be a substantial minimum between them.

The other feature of Peak 1 that can be readily compared with $\rho(E)$ is the position of the half-maximum point on the low kinetic energy side of this peak. On I'(E) this falls in the range 2.8 - 3.0 eV below 1', while in EPM $\rho(E)$ value is 2.9 eV, in excellent agreement. We cannot compare this directly to the OPW results, but the agreement with experiment would almost certainly be worse. This follows because the OPW results have the maximum in the top band near Δ about 3.4 eV above the bottom of the third band (at X_6^-), while the EPM value is 4.0 eV. It is difficult to obtain an experimental value for this quantity from the spectra, but a value of 3.9 ± 0.2 can be estimated by assuming that the peak has a constant slope down to zero intensity, as indicated in the EPM $\rho(E)$.

In summary, our spectrum shows good agreement with the two theories regarding total width of the top band, giving 5.2 ± 0.3 eV vs 5.5 eV (EPM) or 5.2 eV (OPW). In detail there is some disagreement. The position of peak 1' appears to be higher than either theory would predict by ∿ 0.2 - 0.4 eV. Peak 1' is closer to 1" than the EPM results (by ∿ 0.4 eV), and higher above the bottom of these bands than the OPW prediction (by ∿ 0.6 eV).

Peak 2 in PbS has its center 7.0 eV below 1', or about 8.2 eV below E_F and presumably also the top of the valence bands. The FWHM of this peak is 2.5 eV and the total width, based on an uncertain extrapolation to zero intensity, is about 3.5 eV. The centroid in the EPM $\rho(E)$ is 7.1 eV below the top of the bands or 5.6 eV below 1', about 1 eV or more too high. The width that should be compared to the experimental FWHM (in the absence of lifetime broadening) is about 1.2 - 1.4 eV (because of instrumental broadening), and the total bandwidth is about 2.1 eV; both are thus substantially narrower than experiment. The OPW extrema of this band are 5.8 and 8.1 eV below the top of the valence bands. Thus the OPW bandwidth of 2.3 eV is too small. We estimate that the OPW centroid in $\rho(E)$ would lie about 7.3 eV below the top of the valence band, or about 0.9 eV too high. Use of point 1' as a fiducial point would worsen the agreement, since this point is already too low in the OPW results. In summary, Peak 2 is about 1 eV lower and $\sim$ 50% wider than predicted by the OPW and EPM theories. Of course the observed binding energy may be affected by relaxation and the linewidth by lifetime broadening.

The centroid of Peak 3 falls at 12.5 eV below E_F, or about 1.6 eV higher than the 14.1 $\pm$ 0.2 eV that we can estimate as the distance that the bottom band falls below the top of the valence band in the OPW calculations. The peak width shows a larger discrepancy. The OPW band is only 0.7 to 0.8 eV wide, while Peak 3 is about 2.6 eV FWHM or $\sim$ 4 eV in total width. Thus band-structure broadening may be more pronounced for this band than the calculations indicate.

Turning now to PbSe, there is a considerable amount of partially-resolved structure in Peak 1. The shoulder on the high-energy side

(Peak 1') is clearly discernible, although not quite as well-resolved as in PbS. Peak 1' is 1.16 ± 0.10 eV below E_F, in excellent agreement with the highest-energy maximum in the EPM $\rho(E)$, which is also less well resolved from the rest of Peak 1, and is centered 1.18 eV below the top of the valence bands.

The rest of Peak 1 in PbSe is similar to the PbS case, but more structure is evident. The resolution of other features is marginal, but four more features could be reproducibly identified in three samples. They were: 1", an abrupt change of slope similar to 1" in PbS; 1_3, a peak connected to 1' by a gently-sloping line; 1_4, a peak separated from 1_3 by a distinct minimum, and 1_5; another shoulder on the low energy side of Peak 1. The positions of the last four features relative to 1' are given, for all three samples, in Table 5. Also given in Table 5 are the positions of the five most prominent peaks in the EPM $\rho(E)$. The agreement with experiment is very good. Equally impressive (and more important) is the agreement between the general shapes of this peak in $\rho(E)$ and $I'(E)$. Again Peak 1' is slightly closer to the rest of Peak 1 and not as well resolved as the EPM results would suggest, but the overall agreement is really extraordinary.

Further comparisons with the EPM $\rho(E)$ give $1' - 1_6 = 2.9$ eV (expt) and 2.7 eV (EPM) and $1' - 1_7 \cong 4$ eV (expt) and 3.7 eV (EPM), where 1_6 is the position of half-maximum height on the low energy side of Peak 1, and 1_7 is the bottom of these bands, extrapolated from the slope. Again the agreement is excellent. The experimental $I'(E)$ and the EPM $\rho(E)$ are plotted in Fig. 2.

No $\rho(E)$ is available from the OPW calculations, but it is clear that the OPW and EPM results for Peak 1 in PbSe agree very well, as point-by-point comparison of the energy bands will show. The OPW results give the maximum in the top band near Δ as 1.1 eV below the top of the valence bands at L_6^+. If this may be taken as a measure of the position of 1', the agreement is excellent. The next two bands have flat regions along Γ - L, at $\sim$ 2.0 and 2.4 eV below L_6^+ (OPW), or 2.1 and 2.5 eV (EPM). These two bands probably contribute significantly to the features 1" and 1_3 in I'(E), at $\sim$ 1.85 eV and 2.3 eV below E_F. It would be very plausible simply to interpret these features as determining the positions of L_{45}^+ and L_6^+, but such an interpretation is not unique. Finally, the total width of these top three bands is 4.9 eV (OPW), in good agreement with 4.9 eV (EPM) and $\approx$ 5 eV (expt).

Peak 2 in PbSe shows no appreciable structure. Its position at 7.1 eV below 1', or 8.3 eV below E_F, is about 1.5 lower than the corresponding peak in the EPM $\rho(E)$, at 6.8 eV, and its width (FWHM = 1.8 eV) is about twice that of the EPM peak (FWHM = 0.9 eV). In the OPW results this band appears to be about the same width as in the EPM case, although comparison is difficult because X_6^+ lies below Γ_6^+ in OPW and above it in EPM. We estimate the centroid of this band to lie about 6.6 eV below 1' in the OPW case, in better agreement with experiment, but still slightly high.

Peak 3 in PbSe is centered 11.7 eV below 1' or 12.9 eV below E_F, about 1 eV higher than the lowest OPW band, which would give a peak at an estimated 12.8 eV below 1' or 13.9 eV below the top of the valence bands. Again the peak is wider (1.9 eV FWHM, or $\approx$ 3.5 eV total) than the OPW band (0.8 eV total), though not as wide as Peak 3 in PbS.

In PbTe, Peak 1 has a rather different structure from the same peak in PbS and PbSe. First, the shoulder attributed to Peak 1' is not evident. This is in very good agreement with the EPM $\rho(E)$, which does not show the well-separated peak found in the other salts. This is a consequence of the general tendency for the top three bands to be compressed upward in PbTe relative to PbSe and PbS. Table 6 contains the positions of several symmetry points relative to the top of the valence bands (L_6^+), from the OPW and EPM calculations. The compression of these bands in PbTe is especially pronounced for features near the top of the band.

Since there is no Peak 1' in PbTe, another fiducial point is needed. We shall use the energy of the leading edge at half height, denoted 1_H. Its value is 17.99 eV above $E(5d_{5/2})$, or 0.34 ± 0.05 eV below E_F. This agrees very well with the value 0.4 ± 0.1 eV estimated from the EPM $\rho(E)$ as the energy of this feature below the top of the valence bands (at L_6^+). The error in this estimate follows from uncertainties in converting $\rho(E)$ to $I'(E)$.

Peak 1 in the PbTe $I'(E)$ can be characterized as "blunt". This agrees well with the EPM $\rho(E)$ after due allowance for experimental resolution has been made. At slightly higher resolution considerably more structure should be discernible. The peak is somewhat wider than the theoretical results would indicate. The trailing edge at half height falls at E_F - (3.84 ± 0.02) eV, compared with E_F - 3.2 eV for this feature from the EPM $\rho(E)$. Rough extrapolation gives the total bandwidth as $\sim$ 5 eV, compared to 4.3 eV (OPW) and 3.7 eV (EPM).

The positions and widths of Peaks 2 and 3 in PbTe are set out in Table 7. Peak 2 is about 1 eV lower than the OPW result and nearly 2 eV

below the EPM value. The OPW peak positions for Peak 3 is in very good agreement with experiment. Again both of these peaks are wider than the band structure $\rho(E)$ would predict.

We have identified the peaks in the XPS $I'(E)$ spectrum with peaks of corresponding energy in $\rho(E)$ of band theory. The same assignments can be obtained empirically by comparing the XPS valence-band spectra of the lead salts with those of the pure elements comprising them. For example there is a one-to-one relationship between the peaks in $I'(E)$ of PbTe and the sum of peaks in the $I'(E)$ spectra of single crystal Pb[15] and single crystal Te.[16] The binding energies of these peaks are listed in Table 7. It can be seen that the difference between any two corresponding peaks, one from the salt and one from the element, is at most ~ 0.6 eV. These differences are consistent with the ionic character of the salt which is demonstrated by comparing the separation in binding energy of the Pb $5d_{5/2}$ and Te $4d_{5/2}$ peaks in PbTe (20.01 eV) with the separation between these peaks in pure Pb and pure Te (21.48 eV). The difference of separations is 1.47 eV. The observed peak widths (FWHM) of the Pb 6s and the Te 5s in the pure elements are approximately a factor of two wider than peaks 2 and 3 in PbTe possibly indicating a larger crystal field interaction for these bands in Pb and Te than in the partially ionic PbTe.

E. Conclusions

We have presented the high-resolution XPS spectra of PbS, PbSe, and PbTe valence bands, assigned the peaks to bands in available calculated band structures, and compared the structure of each peak with theory. The

agreement observed between theory and experiment is encouraging. Nevertheless there are questions which remain to be answered before the full value of XPS valence-band spectra can be realized. We have assumed the one-electron transition model where the measured binding energy is equated to the one-electron orbital energy. This implies that all other one-electron orbitals remain frozen during photoemission. We have also assumed that the density of states $\rho(E)$ generated from band structure calculations corresponds to the one-electron orbital energy spectrum. The existence of possible deviations from the above model are recognized; however they have to be defined and quantified before a more sophisticated model can be applied. Only by further experimental and theoretical study can the magnitude of the final state and relaxation effects in the photoemission process and the sensitivity of the theoretical band structure to an approximate exchange potential be taken into account.

We thank Professor G. Somorjai for giving us single crystal PbS, PbSe, and PbTe.

REFERENCES

1. H. E. Swanson and R. K. Fuyat, Nat. Bur. Stand. Circular No. 539, Vol. 2, p. 18 (1955).
2. H. E. Swanson, N. T. Gilfrich, and G. Ugrinie, Nat. Bur. Stand. Circular, Vol. 5, p. 39 (1955).
3. N. R. Short, Brit. J. Appl. Phys. 1, 129 (1968).
4. Pay June Lin and Leonard Kleinman, Phys. Rev. 142, 478 (1966).
5. Y. W. Tung and Marvin L. Cohen, Phys. Rev. 180, 823 (1969).
6. Y. W. Tsang and Marvin L. Cohen, to be published.
7. F. Herman, R. L. Kortum, I. B. Outenburger, and J. P. Van Dyke, J. de Physique 29, C4-62 (1968).
8. J. B. Conklin, Jr., L. E. Johnson, and G. W. Pratt, Jr., Phys. Rev. 137, 478 (1966).
9. S. Rabii, Phys. Rev. 167, 801 (1968); 173, 918 (1968).
10. C. S. Fadley and D. A. Shirley, in Electronic Density of States, Nat. Bur. Stand. special publication No. 323, 163 (1971).
11. F. Herman, I. B. Outenburger, and J. P. Van Dyke, Intern. J. Quantum Chem. III S, 82 (1963).
12. H. Overhof and U. Rössler, Phys. Stat. Solidi 37, 691 (1970).
13. M. Cardona and D. L. Greenaway, Phys. Rev. 113, A1658 (1964).
14. R. A. Pollak, L. Ley, S. Kowalczyk, D. A. Shirley, J. D. Joannopoulos, D. J. Chadi, and Marvin L. Cohen, Phys. Rev. Letters 29, 1103 (1972), and Sec. VIII.
15. L. Ley, R. A. Pollak, S. Kowalczyk, and D. A. Shirley, Phys. Letters 41A, 429 (1972), and Sec. VI.
16. R. A. Pollak, S. Kowalczyk, L. Ley, and D. A. Shirley, Phys. Rev. Letters 29, 274 (1972), and Sec. IV.

Table 1. Ratio of Pb $4f_{7/2}$ to O 1s peak areas

	PbS	PbSe	PbTe
Before VB Run	30:1	> 50:1	10:1
After VB Run	44:1	> 50:1	33:1

Table 2. Pb salt VB binding energies (eV)

	Pb $5d_{3/2}$	Pb $5d_{5/2}$	3	2	1	1'
PbTe	20.94±0.05[a]	18.33±0.05	11.7±0.2	8.20±0.1	2.30±0.1	--
PbSe	20.99±0.05	18.38±0.05	12.92±0.15	8.64±0.1	2.19±0.1	1.21±0.15
PbS	21.10±0.05	18.52±0.05	12.81±0.15	8.43±0.1	2.53±0.1	1.20±0.1

[a]The quoted errors do not include uncertainties in the determination of the Fermi level.

Table 3. Calculations of Lin and Kleinman[4] compared to experiment

	PbS		PbSe		PbTe	
	L&K	Expt	L&K	Expt	L&K	Expt
Peak 1	1.8	2.5	1.7	2.2	2.5	2.3
Peak 2	6.3	8.4	5.8	8.6	5.4	8.2
Peak 3	12.2	12.8	11.8	12.9	8.7	11.7

Table 4. Calculations of Herman et al.[7] compared to experiment

	PbS		PbSe		PbTe	
	OPW	Expt	OPW	Expt	OPW	Expt
Peak 1	2.6	2.5	∿ 2.6	2.2	∿ 2.0	2.3
Peak 2	6.6	8.4	7.4	8.6	7.4	8.4
Peak 3	14.0	12.8	14.0	12.9	11.5	11.7

Table 5. Features in Peak 1 of PbSe (Energies in eV)

Sample	1'	1"	1_3	1_4	1_5
I	(0)	0.7[a]	1.0_5	1.5_5	2.2_5
II	(0)	0.7_1	1.2_5	1.7_5	2.4_8
III	(0)	0.6_5	1.1	1.6_5	2.3_5
Theory(EPM)	(0)	0.9	1.35	1.8	2.2

[a]These positions are known to ± 0.1 eV relative to one another.

Table 6. Characteristic energies in Pb salts (eV)

Description	PbTe		PbSe		PbS	
	OPW[a]	EPM[b]	OPW[a]	EPM[b]	OPW[a]	EPM[b]
L_6^+	0	0	0	0	0	0
Δ_6	0.7	0.6	1.1	1.1	1.8	1.6
$L_{4,5}^+$	1.0	0.9	1.9	2.2	2.3	2.8
X_6^-	4.3	3.7	4.9	4.9	5.2	5.5

[a] Taken from references 5 and 6.

[b] Taken from reference 7.

Table 7. Comparison of PbTe results with those for Pb and Te. Binding energies are relative to the measured Fermi levels.

	PbTe	Pb[a]	Te[b]
Binding energy Te $4d_{3/2}$ (eV)	40.95(7)	--	41.80(9)
Binding energy Te $4d_{5/2}$ (eV)	39.49(7)	--	40.31(9)
FWHM $4d_{3/2}$ = FWHM $4d_{5/2}$	1.50(2)	--	0.94(2)
4d splitting (eV)	1.46(2)	--	1.51(1)
Binding energy Pb $5d_{3/2}$ (eV)	20.94(7)	20.32(5)	--
Binding energy Pb $5d_{5/2}$ (eV)	18.33(7)	17.70(5)	--
FWHM $5d_{3/2}$ = FWHM $5d_{5/2}$	1.20(5)	0.94(5)	--
5d splitting	2.61(2)	2.62(2)	--
Binding energy Te 5s, PbTe "3" (eV)	11.7(2)	--	11.5(2)
FWHM Te 5s, PbTe "3" (eV)	2.5(3)	--	4.8(5)
Binding energy Pb 6s, PbTe "2" (eV)	8.20(11)	7.68(20)	--
FWHM Pb 6s, PbTe "2" (eV)	2.3(2)	2.7(2)	--
Binding energy Pb 6p, Te 5p, PbTe "1"	2.30(11)	{2.33(8) 0.53(5)	{4.0(2) 1.13(5)
FWHM Pb 6p, Te 5p, PbTe "1"	3.5(2)	3.1(2)	5.0(2)

[a] Ref. 15.

[b] Ref. 16.

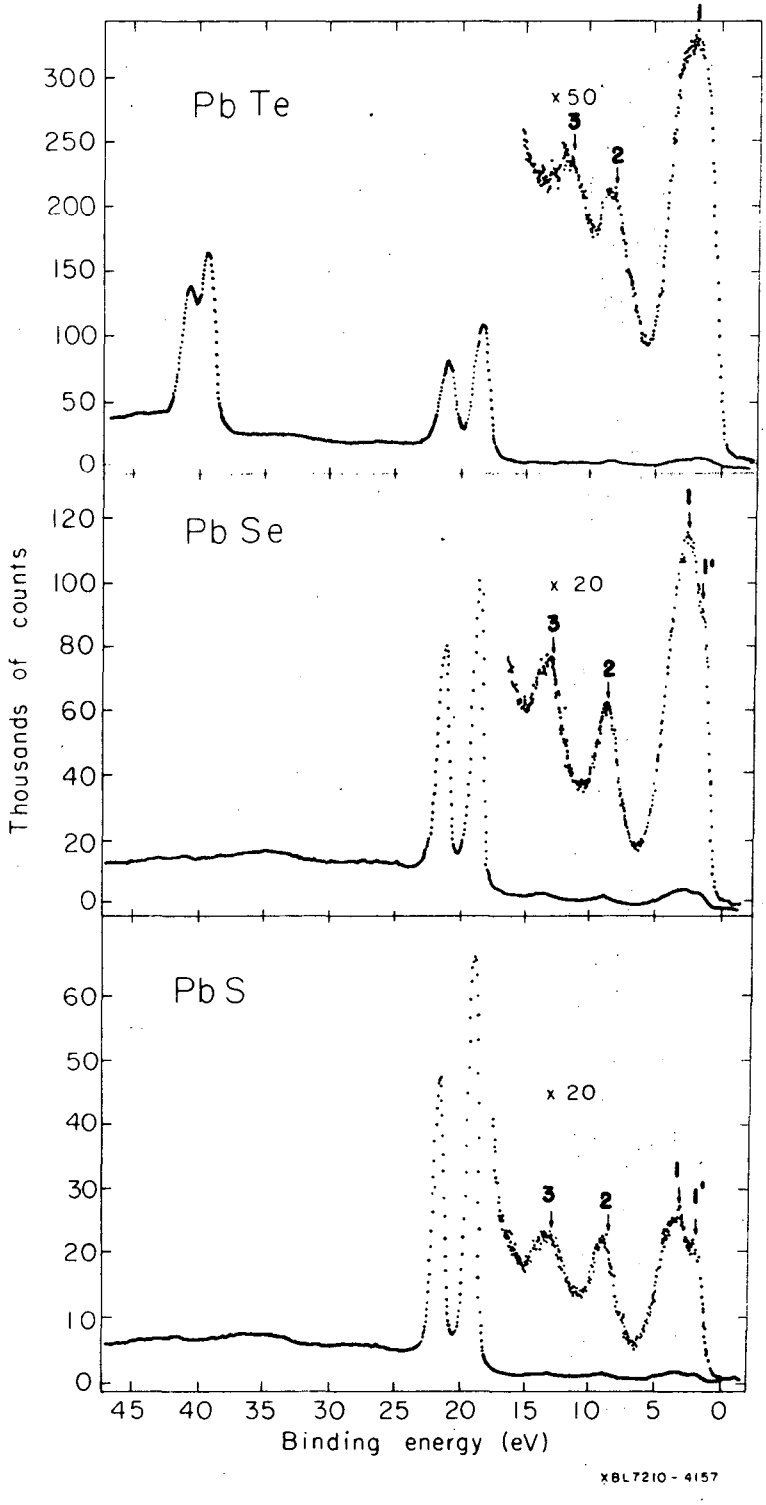

Fig. 1. Raw valence-band spectra of the lead salts; the strong double peaks at ∿ 20 eV are the lead $5d_{3/2}$ and $5d_{5/2}$ levels; the tellurium 4d levels are at about 40 eV binding energy.

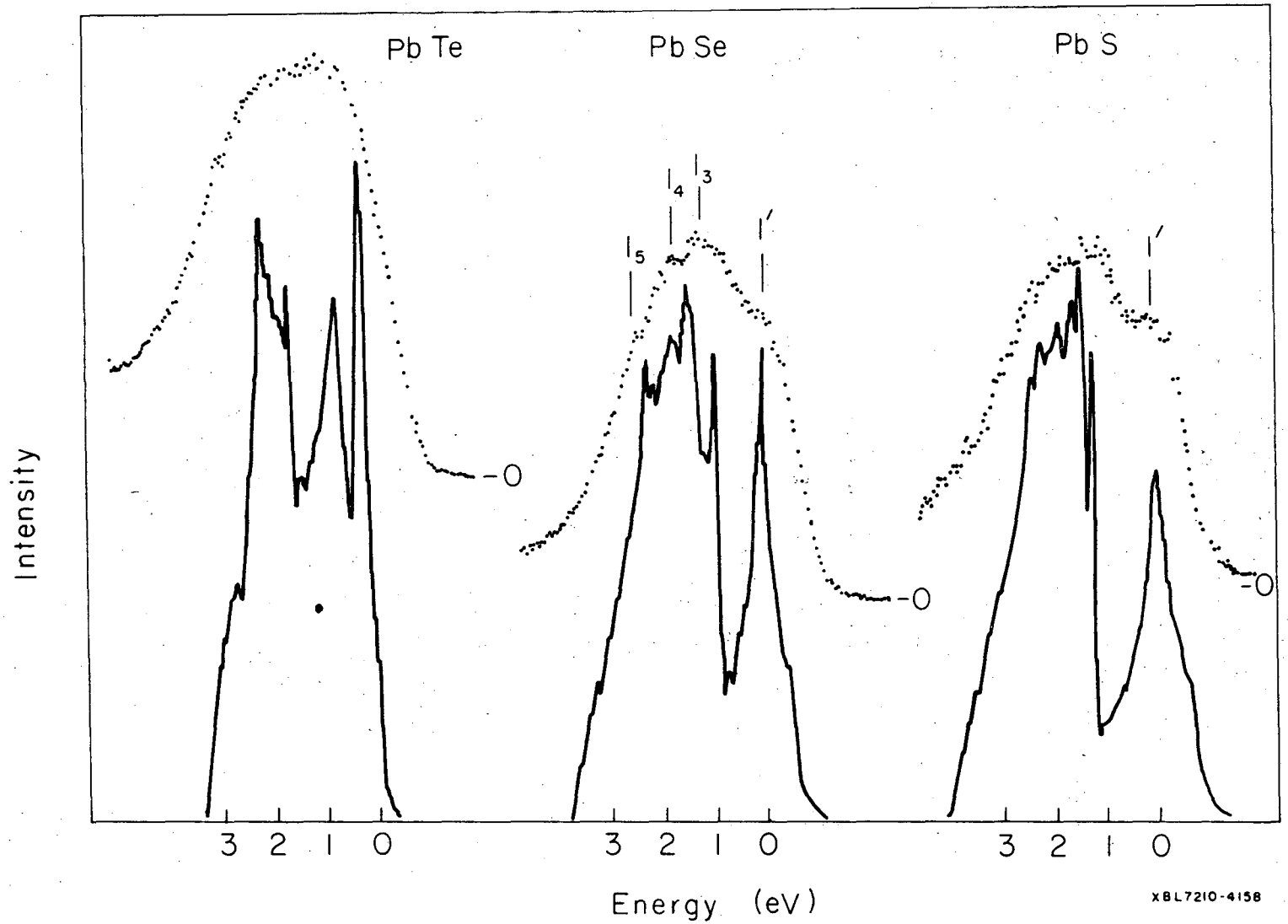

XBL7210-4158

Fig. 2. EPM densities of states[5,6] compared with the shape of the (1-1') peaks in the valence bands of the lead salts (relative energy scale).

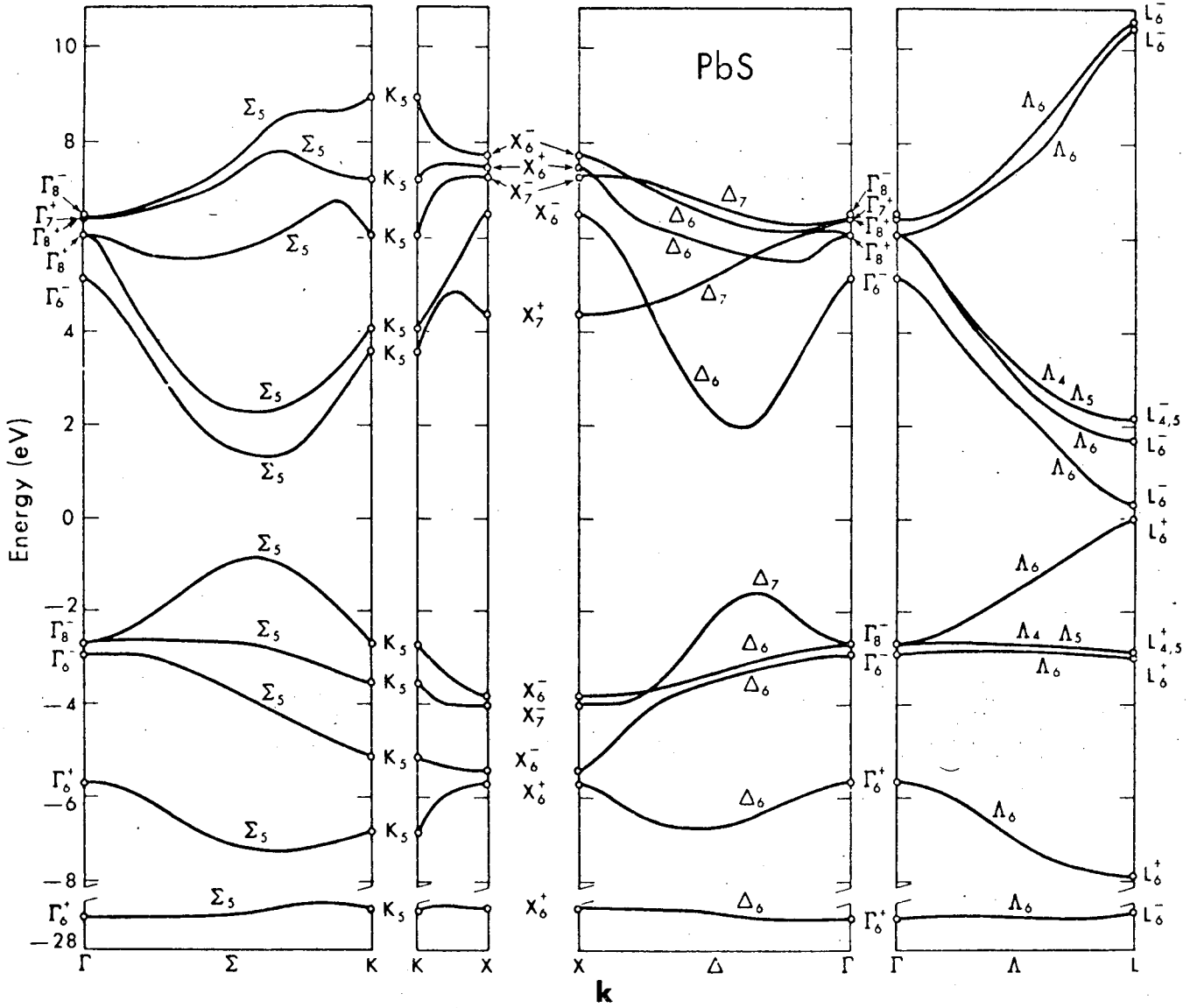

Fig. 3a. Band structure of PbS calculated by the Empirical Pseudopotential Method.[6]

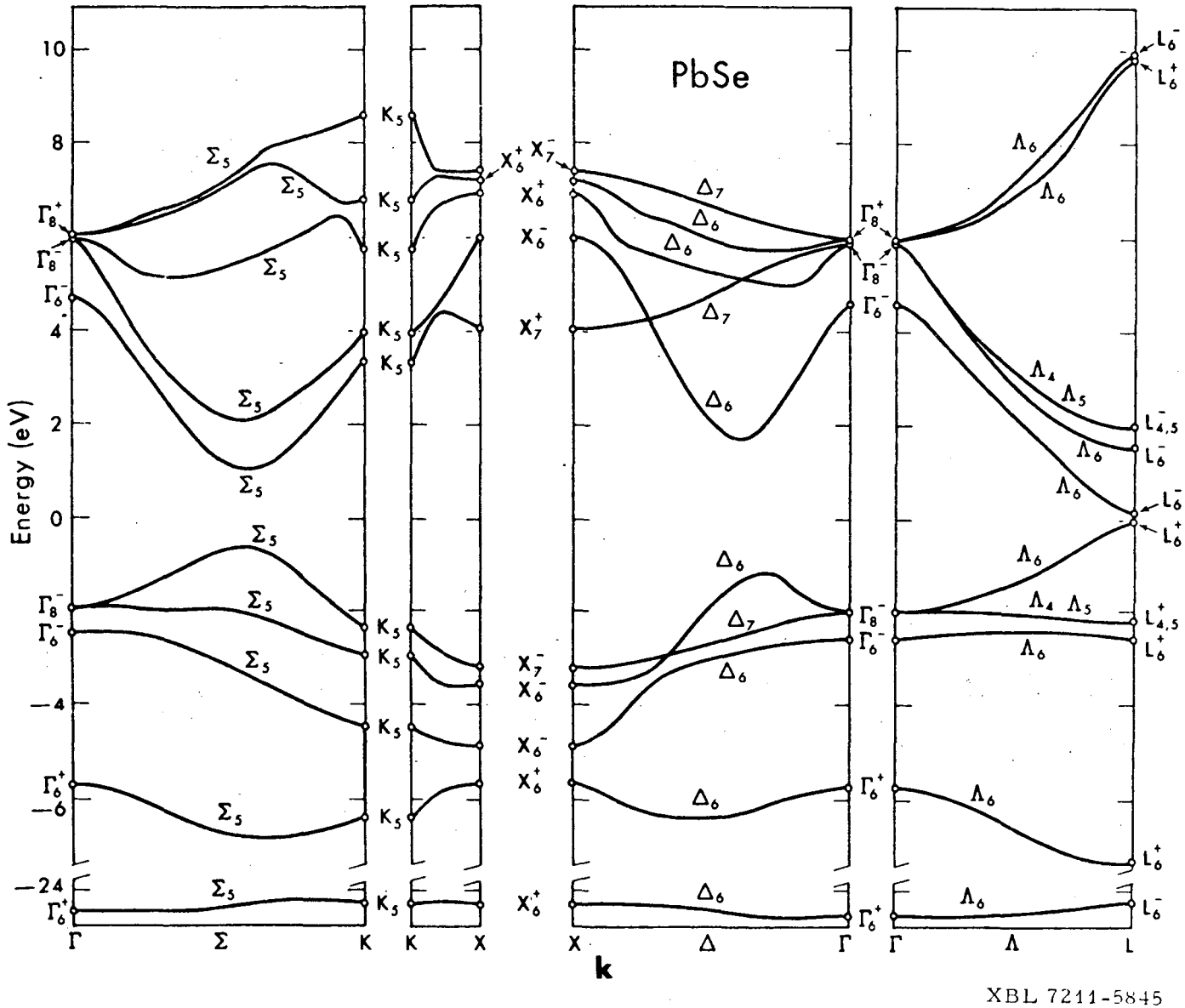

Fig. 3b. Band structure of PbSe calculated by the Empirical Pseudopotential Method.[6]

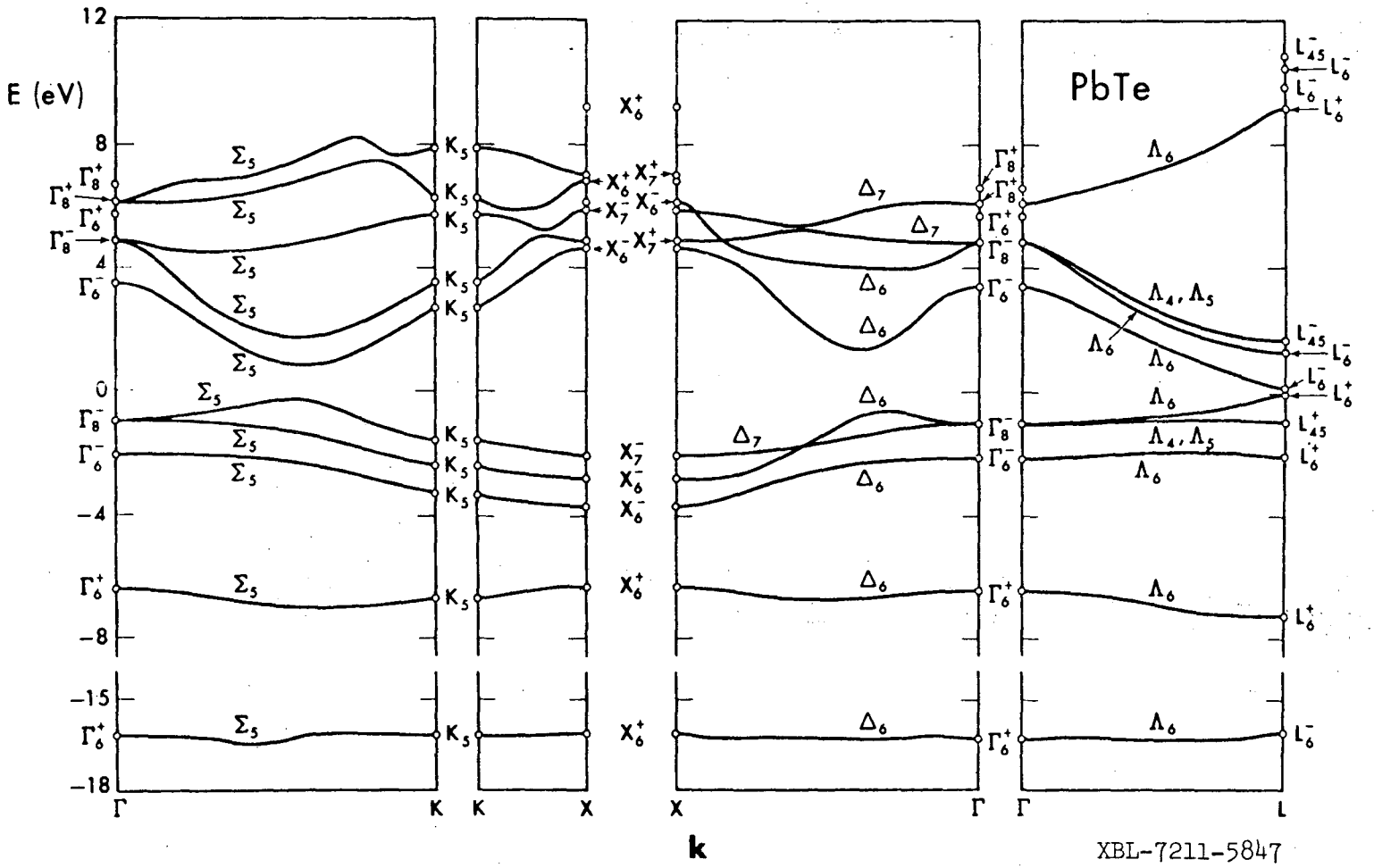

Fig. 3c. Band structure of PbTe calculated by the Empirical Pseudopotential Method.[5]

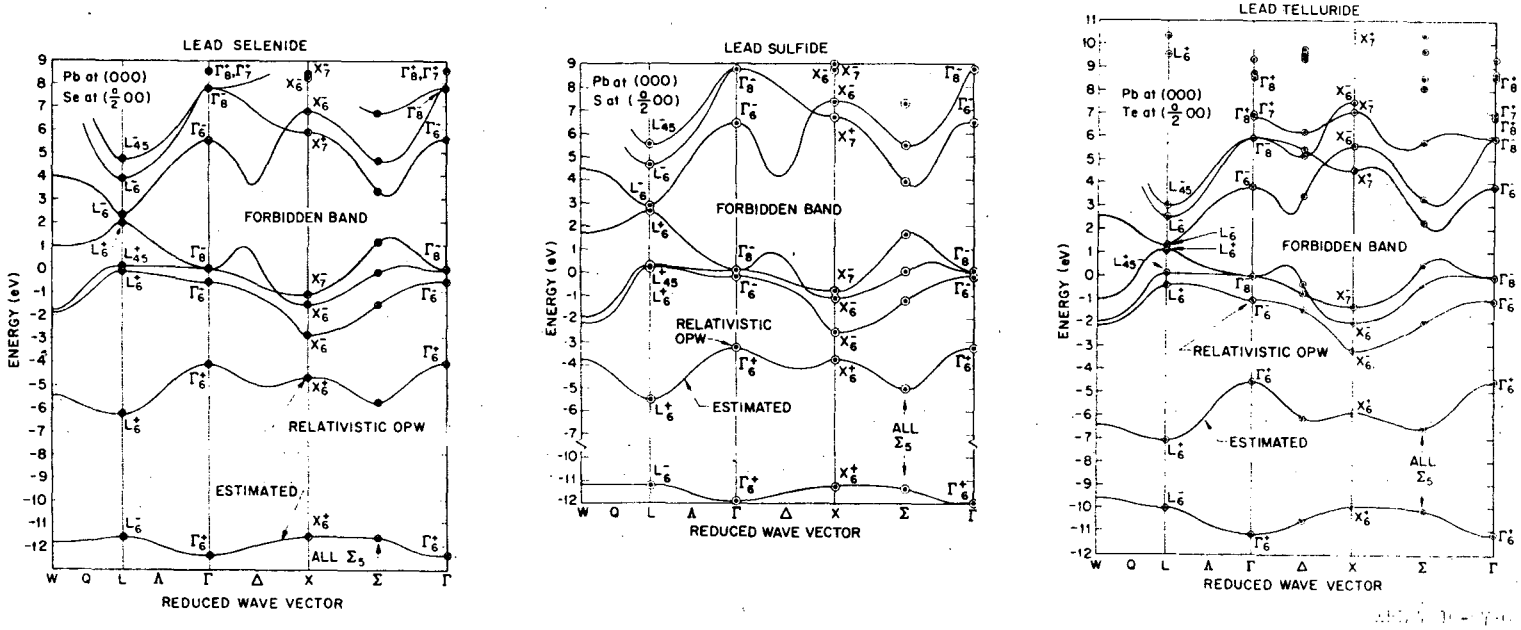

Fig. 4. Band structures of the lead salts calculated by the OPW method.[7]

SECTION XII. CHARGING OF INSULATORS AND SEMICONDUCTORS

Charging of insulating samples is an effect that is as yet not under control in the field of x-ray photoemission spectroscopy. The x-rays striking the sample produce photoelectrons which in turn excite secondary electrons. Many electrons are energetic enough to escape the sample at its surface. If these electrons are not replaced charge neutrality no longer exists and the sample becomes positively charged. The charged state is manifest by a shift of the XPS structure to lower kinetic energy. The binding energy is given by Eq. (3),

$$E_B = h\nu - E_{kin} - q\phi_{sp} - q\psi_{sa} \quad .$$

Charging produces a change in the Volta potential ψ_{sa}. Charging can be considered under control when the Volta potential can be either measured or nulled.

The Volta potential is a function of the photoelectron and secondary electron emission current I_e and the neutralizing electron current I_n which usually originates from ground or ambient space charge. Initially $I_e > I_n$ in insulators and the sample charges positively until I_e decreases or I_n increases such that $I_e = I_n$. I_n and I_e are a function of sample conductivity, mobility, photoconductivity, surface states, space charge layers, trapping centers, recombination centers, and contacts. These parameters are in turn sensitive to the geometry of the experiment and therefore different types of spectrometers and different sample configurations within each type of spectrometer can yield different results for the same substance. The experiments reported in this

section were performed on an HP 5950A ESCA photoelectron spectrometer. For other instruments the sources of I_n will not be the same and different charging behavior will be observed.

The HP 5950A produces a focussed beam of x-rays which has a cross sectional area of 1 mm × 5 mm where it strikes the sample surface. Most of the samples studied were single crystals of approximately 12 mm diameter. The x-ray beam irradiates the center of the sample surface. The perimeter of the sample is not hit by x-rays. Figure 1 illustrates the experimental arrangement.

Volta potentials (charging shifts) of over 40 volts were observed. Figure 2 is a plot of charging versus band gap for 26 semiconductors and insulators. The charging shift was determined by evaporating a thin film (probably islands) of gold onto each sample surface and referencing a core level of the sample to the Au $4f_{7/2}$ line of known binding energy (84.00 ± 0.01 eV). The difference between the binding energy of a core peak of the sample referenced to gold and the absolute binding energy of a clean surface measured from the spectrometer voltages yields the Volta potential (charging) plotted in Fig. 2. The difference in energy between the gold referenced binding energy and absolute binding energy of the gold covered surface measured from the spectrometer voltages is plotted versus band gap in Fig. 3. The gold covered the sample surface and the spectrometer-sample contact.

The general trend in Figs. 2 and 3 is for charging to increase with band gap. The materials with small band gaps charge to values near or less than the band gap, and those with large band gaps charge to values near or greater than the band gap. In most cases the application of the thin surface film of gold reduced the charging (compare Figs. 2 and 3) indicating a lower resistance path to ground.

The unusually high charging in ZnSe is probably attributable to the photovoltaic effect. Exceptionally high photovoltages have been reported for ZnSe single crystals.[1] In some cases photovoltages of several hundred volts were observed.[1] It is believed the effect results from the addition of photovoltages from many individual junctions which are associated with stacking faults in the single crystal.[1] The XPS charging shift of 21.6 eV on cleaved ZnSe decreased to 1.2 eV after evaporating the Au reference layer onto the surface.

The crystals charge until I_n equals I_e. I_e decreases and/or I_n increases as ψ_{sa} increases. In the case of single crystals the region from which the photoemission spectrum originates is bathed in x-rays and the induced photoconductivity allows uniform charging over the photoemitting surface. In the case of powders contact resistance between crystallites can broaden lines as a result of non-uniform charging.

The fact that charging follows the band gap so closely suggests that a mechanism such as breakdown as a consequence of the tunnel effect (Zener breakdown) switches on a higher I_n at Volta potentials near the band gap value. This mechanism is especially likely in the materials with thin depletion layers (high carrier concentrations). The depletion layer in this case is the region between the irradiated and non-irradiated portion of the sample. As the depletion layer gets thicker (carrier concentration decreases) one expects the charging to increase above the band gap value. We see this behavior in the alkali halides. Breakdown by carrier multiplication (avalanche breakdown) would tend to limit this increased charging effect. Surface conductivity must not be forgotten and may contribute significantly to I_n in those cases where the charging

is less than the band gap. Bulk conductivity in the small band gap materials can also limit the charging to values less than the band gap. Finally it should be mentioned that non-ohmic contact between sample and spectrometer adds another degree of complexity to the charging problem and should be avoided.

At present we correct for charging by subtracting the Volta potential from our measurements. Definite broadening occurs in insulating powders and possibly even in single crystals. Nulling the Volta potential by neutralizing the sample with low energy electrons appears to offer a solution to some of these problems.

REFERENCES

1. R. H. Bube, Photoconductivity of Solids (John Wiley and Sons, Inc., New York, 1960).

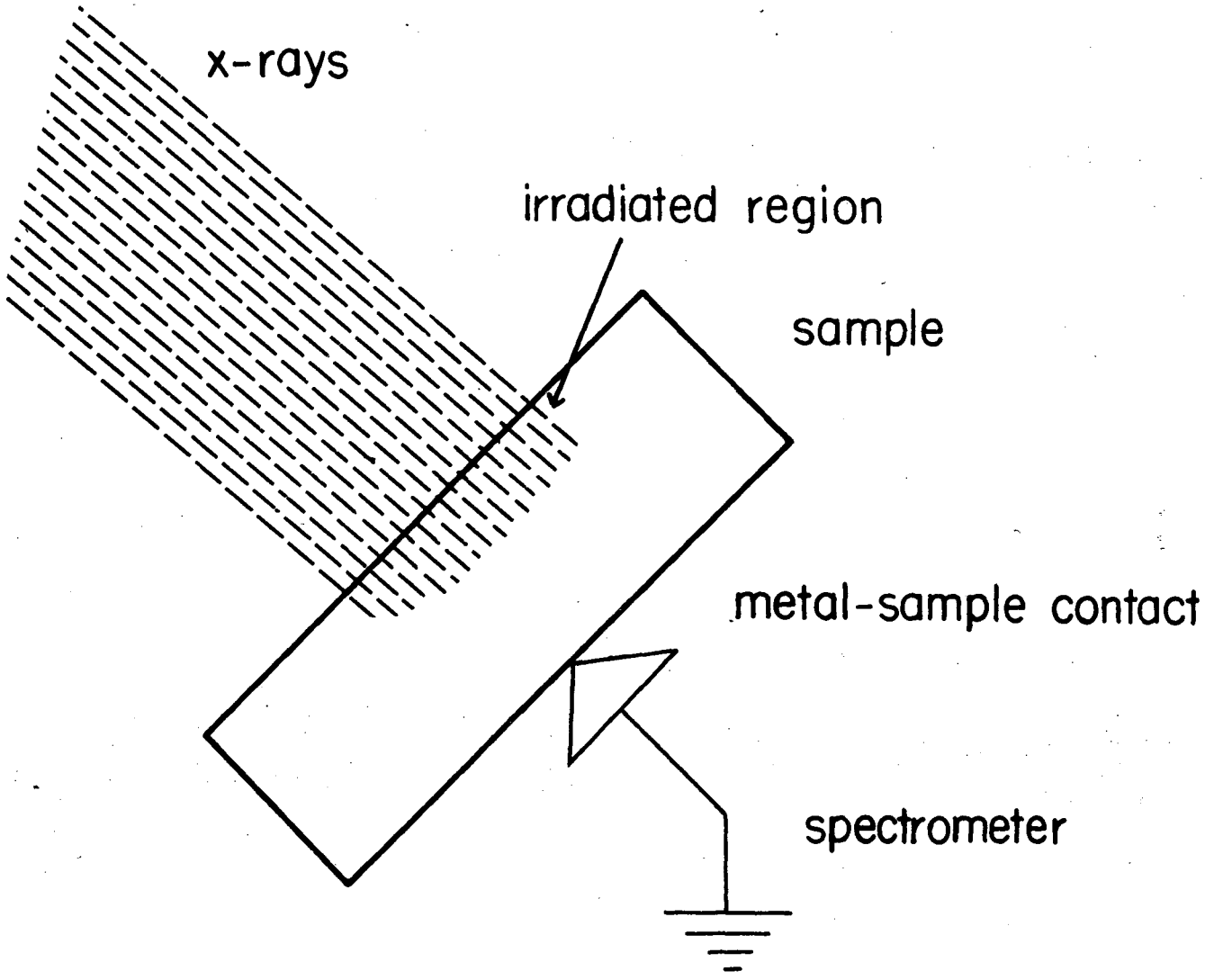

XBL 7211-7404

Fig. 1. The resistance between ground and the sample depends upon surface resistance, bulk resistance and the spectrometer-sample contact resistance. Photoconductivity induced in the irradiated region tends to neutralize nonuniform charging.

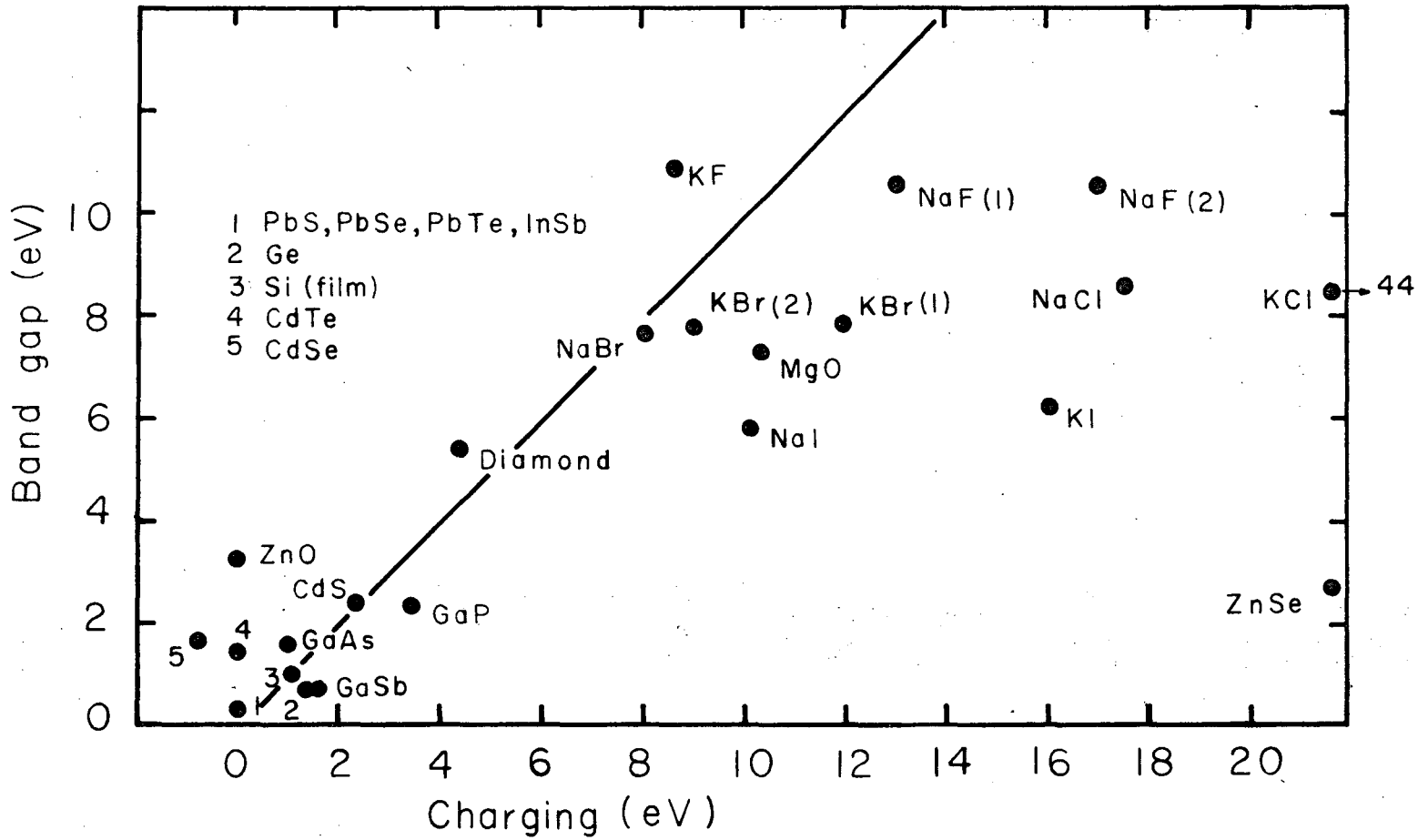

XBL 7211-7406

Fig. 2. Volta potential ψ_{sa} (charging) of cleaved sample plotted versus the band gap.

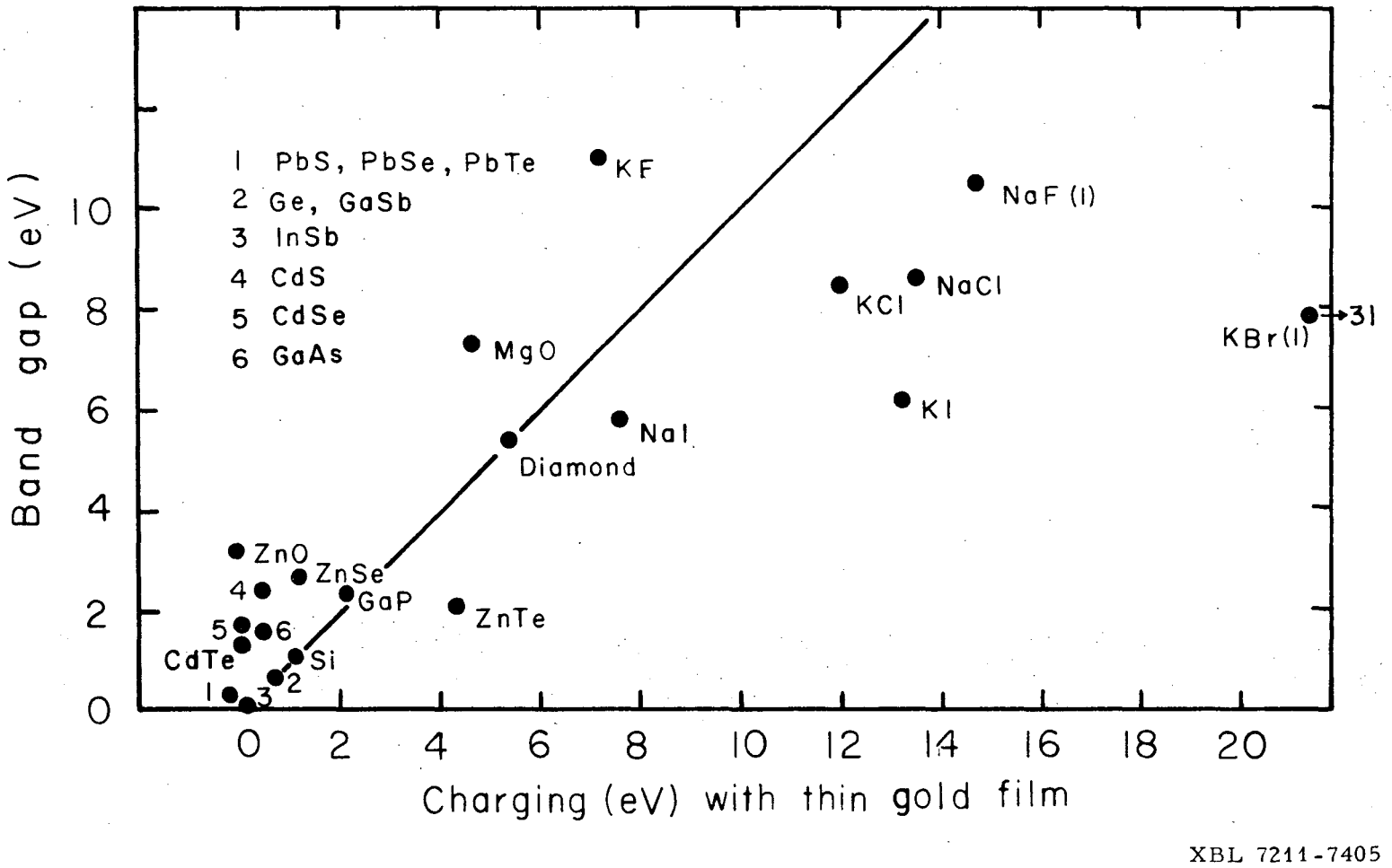

XBL 7211-7405

Fig. 3. Volta potential ψ_{sa} (charging) versus band gap of cleaved samples onto which a thin layer of gold has been evaporated.

SECTION XIII. CHARACTERISTIC ENERGY LOSS SATELLITES OF Al, Cd, In, Sn, Sb, AND Te

During the XPS process the number of primary photoelectrons which escape from the solid is much smaller than the number of escaping secondary electrons (see Sec. II). As long as the secondary electron emission is a relatively smooth function of kinetic energy, it can be subtracted from the spectrum as background (cascade background). However there are discrete energy loss mechanisms which produce structure to the low kinetic energy side of primary electron peaks. This structure, which is mainly composed of electrons that have excited plasmons, will be the subject of this section.

An electron passing through a solid can couple through its longitudinal electric field to electron density fluctuations (plasmons). Many plasmon resonance energies have been determined by measuring the energy losses of electrons reflected from solid surfaces or transmitted through thin films.[1] Almost all structure reported here can be attributed to this type of plasmon energy loss.

For a process such as XPS, many-body calculations[2] predict structure resulting from plasmons coupled to core electrons. This type of plasmon excitation is intrinsic to the photoemission of a core electron while being coupled to its surrounding plasma rather than a free electron passing through a plasma. The total spectral density in this model consists of a sharp quasiparticle peak with a broader plasmon satellite structure to higher binding energy. The plasmon structure is predicted to be 50 to 100% as intense as the quasiparticle level and the total spectral density follows a sum rule such that it is centered about

the Hartree-Fock orbital energy. The quasiparticle peak is shifted from the Hartree-Fock value to higher kinetic energies by polarization about the final state hole (relaxation) and the plasmon structure compensates for this shift. In the results reported here structure resulting from this type of plasmon resonance is not distinguishable from that which corresponds to a free electron passing through a plasma.

In Sec. A the results for Al are discussed and in Sec. B those for Ag, Cd, In, Sn, Sb, and Te are discussed.

A. Aluminum

The x-ray photoemission spectrum of the Al 2s core level is shown in Fig. 1a. The high binding energy shoulder on the Al 2s metal peak is attributed to surface oxide. Spaced at even intervals of 15.7(2) eV are five orders of bulk plasmon losses P_1 through P_5. The electron reflection measurements of Powell and Swan yielded a value of 15.3 eV.[3] The sum of the area under the five loss peaks is greater than 75% that of the Al 2s metal peak. The absence of the surface plasmon peak at 10.4 eV is consistent with the surface being slightly oxidized.[3] It should be mentioned that in XPS experiments plasmons of all scattering angles are observed and thus dispersion results in peaks which are asymmetrically broadened to higher binding energy and thus shifted to slightly higher binding energy than for the case where only zero scattering angle is considered. The reflection results of Powell, Swan, and Robins should compare well with XPS results because the geometry[4] of their experiments should yield similar effects of dispersion.

We were unable to keep Al clean in the HV mode of operation (see Sec. III). A surface oxide formed immediately. Preliminary results for

Al obtained in the UHV mode of operation (see Sec. XVI) are shown in Fig. 1b for a single crystal which was annealed in situ and argon etched. The surface plasmon labeled S is now present and the aluminum oxide peak is not. There was some Sb and Ta surface contamination in this particular case. Eight bulk loss peaks associated with the Al 2s level are clearly distinguishable (P_6 to P_8 are not shown). The peak parameters are given in Table 1. The total area of the loss peaks is greater than 175% the area of the zero loss peaks.

B. Plasmon Losses of the 4d5s5p Elements Ag to Te

In some materials interband and intraband transitions lying near in energy to the calculated free electron plasma resonance energy $\hbar\omega_p$ result in a shift of the measured plasmon energy from this value. These plasmons are termed hybrid resonances and the dielectric theory of energy losses is used to treat these somewhat more complicated resonances.[1] Effects of this type are observed for the elements reported here.

The XPS plasmon structures for Ag to Te are shown in Figs. 2 to 11. The peak parameters are given in Tables 2 to 7 and summarized in Table 8. The experimental procedure is given in Sec. IV where the valence-band spectra for these elements are discussed.

1. Silver

Silver gave the weakest loss structure of all the elements reported here (Fig. 2). However, it had the narrowest loss peak (1 eV). The bulk plasmon resonance energy is shifted from the free electron value of 9 eV to 3.78 eV by an interband transition ($4d \rightarrow E_F$) that begins at 3.9 eV.[1] In the XPS valence-band spectrum of silver (Fig. 12) the low binding energy edge of the 4d band is just 3.9 eV below the Fermi level E_F which is consistent with the above interpretation. This separation between d band edge and Fermi level is denoted ΔE_{IB} in Fig. 13.

The loss at 3.9 eV is assigned to the unresolved bulk and surface plasmon losses of Ag which have been measured by optical experiments to be at 3.6 and 3.78 eV respectively.[1] The width of the bulk loss has been determined optically to be 0.08 eV FWHM.[5] The 1 eV width of the loss reported here is obviously determined by the width of the primary 3d photoelectron energy distribution (1 eV). Optical reflectivity data[6] indicates that the loss structure at 7.8 eV is also attributable to conduction electron oscillations. The peaks at 18.8 and 24.9 eV are unexplained. Peaks at 17.2 and 25.0 eV have been observed in reflection electron loss experiments.[7]

2. Cadmium

Four loss peaks at 7, 9.3, 13.9, and 19 eV were observed. We interpret the peaks at 7 and 9.3 eV as the surface and bulk loss respectively. Electron reflection measurements[8] did not resolve the bulk and surface loss peaks. Powell[8] assigned structure at 7.8 eV to an anomalously intense surface plasmon loss and a weaker peak at 15.2 eV to the bulk loss. Light emission from electron bombarded Cd yielded a sharp (0.8 eV), intense peak at 9.1 eV.[9] This probably results from the decay of the bulk plasmon. Surface plasmons have a very small probability relative to bulk plasmons of decaying by emitting light.[9] The systematics illustrated in Fig. 13 also support the interpretation of the 7 and 9.3 eV peaks. The peaks at 13.9 and 19 eV are unexplained. Peaks at 15.2 and 23.4 eV were observed in electron reflection measurements.[8]

3. Indium, Tin, Antimony, and Tellurium

Indium exhibits four loss peaks at 8.6, 11.7, 19.8, and 23 eV. The electron reflection spectrum yields peaks at 8.7, 11.3, 20, and 22.7 eV.[10] The first results from a surface plasmon loss, the second a bulk plasmon loss, the third is from electrons that have suffered both a bulk and surface loss, and the fourth and fifth are from electrons that suffer two and three bulk losses. The results for Sn, Sb, and Te can be also interpreted solely in terms of bulk and surface losses. See Table 8 for assignments and the corresponding electron reflection results.

4. Systematics

The systematics of the plasmon structure for Ag to Te is illustrated in Fig. 13. The interband transition ($4d \rightarrow E_F$) energy ΔE_{IB} is a strong function of atomic number and varies from 3.9 eV in Ag to 39 eV in Te. Figure IV-2 shows the behavior of the s-like and p-like valence bands. The free electron plasmon energy,

$$\hbar\omega_p = \hbar \left(\frac{4\pi ne^2}{m} \right)^{1/2}$$

varies smoothly from 9 eV in Ag where N, the number of valence electrons, is 1 to 15.6 eV in Te where N is 6. n is the density of the electron plasma and m is the free electron mass. The measured bulk plasmon energy ΔE_B rises smoothly from 3.9 eV in Ag to 17.6 eV in Te. The shift of ΔE_B from $\hbar\omega$ decreases going from Ag to Sn, crosses between Sn and Sb thus changing sign, and then slowly increases. The surface plasmon energy ΔE_S follows ΔE_B according to,

$$\Delta E_B/\Delta E_S = (\sqrt{2} \pm 0.05)$$

which is just the relationship expected for free electron behavior. The intensity (area) relative to the parent, zero-loss peak for the bulk plasmon (I_B) and surface plasmon (I_S) are shown as a histogram in Fig. 13. The intensity I_B of the bulk plasmon loss increases smoothly from a minimum of 2% in Ag to a value of about 28% in Sn, Sb, and Te. The surface plasmon shows more varied behavior. I_S is of the order of 5% for all cases observed. This behavior is not unexpected since I_S is much more sensitive to surface conditions than I_B.[3]

For Ag and Cd where interband transitions play an important role the characteristic loss structure cannot be explained simply by combinations of surface and bulk losses.

C. Conclusions

The XPS characteristic loss structure of Ag to Te can be almost entirely accounted for by excitations similar to those observed in electron reflection experiments. Most of the structure can be assigned to bulk and surface plasmon excitations. The resolution of the bulk and surface plasmons in Cd explains the electron reflection anomaly and allows assignment of the optical plasmon de-excitation results. The bulk plasmon loss intensity and energy are seen to behave systematically from Ag to Te. The surface loss energies were found to be $(\sqrt{2}/2)$ that of the respective bulk losses.

REFERENCES

1. H. Raether, Springer Tracts in Mod. Phys. 38, 84 (1965).

2. B. I. Lundqvist, Phys. Kondens. Materie. 6, 193 (1967); 6, 206 (1967); 7, 117 (1968); B. I. Lundqvist and V. Samathiyakanit, Phys. Kondens. Materie. 9, 231 (1969); B. I. Lundqvist, Phys. Kondens. Materie. 9, 236 (1969); Lars Hedin, Bengt Lundqvist, and Stig Lundqvist, in Proc. 3rd Int. Mat. Res. Symp., Electronic Density of States, Nat. Bur. Stand. (U.S.), Spec. Pub. 323 (1971).

3. C. J. Powell and J. B. Swan, Phys. Rev. 118, 640 (1960).

4. C. J. Powell, J. L. Robin, and J. B. Swan, Phys. Rev. 110, 657 (1958); C. J. Powell and J. B. Swan, Phys. Rev. 115, 869 (1959).

5. J. Daniels, Z. Phys. 203, 235 (1967).

6. H. Ehrenreich and H. R. Phillipp, Phys. Rev. 128, 1622 (1962).

7. J. L. Robins, Proc. Phys. Soc. (London) 78, 1177 (1961).

8. C. J. Powell, Proc. Phys. Soc. 76, 593 (1960).

9. R. J. Herickhoff, E. T. Arakawa, and R. D. Birkhoff, Phys. Rev. 137, A1433 (1965).

10. J. L. Robins, Proc. Phys. Soc. (London) 79, 119 (1962).

Table 1. Al 2s Characteristic Energy Losses

Peak	Al 2s	S	P_1	P_2	P_3	P_4	P_5
Binding energy (eV)	118.4(2)	128.8(2)	134.0(2)	149.8(4)	165.2(4)	180.6(4)	196.1(6)
Separation from Al 2s (eV)	--	10.4	15.6	31.4	46.8	62.2	77.7
Bulk losses (eV)	--	--	15.6	15.8	15.4	15.4	15.5
Relative intensity	100	14	74	56	24	6.8	--
FWHM (eV)	1.1	3.8	3.4	6.1	6.2	4.7	--

Table 2. Ag $3d_{3/2}$ and Ag $3d_{5/2}$ Characteristic Energy Losses

Peak	$3d_{5/2}$	P_1	$3d_{3/2}$	P_2	P_3	P_4	P_5*	P_6
Binding energy (eV)	368.4(1)	372.3(1)	374.5(1)	378.4(1)	382.3(5)	387.2(2)	393.2(5)	399.4(5)
Separation from $3d_{5/2}$ (eV)	0	3.9	6.1	10	13.9	18.8	24.8	31.0
Separation from $3d_{3/2}$ (eV)	--	--	0	3.9	7.8	12.7	18.7	24.9
Intensity relative to $3d_{5/2}$	100	2.5	78	1.2	1.5	0.3	1.8	1.0
Intensity relative to $3d_{3/2}$	--	--	100	1.6	1.9	0.4	2.2	1.2
FWHM (eV)	1.0	1.0	1.0	1.0	2.5	1.5	4.7	3.5

*P_5 is superposition of 18.7 eV loss and 24.8 eV loss. Intensities of P_4 and P_6 indicate relative intensities of two components of P_5.

Table 3. Cd 4d Characteristic Energy Losses

Peak	4d	P_1	P_2	P_3	P_4
Binding energy (eV)	11.0(1)	18.0(5)	20.3(5)	24.9(5)	30.0(5)
Separation from 4d (eV)	0	7.0	9.3	13.9	19
Relative intensity	100	4.2	11.5	2.3	2.2
FWHM (eV)	1.8	1.8	2.5	∿ 3	∿ 3

Cd $3d_{3/2}$ and Cd $3d_{5/2}$ Characteristic Energy Losses

Peak	$3d_{5/2}$	$3d_{3/2}$	P_1	P_2	P_3	P_4	P_5
Binding energy (eV)	405.4(1)	412.1(1)	414.7(2)	418.8(2)	421.4(2)	425.9(5)	432.6(5)
Separation from $3d_{5/2}$ (eV)	0	6.7	9.3	13.4	16.0	20.5	27.2
Separation from $3d_{3/2}$ (eV)	--	0	2.6	6.7	9.3	13.8	20.5
Intensity relative to $3d_{5/2}$	100	73	14	6.7	8	4.7	3.3
Intensity relative to $3d_{3/2}$	--	100	19	9	11	6.4	4.5
FWHM	1.4	1.4	1.6	2.1	2.2	5	5

Table 4. In 4d Characteristic Energy Losses

Peak	4d	P_1	P_2	P_3	P_4
Binding energy (eV)	17.1(1)	25.7(3)	28.8(3)	36.9(5)	40.1(5)
Separation from 4d (eV)	0	8.6	11.7	19.8	23.0
Relative intensity	100	6	23	4	5
FWHM (eV)	1.7	2.5	2.6	4	4

In $3d_{3/2}$ and In $3d_{5/2}$ Characteristic Energy Losses

Peak	$3d_{5/2}$	$3d_{3/2}$	P_1	P_2	P_3	P_4	P_5	P_6
Binding energy (eV)	444.2(2)	451.7(2)	456.0(2)	460.0(2)	463.6(2)	467.5(5)	475(1)	487(1)
Separation from $3d_{5/2}$ (eV)	0	7.5	11.8	15.8	19.4	23.3	30.8	42.3
Separation from $3d_{3/2}$ (eV)	--	0	4.3	8.3	11.9	15.8	23.3	34.8
Intensity relative to $3d_{5/2}$	100	63	16	1	19	1	2.6	1
Intensity relative to $3d_{3/2}$	--	100	25	1.7	29	1.7	4.2	1.7
FWHM (eV)	1.3	1.3	1.5	1.5	2.0	1.5	~ 3	~ 3

Table 5. Sn 4d Characteristic Energy Losses

Peak	4d	P_1	P_2	P_3	P_4
Binding energy (eV)	24.1(1)	34.4(2)	38.2(2)	52.1(5)	65.8(5)
Separation from 4d (eV)	0	10.3	14.1	28.0	41.7
Relative intensity	100	10	30	9	2.2
FWHM (eV)	1.8	3.5	4	5	5

Sn $3d_{3/2}$ and Sn $3d_{5/2}$ Characteristic Energy Losses

Peak	$3d_{5/2}$	$3d_{3/2}$	P_1	P_2	P_3	P_4	P_5	P_6
Binding energy (eV)	485.0(2)	493.4(2)	499.4(2)	507.6(2)	513.0(5)	522(1)	529(1)	536(2)
Separation from $3d_{5/2}$ (eV)	0	8.4	14.4	19.6	28	37	44	51
Separation from $3d_{3/2}$ (eV)	--	0	6.0	14.2	19.6	28.6	35.6	42.6
Intensity relative to $3d_{5/2}$	100	76	27	24	13	8	0.3	0.3
Intensity relative to $3d_{3/2}$	--	100	36	31	17	10.5	0.4	0.4
FWHM (eV)	1.3	1.3	2.5	2.5	~ 5	~ 5	--	--

Table 6. Sn 4d Characteristic Energy Losses

Peak	4d	P_1	P_2	P_3
Binding energy (eV)	32.8(1)	44(1)	48.6(5)	64.5(2.0)
Separation from 4d (eV)	0	11.2	15.8	31.7
Relative intensity	100	6.7	27	9.9
FWHM (eV)	2	4	5.5	6

Sb $3d_{3/2}$ and Sb $3d_{5/2}$ Characteristic Energy Losses

Peak	$3d_{5/2}$	$3d_{3/2}$	P_1	P_2	P_3	P_4
Binding energy (eV)	526.5(2)	537.5(2)	542.5(2)	553.5(2)	562(2)	571(2)
Separation from $3d_{5/2}$ (eV)	0	11	16	27	35.5	44.5
Separation from $3d_{3/2}$ (eV)	--	0	5	16	24.5	33.5
Intensity relative to $3d_{5/2}$	100	77	30	25	∿ 2	∿ 2
Intensity relative to $3d_{3/2}$	--	100	39	32	∿ 3	∿ 3
FWHM (eV)	1.0	1.0	2.0	2.0	--	--

Table 7. Te $3d_{3/2}$ and $3d_{5/2}$ Characteristic Energy Losses

Peak	$3d_{5/2}$	$3d_{3/2}$	P_1	P_2
Binding energy (eV)	572.5(2)	582.8(2)	590.1(4)	600.4(4)
Separation from $3d_{5/2}$ (eV)	0	10.3	17.6	27.9
Separation from $3d_{3/2}$ (eV)	--	0	7.3	17.6
Intensity relative to $3d_{5/2}$	100	68	18	25.2
Intensity relative to $3d_{3/2}$	--	100	27	37
FWHM (eV)	1.6	1.6	~ 5	~ 5

Table 8

	Energy (eV)			Intensity %			(FWHM of CEL / FWHM of zero loss peak)			CEL's from Literature	Ref.	Assignment	$\hbar\omega_p$	ΔE_{IB}
	$3d_{3/2}$	$3d_{5/2}$	4d	$3d_{3/2}$	$3d_{5/2}$	4d	$3d_{3/2}$	$3d_{5/2}$	4d					
Ag	3.9	3.9	--	1.6	2.5	--	1	1	--	3.78	1	Bulk	9	3.9
	7.8	r	--	1.9	r	--	2.5	r	--	7.3	7	--		
	18.7	18.8	--	∿0.5	0.3	--	∿1.5	1.5	--	17.2	7	--		
	24.9	24.8	--	1.2	∿1.5	--	3.5	∿3.5	--	25.0	7	--		
Cd	6.7	r	7.0	9	r	4.2	1.5	r	1	7.8	8	Surface		
	9.3	9.3	9.3	11	14	11.5	1.6	1.1	1.4	9.1	9	Bulk	11.3	10.0
	r	r	13.9	r	r	2.3	r	r	1.8	15.2	8	--		
	20.5	20.5	19	4.5	4.7	2.2	3.6	3.6	1.8	23.4	8	--		
In	8.3	r	8.6	1.7	r	6	1.2	r	1.5	8.7	10	Surface		
	11.9	11.8	11.7	29	16	23	1.5	1.2	1.5	11.3	10	Bulk	12.5	16.5
	r	r	19.8	r	r	4	r	r	2.3	20	10	Bulk + Surface		
	23.3	23.3	23.0	4.2	1	5	2.3	1.2	2.3	22.7	10	2 × Bulk		
	34.8	--	--	1.7	--	--	2.3	--	--	--		3 × Bulk		
Sn	r	r	10.3	r	r	10	r	r	1.9	10.4	8	Surface		
	14.2	14.4	14.1	31	27	30	1.9	1.9	2.2	14.1	8	Bulk	14.3	23.5
	28.6	28.0	28.0	10.5	13	9	3.8	3.8	2.8	27.8	8	2 × Bulk		
	42.6	44	41.7	0.4	0.3	2.2	--	--	2.8	41.9	8	3 × Bulk		

(continued)

Table 8. (continued)

	Energy (eV)			Intensity %			(FWHM of CEL / FWHM of zero loss peak)			CEL's from Literature	Ref.	Assignment	$\hbar\omega_p$	ΔE_{IB}
	$3d_{3/2}$	$3d_{5/2}$	4d	$3d_{3/2}$	$3d_{5/2}$	4d	$3d_{3/2}$	$3d_{5/2}$	4d					
Sb	r	r	11	r	r	6.7	r	r	2	11.3	8	Surface		
	16	16	15.8	32	30	27	2	2	2.8	15.9	8	Bulk	15	31.0
	33.5	35.5	31.7	3	2	9.9	--	--	3	32.5	8	2 × Bulk		
Te	17.6	17.6	--	37	18	--	3.1	3.1	--	17.9	10	Bulk	15.6	39.0

r - not resolved.

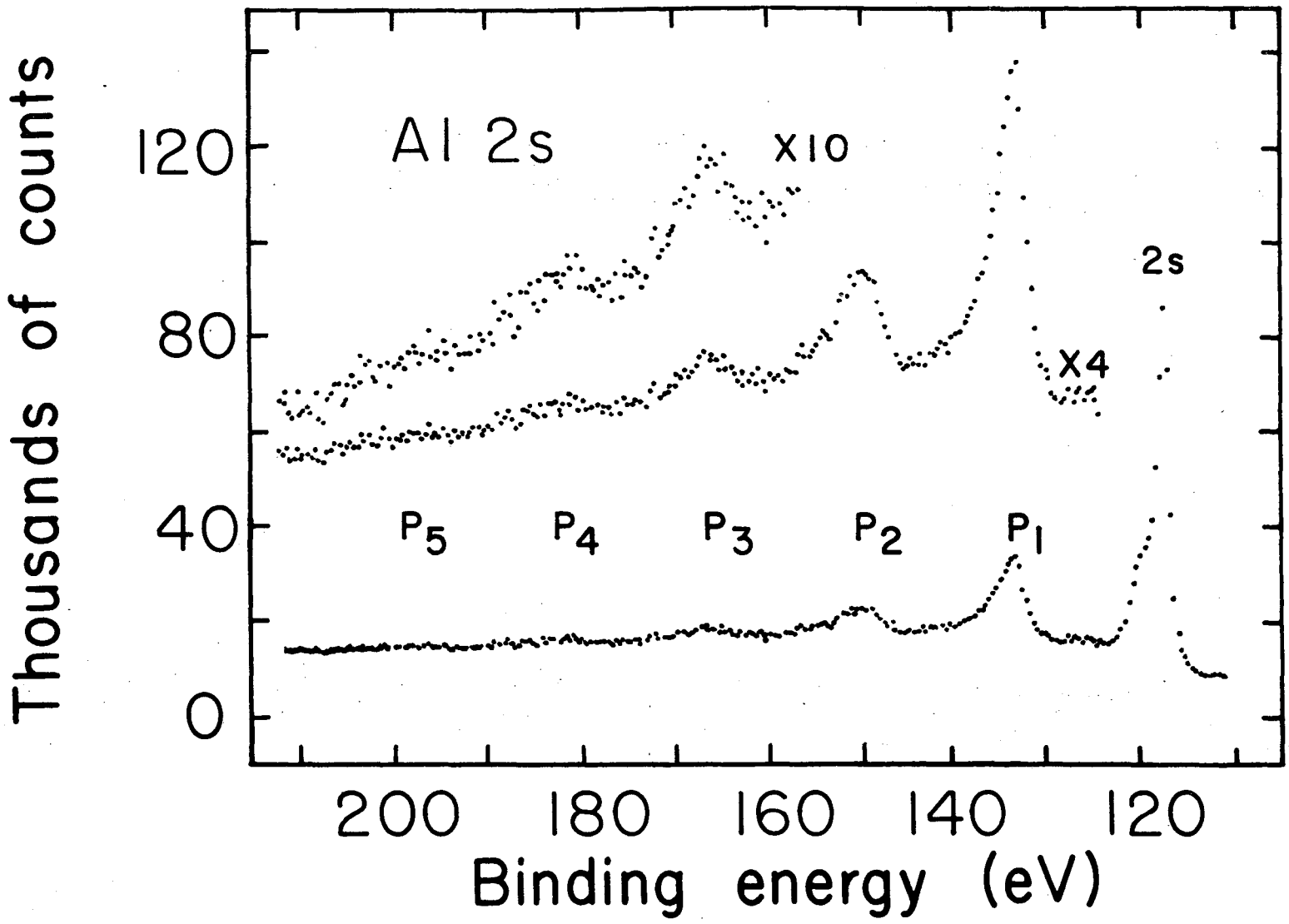

XBL 7211-7417

Fig. 1a. Photoemission spectrum of Al 2s level and its characteristic loss structure (HV).

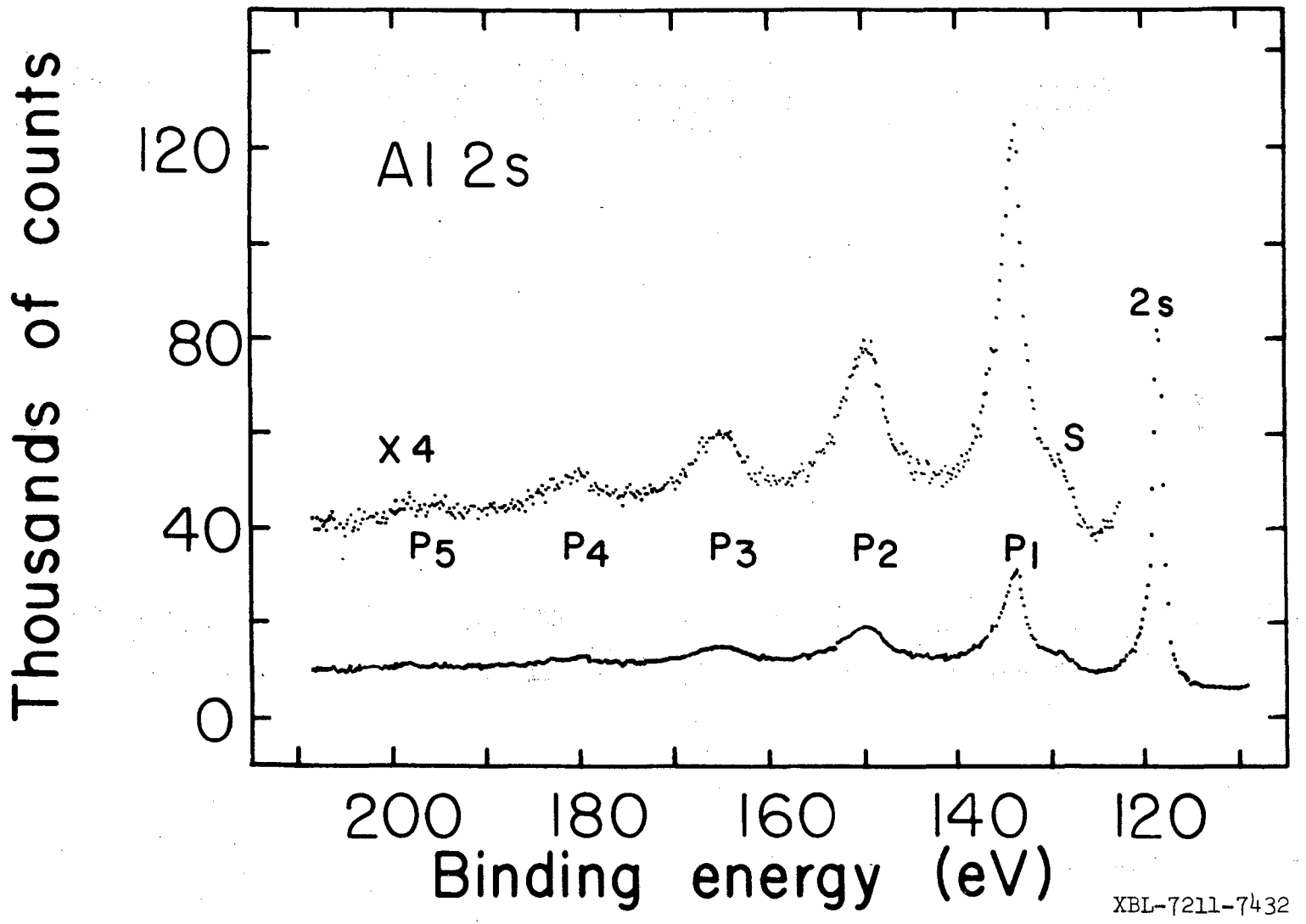

Fig. 1b. Photoemission spectrum of Al 2s level and its characteristic loss structure (UHV).

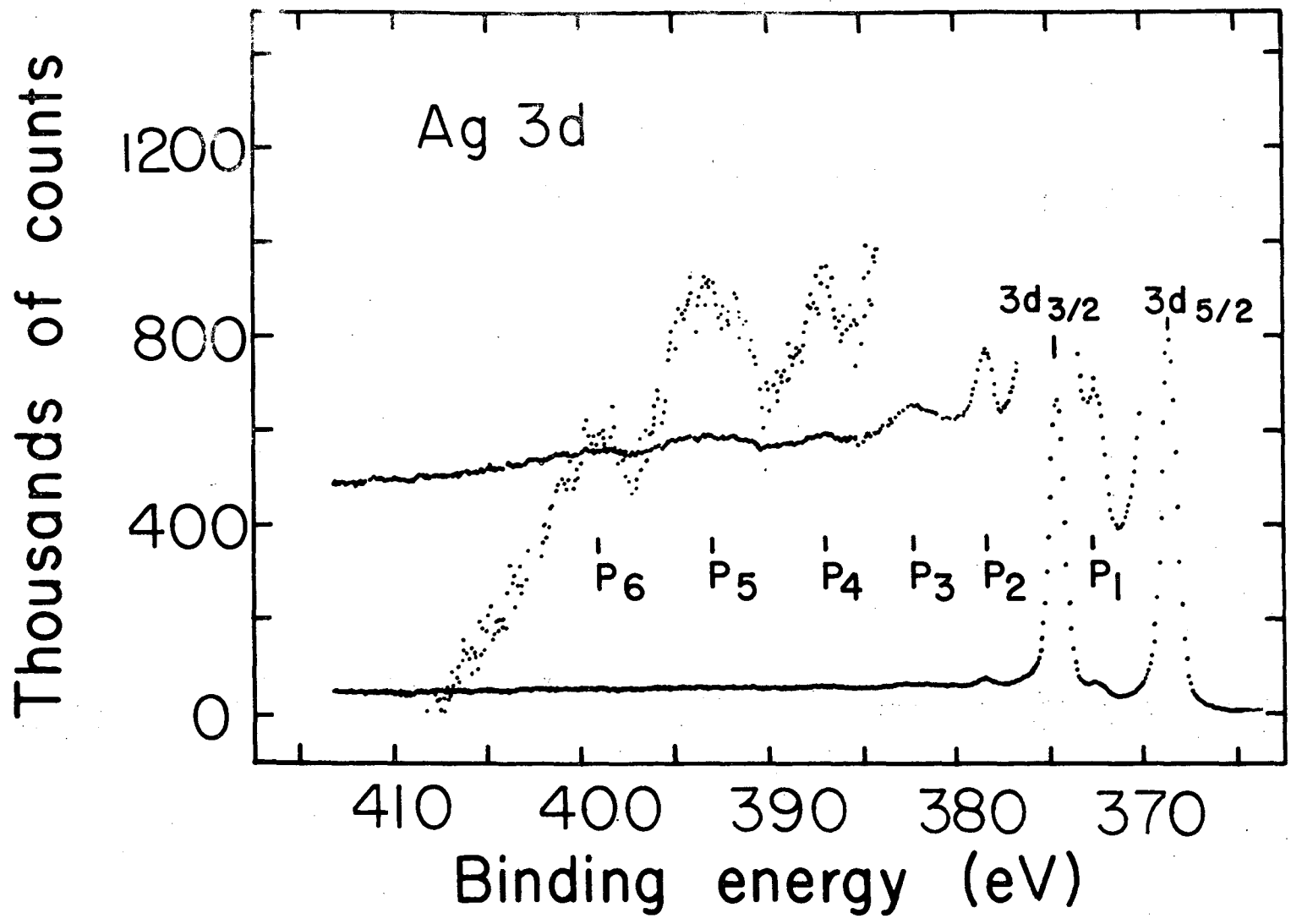

XBL 7211-7416

Fig. 2. Photoemission spectrum of Ag 3d level and its characteristic loss structure.

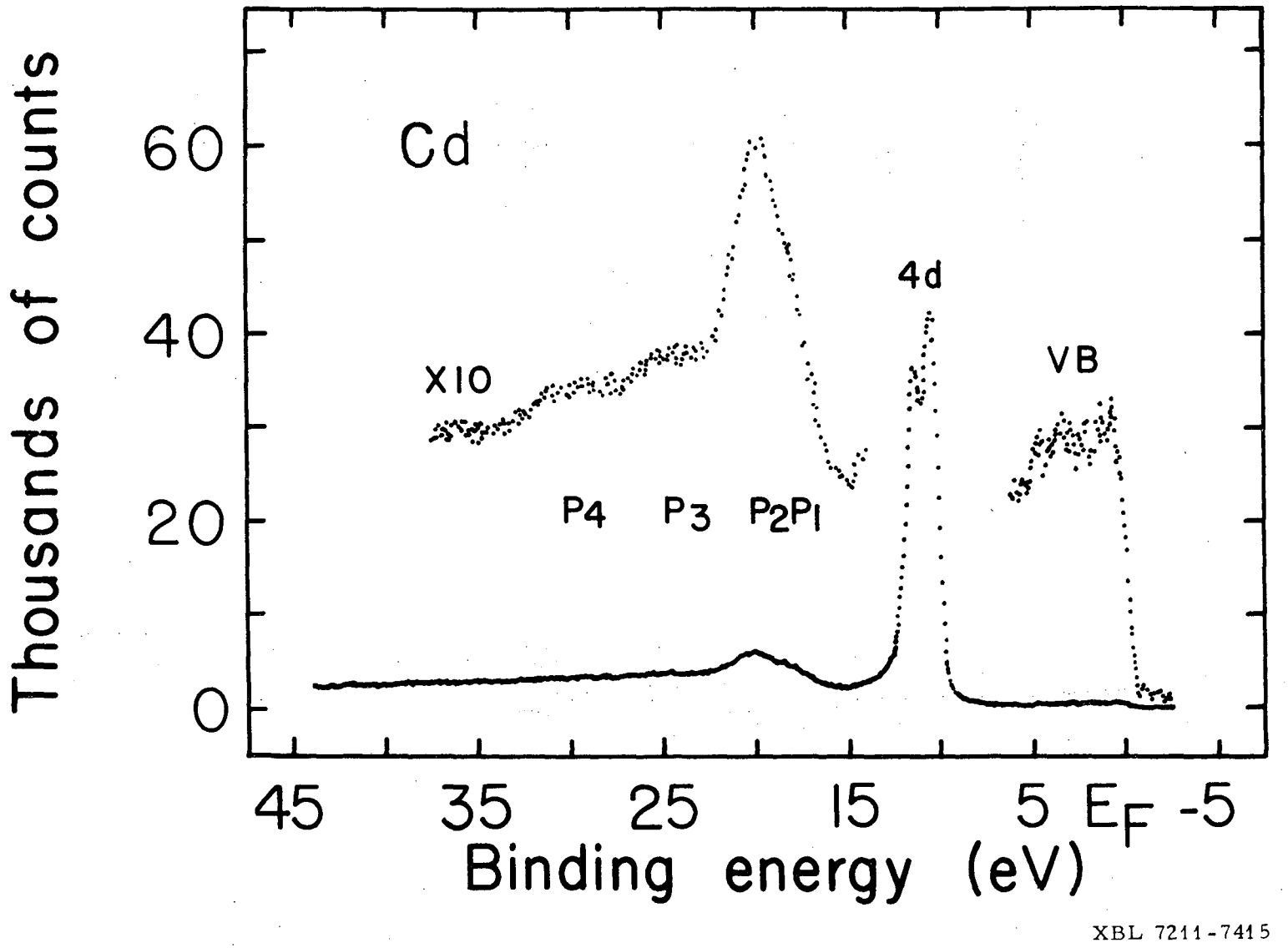

Fig. 3. Photoemission spectrum of Cd 4d level and its characteristic loss structure.

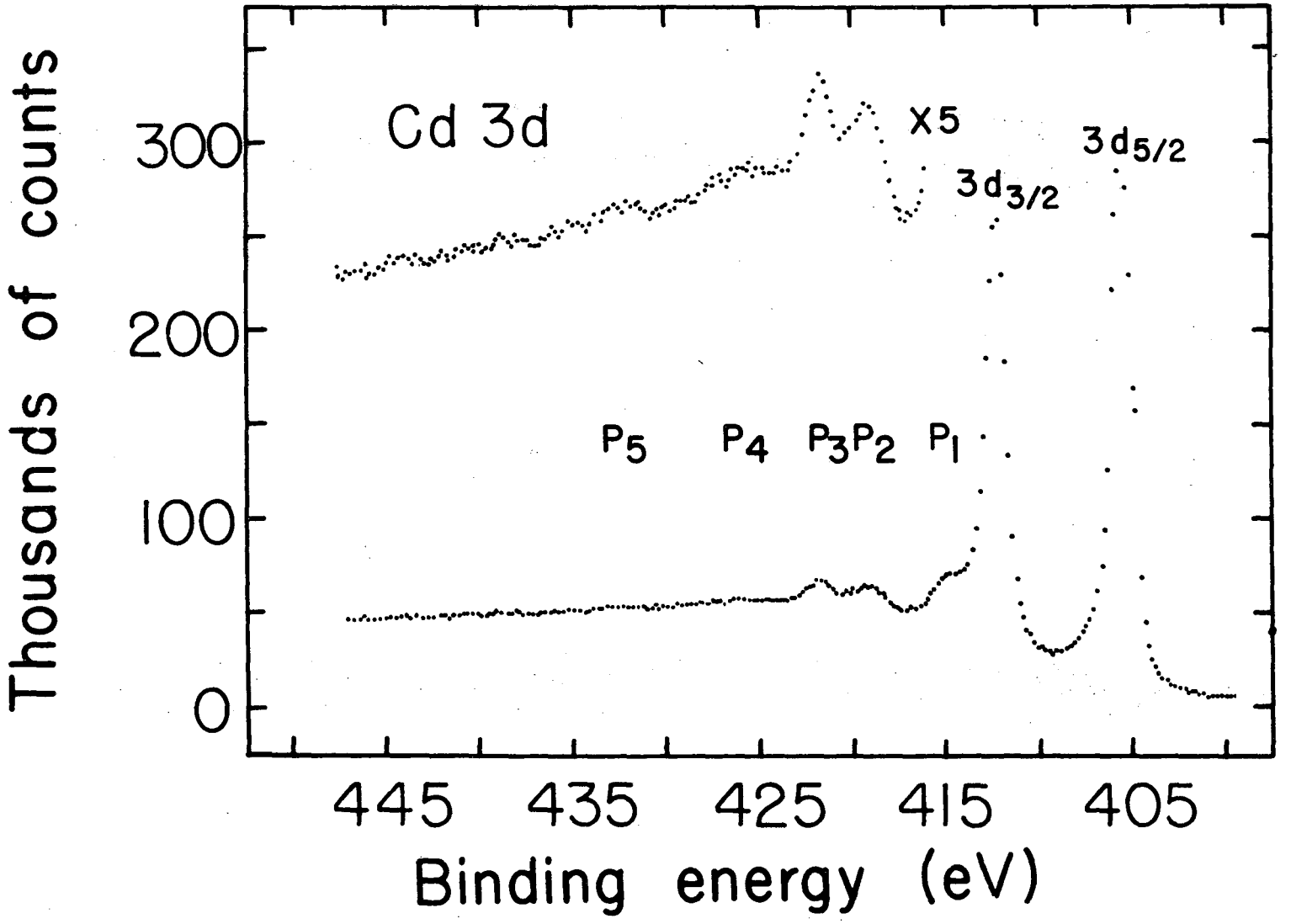

XBL 7211-7414

Fig. 4. Photoemission spectrum of Cd 3d level and its characteristic loss structure.

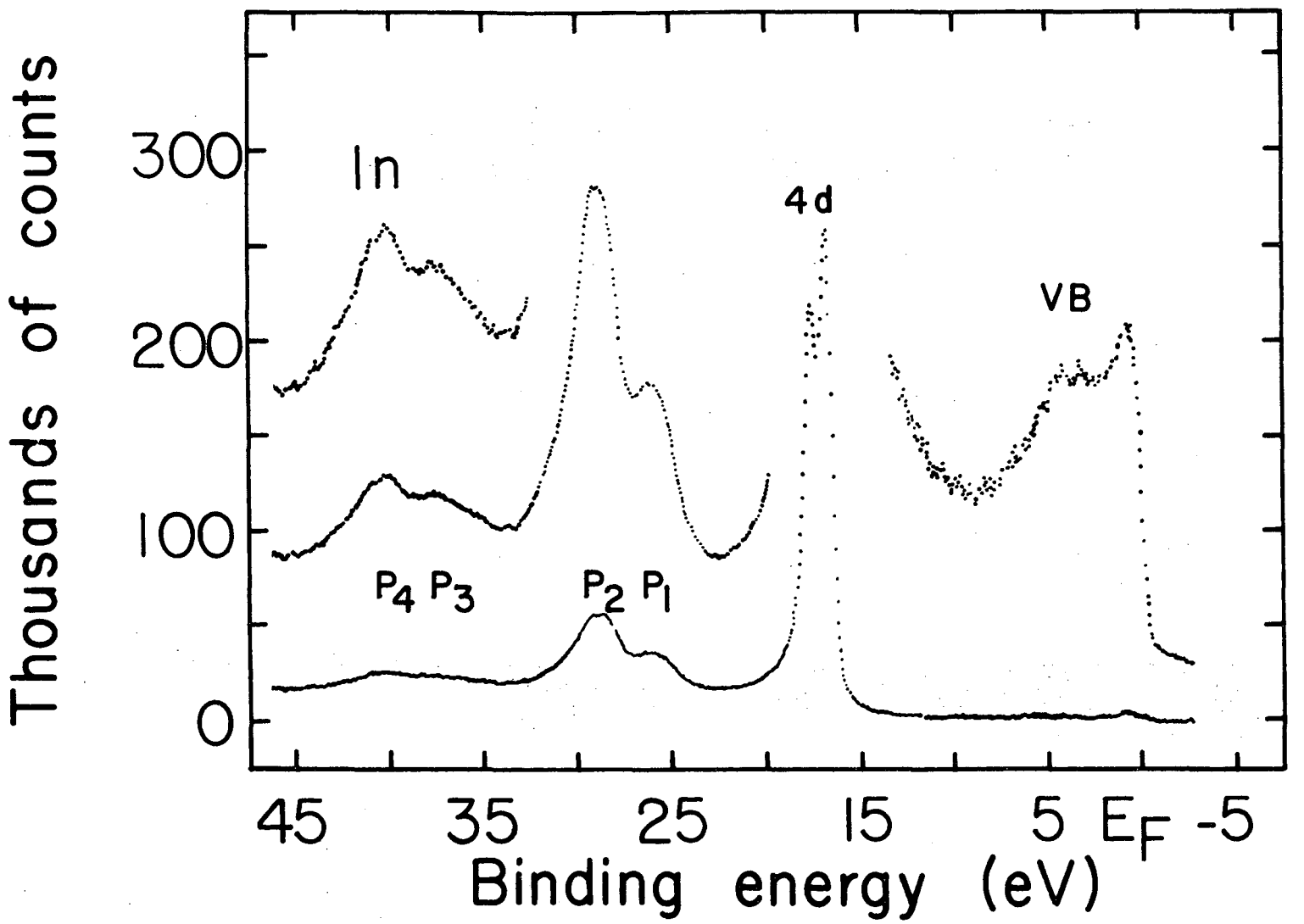

Fig. 5. Photoemission spectrum of In 4d level and its characteristic loss structure.

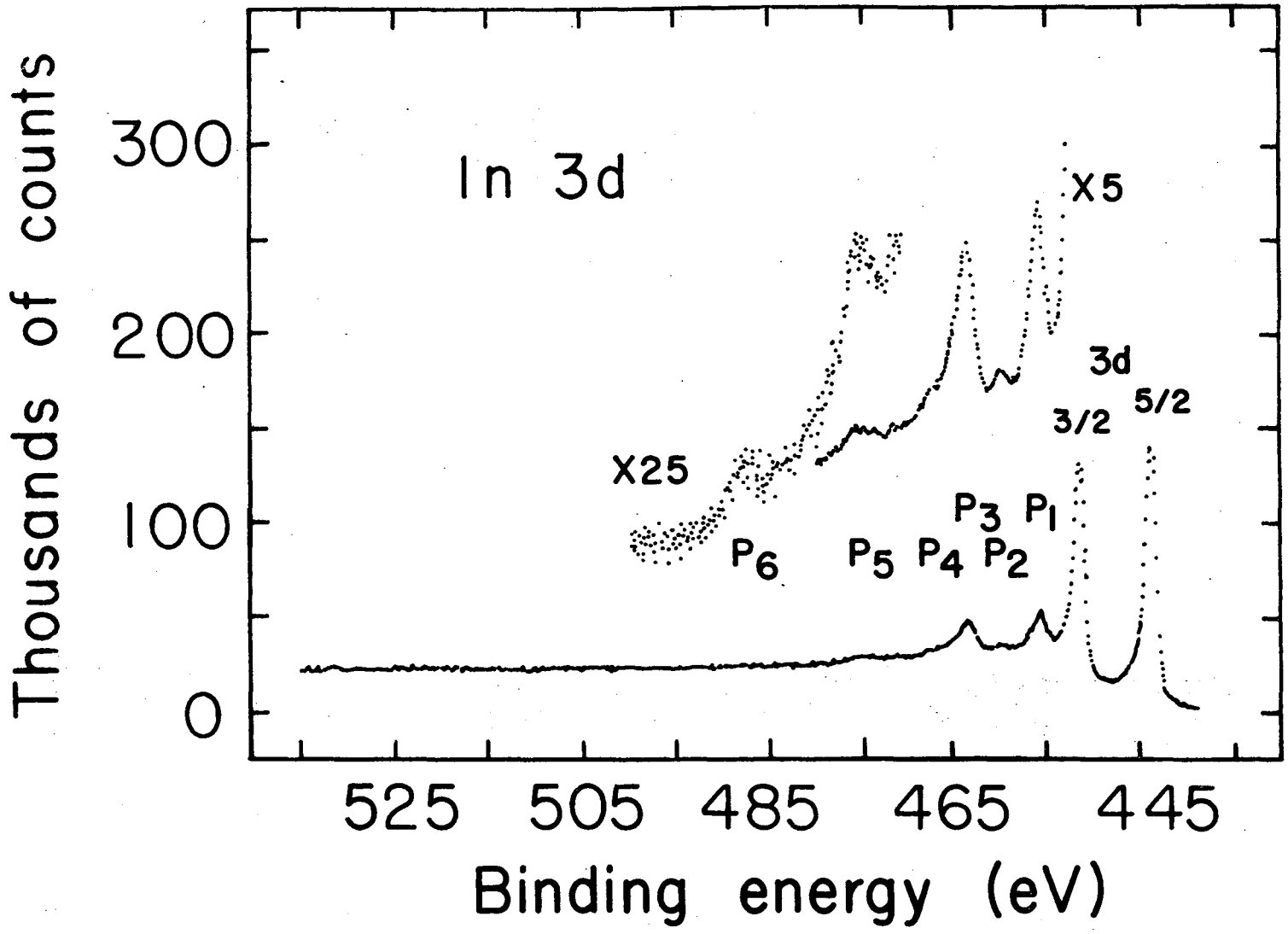

XBL 7211-7412

Fig. 6. Photoemission spectrum of In 3d level and its characteristic loss structure.

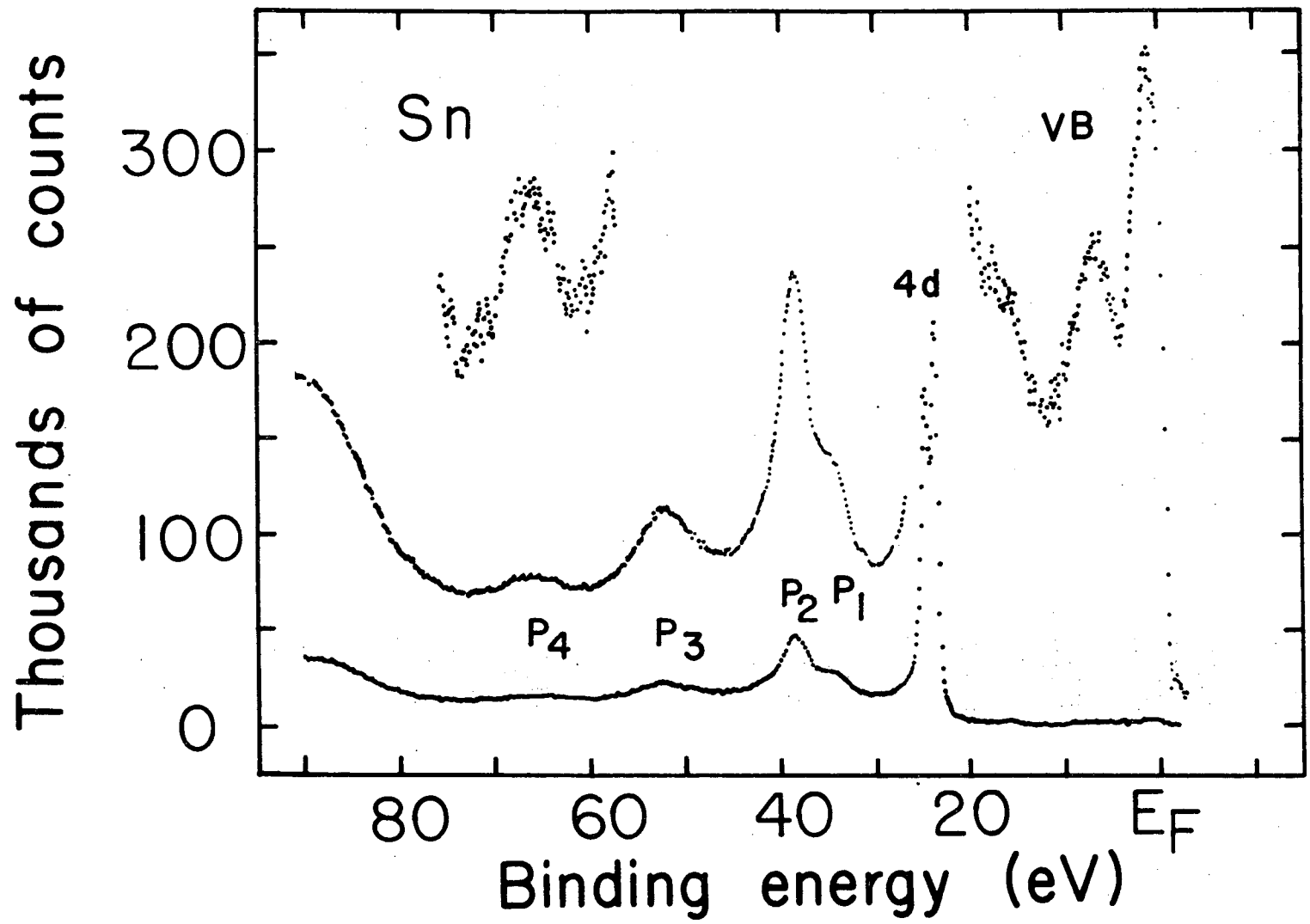

XBL 7211-7411

Fig. 7. Photoemission spectrum of Sn 4d level and its characteristic loss structure.

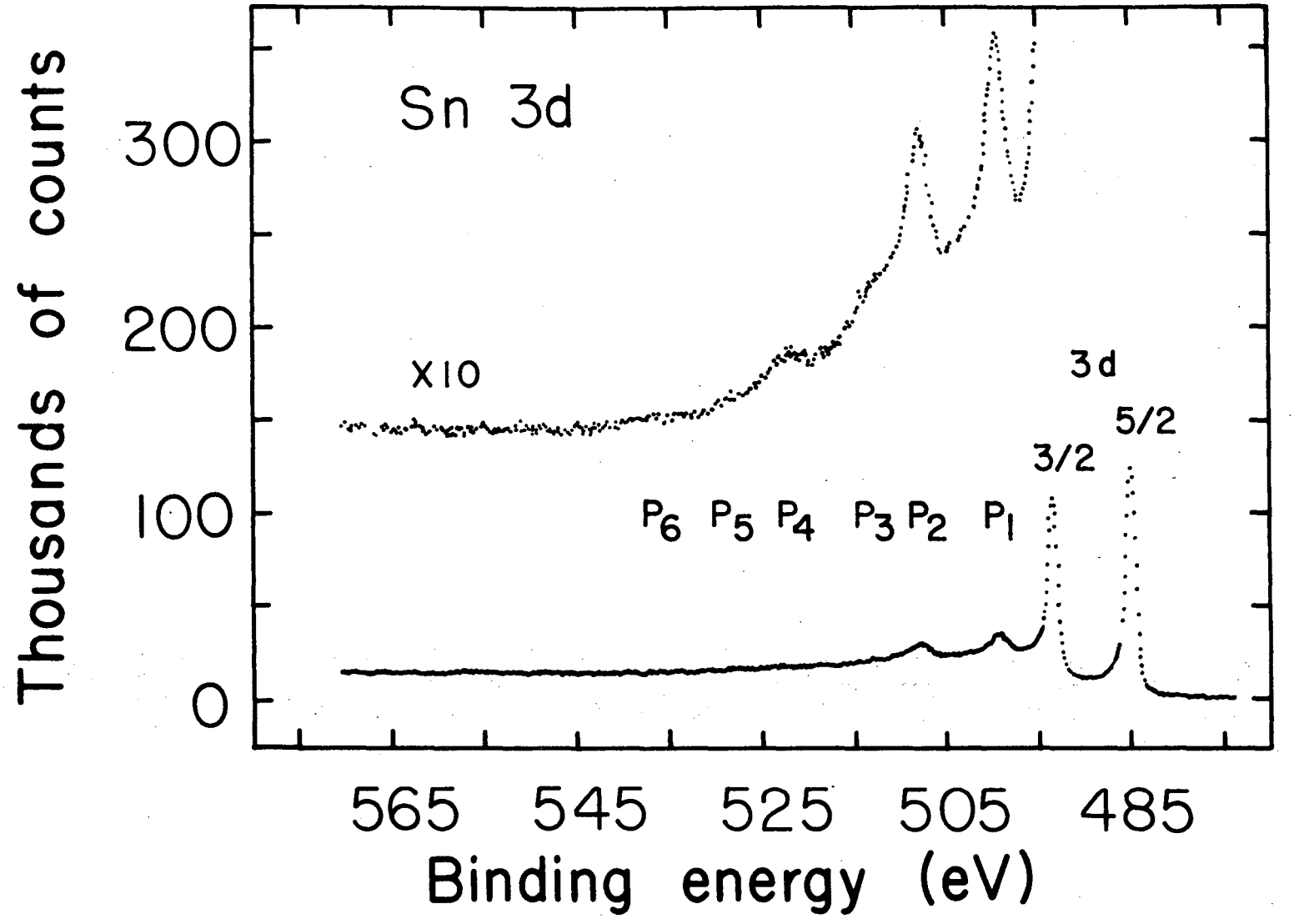

Fig. 8. Photoemission spectrum of Sn 3d level and its characteristic loss structure.

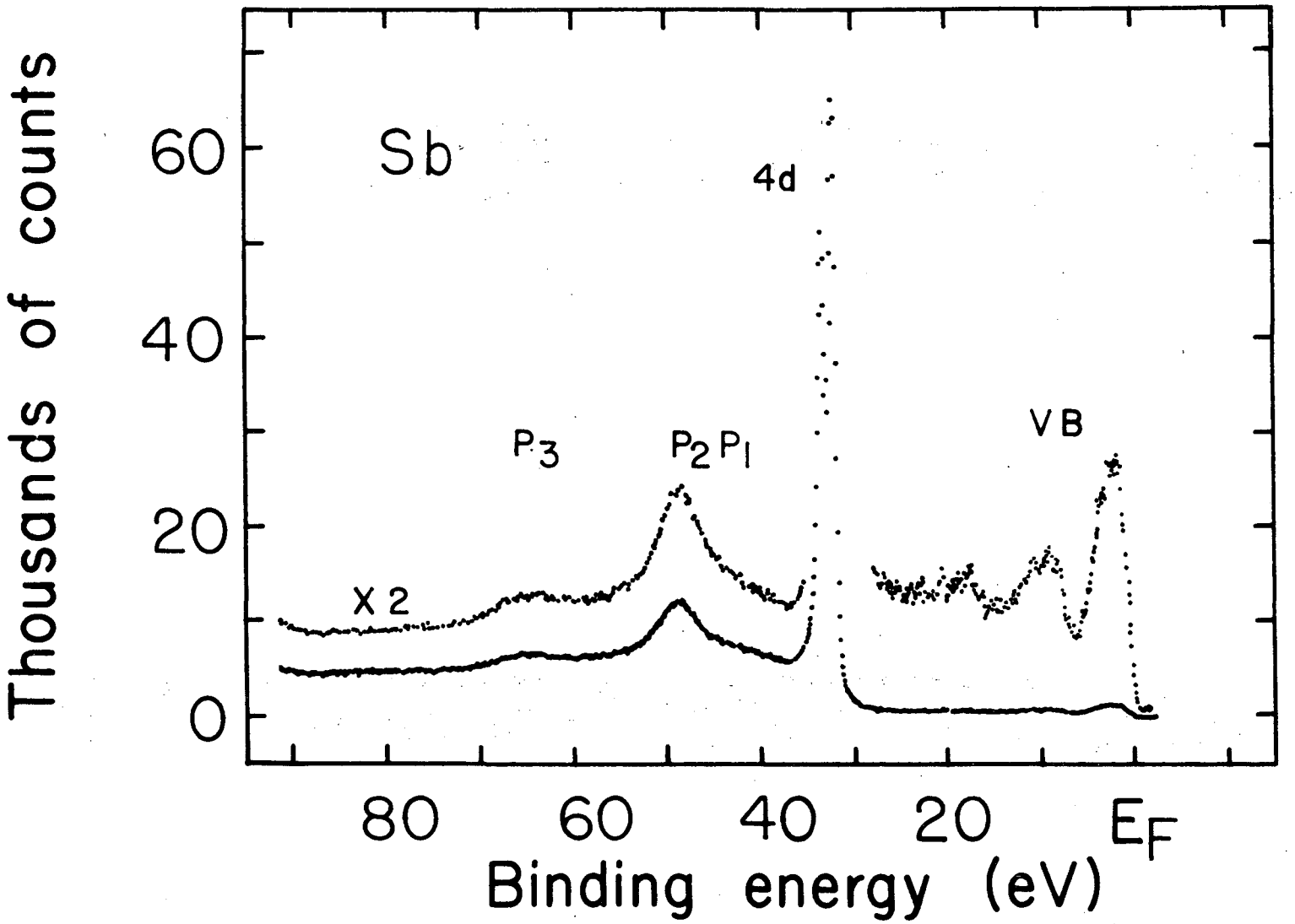

XBL 7211-7409

Fig. 9. Photoemission spectrum of Sb 4d level and its characteristic loss structure.

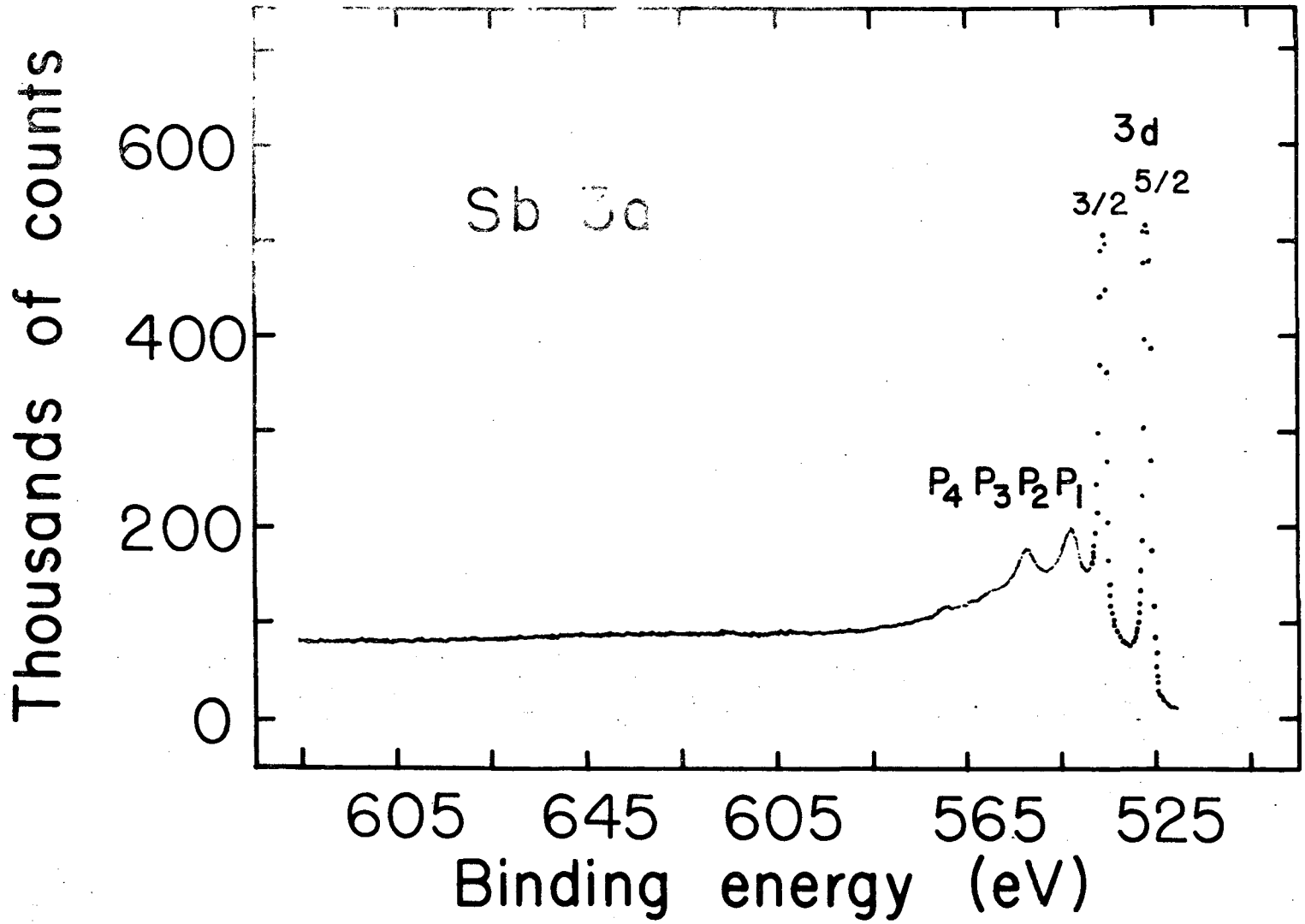

XBL 7211-7408

Fig. 10. Photoemission spectrum of Sb 3d level and its characteristic loss structure.

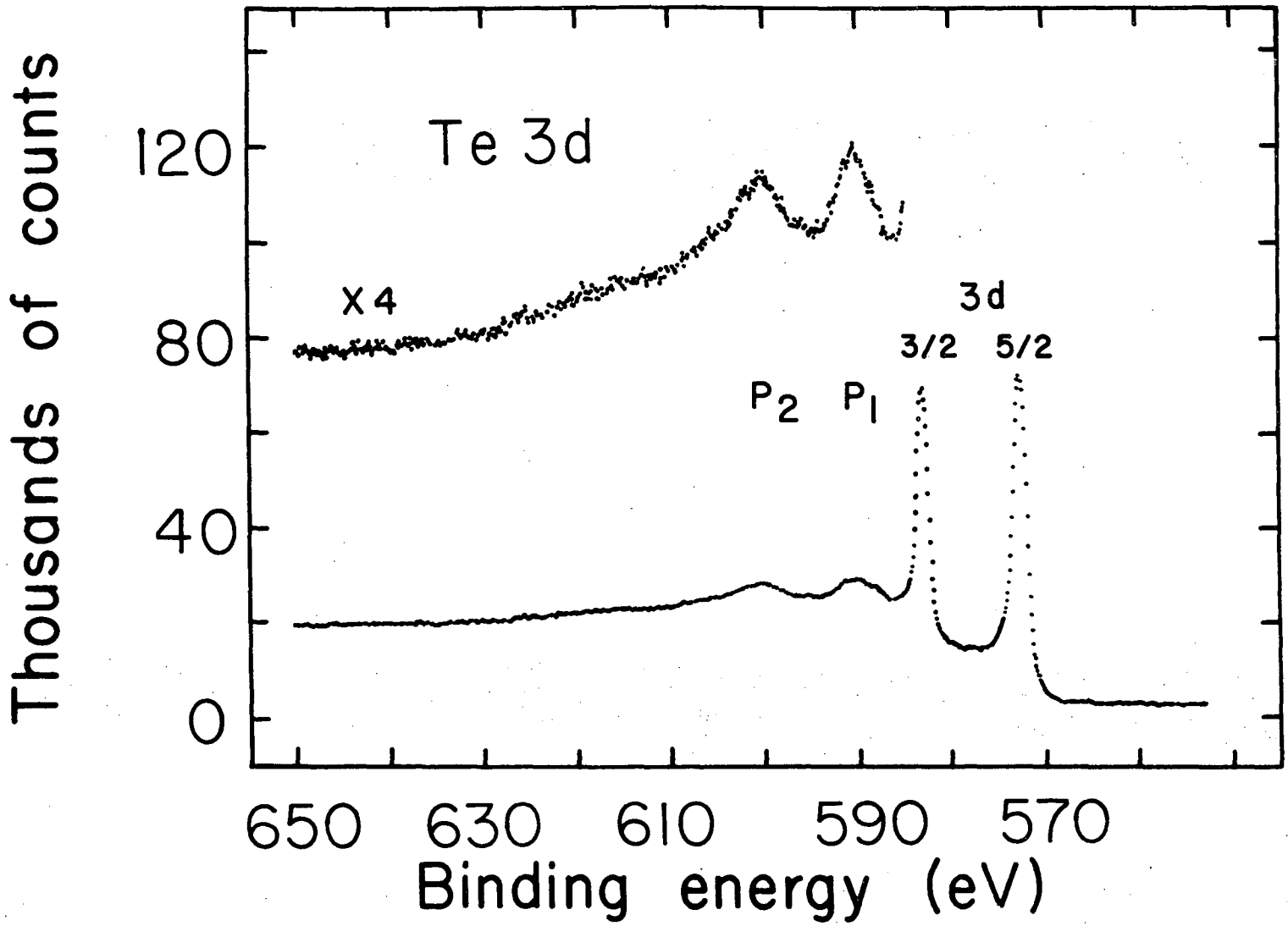

XBL 7211-7407

Fig. 11. Photoemission spectrum of Te 3d level and its characteristic loss structure.

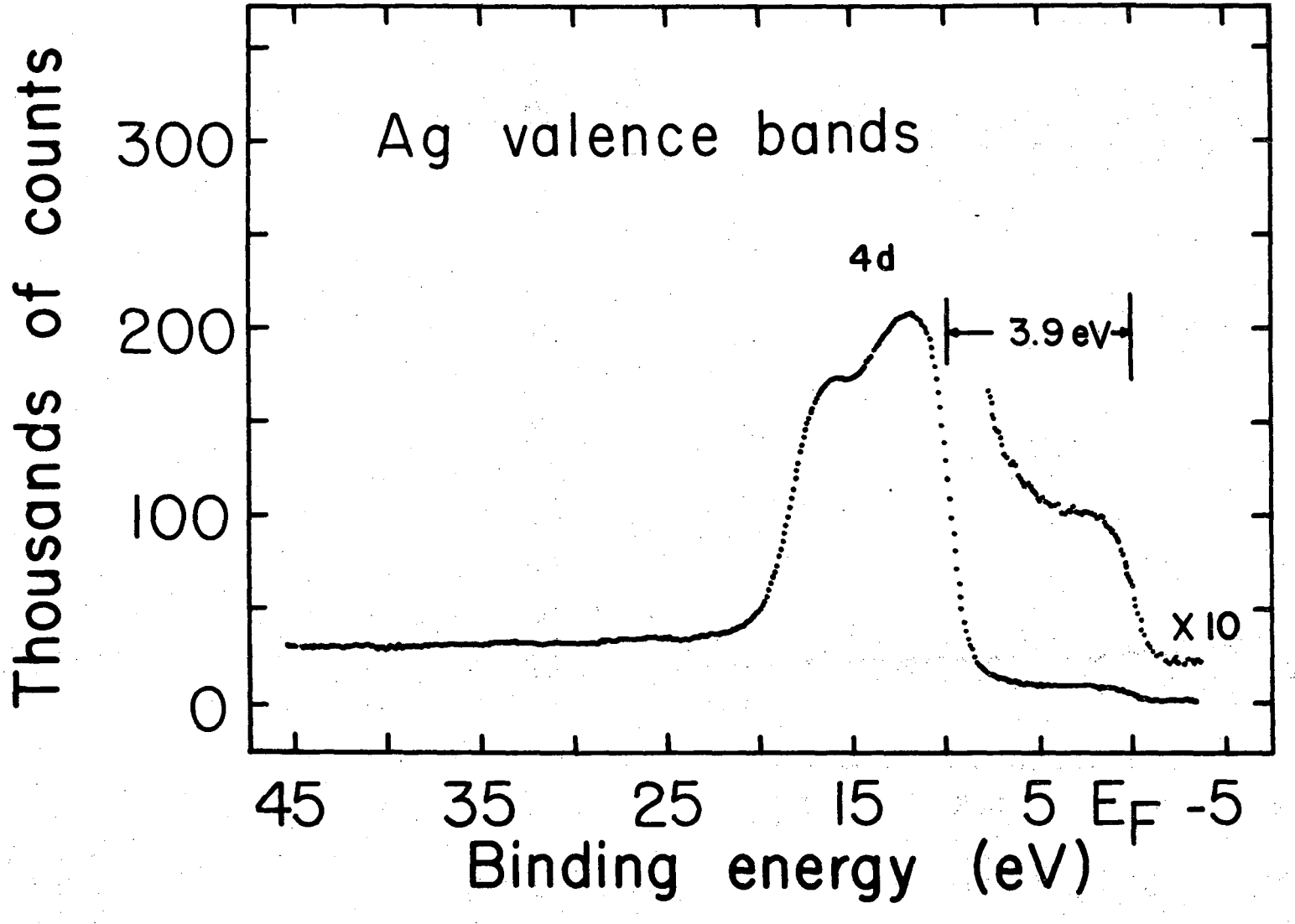

Fig. 12. Photoemission spectrum of Ag valence bands.

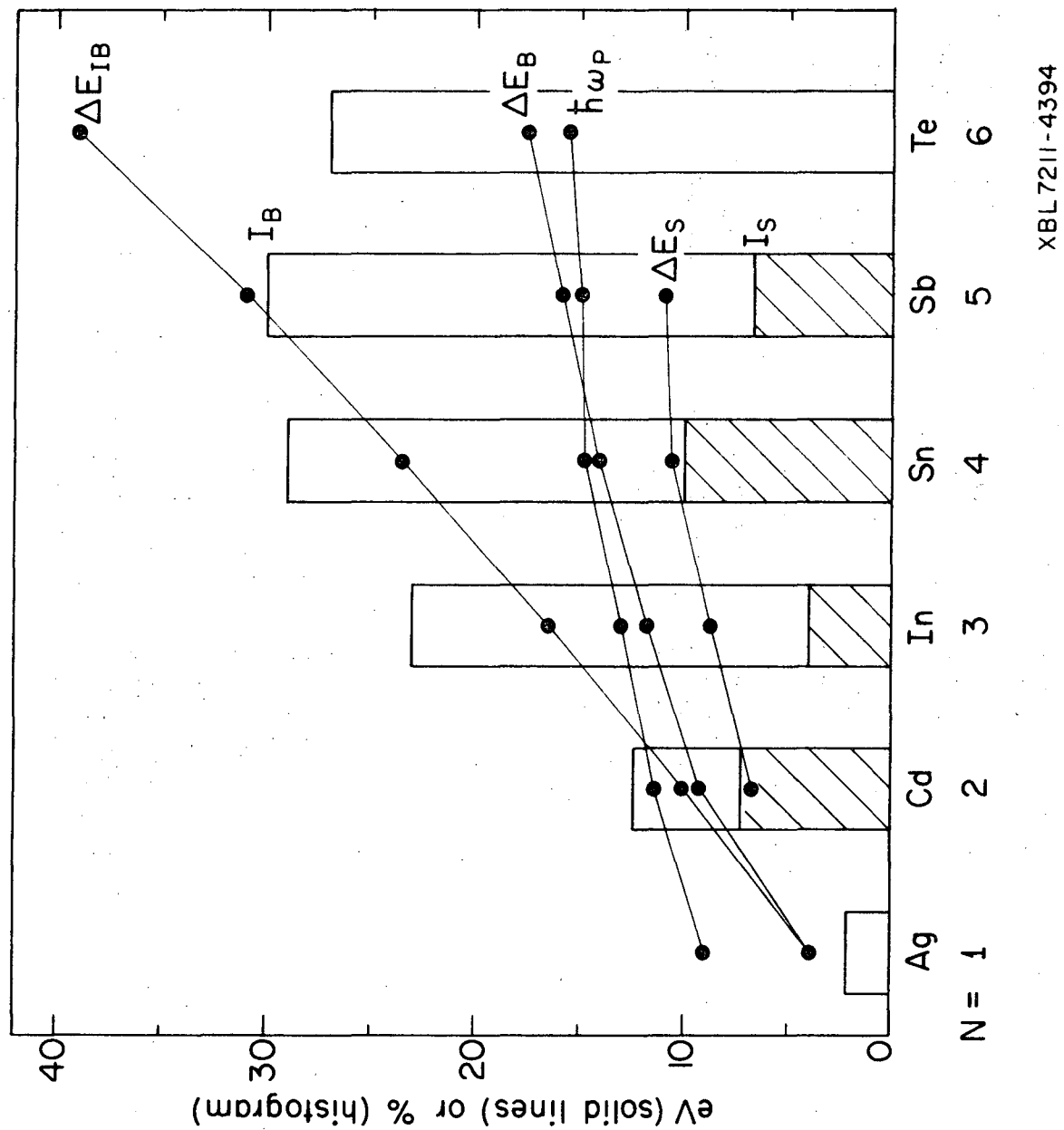

Fig. 13. Systematic of plasmon losses in Ag, Cd, In, Sn, Sb, and Te. ΔE_{IB} is the onset-interband-transition energy ($4d \rightarrow E_F$), ΔE_B is the measured bulk plasmon energy, ΔE_S is the measured surface plasmon energy, $\hbar\omega_p$ is the calculated free electron bulk plasmon energy, and I_B and I_S are the intensity of the bulk and surface plasmon intensity respectively relative to the zero-loss peak.

SECTION XIV. THE TRANSITION METAL OXIDES: CoO AND NiO

A. Introduction

The 3d transition-metal monoxides continue to be the subject of theoretical[1,2,3] and experimental[3] endeavors aimed at elucidating their many varied optical, electronic, and magnetic properties. The x-ray photoemission valence band spectra of CoO and NiO are presented and interpreted in terms of our current understanding of the electronic structure of these compounds.

The x-ray photoemission spectra of CoO and NiO are more complex than those of the pure elements or binary semiconductors reported in earlier sections. Much of this complexity is attributed to the partially filled 3d shell. Core and valence spectra have been interpreted in terms of exchange splittings and multielectron excitations.[4-9]

B. Experimental

The valence band spectra of CoO and NiO are shown in Fig. 1. They were measured with the Berkeley HP 5950A in the HV mode (see Sec. III). Both CoO and NiO were flame fusion grown single crystals[12] which were cleaved in a dry N_2 atmosphere and introduced directly into the spectrometer vacuum of 8×10^{-9} Torr. The cation 2s, 2p, 3s, 3p, and O 1s spectra are included in Figs. 1 and 2 in order to define the conditions under which the valence-band spectra were obtained. Table 1 gives the binding energies of the features marked in Figs. 1 and 2. Previously reported assignments of structure are also listed in Table 1. The NiO XPS valence-band spectrum given in Ref. 7 agrees well with that reported here however the CoO valence band does not. We have observed a spectrum similar to that reported in Ref. 7 for a Co single crystal that had apparently formed a surface oxide layer.

C. Results and Discussion

The results reported here will be discussed in the light of recent NiO and CoO band structure calculations reported by T. M. Wilson[1] and L. F. Mattheiss.[2] Wilson[1] uses a spin-polarized Hartree-Fock (SPHF or UHF) procedure in which the electrons of different spin are allowed to occupy different orbitals. Intra-atomic exchange splits the spin-up from the spin-down electrons and the crystal field splits the spin-down electrons into t_g and e_g bands. Mattheiss[2] uses the augmented-plane-wave (APW) method to calculate the nonmagnetic band structure of CoO and NiO. The APW energy band results at seven symmetry points in the fcc Brillouin zone are fitted with Slater and Koster linear-combination-of-atomic-orbitals (LCAO) interpolation method involving nonorthogonal orbitals. The distance from the top to the bottom of the bands derived from O 2p and Ni 3d orbitals is 6.5 eV and 9.9 eV in the UHF and APW calculations respectively. The experimental width of the (O 2p - Ni 3d) XPS structure (Fig. 1) is 9.8 eV. The APW band structure has a 4 eV gap in the middle of the (O 2p - Ni 3d) bands and the UHF results are 3.4 eV narrower than the XPS structure. The corresponding APW and XPS widths for CoO are 10.5 eV and 10.4 eV respectively. In both the APW and UHF cases the authors stress that the p-d band separations are sensitive to the form of exchange and that an improved treatment of exchange and attempts to approach self-consistency could change the p-d separations.

Both the APW and UHF calculations predict d bandwidths of 3-4 eV; however, in the UHF calculation the lower d-derived bands are hybridized with the O 2p bands whereas in the APW calculation the O 2p and cation 3d derived bands are separated in energy. In previous photoemission

studies[7,10,11,13] the structure corresponding to peak 1 in Table 1 was interpreted to include all the cation 3d bands. Peak 2 of NiO has been interpreted as a multielectron excitation within the d manifold.[7] The results reported here suggest that peak 2 as well as peak 1 (Table 1) in both CoO and NiO represent emission from the 3d bands. This is not inconsistent with previous photoemission results.[10,11,13,17] The UV photoemission spectra of Powell and Spicer[11] and Eastman and Cashion[13] exhibit strong p band emission already at the position of peak 2. The photoemission cross section for UV energies is larger for p than d electrons and thus the p bands could be masking peak 2.

The area of the O 2s peak is assigned a value of 1.0 and will be used as a reference in the following discussion. The total areas of the CoO and NiO valence bands are 3.4 and 5.8 respectively. Peaks 1 and 2 have an area of 0.8 and 1.1 in CoO and 1.25 and 1.95 in NiO. Using the free atom cross section per electron ratio of Gelius,[14]

$$\frac{\sigma_{O\ 2s}}{\sigma_{O\ 2p}} = 8.8$$

one would expect a contribution of 0.3 to the valence band spectra from the O $2p^6$ electrons. The area of peak 3 (5 to 11.5 eV) is 1.3 and 2.6 in CoO and NiO respectively. This is much larger than the calculated free atom value for the O $2p^6$ electrons. Mixing with d orbitals and/or secondary inelastic processes may be responsible for this enhanced structure.

The increase in intensity of peak 1 on going from CoO to NiO is assigned to the eighth 3d electron in the Ni^{2+} ion. The increase in

intensity of peak 3 is believed to be mostly a result of secondary inelastic processes such as multielectron excitations and characteristic energy losses suffered by the photoelectron as it passes through the solid. It must be emphasized that the origin of the XPS satellite structure of the transition metal compounds has generated much speculation but is still uncertain. Bakulin et al.[15] have observed a characteristic energy loss of 5.8(3) eV for 20 keV electrons passing through a thin NiO film. In NiO the maximum in peak 3 (Fig. 1) falls approximately this interval below peaks 1 and 2. Satellite structure on each of the core levels can be found at this interval from the zero loss peaks.

The splitting between the two 3d peaks (1 and 2) is 2.2 eV for CoO and 1.7 eV for NiO which is of the order of empirically derived estimates of the exchange splitting made by Mattheiss.[2] He obtained 3.0 eV and 2.0 eV for the exchange splitting Δ_{ex} of CoO and NiO respectively.

The area ratio of peak 1 to peak 2 is 1.4 for CoO and 1.6 for NiO. If one assumes constant cross section across the d-bands these area ratios correspond closely to electron ratios of 4 to 3 and 5 to 3. These relative intensities can be explained within the UHF model if one had an exchange interaction approximately equal to the crystal field splitting. Under these conditions the majority e_g orbitals would be accidentally degenerate with the minority t_{2g} orbitals at the energy of peak 1. Peak 2 would arise from the majority t_{2g} electrons. Mattheiss[2] argues that the crystal field interaction will not produce a splitting but only a broadening of the t_{2g} and e_g orbitals in NiO and CoO. Another argument against this explanation of area ratios is that if the majority t_{2g} orbitals mixed with the O 2p orbitals more than the other d orbitals one could not expect the XPS cross section to be constant across the d-bands.

D. Conclusion

The CoO and NiO XPS valence-band spectra are composed of; 1) a 3.5 eV wide 3d structure consisting of two components whose separation appears related to the exchange splitting Δ_{ex}, and just below the 3d bands 2) a 6.5 eV wide structure composed of the O 2p bands with some cation 3d mixing and probably also effects of secondary inelastic processes.

REFERENCES

1. T. M. Wilson, Int. J. Quantum Chem. 3, 757 (1970).

2. L. F. Mattheiss, Phys. Rev. B 5, 290 (1972); Phys. Rev. B 5, 306 (1972).

3. D. Adler and J. Feinleib, Phys. Rev. B 2, 3112 (1970).

4. T. Novakov and R. Prins, in Electron Spectroscopy, ed. by D. A. Shirley (North-Holland Publishing Co., Amsterdam and London, 1972), p. 821.

5. T. Novakov, to be published.

6. A. Rosencwaig, G. K. Wertheim, and H. J. Guggenheim, Phys. Rev. Letters 27, 479 (1971).

7. G. K. Wertheim and S. Hüfner, Phys. Rev. Letters 28, 1028 (1972).

8. K. S. Kim and R. E. Davis, to be published in J. Electron Spectroscopy.

9. K. S. Kim, to be published.

10. R. J. Powell, Ph.D. dissertation, Stanford Electronics Laboratory, Technical Report No. 5220-1, May 1967.

11. R. J. Powell and W. E. Spicer, Phys. Rev. B2, 2182 (1970).

12. I thank R. J. Powell for a CoO single crystal and W. E. Spicer for a NiO single crystal.

13. D. E. Eastman and J. K. Cashion, Phys. Rev. Letters 27, 1520 (1971).

14. U. Gelius, Electron Spectroscopy, ed. by D. A. Shirley (North-Holland Publishing Co., Amsterdam and London, 1972), p. 311.

15. E. A. Bakulin, L. A. Balabanova, and V. A. Vasil'ev, Soviet Physics-Solid State 13, 542 (1971).

Table 1a. Cobalt Oxide

Peak number	Binding energy[a] (eV)	Assignments given in the literature	Ref.
Valence bands			
1	1.8(1)	3d	7,10
2	4.0(2)		
3	5.0 to 11.5	O 2p	10
O 2s			
4	21.6(2)	O 2s	7
Co 3p			
5	60.1(3)		
6	62.4(5)		
7	65.2(3)		
8	68.5(3)		
9	81.5(3)		
Co 3s			
10	102.0(1)		
11	107.9(3)		
12	113.1(5)		
13	127(1)		
O 1s			
14	530.2(1)	O 1s	7
15	532.2(2)	ME($3d^8 \rightarrow 3d^{8*}$)	7
16	553.1(5)		
17	573(1)		

(continued)

Table 1a. (continued)

Peak number	Binding energy[a] (eV)	Assignments given in the literature	Ref.
Co $2p_{3/2}$			
18	780.0(2)		
19	786.4(3)		
20	790.4(3)		
21	801.4(5)		
Co 2s			
22	934.5(4)		

[a]Gold film reference.

ME → multielectron excitation.

Table 1b. Nickel Oxide

Peak number	Binding energy[a] (eV)	Assignments given in the literature	Ref.
Valence bands			
1	1.9(1)	3d	7,11,13
2	3.6(2)	ME($3d \rightarrow 3d^*$)	7
3	5.0 to 11.5	O 2p	11,13
O 2s			
4	21.4(2)		
Ni 3p			
5	67.3(2)		
6	69.6(4)		
7	72.8(4)		
8	80(1)	ME(O 2p → Ni 3d)	9
9	88(1)		
Ni 3s			
10	112.0(5)		
11	117.5(5)	MS	8
12	122.5(5)	ME(O 2p → Ni 3d)	9
13	138(2)		
O 1s			
14	530.0(2)	NiO	4,7,8
15	531.9(2)	Ni_2O_3 ME	7,8
Ni $2p_{3/2}$			
18	853.8(1)	NiO	4,7,8
19	855.5(2)	ME($3d^8 \rightarrow 3d^{8*}$)	4
		Ni_2O_3 & MS	8

(continued)

Table 1b. (continued)

Peak number	Binding energy[a] (eV)	Assignments given in the literature	Ref.
Ni $2p_{3/2}$			
20	857.0(4)	ME($3d^8 \rightarrow 3d^{8*}$)	4
21	861.2(5)	ME($3d^8 \rightarrow 3d^7 4s$)	4,6
		ME(O 2p → Ni 3d)	9
22	866.3(5)		
23	874.5(5)		
Ni 2s			
24	1010.8(5)		
25	1015.8(5)	ME(O 2p → Ni 3d)	9

[a]Gold film reference.

ME → multielectron excitation.

MS → multiplet splitting.

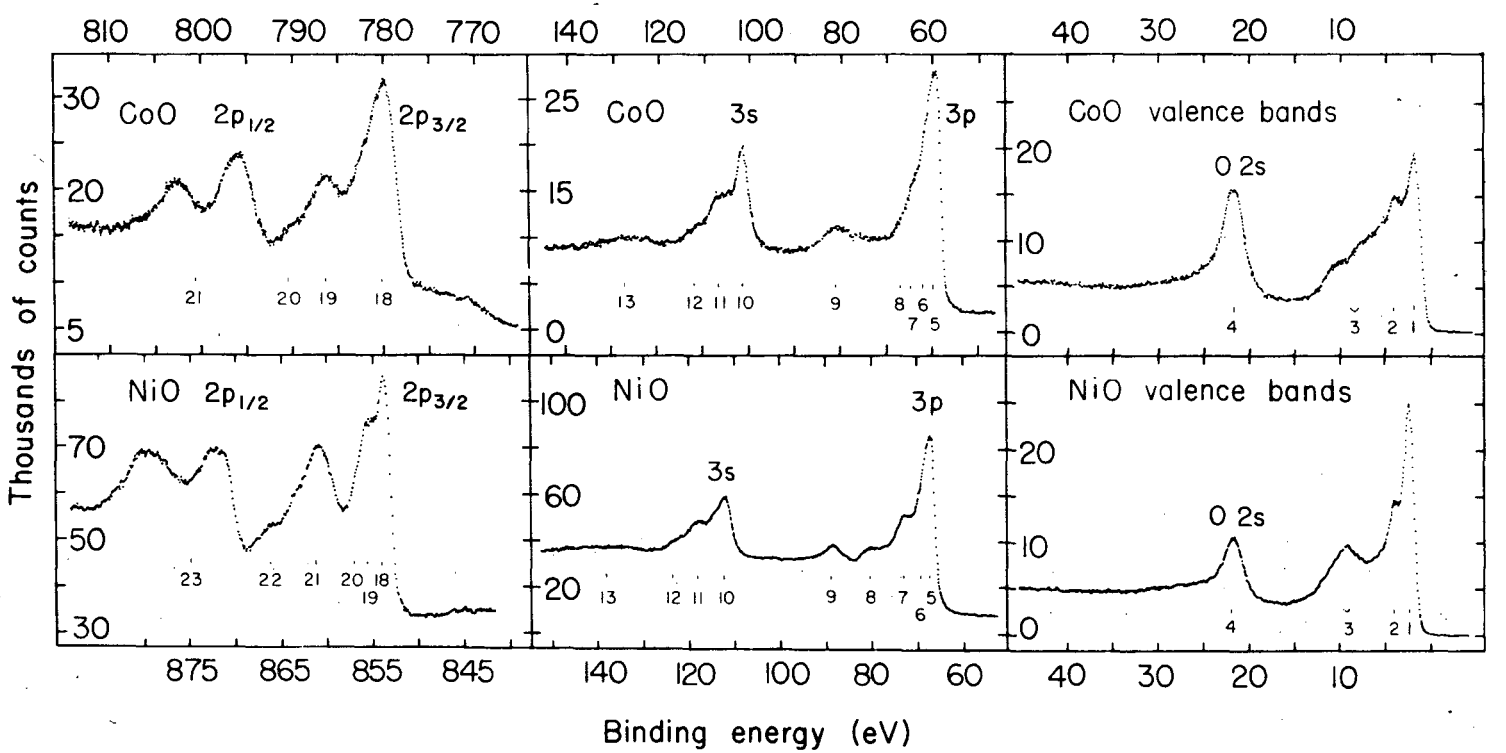

XBL 7211-4430

Fig. 1. CoO and NiO x-ray photoemission spectra.

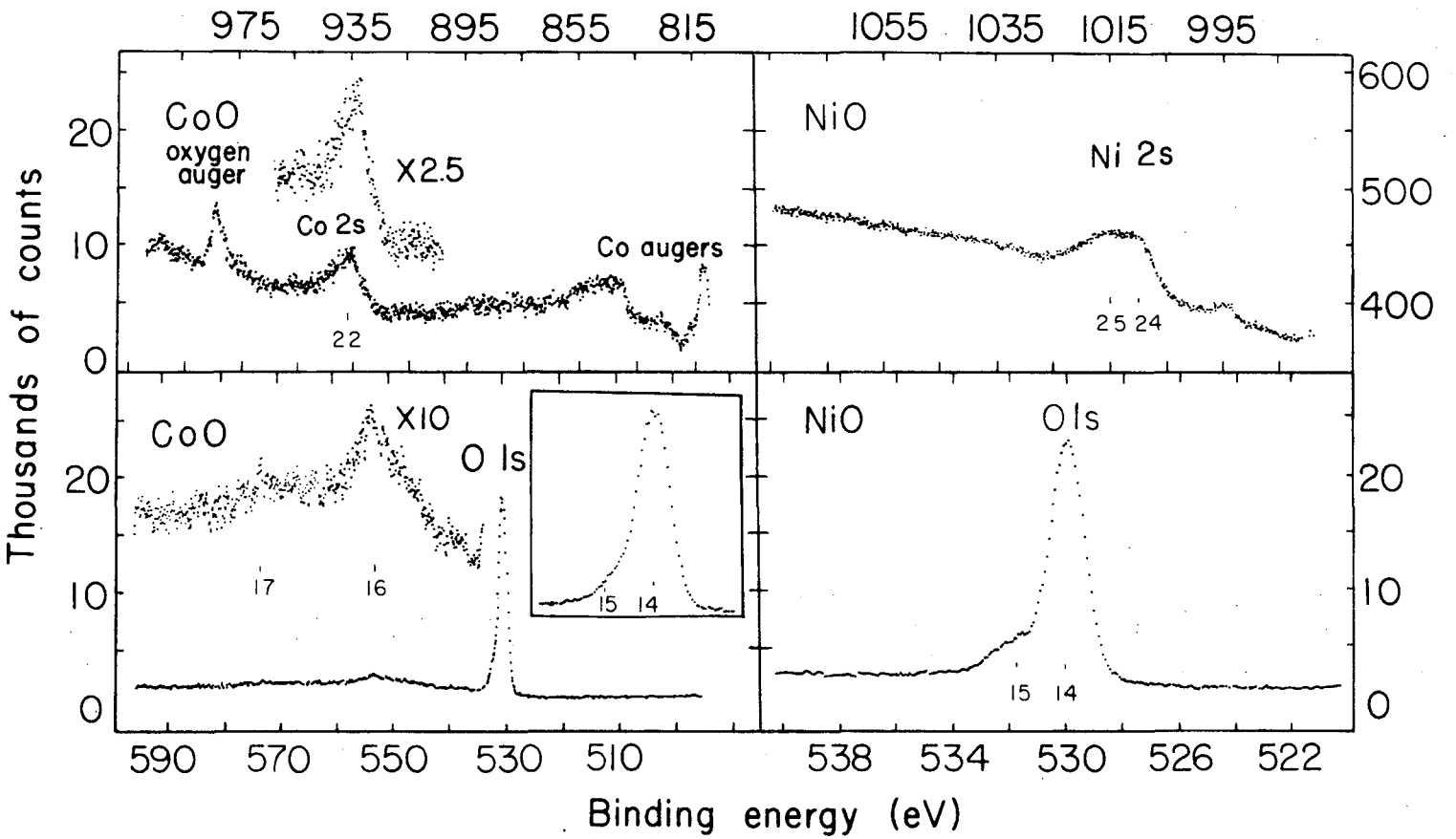

XBL 7211-7431

Fig. 2. CoO and NiO x-ray photoemission spectra.

SECTION XV. SURFACE CHEMISTRY

It is generally accepted that x-ray photoemission spectroscopy has the potential of being quite useful for the study of the chemistry of surfaces. XPS offers us the ability to measure the chemical composition as well as the oxidation state of each species present. These capabilities have not yet been fully exploited; however, the technology of the field is now approaching the point where XPS will soon take its place in the arsenal of the surface scientist.

Historically x-ray photoemission spectrometers evolved from the β-ray spectrometers used in the nuclear sciences where particle energies are high and only moderate vacuums are necessary since penetration depths are much larger and surface contamination is of less consequence. It was recognized quite early that it would be necessary to incorporate the present-day ultrahigh vacuum technology into x-ray photoemission spectrometers before being able to apply XPS to surface chemistry. The first generation of commercial spectrometers, however, did not offer UHV capabilities. The second generation is now available and the variety of instruments is larger. Some offer UHV capabilities with which the utility of XPS in the field of surface chemistry can now be explored. An HP 5950A spectrometer was used in the unbaked, unmodified mode (see Sec. III) for most of the measurements reported here.

Another major technological advance has been the development of a monochromatic x-ray source. Bremmstrahlung radiation and satellite x-rays are eliminated from the x-ray beam striking the sample thus reducing the background signal dramatically. This improvement allows one to study the electronic structure of the valence-band region of essentially

any substance. One is severely limited without monochromatic x-rays, since core-level peaks produced by satellite x-rays often obscure structure in the valence-band region and high background from bremsstrahlung radiation often reduces signal-to-background to impractically small values. The valence-band region yields much information about the chemistry of the system. Dispersion-compensated electron optics have also allowed a factor of two improvement in resolution.

With the advances mentioned above we are now able to begin studying surfaces under defined conditions and thus determine the utility of XPS in surface science. Our overall approach is to survey the x-ray photoemission valence-band spectra of simple substances with clean surfaces and then after setting a foundation build more complicated systems by, for instance, gas-solid reactions and thus enter the field of surface chemistry. At present we are still mainly studying pure substances and have just switched from the unbaked, unmodified mode (HV) of operation to the ultrahigh vacuum mode (UHV). This section presents some preliminary HV results from studies on the oxidation of a clean metal surface. The results are encouraging and indicate XPS will be a useful tool for the surface scientist.

The oxidation of thallium metal is discussed in the next section after which a brief discussion of the oxidation of nickel metal is given.

A. Oxidation of Thallium Metal

Thallium metal exhibits metallic luster when clean and if exposed to air develops a bluish-grey tinge which develops into a thick black oxide. This oxide Tl_2O forms at room temperature and is hygroscopic.[1] Tl_2O reacts

with water to form the hydroxide. A piece of polycrystalline thallium metal was cleaned by argon bombardment and then oxidized in stages. Seven XPS core peaks were monitored at each stage and the peak intensities versus exposure are plotted in Fig. 1.

1. Experimental Method

A fresh surface of polycrystalline thallium metal was produced by slicing with a razor blade just prior to insertion of the sample into the HP 5950A sample preparation chamber where it was argon bombarded (1 keV Ar^+ ions, 10 μA). It was then immediately moved directly to the analyzer chamber where the total pressure was 6×10^{-9} Torr. At this point the C 1s and O 1s x-ray photoemission spectra indicated the presence of 1/10 surface layer adsorbed oxygen and 1/4 surface layer hydrocarbons. The definition of a surface layer will be given below. The Tl valence band spectrum in Sec. VI was accumulated overnight (11 hrs.). In the morning the C 1s and O 1s spectra indicated the accumulation during the night of 1 surface layer of adsorbed oxygen and 1 surface layer of hydrocarbons. The sample was argon bombarded (960 V Ar^+ ions, 12 μA) for 20 minutes to remove this surface contamination. During the next hour an O 1s spectrum was obtained after which a C 1s spectrum was taken. These spectra indicate the presence of approximately 1/10 surface layer Tl_2O, 1/10 surface layer adsorbed oxygen, 1/30 surface layer of hydroxide, and 1/4 surface layer of hydrocarbons. The residual gas spectrum taken in the photoemission energy analyzer is set out in Table 1. It consists of about equal parts H_2O, CO, and H_2 plus small amounts of hydrocarbons and noble gases.

This relatively clean surface was then oxidized in stages (see Table 2) and the seven peaks listed in Table 3 were monitored at each stage. The intensities of these peaks are plotted versus oxygen exposure in Fig. 1.

2. Results and Discussion

As can be seen from Fig. 1 the oxidation of thallium metal is complex. Thallium and oxygen are not the only substances present. Further study is required to confirm the interpretation of the peaks reported here and also to determine that no peaks have been overlooked or unresolved. It is our intention to tackle problems in the UHV mode of operation since, as these results show, the residual gases in the HV mode introduce added complications.

For the meantime a model is proposed to explain the present preliminary results. Peak a (Fig. 1) with 118 eV binding energy is assigned to Tl metal (dashed curve). It is not very sensitive to over six hours of oxygen exposure (3 hrs. at 1×10^{-8} Torr O_2 and 3 hrs. 20 min. at 5×10^{-8} Torr O_2). A small shoulder on the high binding energy side may be present. During this time the oxygen peak d with 530.7 eV binding energy increases to a value about which it remains for the rest of the treatments. It is the only oxygen peak to significantly increase intensity during this initial oxygen treatment. The saturation behavior which it exhibits suggests defining one "surface layer" of adsorbed oxygen as the quantity that yields a d peak intensity equal to the saturation value. It is tempting to assume one surface layer is equal to one monolayer, however this relationship has yet to be shown.

Peak f at 285.6 eV binding energy is assigned to contaminant hydrocarbons which are present in the vacuum and the atmosphere. The behavior of peak f prior to run 980 is similar to the oxygen peak d. It saturates at a value about one-half as large as that of the oxygen peak d. The photoemission cross section for carbon is about one-half as large as that of oxygen and therefore the saturation value of peak f corresponds to an amount of carbon approximately equal to the amount of oxygen present in one surface layer. The saturation of peak f is defined as 1 surface layer of carbon contamination.

The Tl was next twice exposed to 10^{-3} Torr oxygen for 15 min. and then 100 Torr oxygen for 20 min. Peak b at 119.5 eV binding energy which is assigned to the Tl $4f_{7/2}$ peak of Tl_2O and peak c at 529.0 eV binding energy which is assigned to the O 1s level of Tl_2O begin to grow. It is interesting how the sum of the Tl $4f_{7/2}$ oxide and metal peaks increase in intensity as if the Tl_2O was transparent to the photoelectrons during the initial stages of oxidation. This is consistent with the fact that electron-electron scattering lengths are usually longer in insulators than metals.

After the 20 min., 100 Torr O_2 treatment the sample was removed from the spectrometer for 30 seconds and then returned for 20 min., removed for 2 min. and returned for 2 hrs., removed for 20 min. and returned for 10 hrs., removed for 30 min. returned for 1 hr., and finally removed to an oven in air at 100° C for 50 min. and then returned to the spectrometer. The seven peaks listed in Table 3 were monitored between treatments (Table 2). The sample's color turned from metallic to light

brown to brown to blue to black (see Fig. 1). During air exposures the intensity of oxygen peak e increased up to 4 times the value of the saturated surface layer of adsorbed oxygen (peak d). Oxygen peak e is assigned to the hydroxide ion. Tl_2O is hygroscopic and reacts with water in the atmosphere to form the hydroxide. Note peak c, the oxide peak, decreases in intensity when the hydroxide peak e increases whereas the total metal intensity does not decrease. This implys that the water reacts with the oxide and is not just adsorbed. If water was adsorbed on the surface both the metal and oxide peaks would be attenuated and not just the oxide. Trace e shows that under vacuum the hydroxide decomposes to the oxide.

Carbon peak g at 290.2 eV binding energy appears only after the sample is exposed to the air. It closely follows the behavior of the hydroxide peak. This is a high binding energy for a carbon compound in the condensed phase. The assignment of this peak is uncertain at this time. Possibly loosely physisorbed gases that would not feel full extra-atomic relaxation[2] are responsible for this peak. Other candidates include the carbon oxides.

In Fig. 2 it is seen that the XPS valence band spectrum of clean thallium metal is quite different than that of the complicated surface oxide plus hydroxide plus carbon compounds that results after the treatment listed in Table 2. The oxidized metal spectrum exhibits at least two sets of Tl 5d levels as is evidenced by the low binding energy shoulder on the Tl $5d_{5/2}$, the shoulder on the s-like and p-like bands at 7.5 eV and 4 eV binding energy, and the filling of the valley between the Tl $5d_{5/2}$

and Tl $5d_{3/2}$ peak. There are peaks originating from the O 2s level at about 25 eV and the O 2p level at 9 eV.

Oxidation involves the transfer of electrons from the metal. The effect of this transfer is evident in the s-like and p-like bands which are seen to shift on the average to higher binding energy upon oxidation of the metal. The bands also get narrower.

The valence bands of pure systems are now receiving most of our attention and after we develop an understanding of them we can proceed to utilize the bonding information in the more complicated spectra such as the one in Fig. 2.

3. Conclusions

XPS is a useful tool for studying the chemistry of the first few atomic layers of a solid; however, before it can be fully utilized several problems have to be solved. The quantitative relationship between a monolayer and a surface layer has to be determined. The electron penetration depths for substances with different electrical properties have to be further explored. The degree of extra-atomic relaxation during XPS of physisorbed and chemisorbed species must be considered and UHV conditions are desirable.

In the present results both a surface layer of carbon (peak f) and oxygen (d) containing substances collect and remain stable on the surface of Tl in the HV environment described above. UHV conditions are desirable as the HV conditions were not adequate to maintain a clean surface. The surface layers that formed in vacuum under the HV conditions, however, did not alter the clean metal spectrum noticeably. More severe

conditions which produced the oxide were necessary to do that. A carbon containing substance was present with a rather high C 1s binding energy which suggests that possibly its environment was such that it was not receiving the full extra-atomic relaxation of a condensed phase.

B. Oxidation of Nickel Metal

Nickel metal was heated to 640° C on the high temperature sample holder of the Berkeley Iron-Free photoelectron spectrometer. The experimental equipment is described elsewhere.[3] Hydrogen was used to reduce the surface oxide and then the surface was oxidized in two stages. The spectra at each stage are shown in Figs. 3 and 4. The reduced nickel was exposed to a few seconds of O_2 at 5×10^{-5} Torr and the measurements in the middle panel of Figs. 3 and 4 were collected. The nickel was then exposed to oxygen for 1 hr. at which time the spectra in the lower panels of Figs. 3 and 4 were taken. The sample was maintained at 640° C during the whole experiment.

The metal peaks are replaced by the more tightly bound structures of NiO upon oxidation.

REFERENCES

1. A. G. Lee, The Chemistry of Thallium (Elsevier Publishing Co., Amsterdam, 1971).

2. D. A. Shirley, Chem. Phys. Letters 16, 220 (1972).

3. C. S. Fadley, Ph.D. Thesis, Lawrence Radiation Laboratory Report UCRL-19535, April (1970).

Table 1. Residual gas spectrum in photoemission energy analyzer. The total pressure was 9×10^{-9} Torr with the RGA on. Measured with an EAI Quad 250 RGA with 50 V electron energy.

Mass	2	14	15	16	17	18	20	26	27	28
Relative intensity	2.4	0.2	0.4	1.2	2	3.4	0.2	0.2	0.25	3.0
Mass	29	30	32	39	40	41	42	43	44	
Relative intensity	0.4	0.2	<0.1	0.1	1	0.2	0.1	0.2	0.4	

Table 2

Run Number	Treatment just prior to measurement		Time
945	Argon cleaned	5/25	13:35
948	Start leaking O_2 into spectrometer at a partial pressure of 1×10^{-8} Torr		14:21
951			14:49
954			15:16
	(continue for 3 hrs.)		
957			16:00
960			16:48
963	Increase pressure to 5×10^{-8} Torr		17:40
967			19:47
	(continue for 3 hrs. 20 min.)		
970			20:35
973	Expose Tl to 10^{-3} Torr O_2 for 15 min.		21:59
976			22:35
977	Repeat 973		23:07
980	Expose Tl to 100 Torr O_2 for 20 min.		23:55
983	Remove sample from spectrometer into air for 30 sec.	5/26	00:30
986	In air for 2 min.		00:56
989			01:26
992			01:55
995			02:22
998	In air for 20 min.		03:06
1001			03:32
1003	Five hours after run 1001		09:10
1006			10:00

(continued)

Table 2 (continued)

Run Number	Treatment just prior to measurement		Time
1012	In air for 30 min.		13:10
1015	Fifty min. at 100 C in air		14:10
1019			17:07
1025		5/27	09:30

Table 3

Level	Assignment	Binding energy
Tl $4f_{7/2}$	a. Metal	118.0
	b. Tl_2O	119.5
O 1s	c. Tl_2O	529.0
	d. Adsorbed oxygen	530.7
	e. Hydroxide	531.5
C 1s	f. Hydrocarbons	285.6
	g. Adsorbed compound*	290.2

*See text.

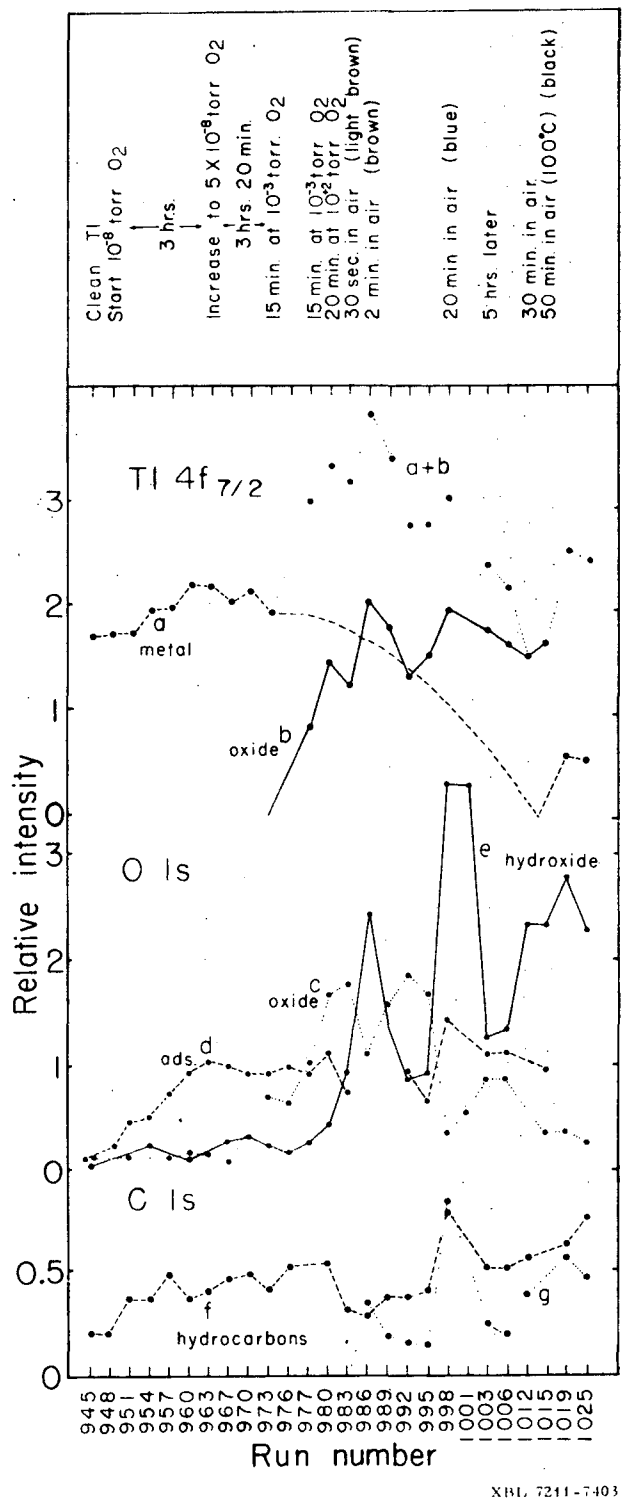

Fig. 1. Peak intensity versus exposure.

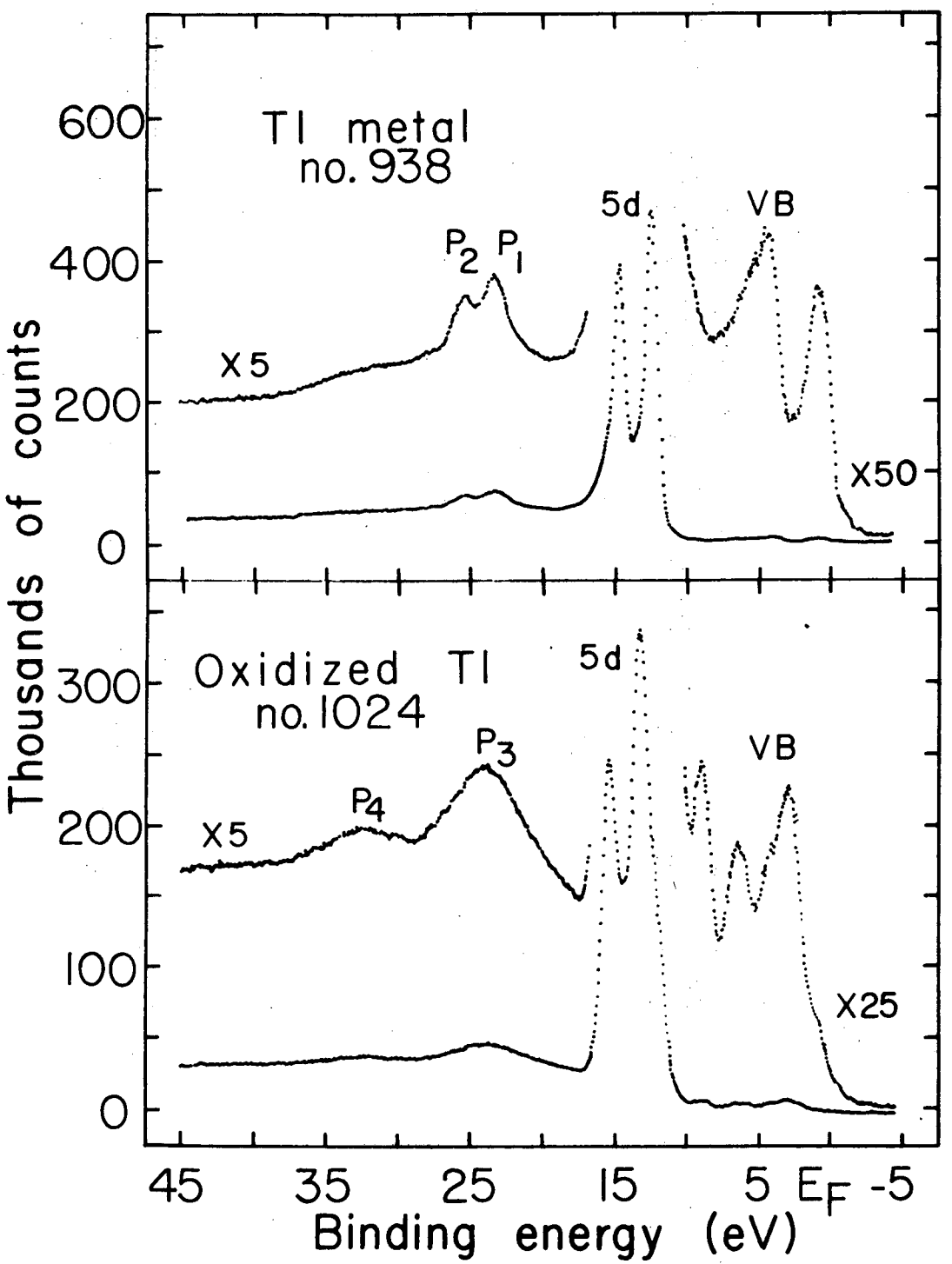

XBL 7211-7428

Fig. 2. Tl metal and oxidized Tl valence bands.

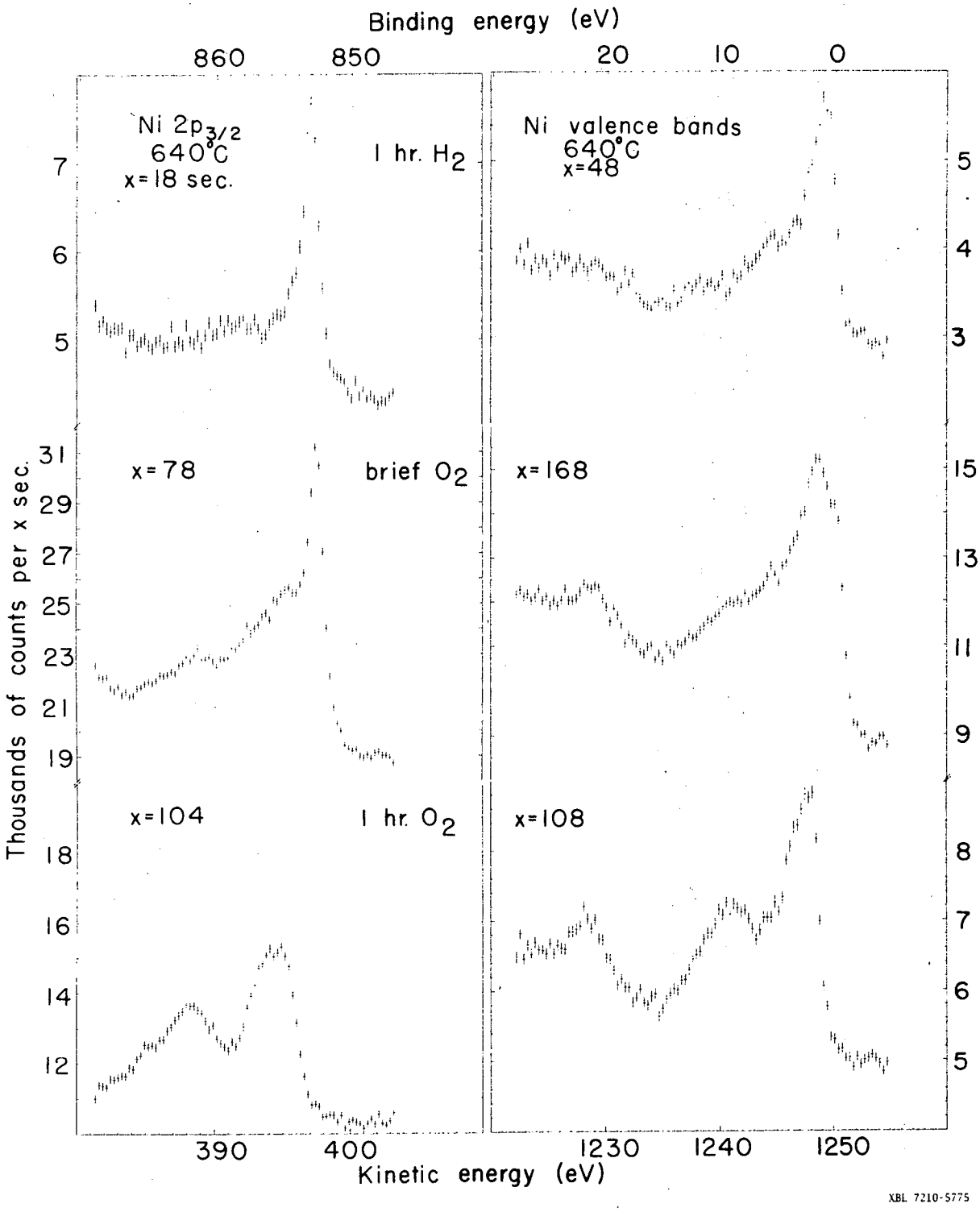

Fig. 3. Oxidation of Ni metal.

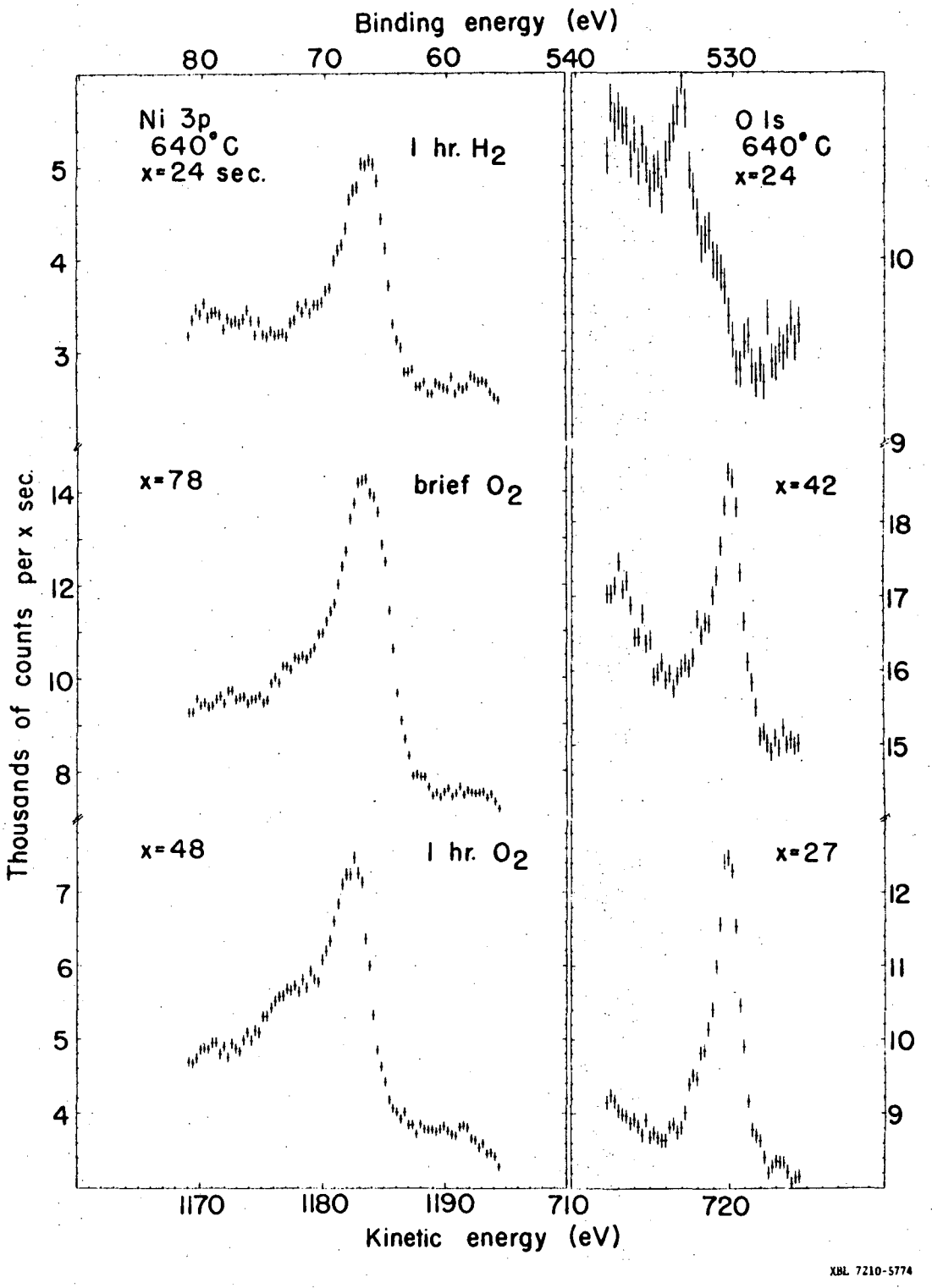

Fig. 4. Oxidation of Ni metal.

SECTION XVI. PRELIMINARY ULTRAHIGH VACUUM RESULTS

The need for ultrahigh vacuum was discussed in Sec. III and the UHV modified HP 5950A was described. After the first bakeout the base pressure was 1×10^{-9} Torr throughout the whole machine. A single crystal of aluminum was annealed at 360° C by electron bombardment for 1 hour and then argon etched for 1/2 hour (8 μA, 1 keV Ar^+). After this treatment antimony, oxygen, carbon, and tantalum contamination was detected in amounts that should not affect the valence band noticeably. The uncorrected valence band of Al is shown in Fig. 1 and that of the Al 2s level in Fig. XIII-1b.

Previously in the HV mode of operation an aluminum oxide peak appeared immediately after cleaning the Al and it would grow with time. No oxide peak was detected 12 hours after cleaning the sample in the UHV system. The spectra reported were recorded more than 12 hours after cleaning.

The Al valence band exhibits the free electron behavior expected. There appears to be a bulk plasmon (15.7 eV) replica of the valence band beginning at the energy labeled P.

These preliminary results are very encouraging, and indicate ultrahigh vacuum conditions will allow us to study systems heretofore inaccessible to x-ray photoemission spectroscopy.

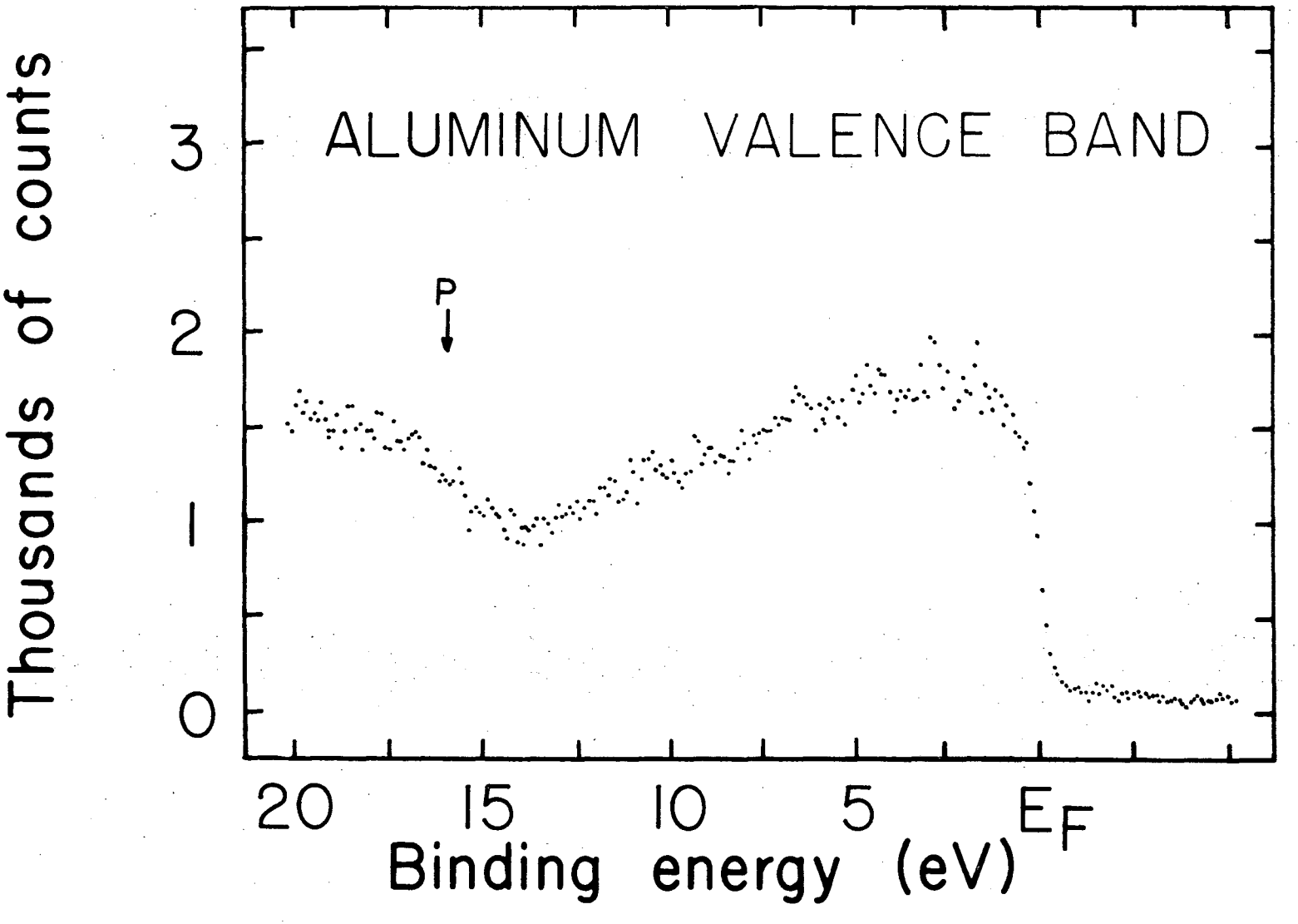

XBL 7211-7433

Fig. 1. X-ray photoemission valence band of aluminum.

APPENDIX

The spectra compiled in Secs. A and B of the appendix are obtained from single crystals except in the cases of Ga and Tl where polycrystalline material was used. All the elements in Fig. A-1 were argon etched except Ge and As which were cleaved. Gallium metal was partially oxidized by residual gases in the spectrometer. The structure at 5 through 10 eV and shoulder on the 3d level are a result of this contamination. The experimental procedure for the spectra following Fig. A-1 is similar in all cases to that used in Secs. VII through XI. The samples were cleaved single crystals. A detailed analysis is in progress and will be published shortly for those materials not reported in earlier sections.

Section A illustrates the relationship among the XPS valence-band spectra for some elemental, III-V, II-VI, and IV-VI semiconductors. Section B is a compilation of XPS spectra in order of increasing ionicity. The ionicity scale is that of Phillips.[1] HgTe and the Pb-salts have been placed between the semiconductors and insulators.

The KI spectrum exhibits weak Au 4f lines originating from the sample mount.

I thank Dr. R. Dalvin, Dr. Y. Petroff, Dr. D. Reynolds, and Professor Y. R. Shen for their gifts of crystals.

REFERENCES

1. J. C. Phillips, Rev. Mod. Phys. 42, 317 (1970).

CRYSTAL STRUCTURES

Diamond	Diamond
	Si
	Ge
Zinc Blende	GaP
	GaAs
	GaSb
	ZnSe
	ZnTe
	CdTe
	HgTe
	InSb
Wurtzite	ZnO
	ZnS
	CdS
	CdSe
Rock Salt	PbS
	PbSe
	PbTe
	Alkali halides

SECTION A

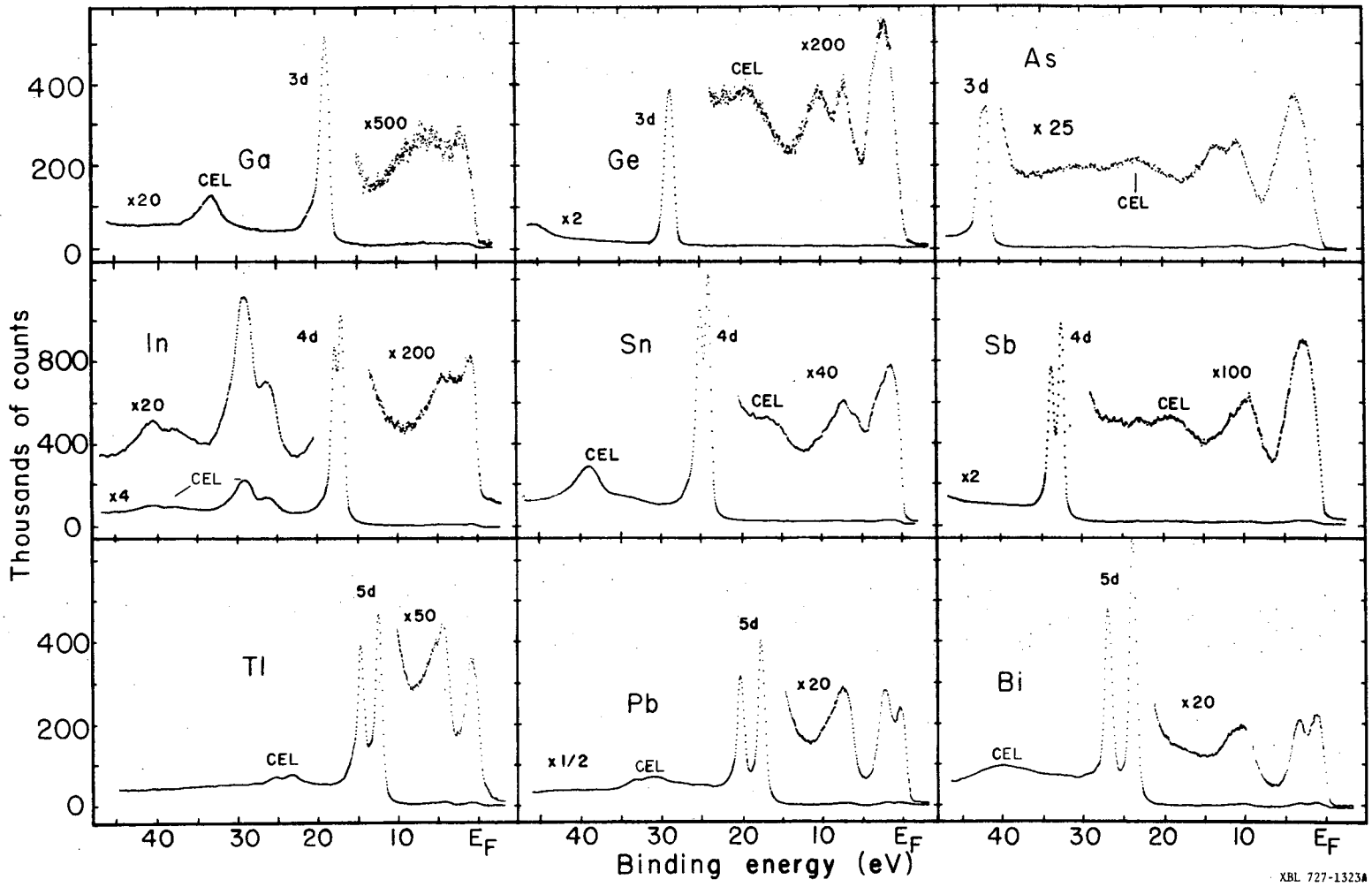

Fig. A-1. Pure elements.

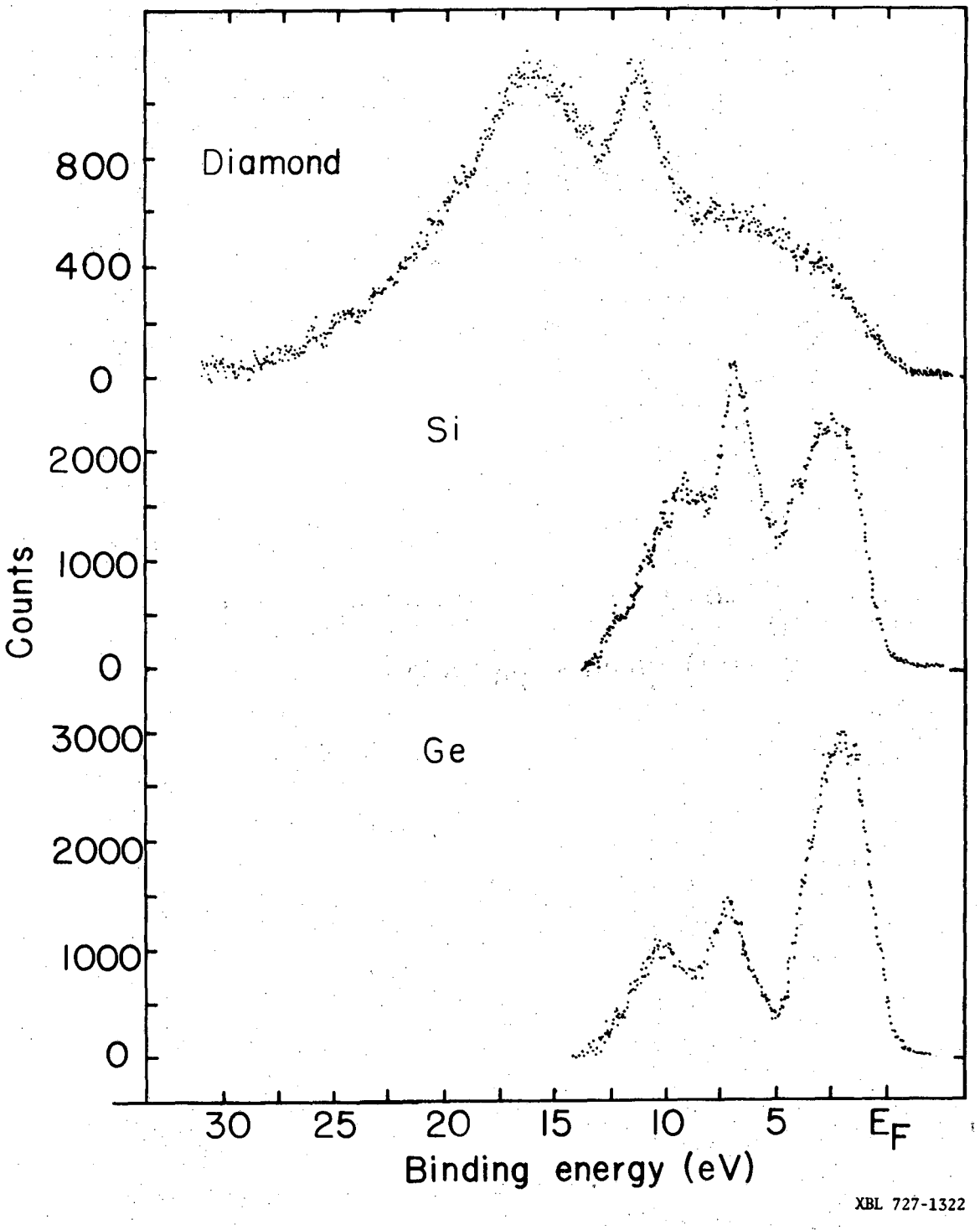

Fig. A-2. Group IV elements.

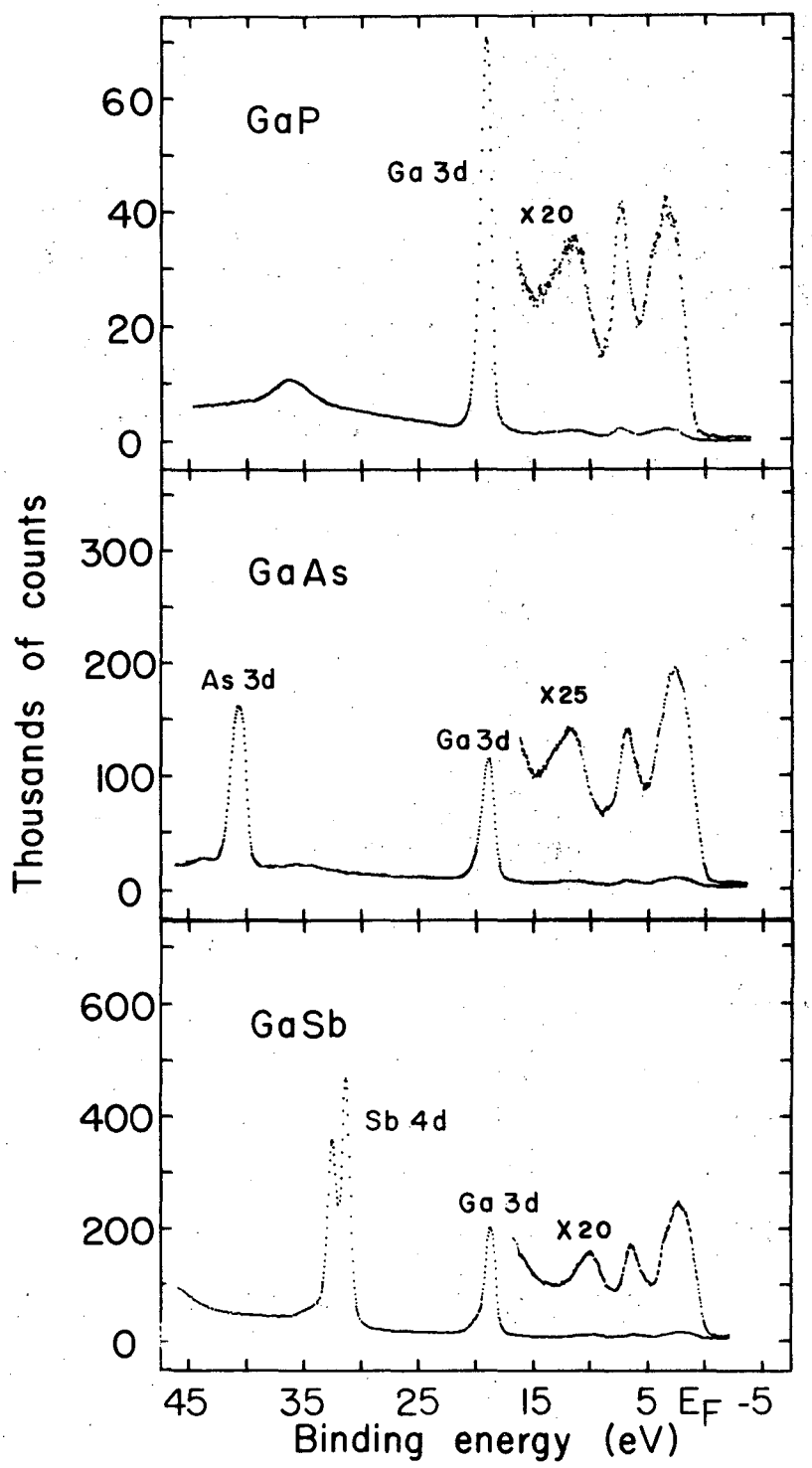

XBL 7210-5822

Fig. A-3. III-V gallium salts.

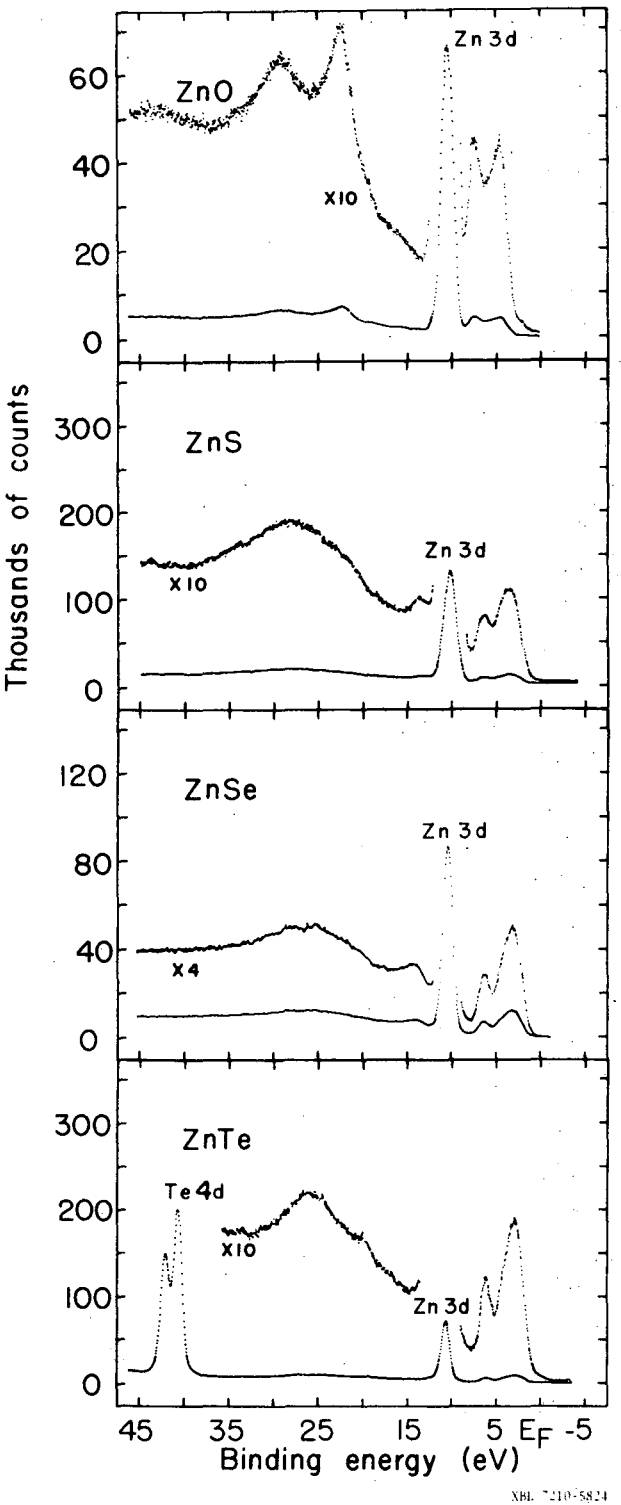

Fig. A-4. II-VI zinc salts.

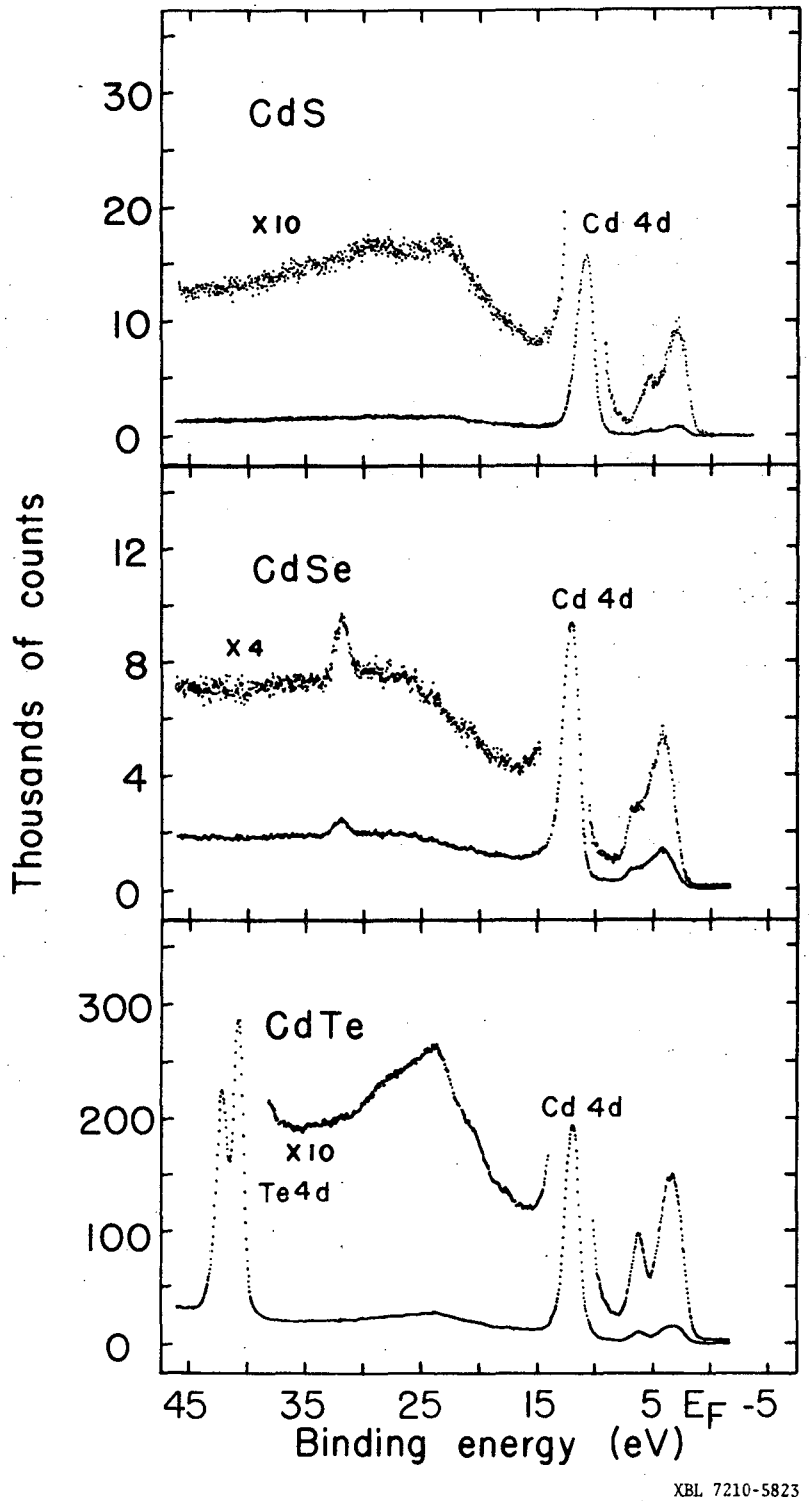

Fig. A-5. II-VI cadmium salts.

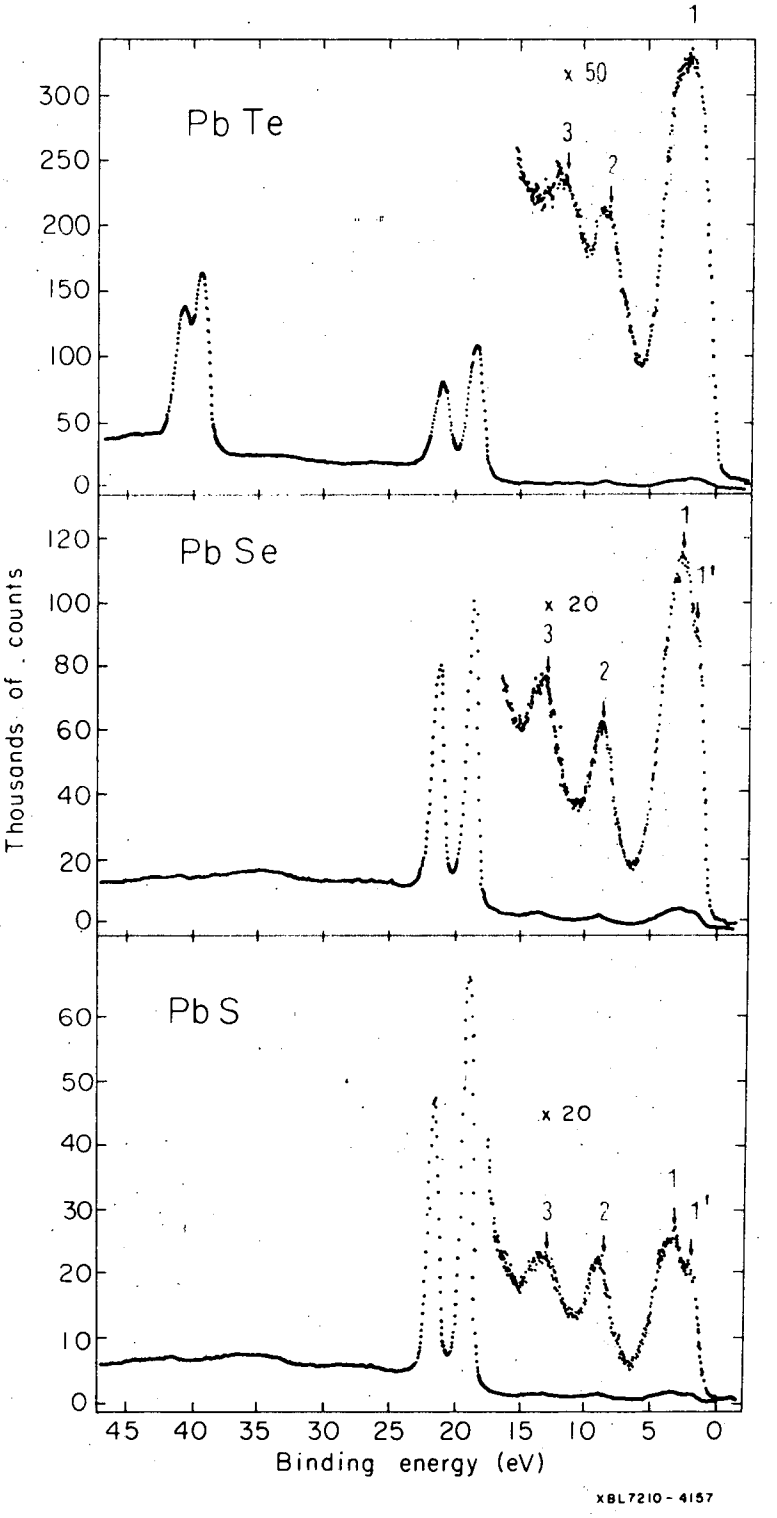

Fig. A-6. IV-VI lead salts.

SECTION B

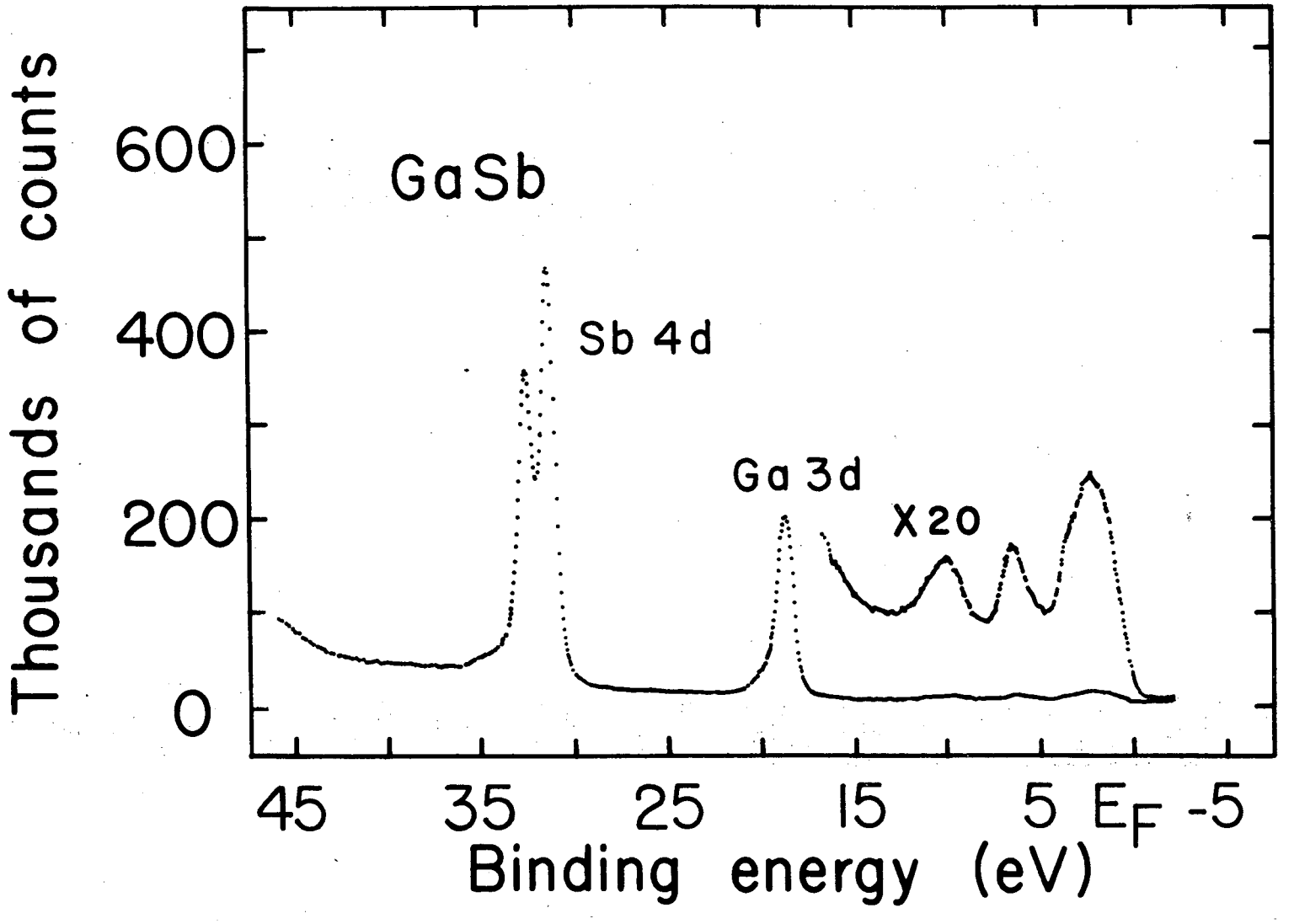

XBL 7210-5795

Fig. B-1. Valence bands of GaSb.

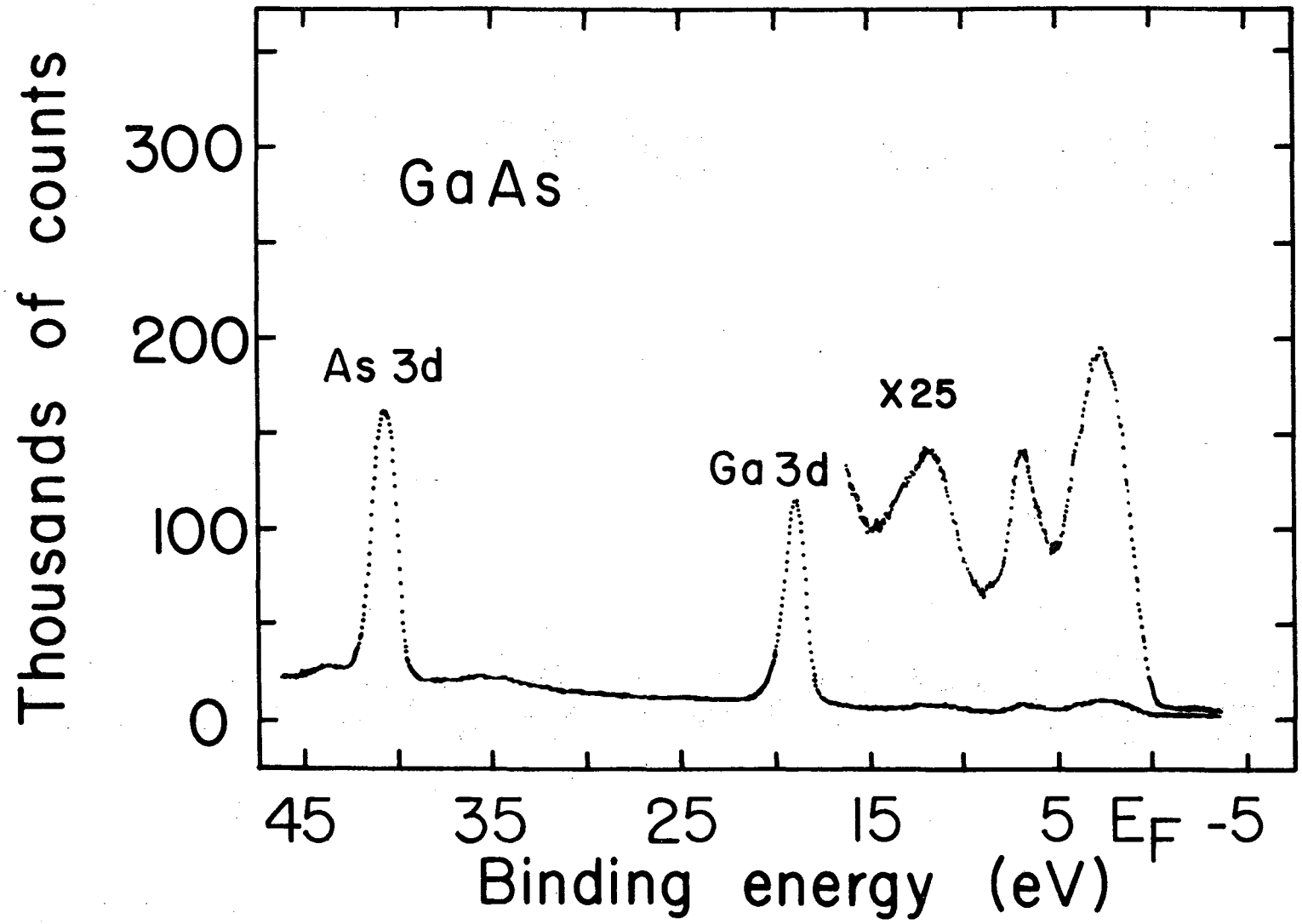

Fig. B-2. Valence bands of GaAs.

XBL 7210-5793

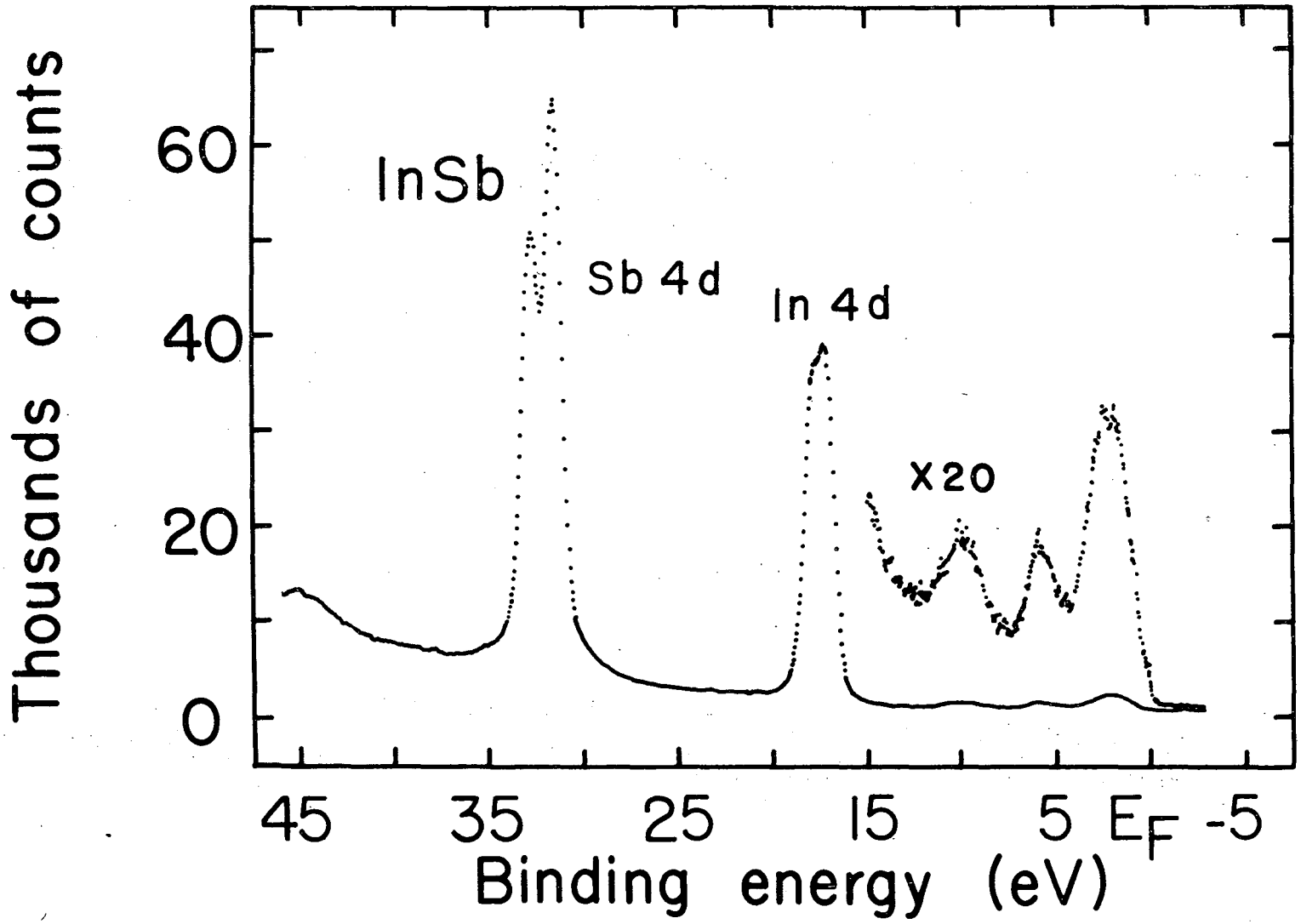

XBL 7210-5796

Fig. B-3. Valence bands of InSb.

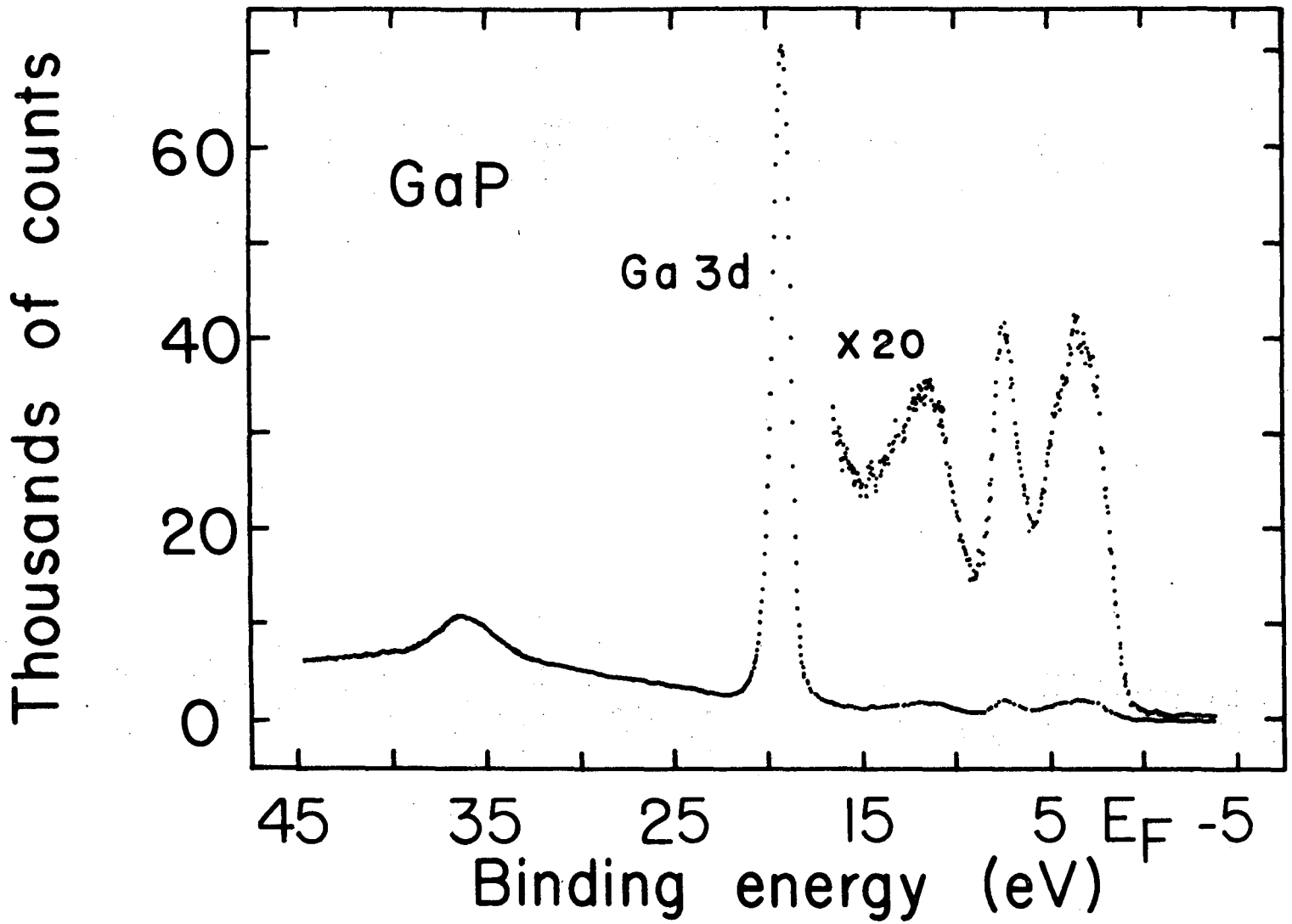

Fig. B-4. Valence bands of GaP.

XBL 7210-5794

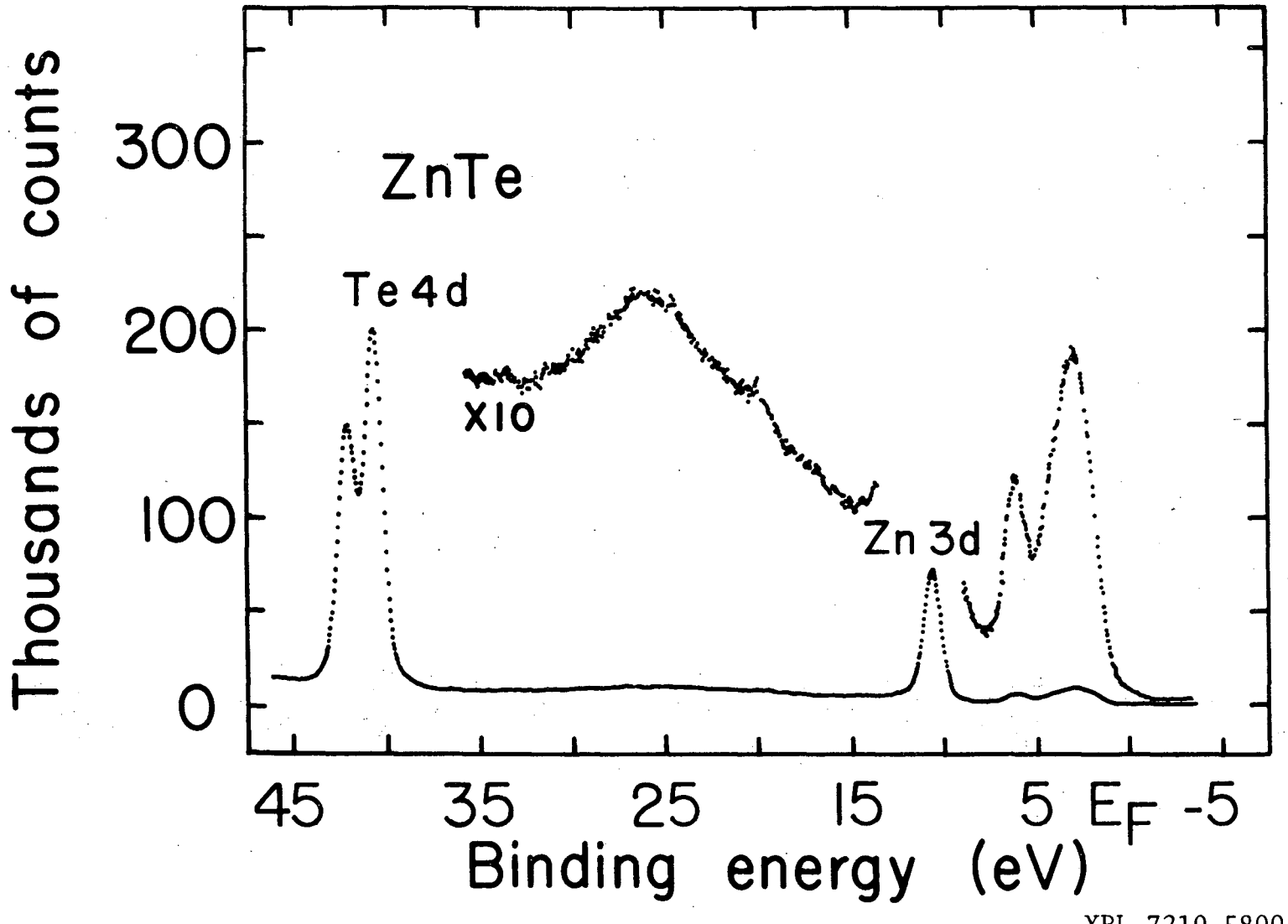

Fig. B-5. Valence bands of ZnTe.

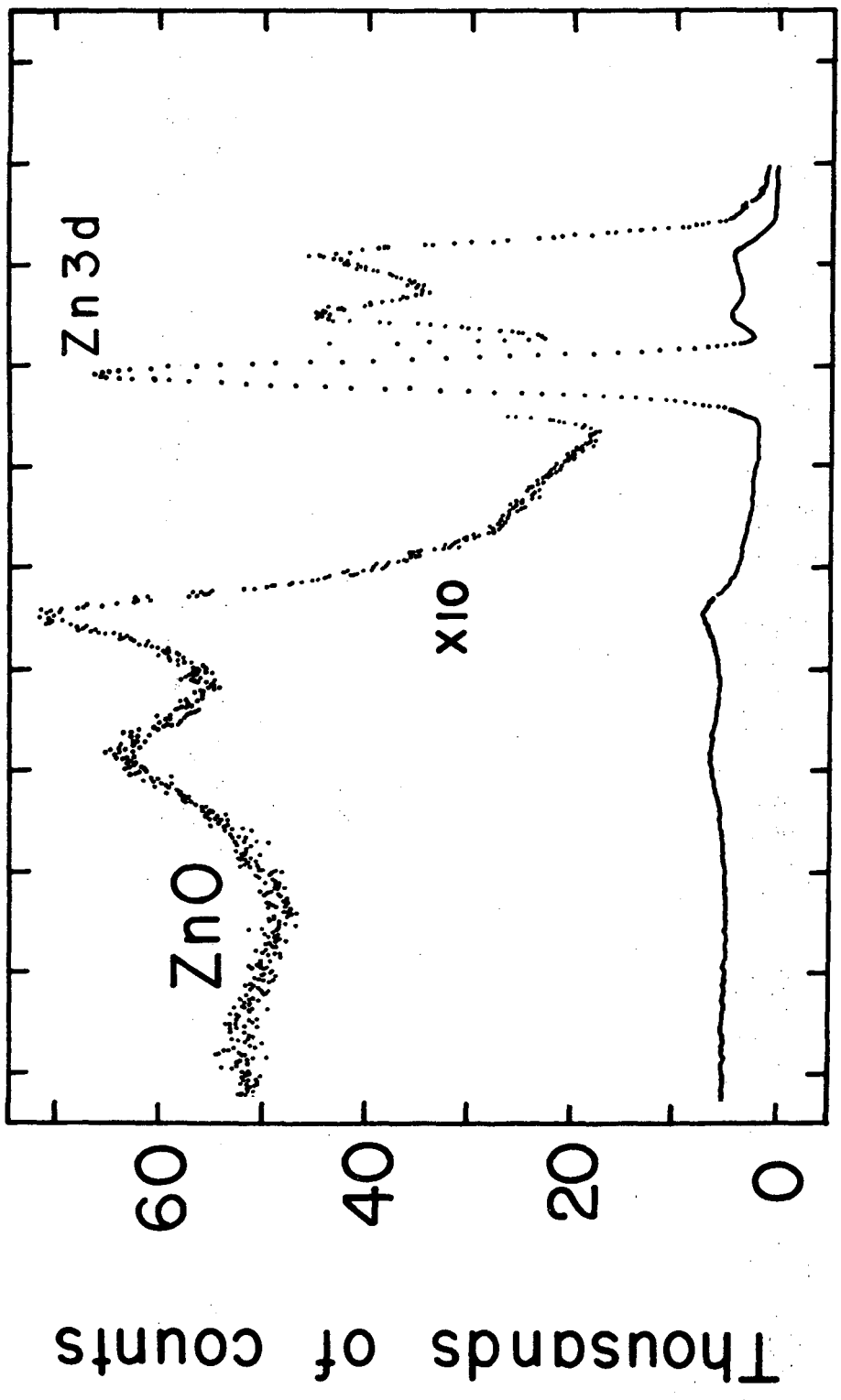

XBL 7210-5797

Fig. B-6. Valence bands of ZnO.

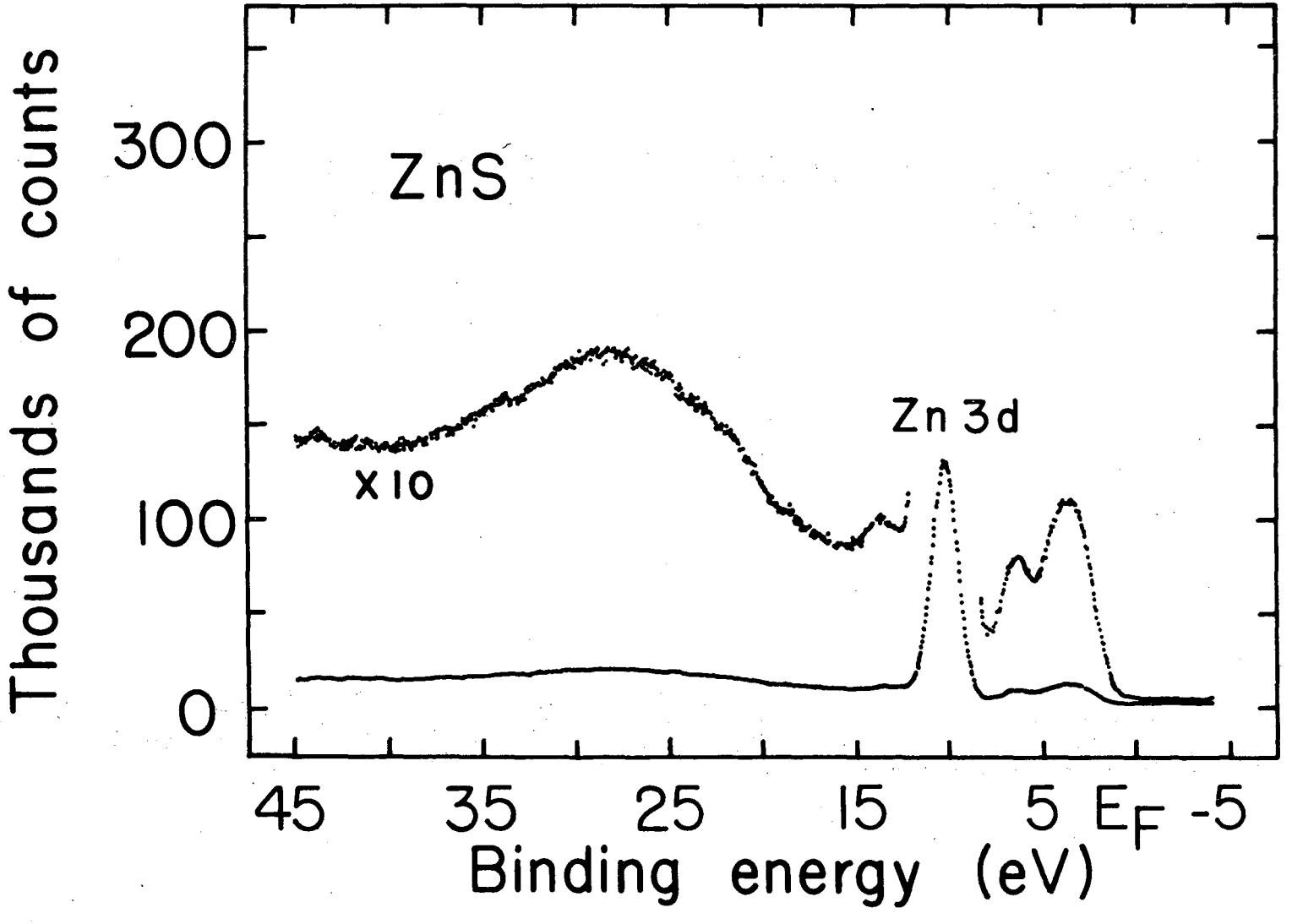

Fig. B-7. Valence bands of ZnS.

XBL 7210-5798

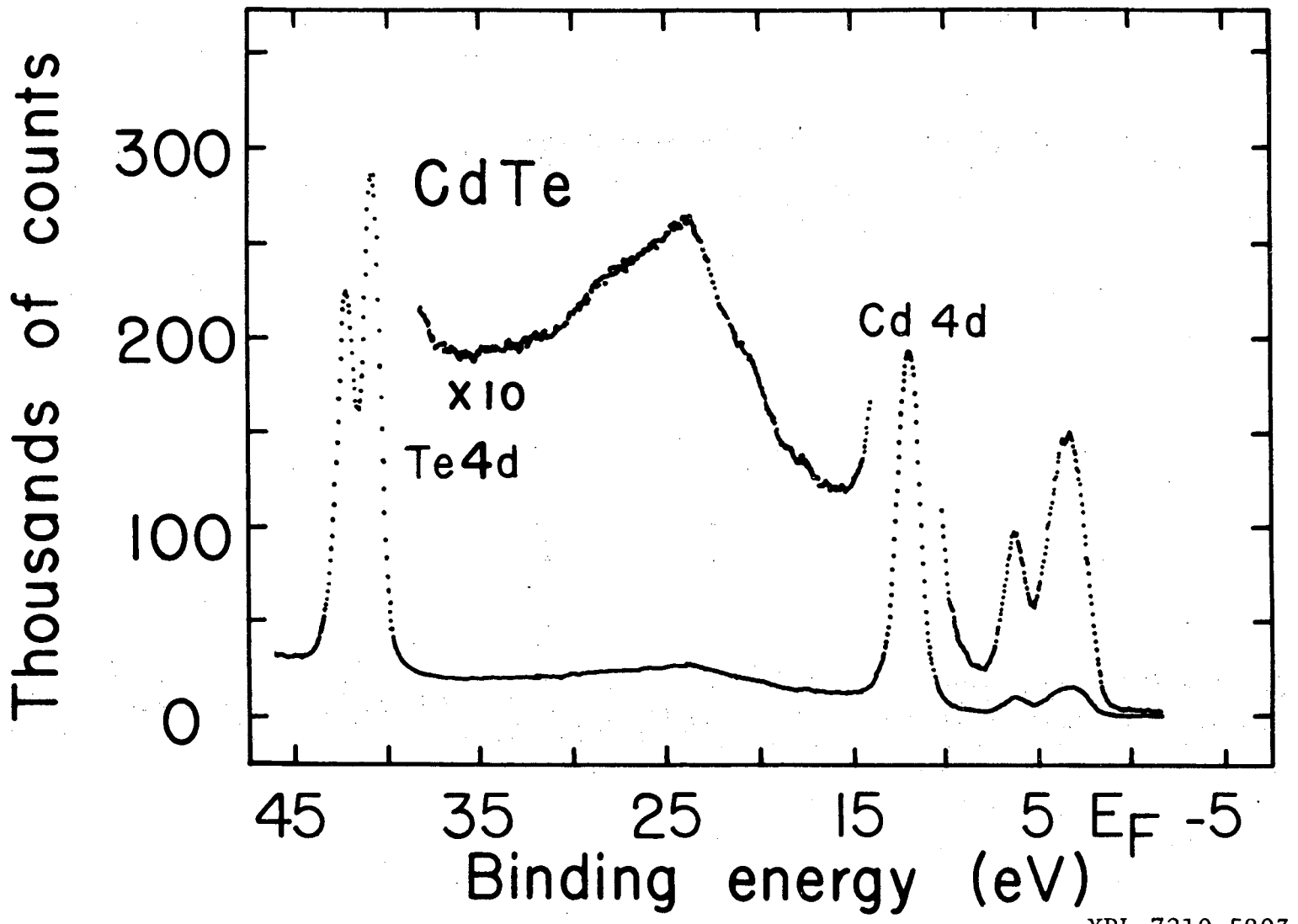

Fig. B-8. Valence bands of CdTe.

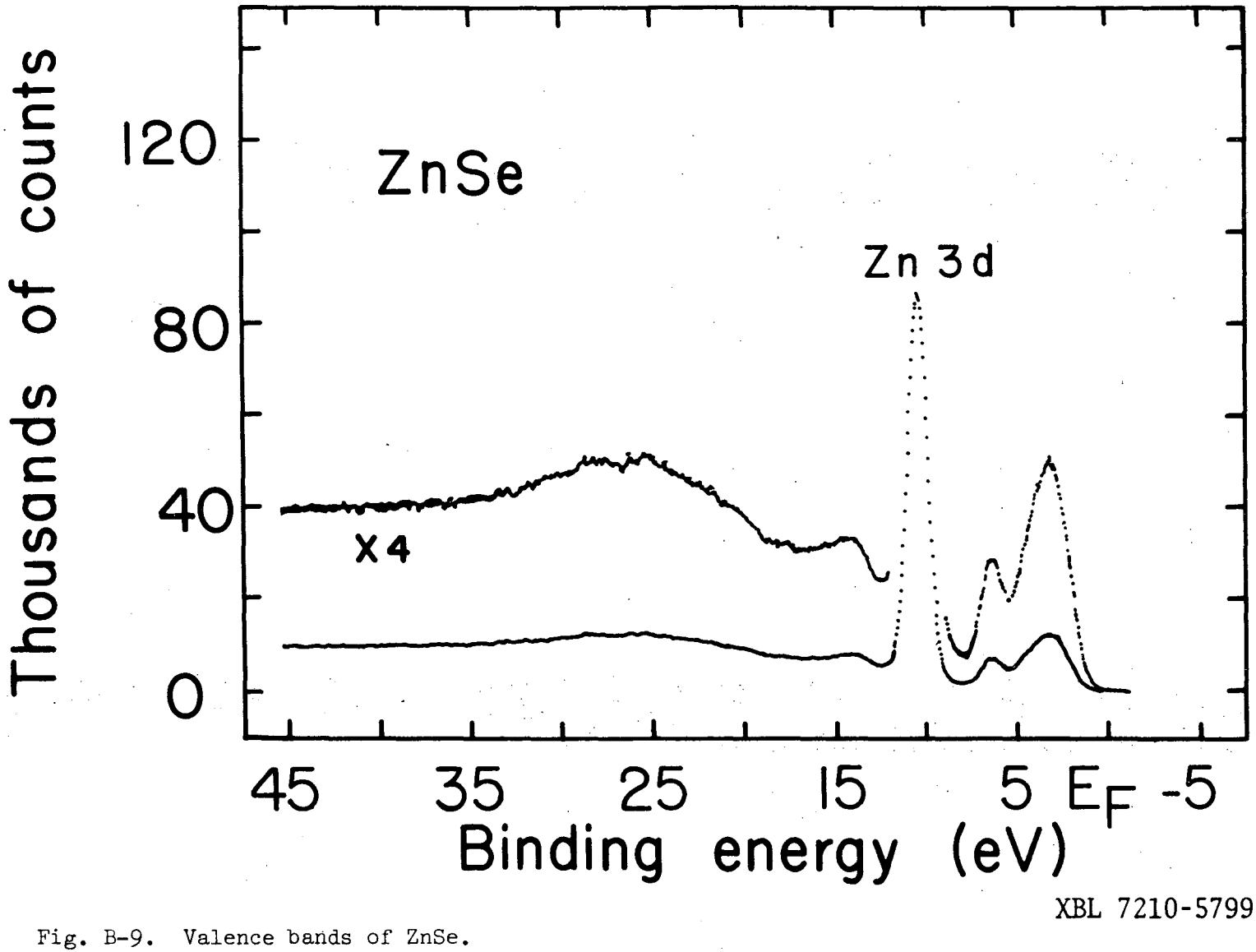

Fig. B-9. Valence bands of ZnSe.

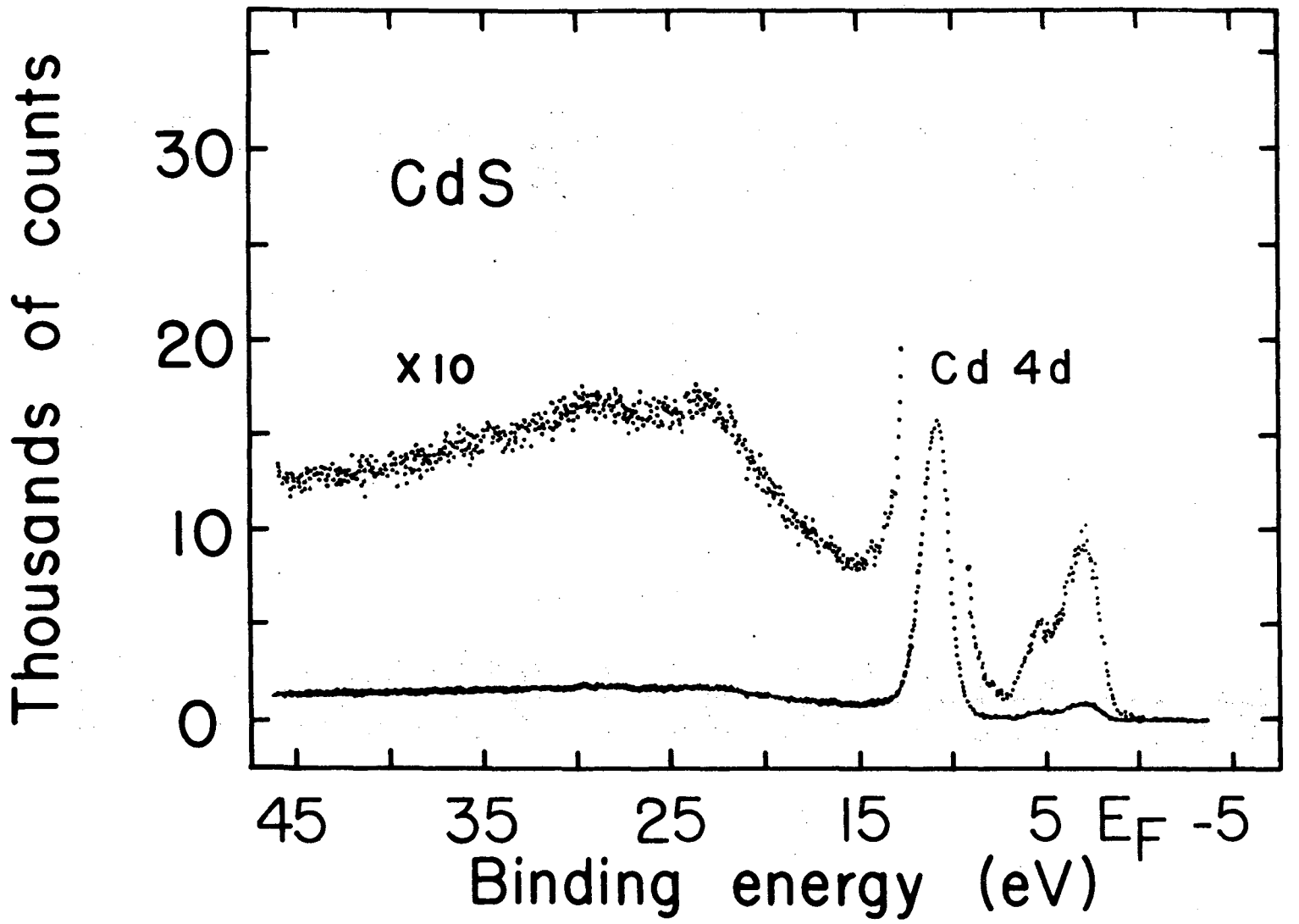

XBL 7210-5801

Fig. B-10. Valence bands of CdS.

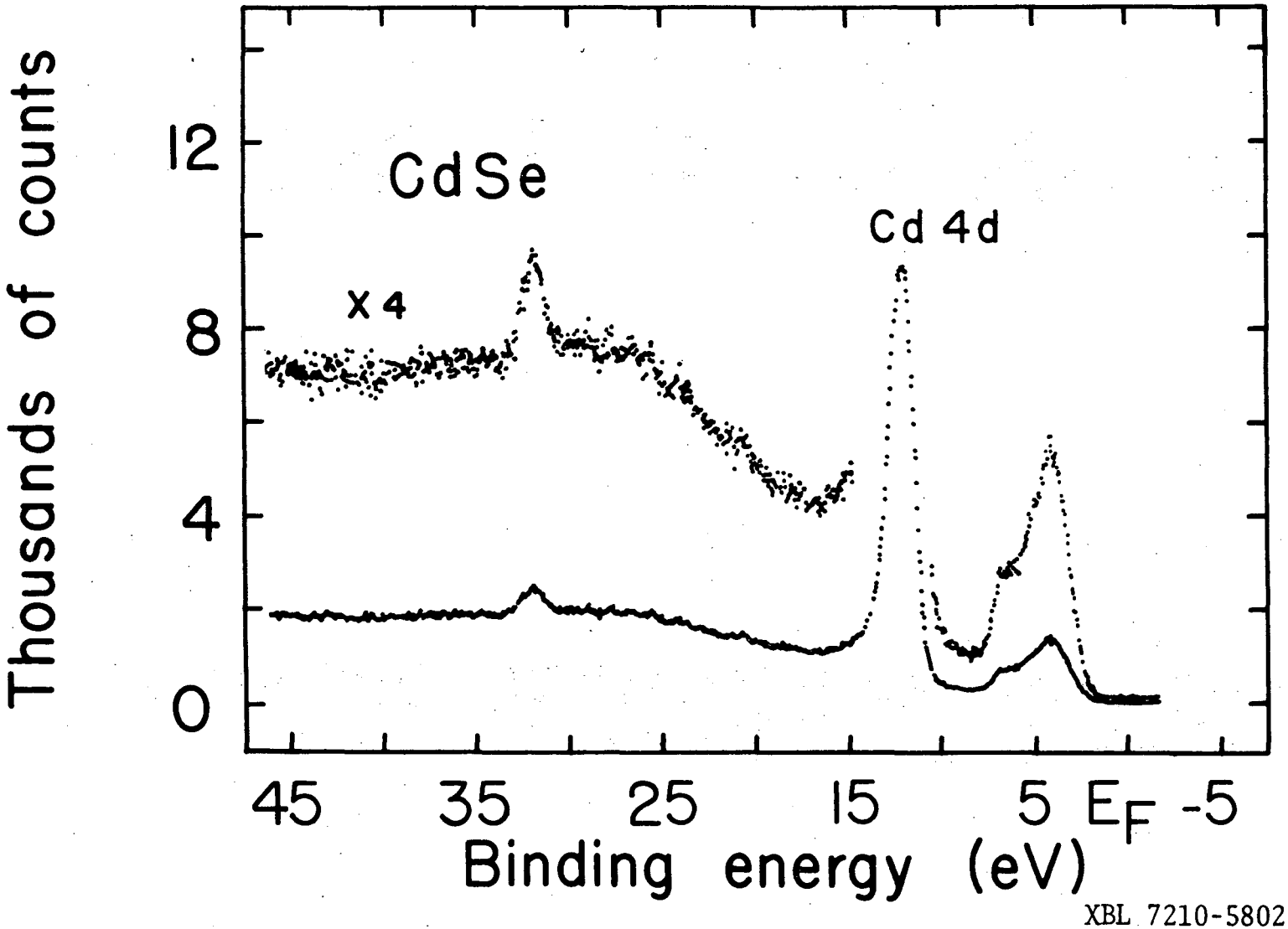

Fig. B-11. Valence bands of CdSe.

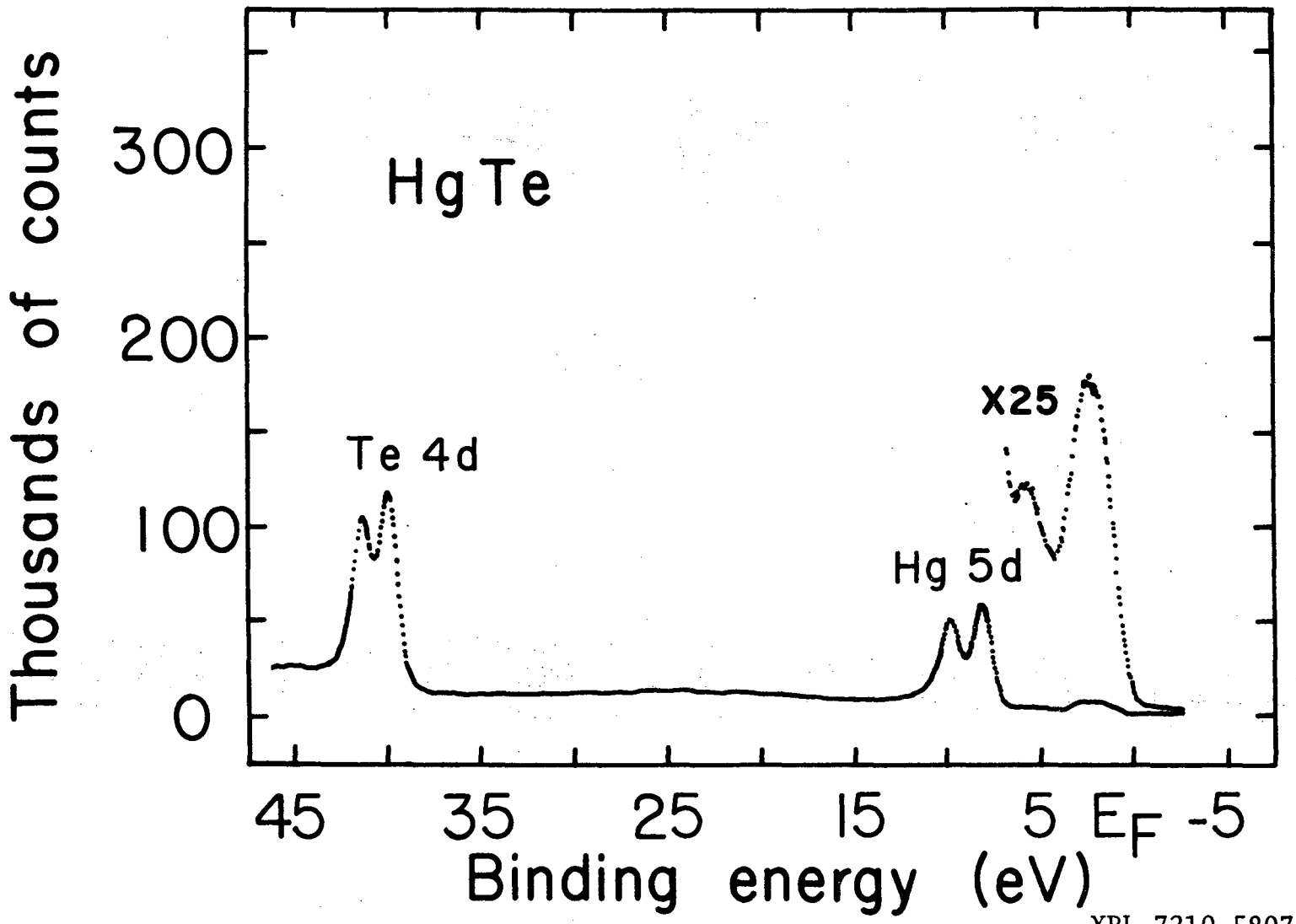

Fig. B-12. Valence bands of HgTe.

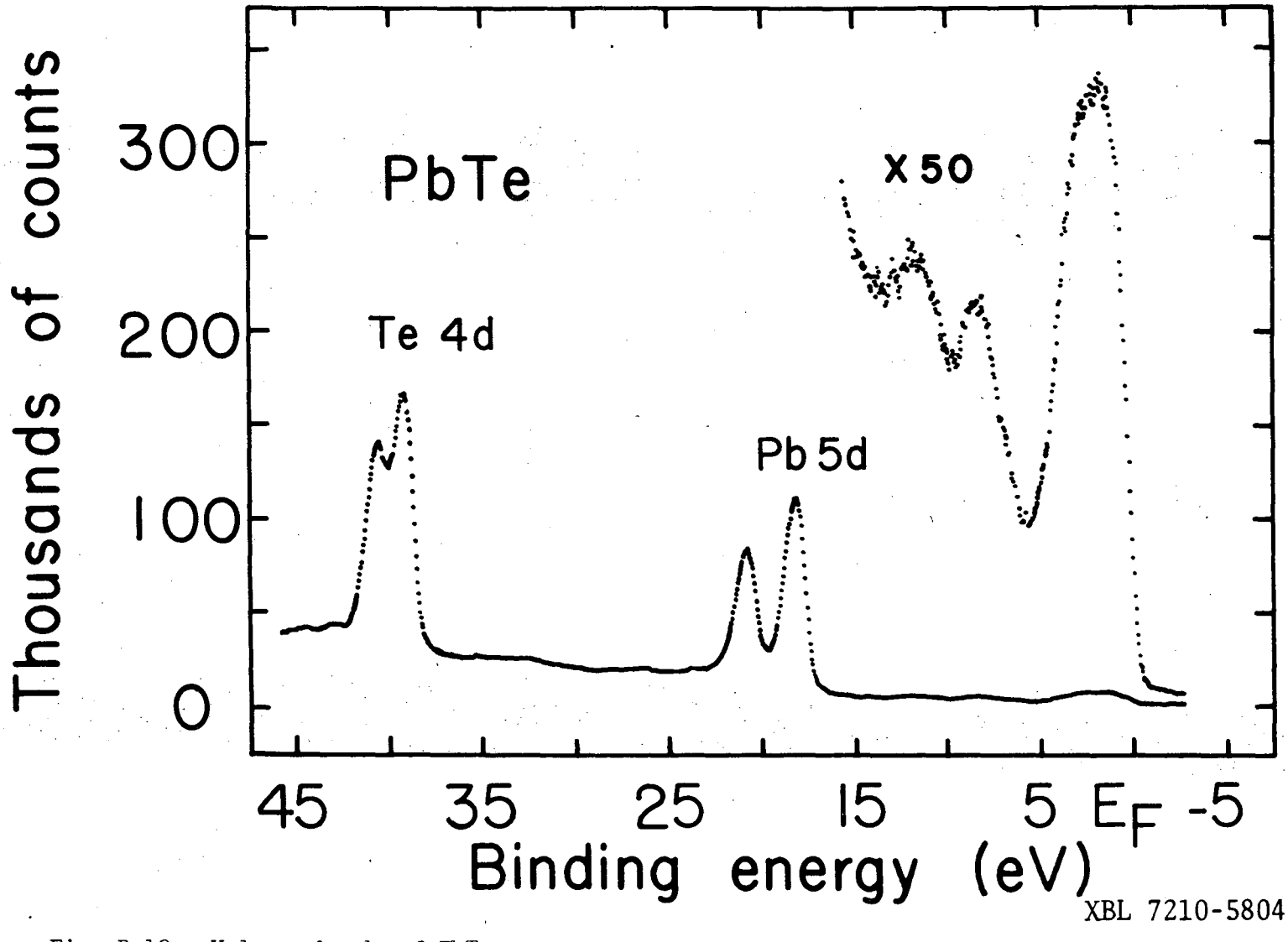

XBL 7210-5804

Fig. B-13. Valence bands of PbTe.

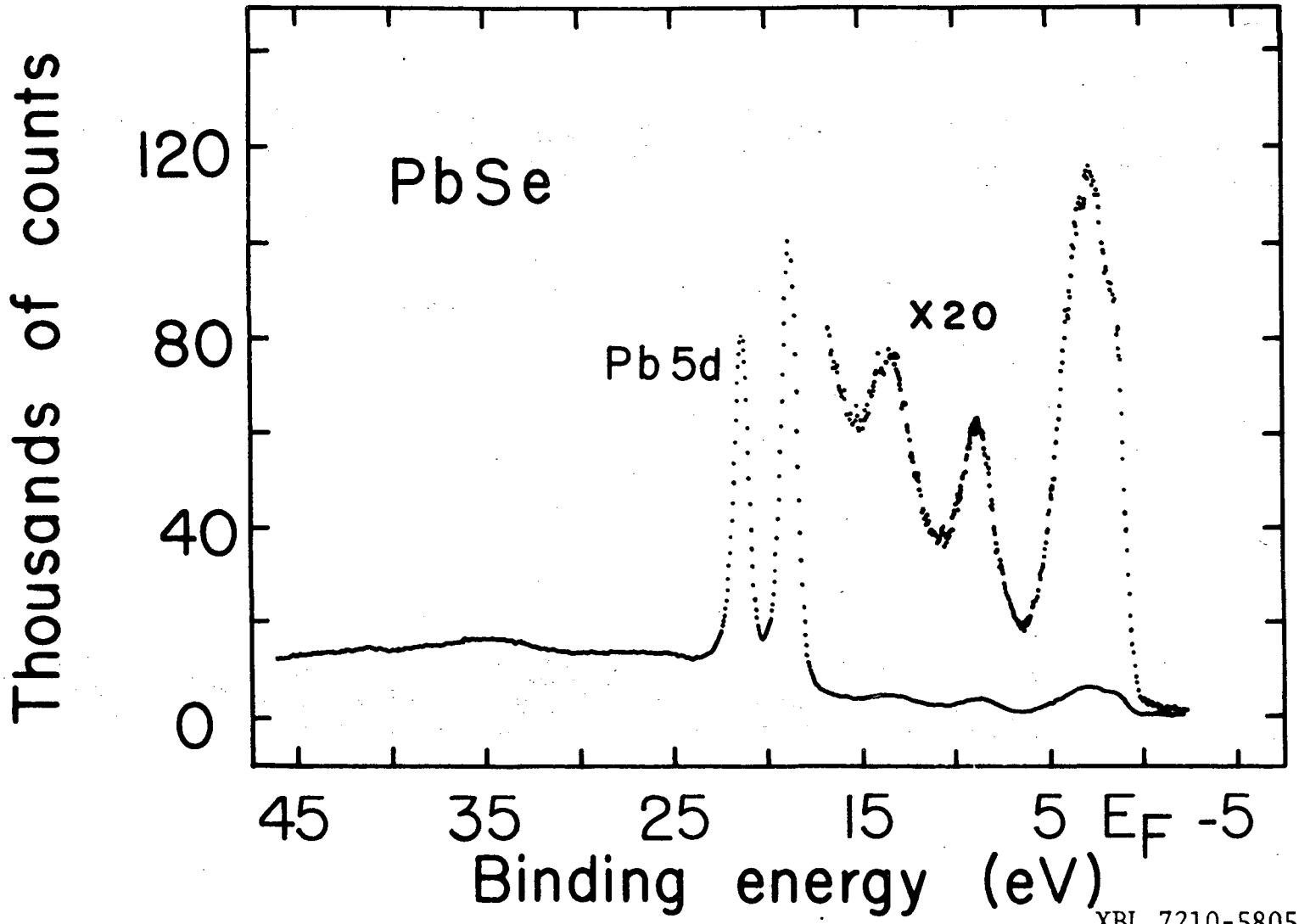

Fig. B-14. Valence bands of PbSe.

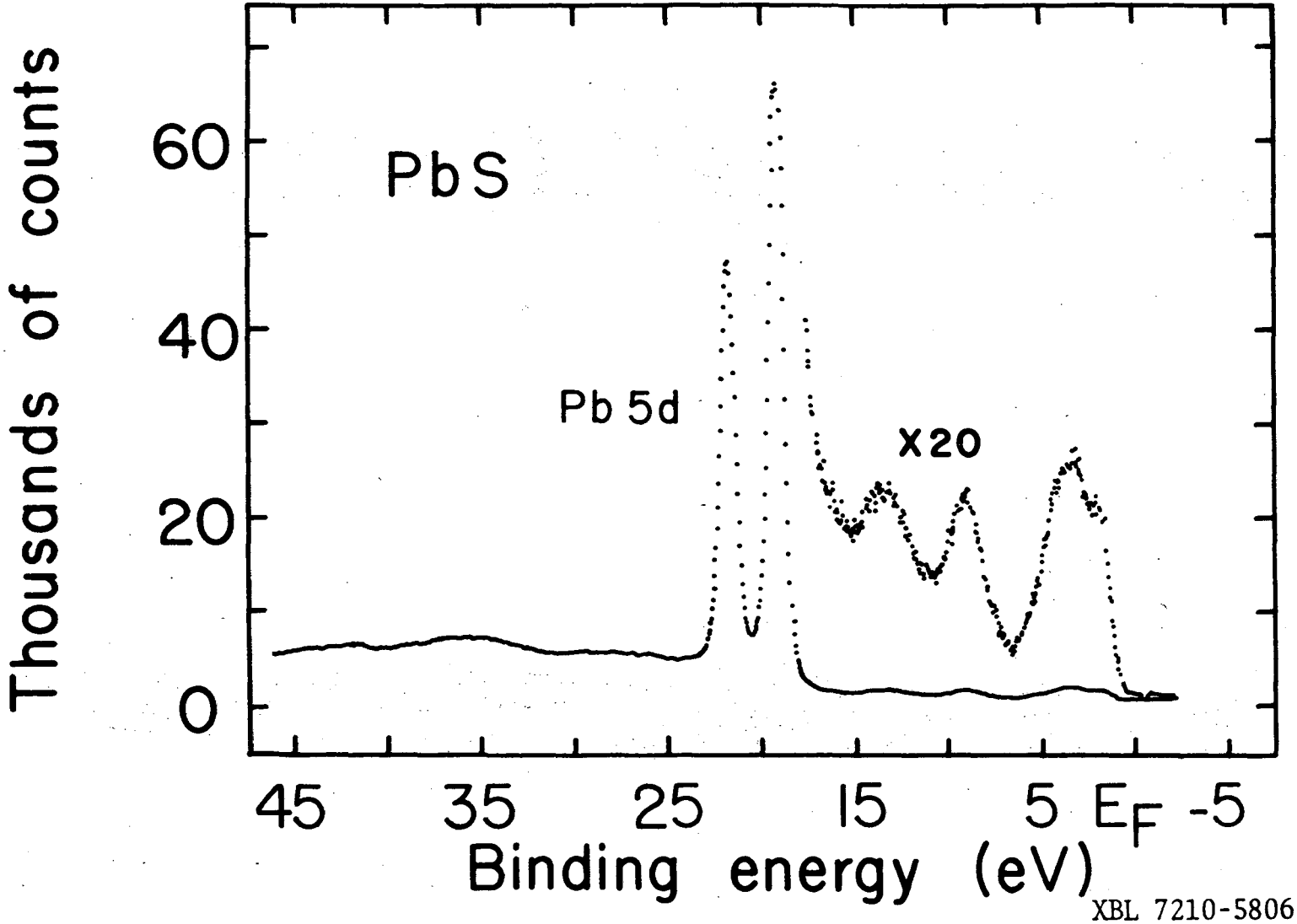

Fig. B-15. Valence bands of PbS.

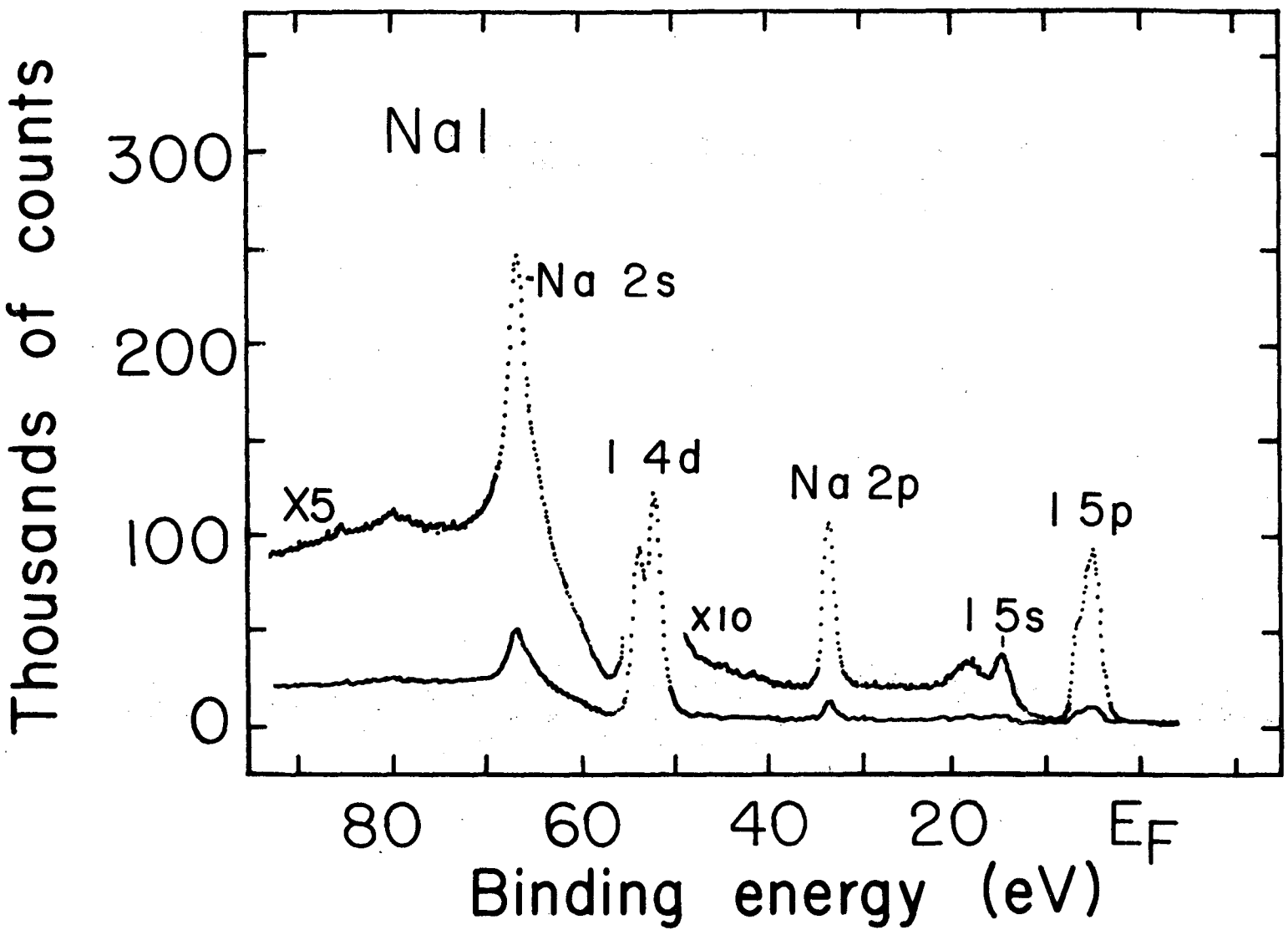

Fig. B-16. Valence bands of NaI.

XBL 7211-7420

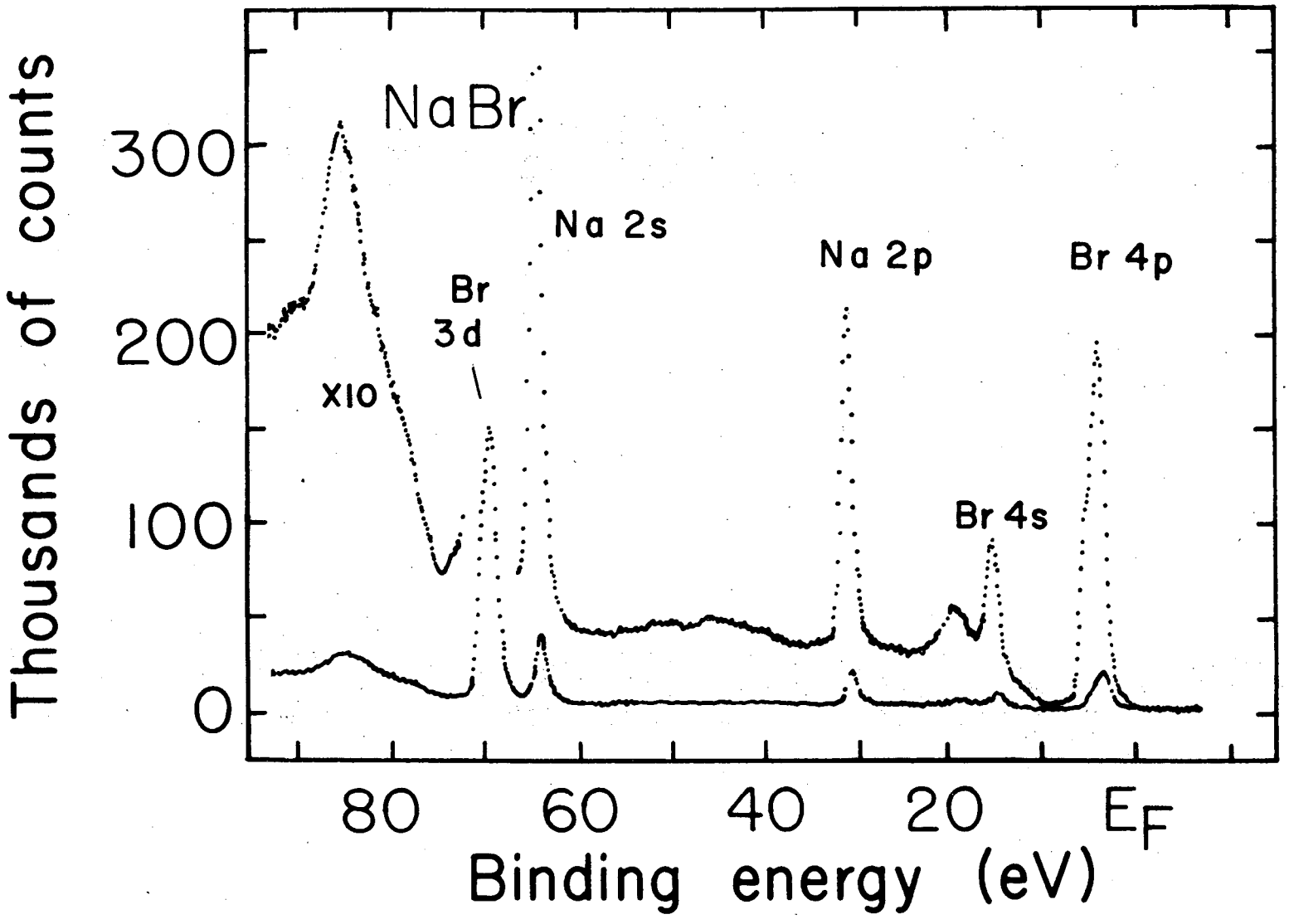

Fig. B-17. Valence bands of NaBr.

XBL 7211-7424

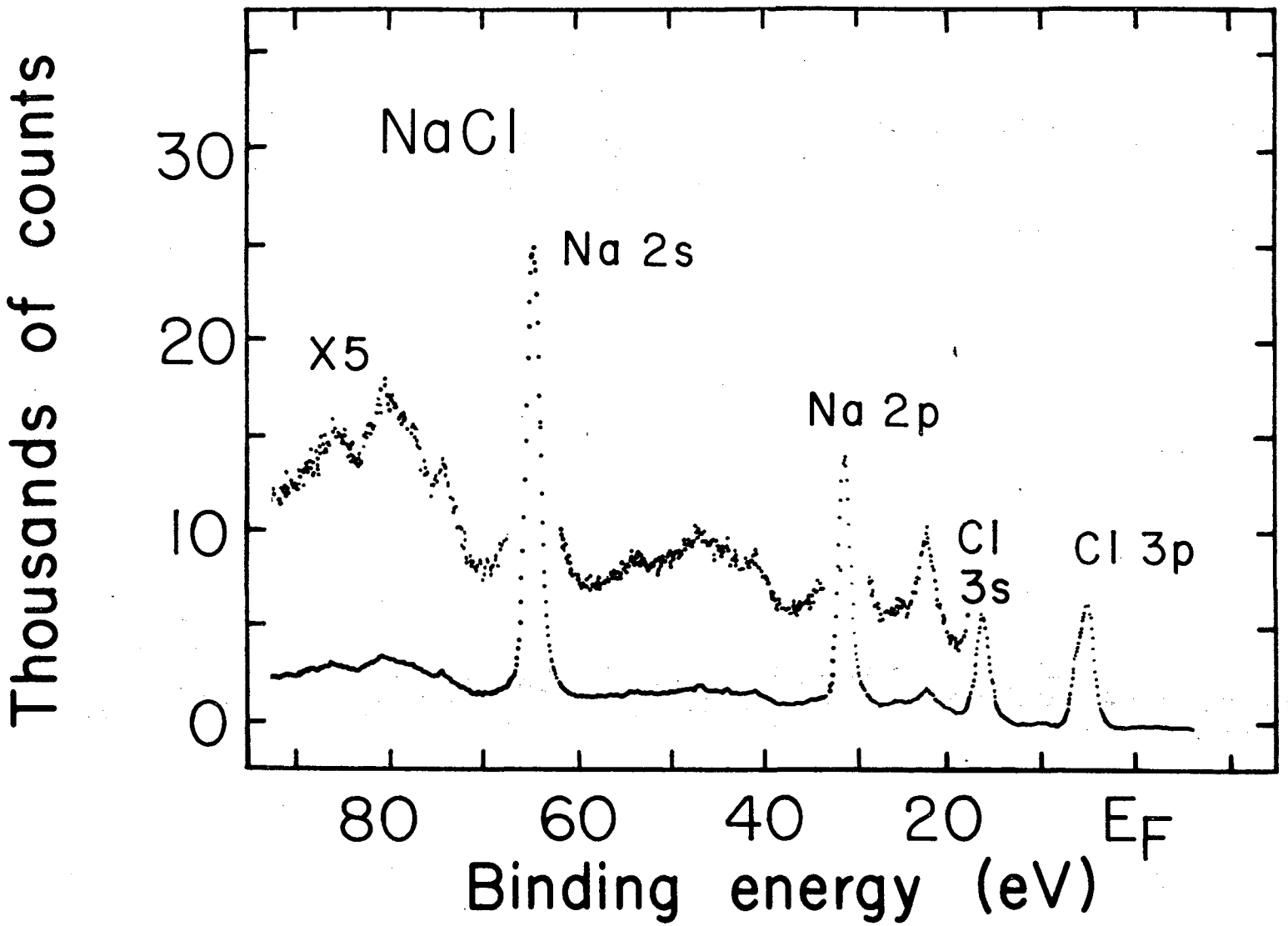

Fig. B-18. Valence bands of NaCl.

XBL 7211-7423

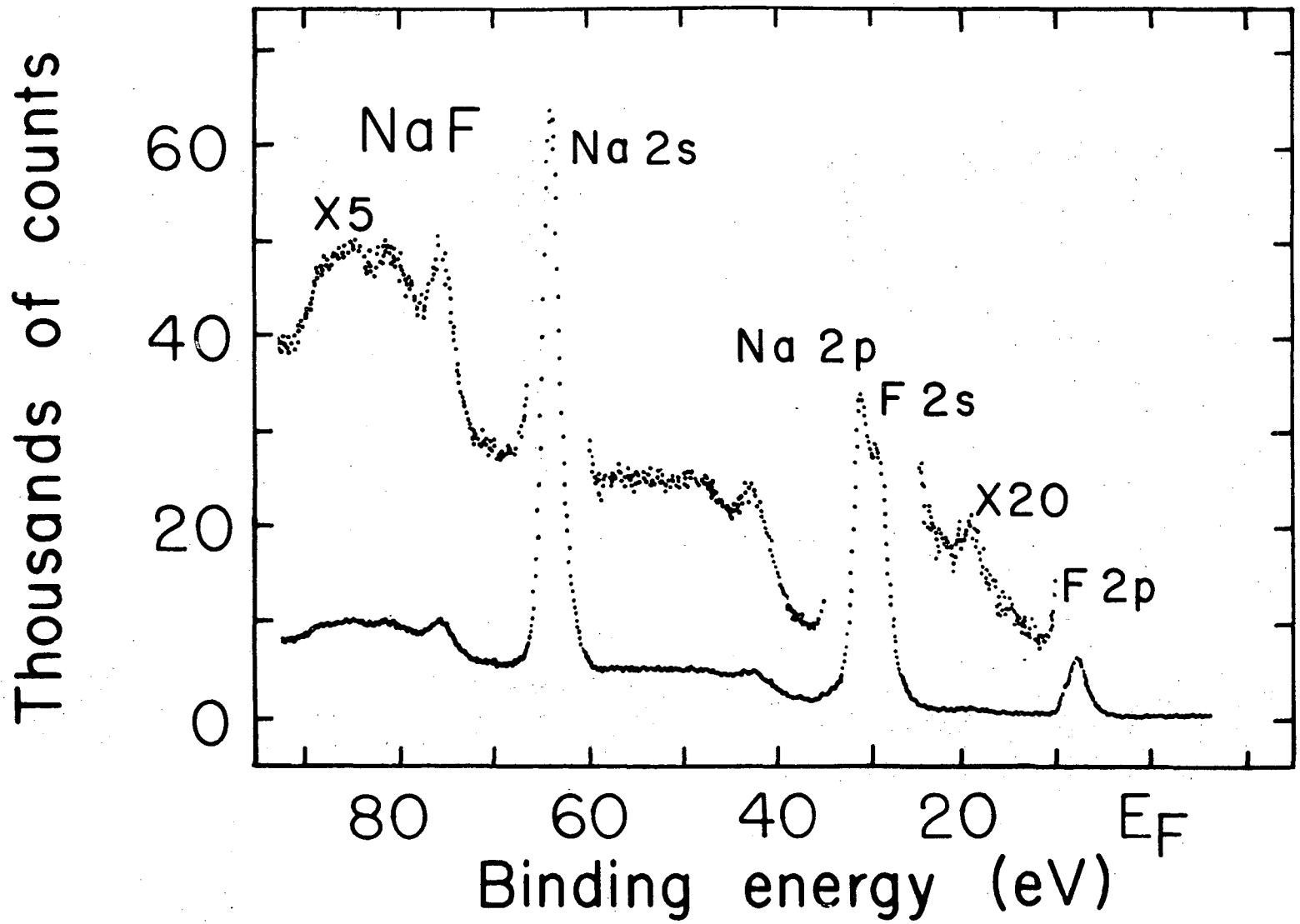

Fig. B-19. Valence bands of NaF.

XBL 7211-7421

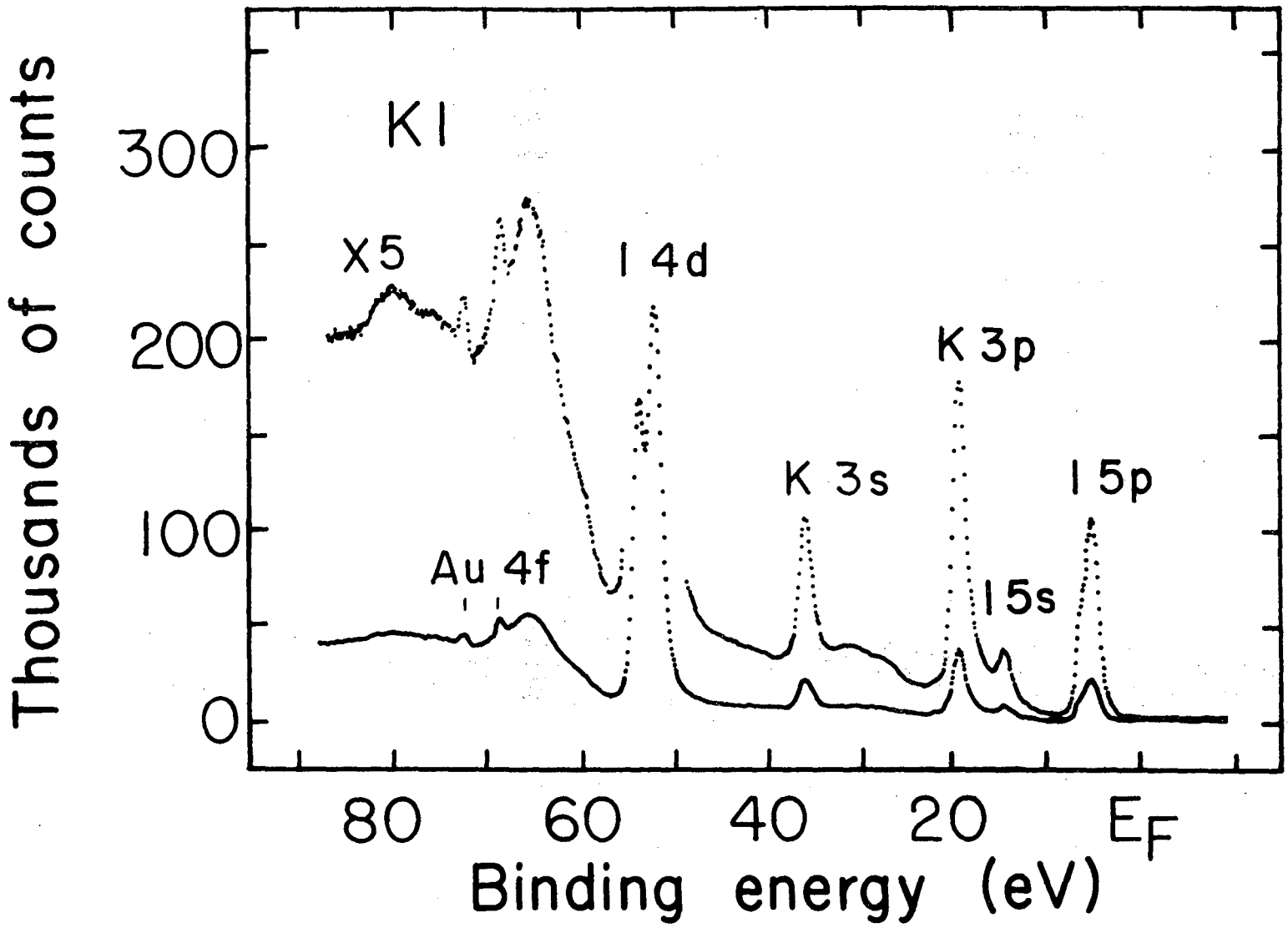

Fig. 20. Valence bands of KI.

XBL 7211-7422

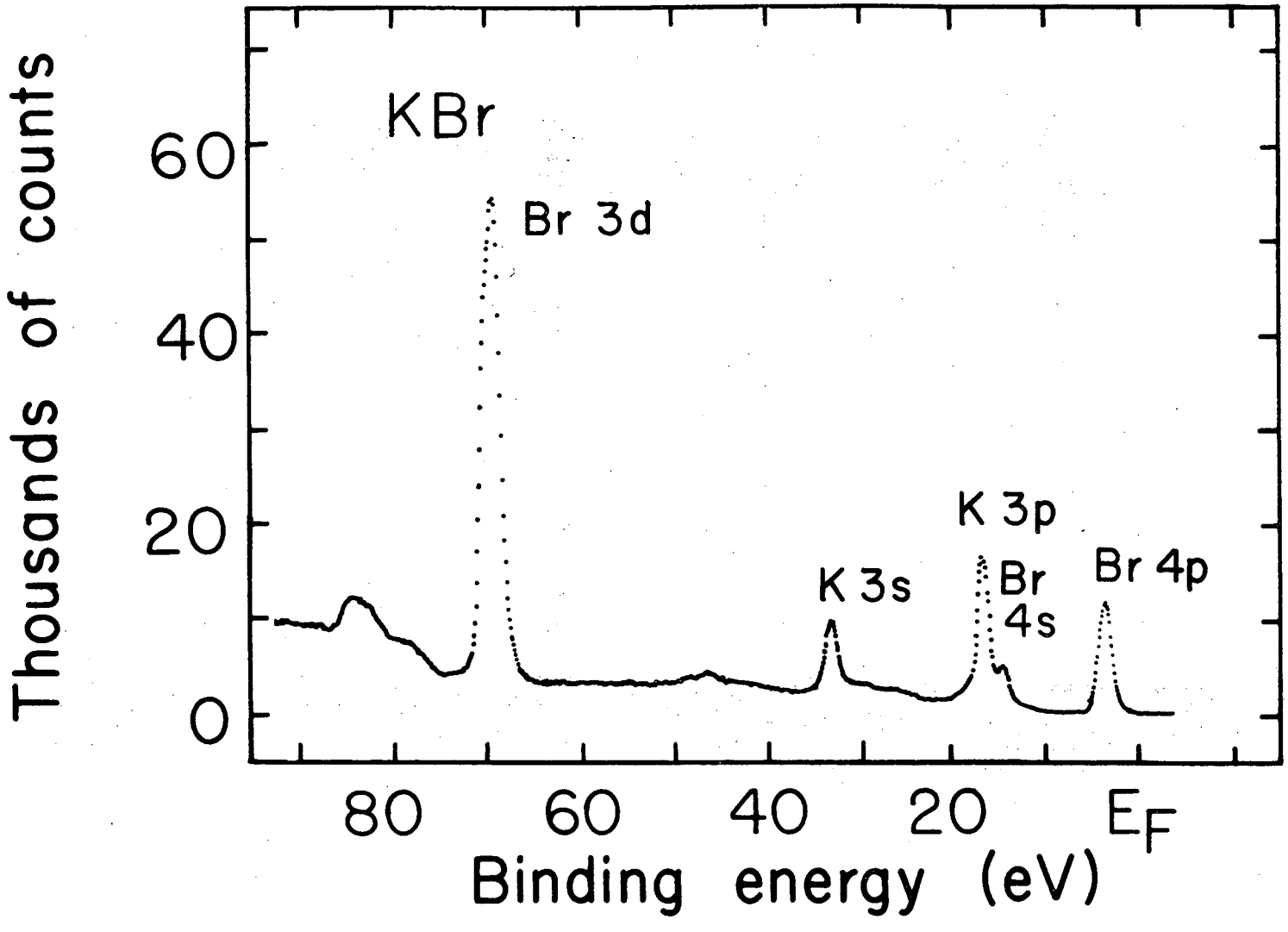

Fig. B-21. Valence bands of KBr.

XBL 7211-7427

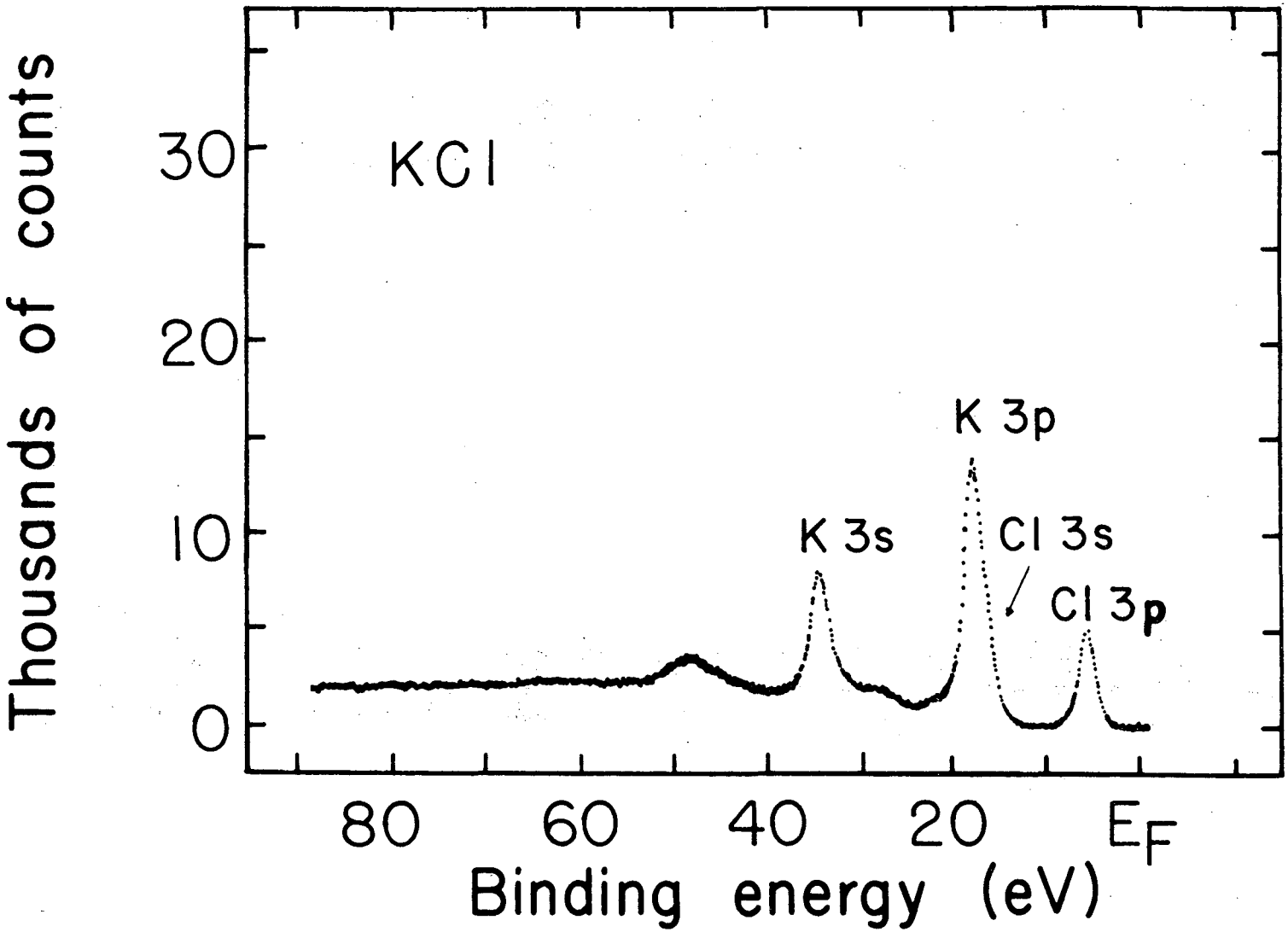

Fig. B-22. Valence bands of KCl.

XBL 7211-7426

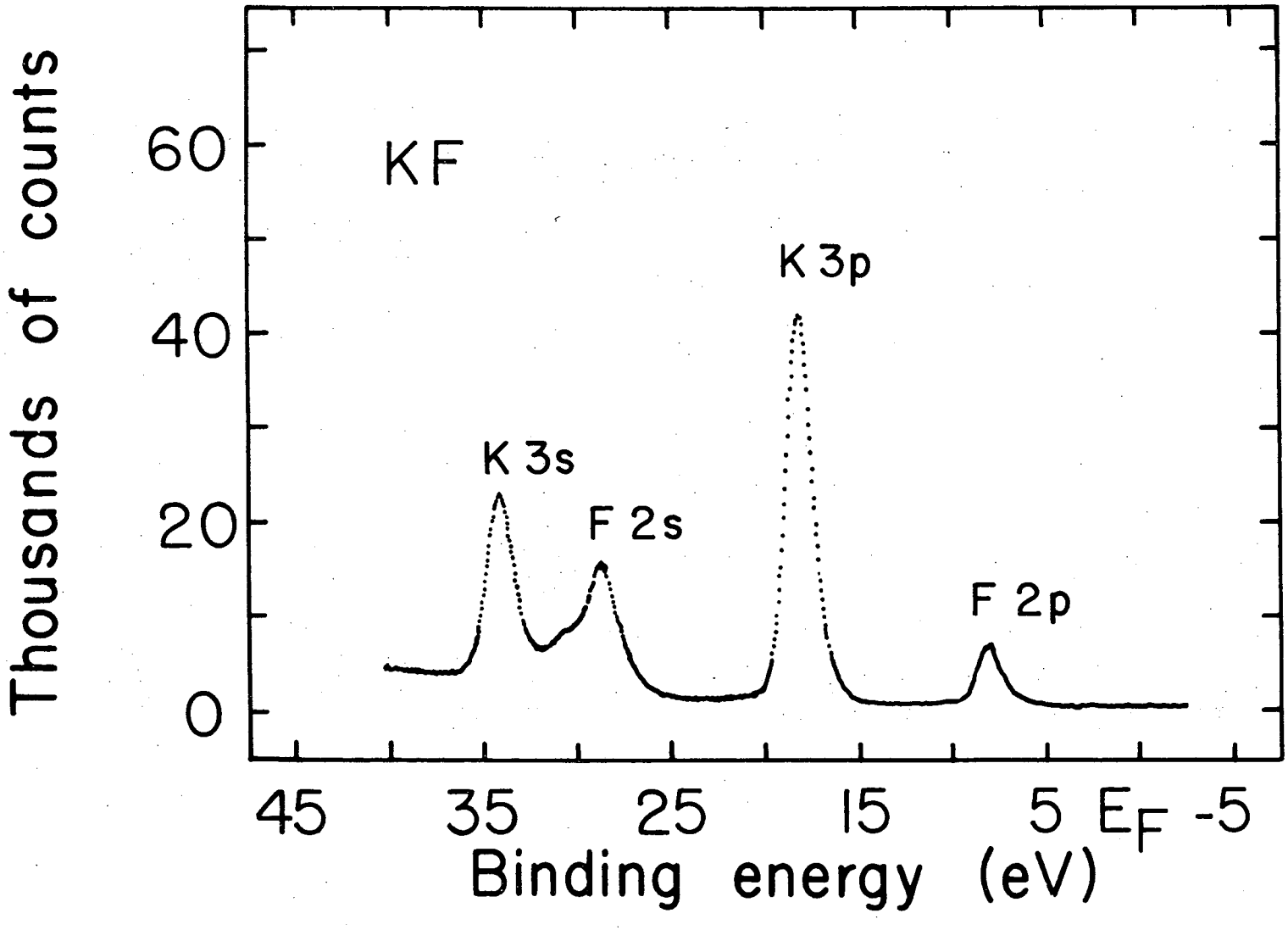

Fig. B-23. Valence bands of KF.

XBL 7211-7425

ACKNOWLEDGMENTS

The research reported in this thesis was performed at the Lawrence Berkeley Laboratory which is part of the University of California operated under contract to the United States Atomic Energy Commission. I thank the many people both on campus (UCB) and on the hill (LBL) who have participated in the photoemission spectroscopy program. Special thanks go to:

My colleagues at the Field Free Laboratory--Professor David A. Shirley my research director, Dr. Lothar Ley, Mr. Steve Kowalczyk, and more recently Mr. F. Read McFeely.

Mr. Joseph E. Katz who maintained and often designed the electronic equipment used in this work.

Mr. Eugene C. Miner who designed and supervised the construction and assembly of the ultra-high vacuum sample handling system.

Mr. Charles J. Butler who managed and maintained the Field Free Laboratory and the experimental equipment there.

Mrs. Winifred B. Heppler, Mr. Richard Escobales, and Mr. Dimitri N. Voronin for technical assistance.

Mrs. Kathleen A. McCracken of the Nuclear Chemistry Division office for her help in the preparation of this and other manuscripts.

I also acknowledge the love and support of my wife Petrea during these years of graduate study.

TECHNICAL INFORMATION DIVISION
LAWRENCE BERKELEY LABORATORY
UNIVERSITY OF CALIFORNIA
BERKELEY, CALIFORNIA 94720